Integrating Droplet and Digital Microfluidics for Single-Cell Analysis

Kenza Samlali

A Thesis

in

The Department

of

Electrical and Computer Engineering

Presented in Partial Fulfillment of the Requirements

for the Degree of

Doctor of Philosophy (Electrical and Computer Engineering) at

Concordia University

Montréal, Québec, Canada

October, 2021

CONCORDIA UNIVERSITY

School of Graduate Studies

This is to certify that the thesis prepared

By: **Kenza Samlali**

Entitled: **Integrating Droplet and Digital Microfluidics for Single-Cell Analysis**

and submitted in partial fulfillment of the requirements for the degree of

Doctor of Philosophy (Electrical and Computer Engineering)

complies with the regulations of this University and meets the accepted standards with respect to originality
and quality.

Signed by the Final Examining Committee:

_____ Chair
Dr. Ramin Sedaghati

_____ External Examiner
Dr. Scott Tsai

_____ External to Program
Dr. David Kwan

_____ Examiner
Dr. Nawwaf Kharma

_____ Examiner
Dr. Sana Anbuhi

_____ Thesis Supervisor
Dr. Steve C. C. Shih

Approved by   _____
                 Dr. Yousef R. Shayan, Chair Dept. Electrical and Computer Engi-
                 neering

December 17th, 2021   _____
                         Mourad Debbabi, Dean
                         Faculty of Engineering and Computer Science

Abstract

Integrating Droplet and Digital Microfluidics for Single-Cell Analysis

Kenza Samlali, Ph.D.

Concordia University, 2021

The motivation to engineer biological systems through standardization and abstraction sparked the development of technological advances in automation of life-sciences since the early 2000's. Now, robotics are performing high-throughput tasks with increasingly higher precision and control over the environment of precious biological samples. At the same time, a different set of hardware has emerged in the life-sciences: while robotics enable for high-throughput automation, microfluidics - the discipline of handling fluids on a micro scale - allows researchers and clinicians to perform experiments they could not have imagined before. These highly controlled devices can purify proteins, engineer cells, gain insights to single-cell 'omic' information, or filter out a patient's cancer cells in a fully automated fashion. In this work, we are focused on designing novel microfluidic devices for single-cell analysis. Currently, the use of single-cell analysis microfluidic devices open up the possibility of gaining detailed insights in heterozygosity of cell populations when coupled with next-generation sequencing technologies. We propose the design of a microfluidic setup that has improved control over single-cell operations within droplet-in-channel microfluidic architectures compared to current systems. Expanding these 'droplet-digital' tools, we have developed a microfluidic system for binary sorting of droplet libraries, on-demand droplet generation, droplet mixing, droplet storage and release, and deterministic encapsulation of single-cells . We propose new methods to sort cells, such as filamentous fungi libraries based on enzyme production, yeast based on growth rate and mammalian cell single-clones based on gene-editing efficiency. This work involves the development of novel hardware and software, and the integration of our microfluidic device within an automation system to operate droplet-digital microfluidics. Such systems are expanding the toolbox of those who are 'engineering biology'.

Acknowledgments

In spring 2017, I traveled to Montréal, living in a tiny Plateau student apartment, embracing the post-graduation crisis. One thing led to another, and I visited Steve's lab. The lab was just a couple of months old. I remember vividly, Fatemeh and Lea trying to figure out how to make some droplets, on a GE300 bench with a wonky camera. On the other side of the bench was James, between a soldering set-up and some *E.coli* plates. A beautiful inter-disciplinary mess: It was exactly what I needed! Only during my last year, I realized what Steve's lab is all about: giving everyone an equal opportunity at exploring their scientific research desires. And I'm so profoundly grateful to my supervisor Dr.Steve Shih, for granting me this opportunity of working with him in his early career. His guidance, support, and encouragement helped me reach my goals throughout my Ph.D. studies. It's an honor to be his first Ph.D. graduate. I wish to thank all the colleagues I've been blessed working with throughout the years: Fatemeh, Angela, Chiara, Guy, James, Sam, Alen, Alaa, Zhiyang, Jenny-Ann, Rob, Ziuwin, Jay, Felipe, Ehsan, Laura, Mara, Chris, Cesar, Hugo, Lea, Amin. Your kind hearts have truly lifted my spirits when times were tough, and I'm grateful for all of the knowledge sharing and learning you've been open to. A special thanks to Fatemeh, Chiara, and Angela, who have contributed to some major ideas presented in this thesis. To my committee, Dr. Kharma, Dr. Kwan, Dr. Anbuhi, and Dr. Tsai, I wish to extend my gratitude for their meaningful contributions that guided the reasoning behind this thesis. Finally, my peers at the Center of Applied Synthetic Biology have always encouraged me to explore the synthetic biology community freely beyond my academic endeavors, thanks to which I've been able to shape my career goals. This was a special journey for me.

I also truly recommend having a pet for comfort and listening ears during your Ph.D. journey. Rabbits are great. And even better, is a life partner who can cheer you up and admire your strengths. I'm eternally grateful to Kevin, for being by my side at all times. Last, I would like to thank my Mama and Broer. Mama, you grew me, you nurtured me. While the world around us came down, you kept me dreaming. That is the most wonderful gift a growing human can ask for. I will always live my life carrying courageous hope, and big dreams.

Contributions

Chapter 2

Samuel R. Little (S.R.L) performed a literature review on building methods using microfluidics, James M. Perry (J.M.P.) performed a literature review on learning methods using microfluidics, Kenza Samlali (K.S.) performed a literature review on testing methods using microfluidics. S.R.L, J.M.P , K.S. and S.R.L designed figures and edited. All authors and Steve C. C. Shih (S.C.C.S), wrote the paper and reviewed the final version of the manuscript before submission.

Chapter 3

K.S. designed and fabricated the device, carried out experiments, analyzed the data and wrote custom software. K.S. and S.C.C.S designed the experiments. Chiara Leal Alves (C.L.A.) helped in device design, fabrication, fungal culture and assays. Mara Jezernik performed initial fungal culture and media establishment, and determined *C.rosea* growth rate. K. S. and S.C.C.S. wrote the paper, and all authors reviewed the final version of the manuscript.

Chapter 4

Fatemeh Ahmadi (F. A.) and S. C. C. S designed the experiments. F.A. fabricated the ID2M devices, integrated the device with the automation and detection setup. F. A performed all proof of concept experiments and constructed a fluorescein standard curve on chip with the help of K.S. Phillipe Vo (P.Q.N.V.) wrote the software to operate the experiments on device. F.A. and K.S. carried out the mutagenesis and generated IL-resistant strains. F. A. performed the yeast cells n-ary sorting on chip and analysed the data with S.C.C.S. F.A. and S.C.C.S. wrote the paper, and all authors reviewed the final version of the manuscript before submission.

Chapter 5

K.S. built the device, carried out experiments, analyzed the data and wrote custom software. K.S. and S.C.C.S designed the experiments. F.A. helped in device design, fabrication and characterization. Angela B.V. Quach (A.B.V.Q.) assisted in cell culture and transfection. Guy Soffer (G.S.) designed automation system software and hardware. K. S. and S.C.C.S. wrote the paper, and all authors reviewed the final version of the manuscript before submission.

All authors reviewed the final manuscript and approved of the contents.

Contents

Bibliography   **155**

List of Figures

List of Tables

List of Abbreviations

4MU-GalNAc   4-methylumbelliferyl N-acetyl-β-D-galactosaminide

4MU-GlcNAc   4-methylumbelliferyl N-acetyl-β-D-glucosaminide

4MU-Glc   4-methylumbelliferyl β-D glucopyranoside

A.niger   *Aspergillus niger*

AC   Alternating current

B. cinerea   *Botrytis cinerea*

DC   Direct current

CAR   Chimeric antigen receptor

C. rosea   *Clonostachys rosea*

CCMM   Colloidal chitin minimal media

CE   Constant electrode

CFD   Computational fluid dynamics

CRISPR   Clustered regularly interspaced short palindromic repeats

CTC   Circulating tumor cell

CWDE   Cell-wall degrading enzymes

DEP   Dielectrophoresis

DBTL   Design Build Test Learn

DMEM   Dulbecco's Modified Eagle Medium

DMF   Digital microfluidics

DNA   Deoxyribonucleic acid

DSB   Double strand break

E. coli   *Esterichia coli*

eGFP	Enhanced green fluorescent protein
ELISA	Enzyme-linked immunosorbent assay
EWOD	Electrowetting-on-dielectric
FACS	Fluorescence-activated cell sorting
FADS	Fluorescence activated droplet sorting
FL-GalNAc	Fluorescein mono-N-acetyl-β-D-galactosaminide
FL-GlcNAc	Fluorescein mono-N-acetyl-β-D-glucosaminide
FD-Glc	Fluorescein-di-β-D glucopyranoside
FITC	Fluorescein isothiocyanate
F. graminearum	*Fusarium graminearum*
GE	Ground electrode
GH	Glycoside hydrolase
GMM	Glucose minimal media
gRNA	Guide Ribonucleic acid
hpi	Hours post incubation
ID2M	Integrated droplet digital microfluidics
IL	Ionic liquid
ITO	Indium tin oxide
KO	Knock out
LOD	Limit of detection
MM	Minimal media
mRNA	Messenger Ribonucleic acid
NSCLC	non small cell lung carcinoma
OD	Optical Density
OET	Opto-electronic tweezers
OF	Optical fiber
PBS	Phosphate buffer saline
PCR	Polymerase chain reaction
PDA	Potato dextrose agar
PDB	Potato dextrose broth

PDMS	Polydimethylsiloxane
PE	Pulsing electrode
RFU	Relative fluorescence units
RNA	Ribonucleic acid
RT-PCR	Reverse transcriptase Polymerase chain reaction
S.cerevisiae	*Saccharomyces cerevisiae*
SAW	Surface acoustic waves
SCL	Serial clock line
scRNA-seq	Single-cell RNA sequencing technology
SDA	Serial data line
SDK	Software development kit
SCA	Single-cell analysis
SSF	Solid-state fermentation
SSDF	Solid-state droplet fermentation
E. coli	*Trichoderma reesei*
TEC	Thermoelectric cooler

List of Symbols

θ	Contact angle
ϵ_0	Permittivity of vacuum
ϵ_r	Relative permittivity or dielectric constant
γ_{LV}	surface tension at liquid vapor interface
C	Capacitance
f	Frequency
Q	Volumetric flowrate
R_h	Hydrodynamic resistance
V_{RMS}	Root mean squared voltage
V_{PP}	Peak-to-peak voltage
E	Energy
F	Force
ρ	Density
μ	Dynamic viscosity
u	Velocity

Chapter 1

Introduction

1.1 Motivation

Microfluidics is a technology that uses the interesting physics of fluids on the microscale, to automate experiments on credit-card sized devices. Also called "lab-on-chip" technology, these devices are changing the way experiments can be rationalized. Tools such as organs-on-chip, single-cell and single-molecule analysis devices, devices for real-time processing of cells and tissues, or rapid diagnostic devices, expand the toolkit of biotechnologists. One area for which microfluidics have been frequently used is single-cell analysis.[1, 2] This technology has allowed researchers to study heterogeneity in biological samples on a single-cell scale. With the introduction of single-cell encapsulation and single-cell trapping systems, single-cell sequencing technologies have become popular.[3, 4, 5, 6, 7] Instead of looking at population average results, developmental biologists are now dissecting single-cell fate, while cancer researchers can easily study tumour heterogeneity. The invention of these tools has resulted in very significant new findings in biology and genomics.[8, 9] Cross-disciplinary work allows for such successful technology adoption.

The current single-cell microfluidic devices have two limitations. First, it remains a challenge to individually control specific droplets – and thus cells – in a channel microfluidic device. Second, it is not yet possible to perform fluidic operations with these selected droplets, such as mixing, sorting and isolation for incubation or storage. Similarly, in droplet-in-channel microfluidic systems, cells are often at random encapsulated inside droplets. In summary; there is currently no platform to easily control an individual single-cell-containing droplet in channels or to control how the droplets are generated. These are limitations for those wanting to develop microfluidic systems that can perform multi-step biological assays.

In this thesis, we are proposing foundational new microfluidic tools that can alleviate some limitations of the current single-cell microfluidic devices. Chapter 1 provides a summary of microfluidic single-cell technologies and identifies some gaps in the current microfluidic tools available. A comprehensive literature review on the use of microfluidics in synthetic biology is presented in Chapter 2. Chapter 3 demonstrates a method to sort droplets containing single filamentous fungi clones, expanding the high-throughput droplet sorters toolkit. This is the first application of droplet-digital microfluidics (co-planar electrodes under channels). In Chapter 4, we show several new droplet operations that can be performed with this droplet-digital architecture, such as on-demand droplet generation and mixing or storing of droplets in channels. We show this device's functionality by screening a yeast mutant library based on cell growth in various conditions. Finally, in Chapter 5 we show a method for deterministic single clone encapsulation. In combination with other droplet operations, in this chapter, we show the power of this hybrid droplet-digital technology by sorting out single gene-edited mammalian cells into a stable KO cell line.

Expanding on this motivation, we believe that the development of new microfluidic tools is pushing the field of microfluidics in new directions. We are especially motivated to look at the needs of synthetic biologists and those engineering biology.

1.2   Microfluidic theory

Fluids behave differently on the microscale. When volumes shrink, gravity becomes insignificant (viscous forces dominate over inertial forces), surface tension turns into a powerful force, and simple physics such as evaporation can make droplets move or their laminar flow can prevent fluids from mixing, as mass transfer now becomes purely dependent on diffusion.[10, 11, 12] These fluidic behaviours can become very useful for applications in chemistry and biotechnology, as they mimic the physics experienced at the scale of a cell. Microfluidics is the field in which we try to use these physics to manipulate fluids on the micro or pico-scale. Although microfluidics was established in the 1980s, the field started becoming more widely applied after the 2000s, when its analytical applications for biochemical and biological sciences were uncovered. Although there are many types of microfluidics, for this thesis the two relevant types of microfluidics are digital microfluidics and droplet-in-channel microfluidics.

1.2.1 Digital microfluidics

In digital microfluidics (hereafter referred to as DMF), microliter sized droplets are moved across an array of electrodes by sequentially applying electric potentials to these electrodes (**Figure 1.1**). This basic operation can be used to dispense, split, mix, merge, and design complex patterns. This technology can be used to automate advanced procedures that contain multiple steps of liquid handling and can eliminate manual steps.[13] For example, this can be useful for sample preparation (sequencing, protein purification), quantifying methods (PCR, ELISA), and analytical methods. More detailed examples are given in Chapter 2. Commercial examples of DMF include Oxford Nanopore's sequencing sample preparation cartridge [14], Illumina's sequencing pipelines [15], GenMarkDx's cartridge for amplification and detection of pathogenic DNA [16], and core technologies of other small companies such as Nicoya [17], Miroculus [18] or Nuclera [19]. The basic mechanism behind the droplet movement is the result of an electrostatic field that forms between the actuated electrode and the ground electrode. A high AC voltage is applied to an electrode, after which the dielectric layer between electrode and droplet acts as an insulator and can accommodate a voltage drop (**Figure 1.1**). This droplet movement is often called electrowetting (electrowetting-on-dielectric, EWOD). Various hypotheses have been proposed for the true mechanism underlying the movement of droplets. But generally, there are two types of physical models by which DMF droplet manipulation is described: the contact-angle model [20], and the electromechanical model [21, 22]. The contact-angle model is based on the Young-Lipmann equation (**eq. 1.1**),

$$\cos\theta_V = \cos\theta_0 + \frac{1}{2\gamma_{LV}}CV^2 = \cos\theta_0 + \frac{\epsilon_0 * \epsilon_r}{2d\gamma_{LV}}V^2 \qquad (1.1)$$

with θ_V the contact angle under an applied potential V, θ_0 the static (initial) contact angle , and γ_{LV} the surface tension between liquid and vapor phase. According to the contact-angle model, under an applied potential V, the droplet contact angle with the surface θ_V will decrease, leading to capillary pressure, resulting in a force causing droplet movement to obtain lower surface tension.[20] This surface 'wetting' marked the EWOD terminology.

The electromechanical model describes droplet movement through Coulomb interaction. It is rather the system's unbalanced energy (**eq. 1.3**) within predominantly the dielectric layer, that will cause a driving force on the droplet (**eq. 1.4**). This driving force can be derived from the total energy stored in a classic

capacitor and resistor circuit (**eq. 1.2**), with the electrical capacitance C,

$$C = \frac{\epsilon_0 \epsilon_r A}{d} \tag{1.2}$$

with A and d the area of the theoretical capacitors (area to which potential is applied) and the distance between the two capacitor plates (thickness). The total energy (here just looking at the x-plane) $E(f, x)$ can be defined by the sum of the energy stored in the capacitors in series. If we are looking at a two-plate DMF, with a droplet squeezed between a bottom actuated electrode and a top grounded electrode, filling in for C, that becomes

$$E(f, x) = \sum_i \frac{C_i V_i^2}{2} = \frac{L}{2} \left(x \sum_i \frac{\epsilon_0 \epsilon_{ri,liq} V_{i,liq}^2 (j2\pi f)}{d_i} + (L - x) \sum_i \frac{\epsilon_0 \epsilon_{ri,fill} V_{i,fill}^2 (j2\pi f)}{d_i} \right) \tag{1.3}$$

, with $j2\pi$ the frequency dependent imaginary part of the permittivity, and L the length of the droplet when approximated as a square area. The driving force acting on the droplet can then be represented by a potential energy function,

$$F(f) = \frac{\partial E(f, x)}{\partial x} = \frac{L}{2} \left(\sum_i \frac{\epsilon_0 \epsilon_{ri,liq} V_{i,liq}^2 j2\pi f}{d_i} - \sum_i \frac{\epsilon_0 \epsilon_{ri,fil} V_{i,fil}^2 (j2\pi f)}{d_i} \right) \tag{1.4}$$

. Another important distinction to be made is the difference between co-planar electrodes versus a system where a droplet is squeezed between a top and bottom electrode (**Figure 1.1**). In a two-plate DMF system, droplet movement follows the actuated electrode pattern, since a homogeneous electric field forms with field lines orthogonal to the electrode pair. In a co-planar system, when one electrode is actuated with a potential, the neighbouring electrodes are used as a ground and a curved electrostatic field forms above the gap between the two electrodes. [23, 24] So, in this case, the shape of the electrode gap is an important design consideration. [25]
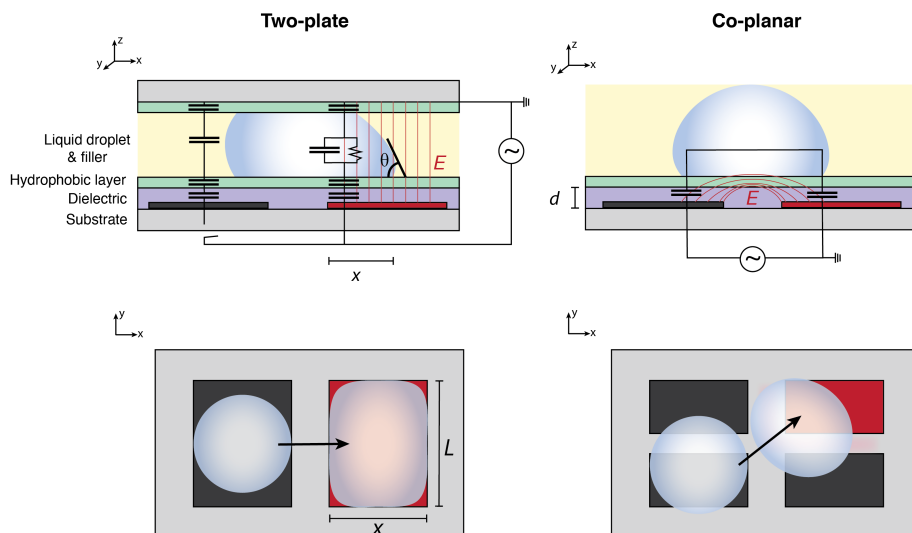
Figure 1.1: Digital microfluidics overview. Side view of a two-plate and one-plate digital microfluidics (DMF) device, showing electric field location upon actuation of one electrode. Top view of a two-plate and one-plate digital microfluidics (DMF) device, showing droplet movement. Arrow indicates droplet movement and red electrode indicates actuation.

To conclude, one of the main advantages of DMF devices is their ability to control droplets individually. DMF can move, mix, merge, or dispense droplets in patterns defined by the user. The small volumes, low cost, ability to integrate with other instrumentation, and biocompatibility make this platform suitable for automating biological assays with droplets containing DNA, cells, proteins or functional enzymes.[26] On the other hand, the throughput of these platforms is low and other microscale manipulations beyond droplet movement (such as cell trapping, cell culture) are still in development. The DMF field is still young, and problems any nascent field struggles with are apparent. For example, fabrication and operation methods are not standardized, making it hard for other researchers to try and apply these devices.

1.2.2 Droplet-in-channel microfluidics

In channel microfluidics, we use pressure or capillary forces to manipulate fluids in channels, often driven by pumps or vacuum systems. Next to using these systems to manipulate fluids in a continuous flow, we can also make droplets in channels. Using micron-sized channels, typically immiscible two-phase flows (aqueous and oil) can be used to generate femtoliter (fL) to nanoliter (nL) sized droplets at rates of up to thousands of droplets per second (kHz), with an oil and water flow rate in the μL/min range.[27] The system's oils, surfactants and materials are biocompatible (have negligible effect on viability of cells),

making it an ideal platform for biological applications.[3] Droplet-in-channel technologies' high-throughput capabilities are frequently used to perform single-cell sequencing library preparation or to automate screening procedures.[28] For single-cell sequencing library preparation, typically a bead with barcodes is co-encapsulated with a single cell. These barcodes are unique and can mark the products of a single cell such as DNA, RNA, antibodies, proteins for identification during the analysis of different sequencing methods.[7] To screen libraries of single-cells, typically high-throughput instrumentation is needed for microtiter plate-based methods, or the use of flow cytometry and fluorescence-activated cell sorting (FACS) is needed. Using droplet-in-channel microfluidics, single-cell containing droplets can be sorted in high-throughput based on intracellular, cell-wall bound, or secreted products [29] using absorbance [30] and fluorescence [31]. More detailed examples for screening and sequencing using droplet-in-channel microfluidics will be given in Chapter 2.

One of the main advantages of droplet-in-channel microfluidics is their high throughput and ability to encapsulate single cells. Droplet-in-channel microfluidics is especially useful for biological applications, thanks to their ability to compartmentalize biological samples such as single-cells, the analytes they produce, and their DNA or RNA into droplets. [32] The fabrication of DMF and channel microfluidic devices is usually a procedure performed in a cleanroom, following a standard photolithography process. While we give a short introduction here, please refer to additional literature [33] and materials and methods for a review of the detailed process. During the photolithography process, positive or negative photoresists and a photomask are used to pattern respectively either electrodes or channel outlines on a substrate.[34] For DMF, these electrodes are patterned on a glass substrate and then coated with a dielectric layer (e.g. Parylene C), and a hydrophobic surface (e.g. Teflon) to minimize forces required to move droplets. For two-plate DMF, a Teflon coated indium tin oxide (ITO) top plate is used.[13] To make a channel device, the substrate on which channels are patterned is usually used as a mould for a soft lithography process, in which a polymer (polydimethylsiloxane, PDMS) is cast on top of the mould.[35] The PDMS can be peeled off, inlets can be created, after which the PDMS is bonded to a substrate (e.g. glass slide), typically using oxygen plasma treatment.[36]

1.3 Microfluidic constraints when working with biological material

Microfluidic devices can provide automation capabilities for numerous biological assays, but translating benchtop assay operations onto a device is not always an easy task. It is important to assure that microfluidic assays don't influence cell viability negatively. To be successful in this, in the first place, these samples must have ideally not experienced any unusual stresses during their time on-chip. The laminar regime fluid physics on the micro-scale provide ideal conditions that mimic physiological conditions of heat and mass transport. This makes hydrodynamic applications in channel microfluidics, such as cell trapping, ideal platforms for work with mammalian cells. While DMF platforms exert additional electrostatic forces to move droplets, the surface charges that build up are not impacting cell viability or gene expression. Beyond simple viability studies, a more elaborate transcriptomic study showed no effect on cellular gene regulation while potentials are applied to electrodes.[37] EWOD does not harm cells within droplets, as there is no significant electrical potential that crosses the droplet. The voltage drops across the dielectric. [13] Dielectrophoretic forces or optoelectronic forces which are often applied to control particles in channel microfluidics, apply high electrical potentials on cells.[31]

Beyond physical forces exerted on the cells, materials and reagents used in microfluidic devices are a second contributing factor to platform biocompatibility. The hydrophobic surface treatment [38], the fluorinated oils and the water-oil interface surfactants used in droplet-in-channel microfluidics [39] allow for cells to maintain their typical in vitro cellular metabolism and life cycle. The carrier oils are typically perfluorinated and can carry up to 20 times more oxygen than water [40], allowing for long-term incubation in droplets. In particular for single-cell assays, maintaining expected viability is important. In some applications, high cellular viability is also required to be able to recover cells after performing an on-chip assay. Single-cells can be recovered off-chip into media for further growth into clonal colonies or droplet libraries might require further analysis. When using droplet-in-channel microfluidics, droplet emulsions need to be broken to recover their contents. The use of a chemical (1H,1H,2H,2H-Perfluoro-1-octanol), static gun, or centrifugation are reported methods. Due to their negative effect on cell viability, alternative methods need to be developed, as we demonstrate in Chapter 5 .

1.4 Single-cell analysis with microfluidics

Beyond scientific discovery, the ability to understand the complexity of a cell population is important to develop new products, medicine and diagnostics and advance clinical research. Rather than population level averages, single-cell analysis tools allow us to look at gene expression profiles and cell responses of single cells. As a result, researchers gain a more comprehensive understanding of cells on a spatial and temporal level. Hardware tools that allow for the physical separation of these cells are an essential part of single-cell analysis. At the forefront of this application development space, are microfluidic technologies.

1.4.1 Current microfluidic methods for studying single-cells

To study single-cells in microfluidics, the cells are often isolated either by physical boundaries: rigid wall structures or fluid interfaces. We can distinguish four major microfluidic systems that allow for single-cell analysis: wells, single-cell trapping systems, droplets, and valve-based systems. Several examples are provided in **Table 1.1** and **Figure 1.2**.

Table 1.1: Microfluidic methods to study single-cells.

	Micro- and nanowells	Single-cell trapping systems	Droplets	Valve based
About	Passive cell trapping in microwells	Cell trapping in single-cell traps, two cell traps, droplet traps	Poisson encapsulation of single-cell in drops	single-cell trapping
Method	Gravity	Hydrodynamic, centrifugal, electrical, optical	Microfluidic droplet generation	Microfluidic valves
Throughput (cells per device)	$10 - 10^3$	$1 - 10^3$	10^3 - $10^5 Hz$	$10 - 10^3$
Literature	[27, 41, 42, 43, 44, 45, 46, 47, 48, 49, 50, 51, 52]	[53, 54, 55, 56, 57, 58, 59, 60, 61, 62, 63, 64, 65, 66, 67, 68, 69, 70, 71]	[72, 28, 7, 73, 74, 75]	[76, 77, 78, 79, 80, 81]
Commercial examples		Silicon Biosystems DEPArray	Sphere-Fluidics CytoMine®, Dolomite Bio Nadia, 10X Genomics Chromium Controller, Mission Bio Tapestri	Fluidigm IFC chip

Micro- and nanowells (passive trapping)

Micro and nano-wells are micro or nanoliter sized versions of traditional multi-well plates. The size of the microfluidic wells are close to cell size and thus have typically low walls. The main goal of these devices is to spatially separate cells or pattern them, to then further study the individual cells while being cultured on the device.[42] This is typically done by passively trapping cells in the wells using gravity. Recent examples include Seq-Well, a microwell that captures single cells and beads for single-cell RNA-sequencing [44, 43] , or single-cell barcode chips that contain wells with sandwich antibody based assay [41, 45]. Using the latter device, Lu et al. [41] was able to detect 42 secreted proteins for an array of single macrophages. While micro and nano-wells are often used in a static-solution environment, well-based devices can also be operated under continuous flow. The use of nano and microwells for tissue engineering and tumour modelling has become by far the most popular application of these well slides, as they allow for the controlled growth of 3D tissue cultures such as spheroids.[46] E.g. Järvinen et al. [47] was able to culture spheroids and cell monolayers on the same microfluidic platform, and Lee et al. [48] were able to study lung cancer multicellular tumour spheroid (MCTS) formation under continuous flow.

The integration of microwell devices with other microfluidic techniques that can produce external forces (optical, dielectrophoretic, acoustic) can provide options for improved capture efficiency and control over culture conditions. For example, Antypas et al. [49] used a nanowell device (nwSlide) to study bacterial libraries single colony growth by monitoring the OD_{600} in each well. Cells were deposited into the nwSlide using FACS (**Figure 1.2**). Analysis of the wells can also be facilitated by built-in sensors. Huang et al. [82] developed a microwell slide with integrated surface-enhanced Raman spectroscopy (SERS) surface for the detection of bacterial metabolites related to antibiotic susceptibility.

There are adaptations to microwells that ease sample retrieval. Microcapillary arrays are microwell slides that do not contain a bottom to each well, and in which liquid remains within the well due to capillary action. The advantage here is the easy recovery of well content, for example by using a precise laser, such as Chen et al. [51] used for the recovery of single clones after performing a fluorometric enzymatic assay, or simply pushing cells through such as Andree et al. [52] did for assessing the viability of circulating tumour cells. The use of optical tweezers to retrieve cells from traps is also a popular technique.

To conclude, micro- and nanowells are popular for their simple operation and fabrication methods. However, passive trapping can be undesirable due to uncontrolled well loading. Secondly, the single-cell

analysis methods are often limited since either cells are not fully separated from neighbouring cells leading to cross-contamination, or further environmental manipulation such as adding reagents, mixing etc is not possible due to the static culture conditions.[83]

Single-cell trapping systems

Moving away from gravitation based seeded well slides, active systems of cell trapping rely on other external forces that aid in confining single-cells to specific trap structures. Here we give a brief overview of some of these methods and recent literature.

Hydrodynamic trapping exploits the laminar flow regime fluidic streamlines to guide particles into physical traps. [58] This is the most popular method of active single-cell trapping, with Tan and Takeuchi [84] publishing a leading example of serpentine channel based trapping (**Figure 1.2**), and Huebner et al. [53] a first successful lateral trapping chamber. Devices are designed in such a way that streamlines guide single-cells into traps. If designed well, when a trap is occupied, further cells would not be trapped. Such devices have been used to e.g. trap microbeads functionalized with exosomes [59], to trap and study Influenza A infected mammalian cells [60] and many other hydrodynamic trapping [85, 61, 62].

Centrifugal forces can be used for cell trapping in combination with traps or wells. Li et al. [86] used centrifugal forces in a two-step process to pair two cells and study intercellular communication in a HeLa cell line. Another well-known example of centrifugal based trapping is the 'mother machine', a device with micron-sized trenches for trapping single bacteria and cell physiology, mechanics or gene expression in a single-cell's offspring. [67, 68, 69] The mother machine device has gained popularity among synthetic biologists to study gene regulatory networks and we expect it will assist in many more interesting discoveries beyond its original application.

Acoustic waves, in particular standing ultrasonic waves, will generate stationary pressure gradients in fluids. If particles or cells are present in the medium with different properties than the fluid, in this case density and compressibility, these pressure gradients can exert forces on the particles. Surface acoustic wave (SAW) can thus be used to trap cells without contact, also referred to as acoustic tweezers. [71] Ohiri et al. [70] combined hydrodynamic trapping with surface acoustic waves to improve trapping efficiencies up to 67%. Collins et al. [66] combined the use of microwells with SAWs at high frequency to create a two-dimensional (2D) acoustic force field to fill up wells with precise inter cellular distancing. While single-cell trapping using SAW is an interesting development, the use of acoustic waves is more popular in bulk channel

microfluidics for separation of particles, or for droplet sorting systems.

Electrical trapping of single-cells typically relies on dielectrophoretic (DEP) forces to trap single-cells. Dielectrophoresis is the movement of a dielectric object due to forces generated by a non-uniform electric field. Similar as with acoustic waves, if particles or cells are present in the medium with different properties than the fluid, in this case a difference in the permittivity, DEP forces can act on the particles. DEP force can be negative or positive, defined by the Clausius-Mosotti factor.[87] While there are several microfluidic single-cell DEP trapping devices out there [64, 65], the application of DEP for single-cell trapping is not very popular due to possible negative effects of the electric fields on cell survival and more importantly the low throughput and complex fabrication of these devices. However, DEP is a popular technique for droplet sorting. [31]

Optoelectrical techniques are interesting single-cell trapping methods due to their high precision programmability and flexibility. Optical trapping techniques rely on optioelectronic tweezers (OET), which generate DEP forces, electroosmotic flows and electrothermal flows that can trap particles. [63] OET have been widely used in conjunction with microfluidics to trap single cells. Commercial examples that use this technology include Berkeley Lights [88] and Lightcast Discovery [89].

Finally, magnetic trapping techniques can be used to trap cells, by using magnetic particles. Huang et al. [50] used magnetic beads coupled to human acute monocytic leukemia cells. The trapping efficiency of these systems is not very high (for Huang et al, 56%), and popularity of these single-cell trapping tools has declined as better alternatives are available.

To conclude, many different types of single-cell trapping mechanisms are available, that apply additional forces to single-cells to aid their confinement. Hydrodynamic trapping techniques are easy to execute with no additional equipment and have a high efficiency of trapping. However, trapping is based on a particular device design and fluid flow conditions, and thus expertise is needed to design these devices. Optical trapping is extremely precise in operation and several successful commercial platforms are available that use this technique. However, such systems have a large footprint and development is costly and requires expertise. While optical systems get their high-throughput from their parallelization, single-cell operations are slow. Centrifugal devices simplify the experimental protocol and fluidic setup by eliminating the need to carefully trap cells using precise hydrodynamic or other techniques.

Valve-based systems

Valve-based systems are channel-based devices that contain pressure controlled valves. Microfluidic valves typically are made by designing a multi-layer PDMS based device, of which one layer contains a channel architecture for the assay, and a second layer contains channels that are pneumatically controlled. In between the two layers is a thin soft elastomeric membrane which can be deflected and constrict a channel in the channel layer under pneumatic pressure. Guo et al. [77] developed a simple two layer device for trapping of single-cells and tracking viral infections during incubation by using an external fluorescence reader (**Figure 1.2**). A more complex process was shown by Wang et al. [76], who used a valve-based device to trap single sperm cells. Their device included controlled valves to flush single cell containing chambers with lysis buffer and other reagents for whole genome amplification.

Valve-based devices can offer high throughput single-cell assays of that can perform multiple operations in space and time. It's an ideal platform to perform complex fluidic operations on single cells and can also be integrated with hydrodynamic or well based devices. Additionally, it confines cells in a closed environment, making it possible to study cell secreted products.[78, 79] While these integrated fluidic circuits can be fully automated, both the device as the external fluidics and automation are complex to design as they at minimum consist of as many pumps as there are control channels. Other issues such as channel layer design constraints, biofouling, device assembly and alignment, and the large volumes they use, make them difficult to adopt as technologies.

Droplet encapsulation

In droplet-in-channel microfluidics, droplets are usually generated by flow-focusing and T-junction channel geometries. During this process, cells and living organisms can be encapsulated in droplets by diluting the cells in the aqueous fluid. The advantage of this methodology is the simplicity of single-cell isolation, and the full isolation of single-cells in a controlled environment that can maintain cell secreted products, beads, assay reagents or lysed cells.Zilionis et al. [7] showed the use of a droplet generator, to perform sample preparation for single-cell RNA sequencing. In their method, called inDrops, single cells are encapsulated in droplets, together with hydrogel beads that contain barcodes (**Figure 1.2**). The cells are lysed within the droplets, and a reverse transcription reaction occurs that labels all of the cells mRNA with the barcodes. Only after this reaction, the emulsion is broken, the RNA is purified, and sent for sequencing.

Many others have developed single-cell sequencing techniques based on droplet microfluidics, of which a short review can be found in Chapter 2. Typically, this is performed in water-in-oil emulsions. The fluorinated oil and surfactants that surround the aqueous droplet prevent droplet cross-contamination and have been well characterized for use during long incubation and thermal cycling applications.[75] Besides water-in-oil emulsions, it is also possible to make water-in-water emulsions, termed aqueous two-phase systems (ATPS), which have shown better biocompatibility.[74] To conclude, this method of single-cell isolation is by far the most popular method, because of its simplicity and extremely high throughput. The user is simply required to follow guidelines to dilute cells to a concentration that allows for single-cell encapsulation following the Poisson distribution (**eq. 1.5**) . The device is a simple flow-focusing droplet generator that does not require a complex fluidic setup. As a result of its impact on single-cell sequencing, this is one of the most adopted microfluidic platforms (see Chapter 2). However, there are two major disadvantages to this technology. First, single-cell containment is unreliable.[72] For example in a single-cell sequencing context, if a droplet would contain multiple cells, their sequence information would all obtain the same barcode, resulting into complications during sequence analysis. If a majority of the droplets don not contain a cell, this can also lead to a waste of reagents and barcoded beads. [73] Second, there is no control over any specific droplet.
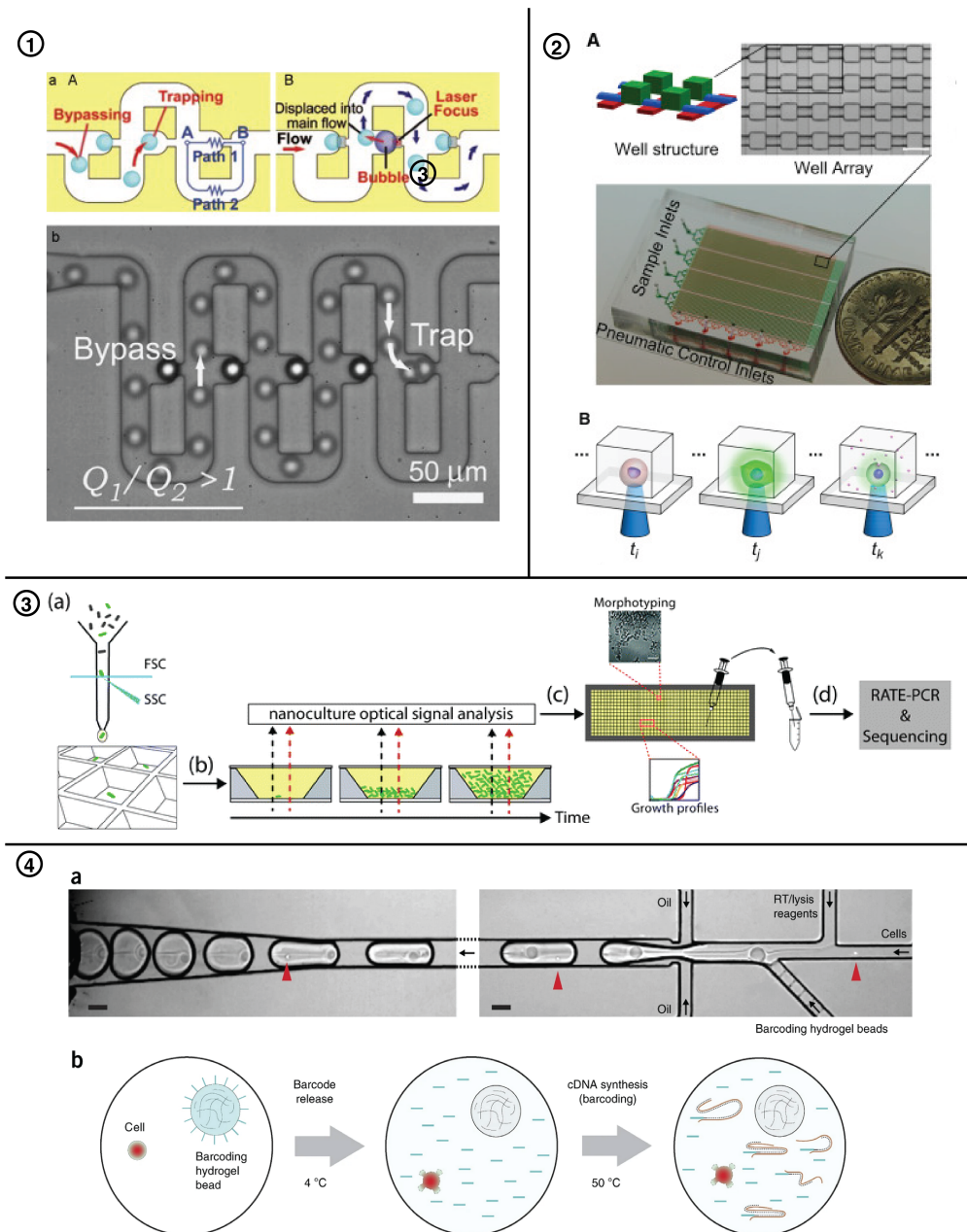
Figure 1.2: Overview of microfluidic single-cell trapping methods. (1) Hydrodynamic single cell trapping. When the trap is empty, flow resistance along the straight channel is lower than that of the loop channel, and the main stream flows along the straight channel, trapping a cell. If the trap is filled, cells bypass the occupied trap (bypassing mode). Reproduced with permission from Tan et al., PNAS 104 (4), 1146-1151 (2007), Copyright 2007 by The National Academy of Sciences of the USA (2) Valve-based trapping. Channels were loaded with cells infected with viruses. Valves were closed to confine single-cell s, after which fluorescence was monitored to observe lysis events. Reproduced with permission from Guo et al., 18(13), 1914 - 1920 (2018), Copyright 2018 Royal Society of Chemistry (3) Nano-wells. Nano-wells were loaded with bacterial libraries using FACS. Subsequently, single-cell growth rates were monitored by tracking growth. Reproduced with permission from Antypas et al., 18(12), (2018), Copyright 2018 by Royal Society of Chemistry (4) Single-cell droplet encapsulation. Single-cell RNA sequencing library preparation involves the co-encapsulation of single-cells and barcoded beads. Reproduced with permission from Zilionis et al., 12 (1), 44–73 (2017), Copyright 2016 by Nature Publishing Group

1.4.2 Single-cell confinement efficiency

Previous systems can be further divided into two groups, depending on whether they can obtain single-cell isolation in a deterministic way i.e. the single-cell isolation efficiency is not dependent on cell concentration (**Table 1.2**). One main aim of this thesis is to explore the development of an easy method to encapsulate single-cells in droplets deterministically.

Table 1.2: Overview of microfluidic single-cell encapsulation methods

		Methods	Disadvantages	Reference
Deterministic Methods	Sorting Post-Encapsulation	FACS (TAW and di-electrophoretic), SAW / DAW, imaging, shear migration, pinched flow fractionation, pneumatic, magnetic, thermal (laser)	Requires additional apparatus or optimized flow rates	[74, 90, 91]
	Passive or Active Encapsulation	Inertial ordering, pico-injection, optical trapping, close packing	Low throughput	[92, 93, 94]
Non-Deterministic Methods	Passive Encapsulation	Random Poisson	Random droplet generation and cell encapsulation	[72]
	Active Encapsulation	SAW, piezoelectric, pulse-inertia, centrifugal, hydrodynamic bridges	Limited throughput and additional actuators needed, no control over cell encapsulation	[95, 96, 97]

Stochastic single-cell isolation

Stochastic isolation of single cells happens in microfluidic systems that do not manipulate or control the flow directionality of single-cells with external forces. In laminar flow without additional external forces, particles (cells) will follow streamlines and do not deviate from them. The distribution of cells in this liquid is not ordered. So, when the trapping of cells occurs, some traps or droplets might have cells while others don not. This can be described by a Poisson distribution (**eq. 1.5**), where k is the number of cells in one trapping entity, λ is the average number of cells in a trapping entity and $P(k, \lambda)$ describes the probability [72].

$$P(k, \lambda) = \frac{\lambda^k e^{-\lambda}}{k!} \tag{1.5}$$

The Poisson distribution is notoriously known in the microfluidics community as a problem that is difficult to overcome. In passive micro-and nanowell devices, this distribution applies to cells filling up wells, leading

to uncontrolled object sedimentation. A Poisson distribution is also applied during flow-focusing droplet generation, in which an aqueous liquid flow is saturated with a low concentration of randomly distributed suspended cells. For single-cell encapsulation, in the first place, we wish $k = 1$. For a $\lambda = 0,05$ and $k = 1$, we get $P(k, \lambda) = 98\%$, however most droplets will be empty. With $\lambda = 0.35$ and $k = 1$, we would reach a more favourable condition with around 25% of droplets containing a single cell, yet around 4.3% of droplets contains doublets.

Deterministic single-cell isolation

In deterministic systems, either the cells or the isolating entities are manipulated to ensure single-cell occupancy (**Figure 1.3**). This can be done by using some of the active single-cell trapping methods mentioned earlier. Antfolk et al. [98] used a combination of SAW and DEP forces to trap single-cells from one set of a mixed library of cells. SAW were used to separate the circulating tumor cells (CTC) from blood cells. The CTC's were then guided to a DEP trapping array, which trapped the single CTC's . Their device showed reliability and precision, as it could trap 80% of all of the suspended CTC's in a blood sample (**Figure 1.3**). Some other recent examples of deterministic single-cell trapping include a deterministic single-cell trapping array by Chai et al 2021 (**Figure 1.3**), a cell-cell trapping microwell device by Zhou et al. [99] and an impressive combination of DEP and microwells by Bai et al. [100] for scRNA-seq.

While these methods offer extremely precise single-cell operations, they are slow and less accessible compared to simple droplet encapsulation methods. Developing deterministic single-cell droplet encapsulation methods is an important priority to advance the single-cell analysis field (**Table 1.2**). Several methods exist to sort out droplets that contain single-cells, after Poisson based encapsulation. E.g. Navi et al (2018) used ferrofluids to sort out single-cell containing droplets from aqueous two-phase systems (**Figure 1.3**). While this does generate a true single-cell droplet library, it requires an additional sorting step. True single-cell deterministic encapsulation is possible, and relies on complex methods such as pico-injection, or methods for evenly distributing single-cells before encapsulation. Sauzade and Brouzes [92] recently published a microfluidic device for deterministic single-cell trapping and encapsulation, that relies just on hydrodynamic forces (**Figure 1.3**). By first trapping single-cells and subsequently changing the cell media phase to an oil phase (a process called phase change), Sauzade et al. demonstrated the deterministic encapsulation of cells (**Figure 1.3**). The devices developed relied heavily on carefully designed traps, for which

optimization of hydrodynamic resistance (**eq. 1.6**) and streamlines was required to successfully achieve efficient cell trapping and phase change events to occur. The hydrodynamic resistance R_h is defined by channel geometries (width w, height h, and length L) and the dynamic viscosity μ of the fluid.

$$R_h = \frac{12\mu L}{wh^3(1 - 0.63\dfrac{h}{w})} \tag{1.6}$$

With a fixed hydrodynamic resistance R_h, there is a linear relationship between flowrate Q and pressure drop ΔP within rectangular channels.

$$Q = \frac{\Delta P}{R_h} \tag{1.7}$$

Sauzade et al.'s channel device consists of a serpentine channel with traps in between (**Figure 1.3**). For cell-trapping, the bypass channel (the corner of the serpentine) technically should have a resistance that is higher than the trap channel resistance, for cells to have a preferred path through the trapping channel ($R_{trap} > R_{bypass}$). Yet for the phase change, Sauzade et al. intended for oil to shear off the trapping area, going through the bypass and passing by the back of the trap, thus forming a droplet. This requires a higher resistance in the trap than in the bypass. By designing guides that push cells toward the traps, Sauzade et al. could amend the $R_{trap} > R_{bypass}$ design rule. Still, there is a lack of control over the droplets that are being generated, and one could not release or make only specific single-cell droplets.
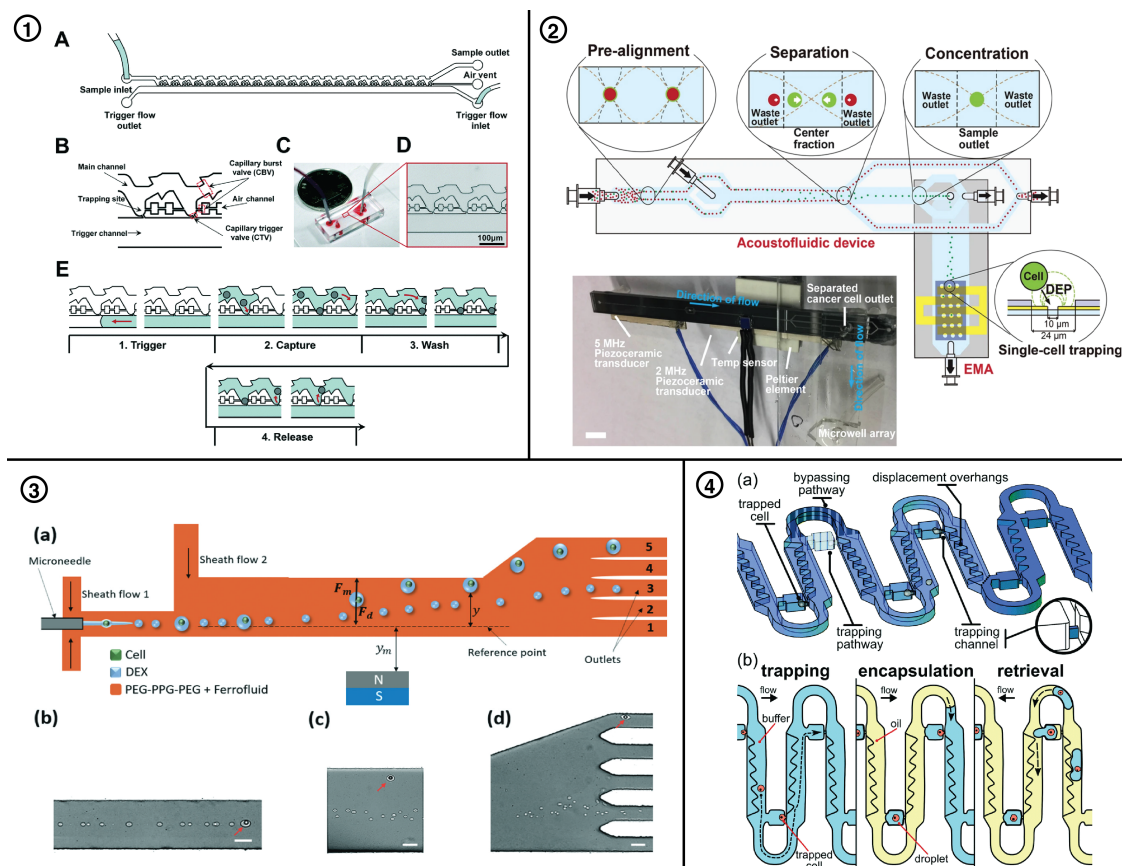
Figure 1.3: Overview of deterministic single-cell encapsulation methods. (1) Deterministic single-cell trapping microfluidic device. The device consists of two types of capillary valves, three channels, and trapping sites. Single-cell trapping and release is performed in four steps. Reproduced with permission from Chai et al., 21(13), 2486-2494 (2021), Copyright 2018 by Royal Society of Chemistry. (2) Ordering of cells before single-cell confinement. Integrated device containing an acoustophoresis chip for ordering cells, followed by a dielectrophoretic trapping array. Reproduced from Antfolk et al.,7(1), 46507 (2017), Creative Commons CC BY. (3) Post-encapsulation sorting. Navi et al (2018) performed diamagnetic separation of cell-containing droplets from empty droplets. A series of images shows the droplet generation region and the size distinction between a particle-encapsulating droplet (indicated by a red arrow) and empty droplets, and the region of high magnetic field gradient where droplets deflect based on their size, towards different outlets. Reproduced with permission from Navi et al., 18(22), 3361 (2018), Copyright 2018 by Royal Society of Chemistry. (4) Deterministic encapsulation. Microfluidic circuit for true single-cell encapsulation. Incoming cells are displaced towards the unoccupied trapping pathway by focusing structures (displacement overhangs). Trapped cells plug the trapping channels, diverting the flow and additional cells through the bypass pathway. The oil phase sequentially flows around occupied traps, generating monodisperse droplets containing single cells. Reproduced with permission from Sauzade et al., 17(13), 2186 (2017), Copyright 2018 by Royal Society of Chemistry

1.5 Droplet-digital methods to improve control over droplets in channels

As discussed previously droplet-in-channel and DMF systems each have their advantages and disadvantages. For this thesis, we consider the benefits of encapsulating single-cells in droplets and the high-throughput of droplet-in-channel devices essential elements for devices that aim to advance the single-cell

analysis field. However, being able to more easily isolate or study single droplets of interest would be beneficial. Combining droplet-in-channel microfluidics with other common microfluidic methods could possibly improve control over droplets. In the last decade, several groups have explored the avenue of positioning co-planar electrodes (DMF method as described earlier, section 1.2.1) under droplet-in-channel microfluidic architectures, with significant advances coming from the Mugele and Wheeler groups (**Figure 1.4**). This can add an additional external force, an electrostatic force, to the equation to control individual droplets.

The ability to generate droplets on-demand using EWOD has previously been explored, with examples of a flow-focusing on-demand droplet generator by Gu et al. [101] (**Figure 1.4**), Chen et al. [102] and Malloggi et al. [103]. Shojaeian et al. [104] used EWOD to eject droplets on-demand from an oil/water fluidic interface. Other EWOD droplet operations in channels have also been explored, such as splitting [105] and coalescing [106, 105, 107] droplets in channels, sorting droplets [108, 24], or guiding and docking droplets using electrostatic forces (**Figure 1.4**). Developments of de Ruiter et al. [109] and Pit et al. [24] were significant to establish a common ground on the physics of droplet movement across co-planar electrodes. The electric field that forms along the gap between them, as Pit and de Ruiter termed 'electrostatic potential wells', can be used to guide droplets along. By playing with hydrodynamic and electrostatic forces, Pit designed a co-planar droplet sorter that could sort droplet binary under lower voltages compared to DEP (**Figure 1.4**)

While these early developments of droplet-digital technology were more fundamental, 'digital-to-channel' and 'channel-to-digital' interfaces demonstrated some of the first relevant biological applications. Particularly Shih et al. [110] and Shih et al. [107] sparked our interest to use these devices to automate end-to-end workflows. Shih et al. [107] made optimal use of a droplet-digital platform by performing single-cell encapsulation using a flow-focusing droplet generator and transferring single yeast cell-containing droplet to DMF which was used for droplet merging, incubation and further analysis (**Figure 1.3**). In their second work, channels were integrated on top of the DMF and droplet merging was shown within channels (**Figure 1.4**).[107] This work was heavily influenced by Abdelgawad et al. [111] and Watson et al. [112]. Abdelgawad et al. [111] showed the first 'hybrid microfluidic' device consisting of a traditional DMF interface for sample preparation, connected with a PDMS based channel interface into which the droplets were driven. Watson et al. [112] first presented a 'digital-to-channel' interface, where electrodes were also located under the channel layer. The main advantage of this system was the simplicity of fabrication, combining two well-established fabrication protocols of DMF and droplet-in-channel microfluidics. Secondly, framing

these hybrid technologies within the context of a typical DMF application, helped researchers transition into implementing the use of electrodes under channels.

In this thesis, we aim to expand the repertoire of these devices by developing additional droplet operations and by showing relevant applications of droplet-digital microfluidics in synthetic biology.
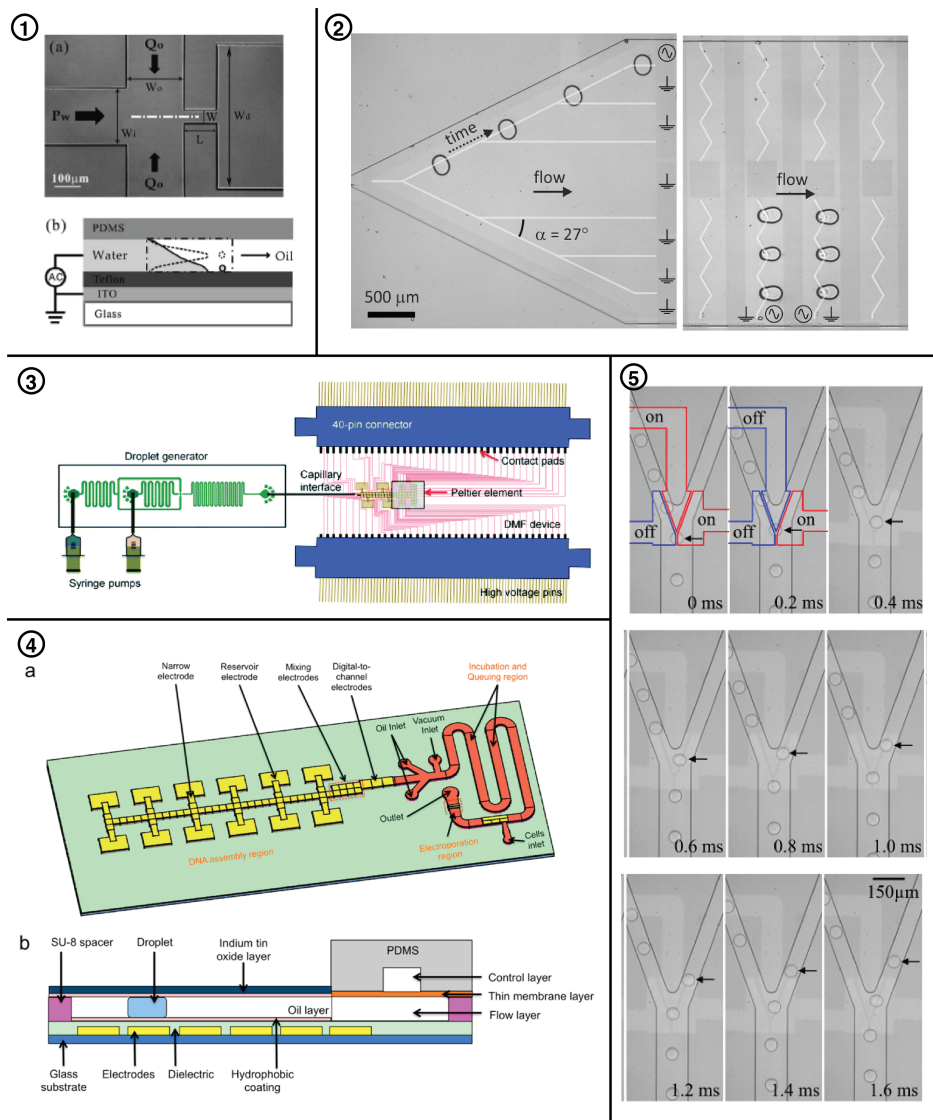
Figure 1.4: Overview of droplet-digital devices. (1) Flow-focusing droplet generator integrated with electrowetting. Dashed square indicates the junction area. Without voltage, the oil-water interface is in the middle of channel dotted curves. With voltage, the oil-water interface is close down to the bottom, releasing a droplet. Reproduced with permission from Gu et al., 93(18), 183507 (2008), Copyright 2008 American Institute of Physics. (2) Guiding, and sorting of drops along the gap between two electrodes, and on-demand trapping and release in a microchannel using EWOD. Reproduced with permission from Ruiter et al., 14(5), 883-891 (2014), Copyright 2014 Royal Society of Chemistry (3) Single-cell droplet digital device. Droplets from the droplet generator are driven to the DMF device (via capillary) and are actuated by high voltage (HV) signals. A Peltier element (to control temperature) is situated below the four cell culture regions on the DMF device. Reproduced with permission from Shih et al., 15, 225 (2015), Copyright 2015 Royal Society of Chemistry. (4) Droplet digital Microfluidic device for automating synthetic biology. (a) Schematic of the device, which comprises a bottom plate with patterned electrodes (shown in yellow) and a channel (shown in orange) to incubate droplets created by DMF and to electroporate cells with the assembled plasmid. Top-plate for DMF and top PDMS layer for the channel are not shown for clarity. (b) Side view of the device showing the digital-to-droplet interface (not to scale) . Reproduced with permission from Shih et al.,4(10), 1151–1164 (2015), Copyright 2015 American Chemical Society (5) EWOD based droplet sorter. Three co-planar electrodes are located under a binary sorter. Sorting of single droplets can be performed using EWOD. Reproduced with permission from Pit et al., 9, 044116 (2015), Copyright 2015 American Institute of Physics

21

Chapter 2

The role of droplet microfluidics in synthetic biology

This chapter was based on: Little, S. R., Perry, J. M., Samlali, K., & Shih, S. C. C. (2020). CHAPTER 8: Droplet Microfluidics: Applications in Synthetic Biology. In Droplet Microfluidics (pp. 193–222). [113] Some section of the original text have been reorganized for conciseness.

Abstract

Synthetic biology is rapidly growing to meet the demand for inexpensive and sustainable resources. So far, the field has developed microbial strains producing biofuels, materials, drugs, as well as new tools for clinical diagnostics and gene therapy. Although rich in potential, synthetic biology still requires development - particularly in the area of automation. The price and footprint of commercially available automation equipment is restrictive to research and these tools are often not tailored to complete the entire workflow of a given project. In response to this, droplet-microfluidic platforms are being developed to expedite synthetic biology. In particular, droplet microfluidic devices have been developed to assemble and transform DNA, perform high-throughput screening assays and perform directed evolution. By consolidating these capabilities and pairing them with design automation and analysis tools, droplet microfluidics will launch a new generation of synthetic biology.

2.1 Introduction

2.1.1 Synthetic biology

Synthetic biology describes the process of engineering a cell for new or improved functionality. The roots of synthetic biology can be traced back to 1953, when Franklin [114], Watson and Crick [115] first discovered the molecular structure of DNA. This discovery cemented the concept of discrete heritability among biologists and sparked a revolution in genetics. In 1973, Cohen et al. [116] produced antibiotic resistant *Escherichia coli* regarded as the world's first genetically engineered organism. Since then, there has been an exponential rise in the use of synthetic biology tools to enable scientists to create biological entities not yet present natural world.

Considered foundational to synthetic biology, genomic research maps structural and functional DNA across the domains of life. Several landmark genomic projects have brought-forth essential synthetic biology tools, such as high-throughput DNA sequencing and cloning techniques. By 1996, the six-thousand genes of the *Saccharomyces cerevisiae* genome were elucidated and with that came DNA hybridization arrays and new techniques in proteomics as well as the first genome databases [117, 118]. By 2001, the first draft of the human genome was presented6. The scale of this project nurtured a revolution in 'next-generation' sequencing [119, 120]. This movement has witnessed the price of DNA sequencing drop from $100 million per human genome to $1000 [121] – removing a massive barrier to entry into the field. Fast-forward 20 years later, these technological advances have led to the discovery of CRISPR-Cas9 [122], regarded widely as one of the most important contribution to the field of synthetic biology and has ushered in a new era of rapid gene editing.

The impact of synthetic biology can be felt throughout many industries including medicine, biofuels, resource and food development as well as manufacturing. In particular, metabolic engineering has produced microbes capable of generating valuable therapeutics such as the antimalarial drug artemisinin [123], opioids [124], cannabinoids [125], and biofuels such as propane-2-diol [126, 127] and farnesene [128, 129]. Major contributions to clinical diagnostics come from Bayer's branched DNA assays capable of detecting HIV and hepatitis DNA in patient samples [130] as well as a paper-based Ebola virus detection system by Pardee et al.[131]. The field of gene therapy is currently in full flight. Patients can now be treated with CRISPR-Cas9-altered lymphocytes with cell-surface receptors targeting a list of common cancers [132, 133, 134].

2.1.2 Design-build-test-learn
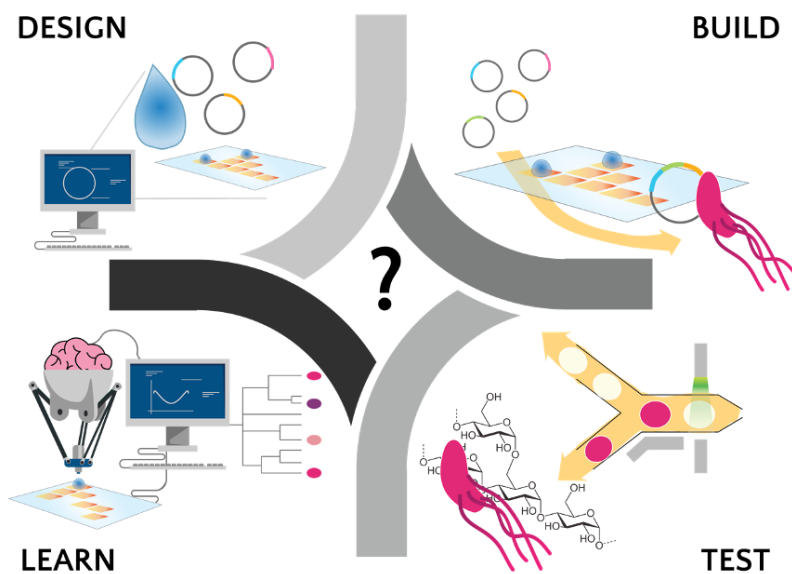
Figure 2.1: Overview of a microfluidic assisted design-build-test-learn (DBTL) cycle. Design software are available to design microfluidic devices and experiments on digital microfluidics, as well as biological CAD tools for construct and experimental design. Building genetic constructs or modified cells can be automated using digital or droplet-in-channel microfluidics for plasmid assembly, cell free protein synthesis, and transformation (electroporation, heat shock, lipid transfection). Typically, this step is followed by a testing step, in which the biological system is tested. Microfluidics can perform high-throughput screening of millions of droplets containing engineered cells and can be easily integrated with analytical platforms and sequencing methods with single-cell resolution. This feeds directly into Learning, where we use microfluidic technology in conjunction with computational learning tools to close the loop. Microfluidics has shown to be a reliable tool for the automation of synthetic biology, yet systems that integrate several or all of the DBTL cycle still need to be developed. Reproduced from Ref. [113] with permission from Royal Society of Chemistry.

Despite this flood of new biological systems and technologies, the process of developing these new biological systems is extremely labour-intensive, expensive and less-than deterministic. Engineering relies on a process of characterizing components so that their performance can be modelled in a wide variety of system contexts. The vast number of biochemical interactions within cells obscures accurate predictions about how biological components will work outside their native hosts. In many cases, high-throughput experimentation must be carried-out to provide a high-resolution picture of how a system's parameters interact while also delivering in the shortest possible timeframe. To categorize different stages of work, synthetic biology has adopted the *design-build-test-learn* cycle of engineering. It is through many rounds of this cycle that researchers can engineer a biological system.

Design in synthetic biology refers to designing a system or experiment. This can take the form of designing transcriptional units using DNA design software [135], gene network design software [135] as well as workflow design tools which optimize across physical and experimental design [136]. Build generally refers to writing DNA, assembling DNA and bringing it into a host organism. DNA can be synthesized

24

de novo using phosphoramidite chemistry or more recently through 'click' chemistry of nucleic acid ana-logues [137]. Constructing large DNA fragments is achieved through DNA assembly. Frequently paired with polymerase chain reaction (PCR) amplification of DNA fragments, DNA assembly techniques such as Golden Gate [138, 139], Gibson [140] and yeast homology recombination [141] are heavily relied-upon in synthetic biology. Addressing standardization and throughput in DNA assembly, synthetic biology 'toolkits' have been developed for numerous applications and chassis organisms [142, 143, 144, 145, 146]. Many of these tool kits provide modular hierarchical cloning systems along with libraries of characterized regulatory element, signal protein and protein purification tags. Test refers to the assays and analytical techniques used to determine genotypic and phenotypic relationships. Learn refers to all work leading to subsequent re-design. Evolving data analysis tools and sequence databases provide the foundation to move forward with new designs.

2.1.3 Automation and the age of the biofoundry

Some of the biggest challenges of synthetic biology are standardization and reproducibility. Even today, where industrial manufacturing is largely automated, much of the work in synthetic biology research is done by hand through frequent pipetting and transferring samples from one platform to another. As a result, technique is learned by trial-and-error, while documented protocols are subject to interpretation. This leads to concerns of data reliability and discourages linking results across different experiments. Addressing this, many institutions have established 'biofoundries', facilities modelled after the industrial spaces such as Gingko Bioworks' Bioworks factory. [147]

The goal of a biofoundry is to expedite synthetic biology research by combining computation with au-tomation. The Global Biofoundry Alliance [148] is an international infrastructure with currently 25 (and growing) non-commercial member facilities. Together, this network promotes best-practices and standard-ization for automation, as well as engages in sustainable project development, while finding ways to expand the role of the biofoundry in the research community. Alongside automation tools, many biofoundries also provide open-source software for design work and analysis such as the Edinburgh Genome Foundry's Cuba software suite [149] and the tools provided by the Agile Biofoundry [150]. These powerful facilities aim to 'close-the-loop' on the DBTL cycle, transcending the limitations of human intervention while providing an educational hub for local synthetic biology communities.

A hurdle when establishing and maintaining a biofoundry is the cost and footprint of the automation

machinery. Their use of consumable plastics also dramatically increases the cost of operation. Yet tools which support the Society for Biomolecular Sciences (SBS) format plastics continue to dominate the market for automation and analysis machines. This is partially because SBS standard microtiter plate formats such as 96 well and 384 well are usable by both humans and machines. This provides an easy transition between manual and automated work but is unnecessary if the goal is to automate the entire DBTL cycle. Despite the vision of expediting the DBTL cycle, biofoundries rely on expensive machines which only automate part of the task – leaving bottlenecks in the total workflow. For example, DNA assembly can be done rapidly using the Labcyte® Echo, as demonstrated by Kanigowska et al. [151]. Yet, bacterial transformation in this study was done manually, since it required delicate temperature control which is not supported by the Echo. Additionally, commercial cell-sorting equipment may not be suitable to handle certain sensitive cell types as they are developed by researchers. A necessary step in the evolution and proliferation of biofoundaries is to integrate affordable and custom automation equipment that completes workflows and does not require human intervention.

2.1.4   Droplet microfluidics

Droplet microfluidics has emerged to provide solutions to "close-the-loop" in synthetic biology (see **Figure 2.1**), lending platforms for automating multiple aspects of the cycle. These platforms are ideal for processing liquid samples in synthetic biology considering how expensive reagents can be. The low footprint of these platforms makes them especially suitable for researcher seeking to maximize the efficiency of their space. Droplet microfluidics falls into two major categories: digital microfluidics and droplet-in-channel. Digital microfluidics allows users control over operations such as mixing and merging of individual sample droplets – a useful tool for precise sample preparation and processing. A clear advantage of droplet-in-channel over conventional automation equipment is throughput, especially in testing. In this review, we describe droplet-in-channel and digital microfluidic platforms and how both platforms contribute to the automation landscape of synthetic biology, as well as discuss how this field can be further developed to 'close-the-loop' on synthetic biology's DBTL process.

2.2 Building

At the heart of synthetic biology is the ability to create, assemble and insert the novel genetic materials into cells. By the end of the *build* stage, synthetic biologists aim to have new genetic constructs inside target organisms. To achieve this, the common workflow is to create genetic sequences by DNA synthesis, amplify those sequences to sufficient concentrations, assemble them into larger more complete constructs, and deliver them into cells. Substantial efforts from different labs have been made to use droplet microfluidics to perform these tasks.

2.2.1 Mammalian gene editing pipelines

A prevalent application of synthetic biology that requires most – if not all – of the steps in the build pipeline, is genetic editing. Since the advent of CRISPR systems (see review papers: [152, 153, 154]), mammalian gene editing pipelines have consisted of designing, synthesizing, and assembling new constructs, delivery of these constructs by transfection, selection and sorting into monoclonal populations, and population expansion. Several droplet microfluidic platforms have been shown in literature to integrate the parts of the process of gene-editing. For example, Sinha et al. [155] demonstrated that the generation and validation of CRISPR knock-outs in mammalian cells can be automated on a digital microfluidic platform. In this work, the authors synthesized and purified plasmids encoding for gRNAs using traditional methods, however they performed the transfection, culture and knockout of lung cancer's RAF1 gene on an automated CRISPR editing platform (see **Figure 2.2 E**). Additionally, furthering previously highlighted work, Li et al. [156] targeted and knocked out the TP53BP1 gene in K562 cells in their continuous flow droplet microfluidic platform. While the transfection and validation of CRISPR plasmids have been performed on-chip, much work needs to be done to integrate the other steps of the pipeline. A logical next step would be to perform the assembly of CRISPR plasmids along with their transfection and validation.

Worth mentioning here is the exciting cell squeeze technology that has been used for genetic editing hard to transfect cells [157, 158]. An interesting avenue of research would be to combine cell squeeze technology with droplet microfluidic automation techniques for end-to-end gene editing of traditionally challenging cells such as primary cell lines.

2.2.2 Microfluidic automation of the build process

While much work needs to be done to integrate devices and capabilities together, a single platform capable of complete end-to-end automation of the Build process (i.e. synthesis, assembly, delivery) using droplet microfluidics is highly achievable (see **Figure 2.2**). The ability to synthesize oligos, amplify material, assemble plasmids, transfect cells, and grow out mutants on a single automated platform will democratize genetic engineering and make prohibitively difficult procedures available to labs, clinics, schools and scientist around the world. Efforts to achieve numerous steps together on a single device have been discussed [159, 107] and furthering this goal should be a main focus for the field moving forward. Beyond the capability to automate conventional building procedures, droplet microfluidic devices have been placed in the spotlight by their important role as one of the only methods to generate and study artificial and edited cells. One of the main reasons for this is the advantage of high throughput that comes with droplets in-channel microfluidics. Although applications are currently sparse in the literature, we envision new single and bench-top sized platforms that can engineer complex strains enabling metabolic engineers to design many different modifications to a cell line with a reduced timeframe and have a successful mutant ready for testing.
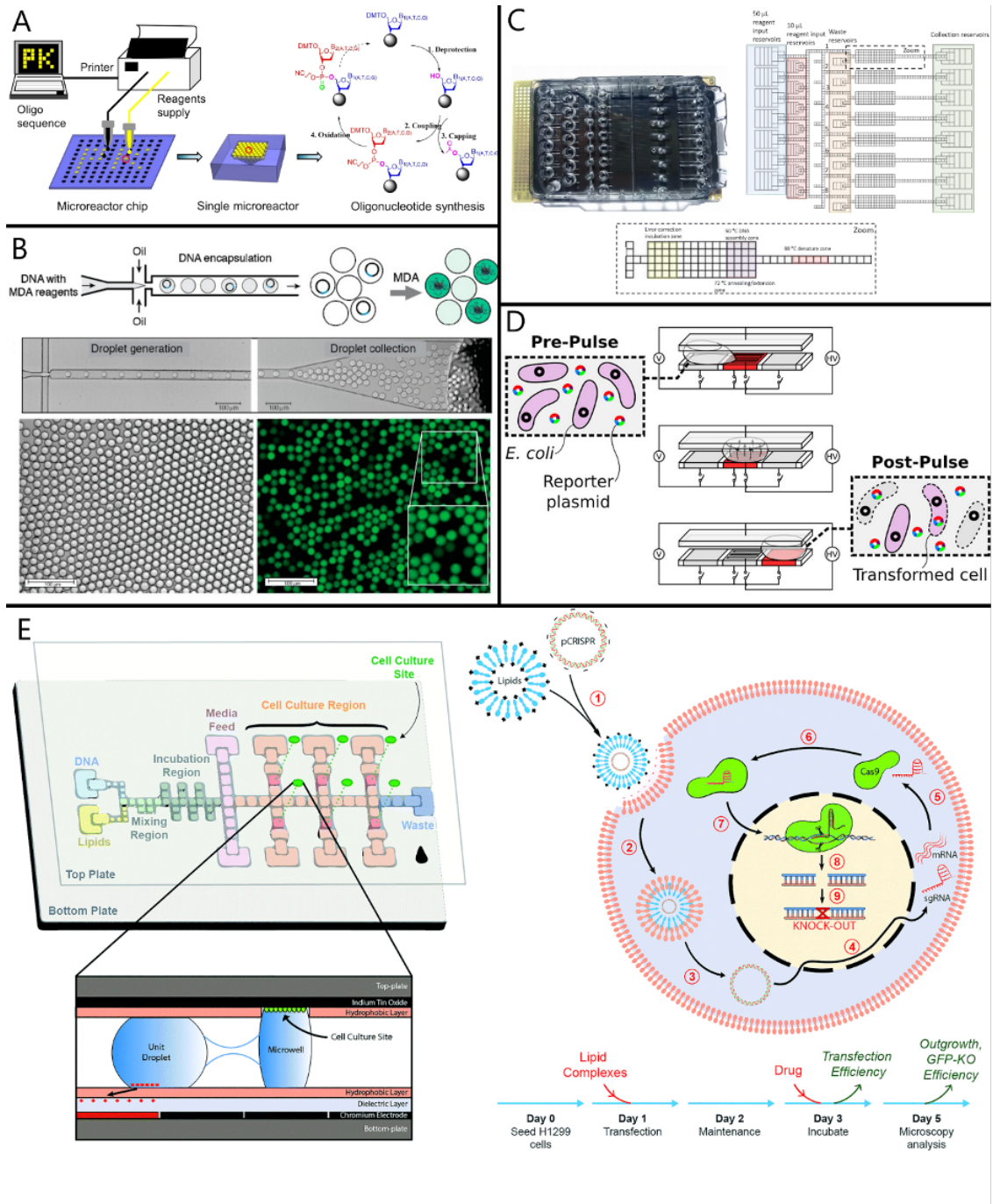
Figure 2.2: Build. a) An oligonucleotide synthesizer based on a microreactor chip and an inkjet printer. b) DNA encapsulation and amplification using an MDA reaction in droplet microfluidics. c) DNA assembly with error correction on a digital microfluidic platform. d) A digital microfluidic device for microbial electroporation. e) An automated genetic editing platform using digital microfluidics. Reproduced from Ref. [113] with permission from Royal Society of Chemistry.

2.3   Testing in droplets

Despite recent advancements in laboratory automation systems, a remaining bottleneck in the DBTL pipeline is the ability to test and analyse whether synthetic designs work as hypothesized. Within this high-throughput robotic framework, analysing phenotypic results of genotypic alterations - the testing step - is still challenging. Detecting compounds of interest from the sea of products found in the cell, requires isolation followed by analytical procedures. The integration of these screening and chemical analysis methods in an automation framework has been limited by their ability to only process samples in series and with limited integration.

Droplet microfluidic devices are suitable candidates as a useful tool for high-throughput testing techniques. Not only do reduced reaction volumes and the hardware setup reduce costs, devices can also integrate in the traditional synthetic biology workflow with other automated systems such as well plate readers and analytical devices. Additionally, these platforms allow for novel testing methods that are unique to microfluidic devices, such as single-cell or single-molecule testing [160].

2.3.1   High-throughput single-cell screening and applications of single-cell encapsulation

The most common method of performing *testing* in droplet microfluidic devices is to encapsulate a single cell in a droplet, generating a library of droplets containing individually engineered cells. During droplet encapsulation, it typically follows a Poisson distribution [72] generating a variety of droplets with different quantities of cells (0, 1 or 2 or more). Typically they are encapsulated at $\sim 100 Hz$, but more recently it has been shown to be capable of encapsulating at kHz speed, allowing for extreme high-throughput cell encapsulation [161].

After generating a library of droplets, the screening process typically relies on analytical based techniques (e.g., fluorescence) to sort the contents of the engineered cells. Sorting droplets after detection of desired compounds is performed by either dielectrophoresis (DEP), acoustic waves, electrodes or thermal energy, most of which allow for binary sorting.[90] In relation to synthetic biology, each droplet is an individual microcompartment containing a single cell that secretes product or is lysed to release a product that can either fluoresce by itself, or can be quantified upon fluorescence.[31] These techniques typically rely on the placement of optical fibers located orthogonal to the channel walls, or using a laser-induced based fluorescence readout system. This creates the possibility to multiplex the droplet experiments with several dyes

that can readout multiple secretions or metabolic activities. A drawback of the high frequency of screening in these devices, is the limited time of exposure of each droplet to the detection systems which can lead to high number of missed droplets or false positives. However, the advantage of being able to detect extracellular secreted target molecules, lyse cells, or study viable samples, truly makes droplet microfluidics a valuable miniaturized and multiplexed platform to inform synthetic biologists their decisions on their engineering design.[162] Within the droplet-in-channel realm, Fluorescence Activated Droplet Sorting (FADS) [31, 163] or more recently, absorbance activated droplets sorting (AADS) [30] have been used for detecting protein expression, enzyme activity, antibodies, aptamers, or cell surface markers [31, 164, 165, 156, 30].

Screening of environmental samples

Bioprospecting refers to surveying environmental samples to discover new enzyme variants or complete metabolic processes. The research starts with the testing phase of the DBTL cycle and provides metabolic engineers with new parts for their building process. Probing environmental samples using droplet microfluidic techniques allows for rapid testing of individual droplets in selective conditions. For example, by sorting enzyme variants by chemical activity and using single-cell sequencing techniques, Nakamura et al. [166] tapped into the advantages of microfluidic technology, and were able to identify 14 novel β-glucosidase genes from previously uncultured marine bacteria. Similarly, Yu et al. [167] used high throughput sorting to determine the characteristics of various heat inducible promoters in plant cells making use of FADS as a pre-screening technique for next generation sequencing.

Screening parts and libraries

Droplet-based microfluidics, with its rapid sorting capabilities, can screen large libraries to inform the synthetic biologist with the necessary genetic modification needed to improve function or production titers. Using UV-based random mutagenesis, Huang et al. [168] built a library of mutant yeast strains and screened for α-amylase production. Using a fluorogenic substrate (BODIPY) and DEP-based sorting, they were able to sort out high α-amylase producing mutants. The authors then performed characterization and deep sequencing of indicated successful mutants, which resulted in new knowledge about protein secretion linked to specific genetic alterations such as a single gene deletion of HDA2 [168]. Since this work, many groups have used similar droplet-in-channel microfluidics systems to screen strain libraries [169, 30]. Romero et al. [169] were able to use high throughput microfluidic screening to characterize the chemical activity

of millions of glucosidase variants expressed in *E.coli* generated by error prone PCR. Eventually the team was able to discover residues crucial to enzyme function and use that as a start point for creating a library of mutations to find increased activity at high temperatures.[169] Similar to enzyme screening, today, this kind of research can be performed by combining single-cell encapsulation, barcoding methods, microfluidic sorting and sequencing. Screening of aptamers is also commonly performed with a droplet-based microfluidic device via a SELEX procedure.[170, 171] Such a procedure is performed using primer-functionalized microbeads followed by emulsion PCR to produce RNA aptamers that have also been used as a target for detection. Upon binding to a target, the conformational change can induce a fluorescent signal, as is the case with a spinach aptamer (see **Figure 2.3 B**), used by Abatemarco et al. [170] for the detection of tyrosine secretion by yeast.[172] Furthermore, screening CRISPR libraries can offer an alternative method to building libraries. Datlinger et al. [173] performed a pooled CRISPR screen with single-cell transcriptome readout to dissect complex signal pathways and other biological mechanisms that are not easily reduced to a single selectable biomarker. Their method (CROP-seq), performs single-cell RNA-seq to sequence both transcriptome and guide RNA (gRNA) of a single-cell lentiviral transduced library. These applications are only few of the examples that show screening parts and libraries can provide a priori data to construct new libraries for building new constructs and cells.

2.3.2 Single-cell sequencing

The ability to accurately sequence genetic material is crucial to the DBTL cycle. It allows the testing process to serve both as a starting point in the cycle, as an ideal path into the learning step, and helps us to use the cycle as a robust iterative method. Precise genetic or transcriptomic sequencing allows metabolic engineers to take naturally occurring genetic material and decipher the code of the DNA or RNA part which will help serve as a basis for further design and engineering or for actual diagnosis or a specific disease. In addition, it allows researchers to determine the sequence variations on the selected clones from designed libraries, which is especially beneficial to analyse sample heterogeneity. With the ability of droplet microfluidic devices to encapsulate individual cells into separate droplet entities, and examples of accurate quantitative single-cell measurements, this enabled a spike in the use these devices for single-cell sequencing.[174] Previous single-cell 'omic' data were unavailable before the implication of microfluidics based single-cell sequencing. The first microfluidic technologies allowing for single-cell RNA sequencing (scRNA-seq) [175], were further

popularized by Drop-seq and InDrop; two simple droplet-in-channel based scRNA-seq techniques developed by Macosko et al. [3] and Zilionis et al. [7]. These technologies sparked the ever increasing popularity of droplet microfluidics within diverse biological research ranging from medicine and immunology [176], to ecology [177]. Currently, the list of microfluidic based RNA sequencing technologies can now be completed with CEL-seq2 [73], MARS-seq [178] and MARS-seq2.0 [179], SCRB-seq [180] and mcSCRB-seq 120, Smart-seq [181] and Smart-seq2 [182], and Quartz-Seq2 [183]. Often, quantities of mRNA could be too low for sequencing. Droplet microfluidic devices that allow for isogenic cell culture have been developed to increase the starting material [128] (see **Figure 2.3 A**). As such, each of these scRNA-seq methods has their advantages and disadvantages [184]. Further applications of single-cell sequencing techniques include XDrop [185], and MATEseq [186]. Many important advancements have been made using scRNA-seq which include the mapping of immune phenotypes of breast cancer tumour environment.[187] Although the transcription level reveals most heterogeneity across tissues, genetic heterogeneity across large single-cell populations such as bacteria is an important field of study for antibiotic resistance and other trait evolution in environmental samples. Ultra-high-throughput genomic sequencing (SiC-seq [188]) allows for deconvolution of genetic heterogeneity in large populations. Further genomic sequencing techniques have been developed to solve challenges related to low starting material - a secondary problem that can also occur during standard DNA sequencing methods. Chu et al. [189] developed SISSOR (single-stranded sequencing using microfluidic reactors) to increase the starting material for sequencing of diploid genomes for haplotyping. By performing multiple displacement amplification in droplets of megabase-sized DNA fragments, they are able to show accurate sequencing data with error rates as low as 10^{-8} of the human genome with just three human cells as starting material. Lastly, using DNA-tagged antibodies, Hughes and Ellington [190] developed AbSeq, a technique to perform ultrahigh-throughput single-cell proteomics to characterize surface proteins.

2.3.3 Droplet microfluidics assisted analytical techniques

The high throughput nature of droplet microfluidics makes it an ideal candidate for rapidly analysing large libraries and making critical observations for each member within the library. However, on-device qualitative and quantitative analysis of droplet content is often limited by the high limit-of-detection. To more thoroughly analyse biological products, coupling droplet microfluidics with established laboratory

analytical techniques will lead to improved analysis, especially for testing the success of metabolically engineered organisms. Several groups have shown the advantages of such devices and their applications in the DBTL cycle. For example, integrating microfluidics with mass spectrometry has been increasingly popular since the device can be directly interfaced with the orifice of the mass spectrometer and does not require the need for specialized matrix plates. Steyer and Kennedy [191] were able to perform nanoelectrospray ionization-mass spectrometry (nESI-MS) of droplets containing enzymes, at a rate of 10 droplets per second. The microfluidic droplet generator was immediately connected to the mass spectrometer without noise contributions from the oil phase containing surfactant, thus achieving very high scan rates. MALDI-MS with droplet-based microfluidics has also been performed [192] by integrating a channel with a specialized fabricated a nanostructure on a Si-layer that contains an initiator – called Nanostructure Initiator Mass Spectrometry (NIMS). Lombard-Banek et al. [193] have also combined devices with capillary electrophoresis (CE), electrospray ionization, and an ultrahigh-resolution mass spectrometer (HRMS) for performing proteomics of single *Xenopus* blastomeres.

Next, the use of droplet microfluidics for PCR has been widely explored as a droplet digital PCR (ddPCR) method. Advantages of performing PCR in droplets are the ability to lyse single-cells in droplets, reduce input volumes, control mixing of reagents, and detection of amplicons. Kim et al. [194] have shown the use of a droplet microfluidic device to perform sample prep for RT-PCR.

Furthermore, droplet microfluidic devices have been integrated with fluorescence microscopy, laser induced fluorescence, Raman spectroscopy, fluorescence correlation spectroscopy electrochemistry, and capillary electrophoresis, and nuclear magnetic resonance spectroscopy [195], however more recent research on integrating microfluidic devices with standard existing analytical tools is lacking.

2.3.4 Directed evolution

While synthetic biology generally aims to develop rational design methods for engineering cells, the current ability to mould biological systems often falls short of achieving desired functionality. Directed evolution is an effective method to optimize a biological system by generating random or selective mutations at the gene of interest and applying selection through performance in an in vitro environment. Directed evolution has been used to discover new proteins or entire metabolic pathways by selecting variants based on cell growth or enzyme activity. The intersection between directed evolution and microfluidics has been thoroughly reviewed elsewhere.[196]

Directed evolution requires the creation of large sample libraries, as well as precise control over environmental factors and large-scale selection. As previously discussed, droplet-in-channel microfluidics possesses all the necessary functions to accommodate high-throughput directed evolution applications. One of the first demonstrations of directed evolution is by Agresti et al. [4] who built a platform which sorted 108 samples per day to select a high-activity horseradish peroxidase (see **Figure 2.3 C**). This platform laid the foundation of implementing the directed evolution workflow in a droplet microfluidic device. It performed an enzymatic reaction inside a pL droplet which produces a fluorophore when the enzyme is highly active. Droplets that exhibited high fluorescence can be sorted dielectrophoretically based on a threshold fluorescence intensity. [4] Many similar platforms have since been used to enhance enzymes for different applications [30, 197, 198]. For example, Ma et al. [198] performed 5 rounds of directed evolution to select an esterase, using two fluorogenic substrates.

Most (if not all) droplet based microfluidic systems that implement directed evolution are limited to binary sorting – hence, lacking the ability to evolve distinct levels of performance in parallel. This can be useful when attempting to scan a diverse space of different samples across an evolutionary landscape. Ahmadi et al. [108] addressed this by using a droplet device with a patterned array of electrodes which sort different levels of a yeast library that are able to grow in harsh ionic liquids used in biochemical processing. Their ability to sort different yeast samples based on multiple concentrations of ionic liquid is the first representation of 'n'-based sorting (as opposed to the usual high/low producer). This can be the first step towards expanding the space of directed evolution and lead to more interesting discoveries of enzymes and metabolic pathways.

A recent and fascinating addition to the field of automatized directed evolution is the eVOLVER platform built by Wong et al. [199]. Although the system does not employ droplet microfluidics, it presents a broad approach to high throughput directed evolution and synthetic biology. The system gives the user control over multiple parameters such as temperature, culture density, and media composition for several evolving cultures in parallel. The researchers offer eVOLVER as a "democratic platform for research by a broad community of users to build, execute, and share experiments". [199] The system's fluidic components may be improved by integrating the control of electrodes or exploring integration of droplet-in-channel platforms to enhance throughput.
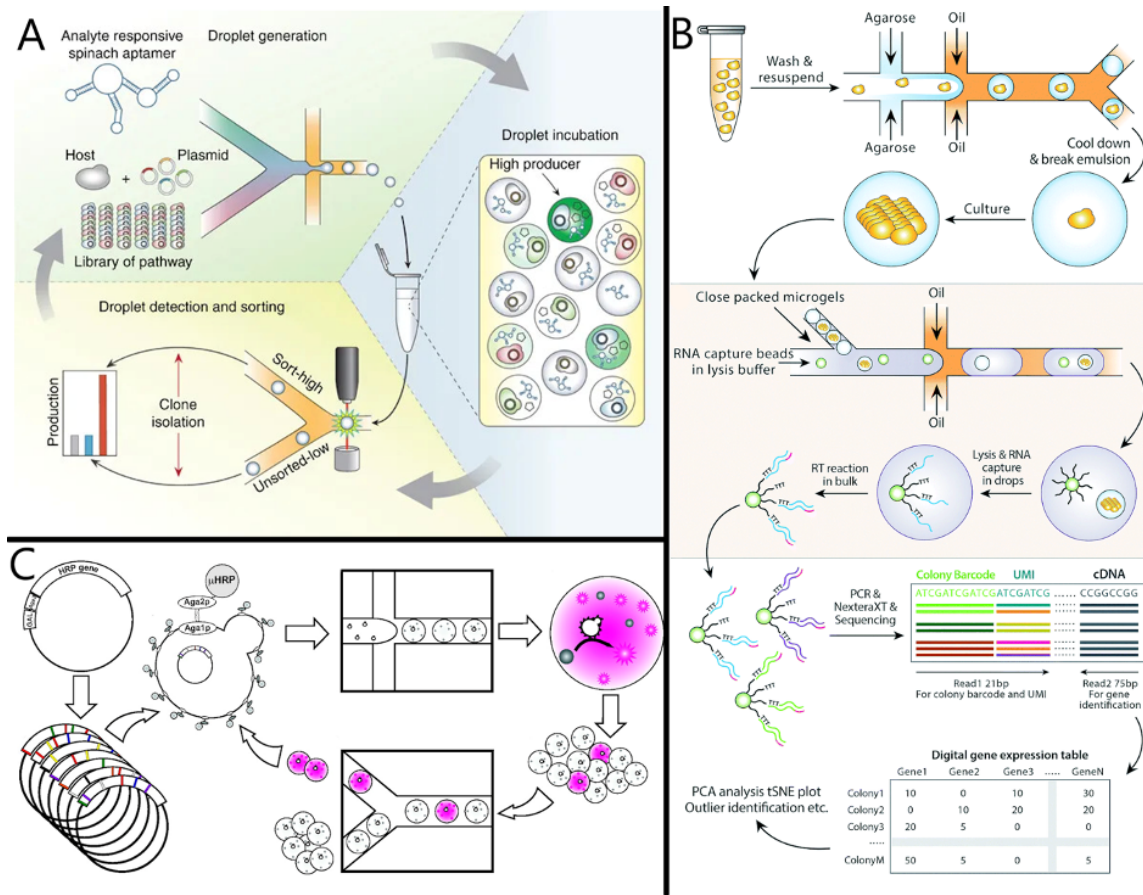
Figure 2.3: Test. a) High throughput screening of secretory phenotypes using RNA aptamers in droplets. b) High throughput gene expression profiling of isogenic colonies using Drop-seq. c) Ultrahigh- throughput screening in droplet microfluidics for directed evolution. Reproduced from Ref. [113] with permission from Royal Society of Chemistry.

2.3.5 Testing to complete the loop

Droplet microfluidics have seen immense adoption across the field of synthetic biology, primarily thanks to their ability to provide platforms for testing (see **Figure 2.3**). Especially, in the single-cell sequencing field with many users setting up or using droplet single-cell sequencing derived technologies. These microfluidic devices for sequencing and screening provide tools to perform experiments we were hardly able to do before. To continue its successful adoption, we need to develop, open-source software and hardware, and integrate to improve system scale-up.

An impressive example of "completing-the-loop" using a testing microfluidic device was performed by Wang et al. [200] who investigated the genetic basis of gene down regulation for improved protein production in yeast. The authors use high throughput droplet microfluidic single-cell analysis to examine a library

of 243,000 RNA molecules known to effect *S. cerevisiae* through RNA interference (RNAi). Once identified, Cas9-mediated recombineering was used to generate yeast strains implementing the identified RNAi molecules for increased protein production. Thus, showing seamless integration of testing and learning, leading to a new design. An often-overlooked challenge in the field of synthetic biology is fermentation. Much attention is paid to high-throughput screening of built strains, yet these screens can be misleading about how strains will behave within an industrial fermentation setting. Scaling-up a research facility's fermentation equipment is an impractical solution which nags for a more affordable option. A set of controlled parameters which move microtiter growth towards fermentation conditions include dissolved gasses, pH, nutrient levels and agitation. Several groups have developed microbioreactors controlling these parameters as discussed by Hegab et al. [201] yet droplet microfluids presents a unique challenge. Controlling oxygen content of droplets can be achieved through monitoring and controlling oxygen in perfluorinated oil used as the continuous phase.[202] Although controlling other parameters in droplets is not altogether feasible, it remains an imperative to integrate bioreactor capabilities into microfluidic workflows to 'complete-the-loop'.

2.4 Learning and outlook

Ultimately, the vision for applying droplet microfluidics to synthetic biology is to take each of the stand-alone elements and combine them into a consolidated device. Much the same way the Arithmetic Logic Units, Control Units, and Memory Units make up a computer's CPU, the microfluidic units capable of designing, building, and testing genetic material will make up the Biological Processing Unit of a future metabolic engineering platform (see **Figure 2.4**).

True automation of synthetic biology requires a platform which performs the core elements of the DBTL cycle in a closed-loop fashion – focusing in on key bottlenecks and eliminating them at successive iterations. A sustainable platform should remain compact and operate under low power and reagent consumption. It is hard for one to imagine this platform would rely on automated pipetting robots or a system dependent on moving cells within the confines of a 96 well plate. Efforts are already being made to incorporate numerous steps into a single device especially within the confines of each individual part of the cycle, as exemplified by Shih et al. [110], and Gach et al. [159], both of whom developed devices capable of plasmid assembly, transformation, and culture on a single platform.[159, 110] Furthermore, examples from the realm

of channel microfluidics such as the eVOLVER platform from Wong et al. [199], show early examples of how multifunctional devices may work.
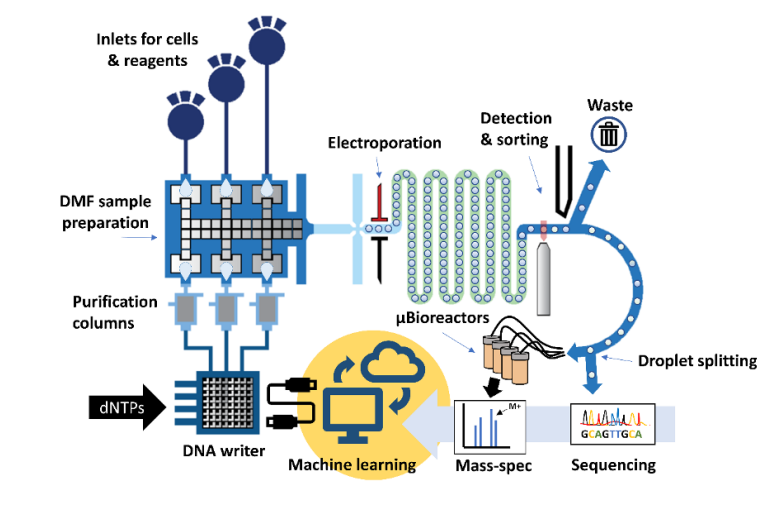
Figure 2.4: Learn. A proposed Bio-Processing Unit (BPU). One vision for synthetic biology could see a single droplet microfluidic device which handles all the aspects of the DBTL cycle and turns the process into a control loop. The system would include: A DMF-based sample preparation zone, a droplet generator, cell encapsulation and electroporation zone, an incubation region with temperature control, sample preparation for integration with sequencing and mass-spectrometry as well as integrated micro-bioreactors. Data collected from each round would pass through a machine-learning core which would control a DMF-based DNA synthesis component, bringing new DNA into the system for subsequent rounds. Reproduced from Ref. [113] with permission from Royal Society of Chemistry.

To keep progressing this vision for the future a link needs to be made between devices that excel at building and those that excel at learning. This will likely mean finding techniques that integrate the low-throughput-high-precision techniques of digital microfluidics commonly used for building with the high-throughput-low-precision techniques of droplet in channel microfluidics commonly used for testing. This may take the form of interfacing the two in series [107], or by integrating actuation electrodes into channels [108]. Furthermore, creating robust "world-to-chip" interfaces, such as that displayed by Tran et al. [203], will allow non-experts to work with these automated platforms without being a microfluidic expert. Achieving these goals should pave the way for a commercially viable all-in-one Biological Processing Unit in the coming years provided that researchers can continue to work towards reliable, robust devices that can have their manufacturing process scaled up.

We believe in the near term an increased focus should be placed on droplet-based oligo synthesis as well as devices that can bridge the gap between building and testing. Oligo synthesis is in high demand as it allows researchers of synthetic biology to be able to design any gene construct they desire. Designing and developing microfluidic platforms capable of on-demand synthesis of short strands (< 1 kb) will be highly useful while simple devices capable of basic elements of both building, testing, and learning will begin to pave the way for how the unique requirements for each part of the cycle will be merged.

Chapter 3

Droplet-digital binary droplet sorting for screening filamentous fungi

This chapter is currently unpublished: Samlali, K., Leal, A. C., Jezernik, M., & Shih, S. C. C. (2021). Droplet-digital system for screening filamentous fungi based on enzymatic activity

Abstract

We report the first droplet-based microfluidic method capable of long term incubation and low-voltage sorting of filamentous fungi inside nanoliter-sized droplets. The new method was characterized and was validated in solid-phase media based on colloidal chitin such that incubation of single spores in droplets was possible over multiple days (2 - 6 days) and were sorted without any droplet breakup. We examined the activity of cell-wall degrading enzymes that are produced by fungi during solid-state droplet fermentation using three highly sensitive fluorescein-based substrates (FL-GlcNAc, FL-GalNAc, FD-Glc). We also used the low-voltage droplet sorter to select clones with high enzymatic activity of cell-wall degrading enzymes such as β-glucosidase, β-glucanases, β-N-acetylglucosaminidases and β-N-acetylgalactosaminidases from a long-term incubated ($\dot{c}$ 3 days) filamentous fungi droplet library. The new system is portable, more affordable, and user-friendly compared to classical DEP-based FADS systems. We propose that this system will be useful for the growing number of scientists interested in fungal microbiology who are seeking high-throughput methods to incubate and to sort fungal cells.

3.1 Introduction

Filamentous fungi are often the preferred choice of a host for industrial biotechnology applications due to their natural ability to produce high yield of extracellular protein. For example, their proteins have been used for hydrolytic degradation of biomass, the production of pharmaceuticals, ingredients for the food industry or applications as agricultural fungicides.[204, 205, 206, 207] *Clonostachys rosea* (also called *Gliocladium catenulatum*, teleomorph *Bionectria ochroleuca*) is a commonly studied fungal mycoparasite that is being used as an agricultural fungicide.[208, 209, 210] While the mechanisms are not fully known, the production of extracellular cell wall degrading enzymes is known to play a key role in *C.rosea*'s mycoparasitism.[211] Cell wall degrading enzymes of C.rosea include chitinases, glucanases and proteases. Chitinases characterized in C.rosea, mostly belong to the glycoside hydrolase (GH) family GH18, of which at least 14 genes were confirmed to be present in C.rosea, including different exo- and endo-chitinases.[212] β-1,3-, β-1,4- and β-1,6-glucanases make up a second group of cell wall hydrolyzing enzymes, of which β-1,3-glucanase is well characterized in *C.rosea*. [210] Due to its commercial application in organic agriculture, there is much interest to screen random mutant *C.rosea* libraries for improved field-relevant properties. Typically, filamentous fungi producing improved enzymes are obtained by implementing an efficient strain improvement strategy, which now frequently involves a high-throughput functional screen to select desired clones out of mutant libraries. [213, 214] There are many high-throughput systems available for bacteria or yeast, however, these are not well adapted to filamentous fungal growth cycle and morphology. Fluorescence activated cell sorting (FACS) and flow cytometry methods for filamentous fungi can only screen conidia and cannot be used to screen for cell secreted products.[215, 216]

Droplet microfluidics has become a popular method for the high-throughput screening of single cells.[30, 217, 218, 219] When cells are encapsulated together with fluorogenic components, single cells can be screened rapidly for enzyme activity with fluorescence-activated droplet sorting (FADS) procedures.[31] Such a method allows for the activity analysis of secreted enzymes [220], cell bound proteins [164], or intracellular protein products [218]. Zang et al. [221], first showed it is possible to incubate filamentous organisms (filamentous actinobacteria) in droplet-in-oil emulsions, followed by Mahler et al. [222] and Tu et al. [223]. More recently, He et al. [224] and Beneyton et al. [225] demonstrated droplet incubation of filamentous fungi, and the first use of FADS droplet microfluidic systems for screening single conidia derived filamentous fungi libraries based on secreted products. However, two limiting factors make the use of

droplet microfluidics for filamentous fungi still challenging. First, the droplet incubation time is limited by the growth rate of the organism. The fungi will start to form hyphae after spore germination, which eventually will pierce through the nano or pico-liter droplets after ∼16 h of incubation, as reported for *T.reesei* and *A.niger* species.He et al. [224], Beneyton et al. [225] As a result, droplets will often merge with neighbouring droplets during incubation or are more prone to splitting and breaking during sorting. Second, when using dielectrophoretic (DEP) sorting, the system needs to be tuned experimentally according to droplet properties such as size or conductivity. The long droplet incubation times needed for protein expression, and different individual growth rates, contribute to droplet volume polydispersity post-incubation which complicates the sorting procedure.[224, 225] Additionally, under high voltages, deformation of hyphae containing droplets can occur, risking a loss of contents in the droplets. This two-fold challenge makes it hard to screen filamentous fungi using standard droplet DEP-based systems and new sorting systems should be developed adapted to the filamentous fungi properties.[226, 90]

Here, we describe the use of a droplet-based microfluidic system for high throughput screening of cell-wall degrading enzyme activity in filamentous fungi. We introduce a solution to the challenges related to using droplet microfluidics for fungal culturing, sorting, and screening, by optimizing the droplet incubation method and by using a low-voltage based sorting method. First, we cultured fungal spores in solid-state fermentation (SSF) media, such that the hyphal growth is maintained in the droplet and incubation times can be prolonged. We incubated single spores of a *C.rosea* mutant library within droplets containing an enzymatic substrate and a colloidal chitin based solid-state media. We used three highly sensitive fluorescein based substrates (FL-GlcNAc, FL-GalNAc, FD-Glc) that will release fluorescein units during incubation to measure the cell-wall degrading enzyme activity. Prolonged incubation using SSF with colloidal chitin as a substrate was explored by evaluating the enzymatic activity of cell-wall degrading enzyme in this media and comparing the activity to liquid culture and observing the droplet integrity over time. Finally, we integrated a low-voltage sorter (using an electrostatic-based sorting technique rather than using dielectrophoresis [24, 109, 108, 227]) tuned to the characteristics of filamentous fungi droplet libraries, to seamlessly couple incubation and sorting. We explored the compatibility of the low-voltage sorter with a droplet microfluidic system to select the clones with high enzymatic activity of cell-wall degrading enzyme such as β-glucosidases, β-glucanases, β-N-acetylglucosaminidases and β-N-acetylgalactosaminidases from a long term incubated (at least 3 days) filamentous fungi droplet library, which were further tested for their biocontrol ability. The addition of solid-phase culture in droplets and low-voltage sorting is the first report,

41

to our knowledge, to show successful autonomous screening of filamentous fungi enzymatic activity several days after germination. The results presented here highlight the optimal use of droplet microfluidics for fungal culturing and screening, illustrating how it can be useful for finding proteins in fungi that can be used for industrial biotechnology applications.

3.2 Results and Discussion

3.2.1 Fungal screening system design and development

Isolation of mutants of interest from a filamentous fungi library requires an efficient high-throughput screening strategy. While there are microfluidic enrichment strategies to sort out active fungi, they suffer from challenges related to droplet incubation and microfluidic sorting. [224, 225] To solve these challenges, we introduce a filamentous fungi droplet screening system that consists of (1) a solid-state droplet fermentation (SSDF) incubation method, and (2) a droplet sorter suitable for maintaining the integrity of the droplets containing filamentous fungi. Our electrostatic co-planar electrode sorter is optimized particularly to sort fragile droplet libraries (preventing 'bursting' of droplets) without the need to frequently tune the sorter parameters (i.e., applied voltage and flow rate) based on differences in droplet volume. Additionally, the system has a small footprint and does not need expensive components (e.g., microscope, lasers and specialized optics) making it more accessible to microbiologists.[226]
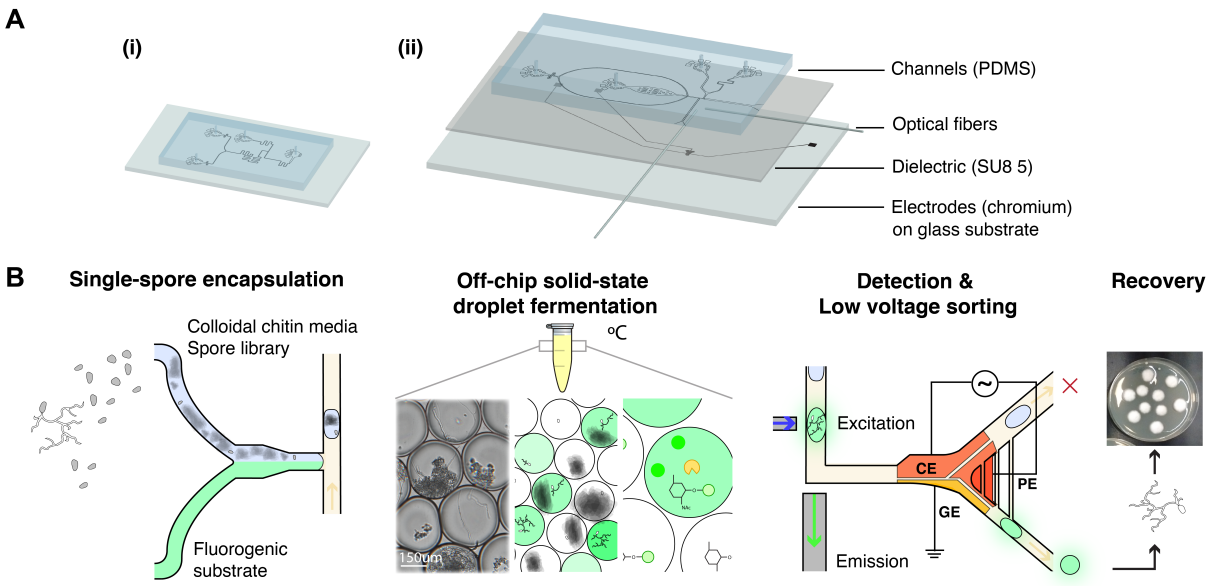
Figure 3.1: Microfluidic device for screening cell wall degrading enzymes in filamentous fungi. (A) Schematic of two microfluidic devices used for screening: (i) a droplet generator and (ii) a sorting device containing electrodes. For (i) and (ii), the microfluidic channel is fabricated via soft-lithography techniques except that (ii) contains an electrode layer with a SU-8 dielectric layer that is bonded to the channel PDMS layer. Two optical fibers (excitation: 105 μm core, 0.22 NA; emission: 200 μm core, 0.39 NA) are inserted into (ii) and are placed orthogonally to the channel to excite and to detect droplet fluorescence. (B) Screening workflow overview. Screening of the enzymes followed five steps. First, the mutant fungal population is generated through UV mutagenesis. Next, a microfluidic mixer T-junction droplet generator (see device (i)) co-encapsulates the conidial library suspended in colloidal chitin minimal media with a fluorescein linked enzymatic substrate for glycoside hydrolases. Droplets are then collected and incubated in HFE 7500 oil 2% fluorosurfactant at 27 ^{o}C for 2 - 6 days. Droplets contain single spores, minimal media with colloidal chitin, and a cell wall degrading specific fluorogenic substrate (FL-GlcNAc, FL-GalNAc, FD-Glc). During incubation, glycoside hydrolase (GH) activity leads to the cleavage of the fluorescein based substrate and the release of fluorescent fluorescein units that remain confined within the droplet. The droplet library was reinjected into a microfluidic low voltage sorter (see device (ii)) and the mutant populations are sorted out when displaying high fluorescence intensity. Finally, mutants with high fluorescence are recovered on PDA plates and grown into clonal colonies after which further testing is performed.

The system presented here (illustrated in **Figure 3.1 A**) consists of a droplet generator and an electrostatics based fluorescence activated droplet sorter (shown in more detail in **Figure B.9**). The droplet generator device is used to create the single-spore droplet library and consists of three inlets that are used for (1) the *C.rosea* spore solution in solid-state fermentation (SSF) media, (2) the fluorogenic enzymatic substrate solution, and (3) the continuous oil phase with 2% fluorosurfactant. Solutions from inlets (1) and (2) were mixed via a serpentine mixer and droplets were generated via a T-junction mechanism. As illustrated in **Figure 3.1 B**, a spore library was exposed to UV to generate a mutant library, and subsequently diluted in a solid-state fermentation media (i.e., colloidal chitin minimal media). In the generator,

the library was mixed with one of three highly sensitive fluorescein based substrates (fluorescein mono-(N-acetyl-β-D-glucosaminide (FL-GlcNAc), fluorescein mono-(N-acetyl-β-D-galactosaminide) (FL-GalNAc), fluorescein-di-β-D glucopyranoside (FD-Glc)) and a single-spore is encapsulated in a droplet emulsion. Following droplet generation, the droplet library was incubated in PCR tubes at $26 - 36\ ^oC$ in the dark for up to four days. The droplets were then injected into the sorter and sorted based on fluorescence. Within the droplets, fluorescein substrates are cleaved by cell-wall degrading enzymes, by which the activity of glyco-side hydrolase (GH) family CAZymes (i.e. carbohydrate active enzymes) such as N-acetyl hexosaminidases (e.g., chitinases) and β-glucanases is measured.[228, 212]

In the experiments described here, we explored the concept of using co-planar electrode sorters. Filamentous fungi will expand their mycelium after several hours of growth and incubation which causes the hyphal tips to exit the droplets. When the tips exit the droplets, it disrupts the water/oil interface and high-field DEP droplet sorting can lead to bursting of the droplets and to losses of the active enzymes during sorting.[225] Previously, electrostatics based sorters showed promising results and reliable droplet sorting without any droplet breakup or damage.[24] This technique is based on applying kHz-frequency potentials to electrodes under a dielectric, and using the generated uniform electrostatic field to move droplets. A binary sorter was designed, (motivated by our previous work in our group [108, 227] and others [24, 109]), consisting of a droplet receiving inlet chamber followed by a spacer oil channel and a binary sorter. The sorter was placed on a dielectric covered electrode configuration directly below the channel. As shown in **Figure B.9 B**, three co-planar electrodes were placed under the sorting Y-junction with a dual purpose to actively sorting positive (P) droplets towards the higher resistance (narrower and longer) channel and maintaining preference of the negative (N) droplets towards the main (wider) channel. The electrodes were configured as a constant electrode (CE) located at the top, a pulsing electrode (PE) located in the middle, and a ground electrode (GE) located at the bottom of the channel. The sorting mechanism is based on a uniform electric field being formed between the gaps of the electrodes with dependency on which electrodes are grounded (see **Figure B.10** for simulation). From our simulations, when a continuous potential (AC, 10 kHz) was applied to the CE (with PE+GE being grounded), an electric field was generated between the gap. This configuration ensures N droplets are directed into the main channel. When a P droplet is detected, the PE is activated with a short and small pulse (300 ms, 10 kHz sine wave, 4.6-51.8 V_{RMS}), such that an electric field forms along the gap between CE/PE and GE such that it directs P droplets towards the narrower channel (**Figure B.10 B**).

Due to the limited number of examples of droplet microfluidic screening of filamentous fungi, and to improve accessibility for using droplet-based microfluidics, we have developed the system to have reduced footprint, more affordable and user intuitive compared to classical DEP-based FADS systems (**Table B.1**).[229] An overview of the software and hardware is written in **Appendix B.2**. Although we used optical methods for observation of the droplets, the system does not use microscope optics for excitation or detection, but uses optical fibers and relies on a single portable detector.[108, 229] OOperation of three electrodes under low voltage opens up the possibility to reduce the electronics further to a smaller footprint and reducing the cost of the system significantly.

3.2.2 Improving droplet incubation for filamentous fungi to analyze cell-wall degrading enzymes

To perform an enzymatic assay on a microfluidic scale, single spores and substrates are encapsulated into pico-liter sized droplets. These are then taken off-chip for incubation to allow for protein expression and secretion. After several hours of incubation, the droplets are reinjected into a device to be sorted for high activity.[29, 230, 231] When culturing filamentous fungi for enzymatic production, longer incubation times ($\sim$ days) are required since certain enzymes are not expressed until several hours after spore germination. [224, 228, 225] The incubation problem was previously shown by Beneyton et al. [225] and He et al. [224] – the sorted positive droplets did not display the expected fold-increase improvement in enzymatic activity. Since these single-spores are confined to liquid bioreactors, this makes culturing of filamentous fungi in droplets challenging because a balance is required between preventing the hyphal exit and obtaining enzymatic production above the limit of detection. Previously *A.niger* hyphal tips have been shown to burst through 250 pl droplets at $\sim$15 hours post-incubation (hpi), and through 18 nL droplets at 32 hpi.[225] *T.reesei* was grown for up to 16 hours, while the organism shows enzymatic production at 24 hpi.[224] Working with larger droplets can increase incubation times, yet this needs systems with a lower limit of detection and adapted microfluidic sorters for larger volume droplets.[224, 225] We address this issue by finding relevant sensitive fluorogenic substrates to allow for early detection of enzymatic production, and by adjusting the incubation media to prolong droplet incubation.

We hypothesize SSF in droplets could potentially solve the incubation issue by maintaining fungi within the SSF substrate such that the solid media will limit hyphal tip exit. Previously, colloidal chitin (CC) has

been shown to be a good addition to liquid culture (for *C.rosea* [232]) and as SSF substrate derived from shrimp shells.[233] In addition to providing support, it also plays a role in inducing cell-wall degrading enzyme expression in mycoparasites, since chitin is a major fungal cell wall component.[232] The use of gel-like or solid supports (microcarriers) in microfluidic water-in-oil droplets prolongs incubation times for mammalian cells [234], yeast [235] or bacterial colonies [236], and for filamentous fungi [237, 238]. However, we believe this is the first demonstration of the use of a solid substrate for SSF of filamentous fungi within pico-liter water-in-oil droplets, and the first demonstration of the encapsulation of colloids for solid support.
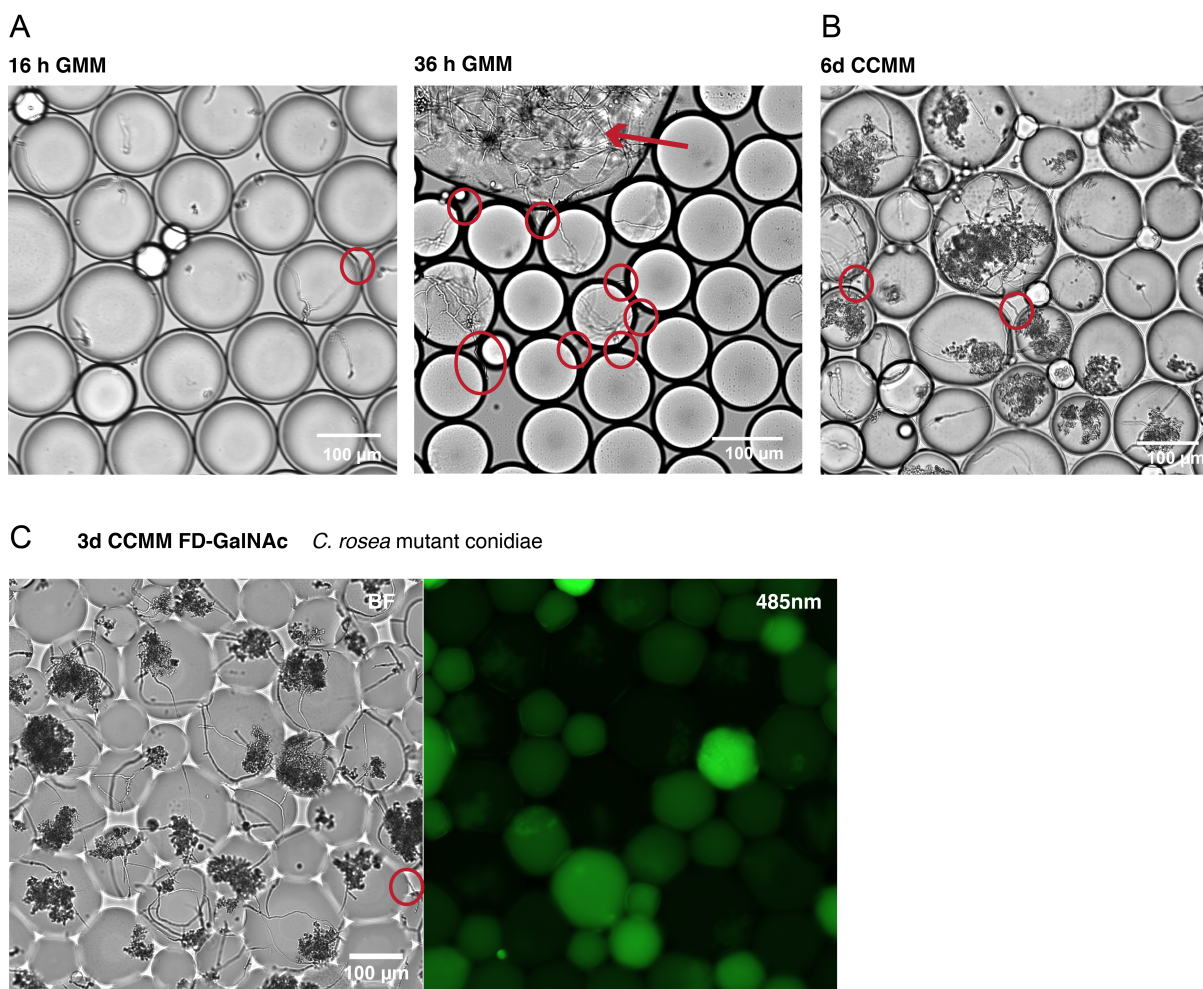
Figure 3.2: Incubation of filamentous fungi in droplets with varying media. Red circles indicate hyphae breaking through droplets. (A) Droplets after 16 and 36 h of incubation with *C.rosea* spores germinating in glucose minimal media (GMM). After 36 h, large hyphal masses can be seen (red arrow), indicating droplet merging events. (B) Solid state droplet fermentation (SSDF). Droplets after 6 days of incubation with *C.rosea* spores germinating in colloidal chitin minimal media (CCMM) show polydispersity and fewer hyphal tip exits. (C) Solid state droplet fermentation (SSDF) with cell-wall degrading enzyme fluorescent substrate. Droplets after 3 days of incubation with *C.rosea* spores germinating in colloidal chitin minimal media with FD-GalNAc. Fluorescein shows no cross contamination across droplets (485 nm, 20X).

To perform SSDF, a mixing channel was used to mix 1:1 2% colloidal chitin solution with the substrate solution prior to droplet generation. To prevent clogging of the device, the colloidal solution was filtered (10 μm) after which spores were dissolved in the solution with constant agitation. Next, the solution was injected at a lower flow rate and gradually increased to an equal flow rate as the substrate solution to avoid sudden clogging. Using colloidal chitin minimal media, we were only able to see hyphal tip exit after 4 days at 27 ^{o}C ($\sim$96 hpi, 1 nL), while with regular minimal media with a glucose carbon source, there was hyphal

tip exit after 16 hpi in $\sim$ 1 nL drops. (**Figure 3.2**). The decreased hyphal tip exit can be explained by the absence of any carbon source beyond complex colloidal chitin, which can only be accessed after sufficient degrading enzymes have been produced.[232] In addition, we observed that the hyphae preferentially grew with high density in the colloid mass within the droplet, while the hyphae present outside of the colloid mass were limited. Interestingly, when droplets were incubated (27 ^{o}C, 2 days) in minimal media droplets without any carbon source, we found several *C. rosea* spores germinating and developing hyphae. While unlikely, C.rosea could have a mechanism to access the carbon chain of surfactants or the highly fluorinated HFE oil., as degradation of fluorinated compounds has been demonstrated for other fungi.[239, 240, 241]

Following culturing on colloidal chitin, we looked at fluorogenic substrates that can be used to monitor the production of a collection of cell-wall degrading enzymes from the glycoside hydrolase family enzymes.[212, 228] Colloidal chitin has previously been used to enhance production of chitinases and β-1,3-glucanases by *C.rosea*,. We examined production of cell-wall degrading enzymes using three substrates: FD-Glc for β-glucosidases and β-1,3-glucanases, FL-GlcNAc for (exo-)chitinases, and FL-GalNAc for the detection of N-acetyl galactosaminidases. Previous reports have shown enzymatic activity measurement of cell-wall degrading enzymes by end-point assays that monitor the release of glucose units for β-1,3-glucanases, or use 4-methylumbelliferyl substrates such as N-acetyl β-D-glucosamine (4-MU-GlcNAc for exo-chitinases).[242, 243] A preliminary well plate assay was performed to confirm enzymatic activity in the parent strain, using 4-methylumbelliferyl-β-D-glucopyranoside (4-MU-Glc), 4-MU-GlcNAc, and 4-methylumbelliferyl-N-acetyl galactosaminide (4-MU-GalNAc) (**Figure B.11**). All substrates showed higher fluorescence after five days of incubation with *C.rosea* agar plugs (P $<$ 0.05 compared to media without *C. rosea*). The higher fluorescence indicates that the parent strain natively produces enzymes that cleave the three enzymatic substrates. When we grew *C.rosea* in colloidal chitin minimal media (CCMM), all three substrates showed a significantly higher fluorescence in comparison to PDB (potato dextrose broth) media (P $<$ 0.05) indicating that CCMM upregulates cell-wall degrading enzyme expression and 4-MU-Glc is a poor choice to represent β-1,3-glucanase production. Next, the equivalent fluorescein based substrates were used for a kinetic assay on spore solutions to further investigate them as substrates for FADS. Common enzymatic substrates (e.g., 4-methylumbelliferone and resorufin based substrates) are difficult to use for detecting enzymatic activity in droplet microfluidics because they require merging at end-point or require UV excitation. Fluorescein based substrates are extremely sensitive, easy to detect under 470 nm excitation, and have previously been used in droplet microfluidics with excellent droplet retention for long

term droplet incubation.[220, 31, 32] We qualitatively examined substrate partitioning and hyphal exit by incubating *C.rosea* spores germinating in colloidal chitin minimal media with FL-GalNAc in droplets for three days. Culturing the spores in the solid media shows no cross contamination of fluorescein across droplets and very minimal hyphal exit (Figure 3.1C). Furthermore, we observed detectable fluorescence after incubation of spores (0.5×10^7 spores mL^{-1}, Poisson spore concentration) with fluorescein substrates (**Figure B.12**). The fluorescence signal using all three fluorescein based substrates displays an increasing trend over the 16 h of incubation. The change in fluorescence over time for all three substrates are significantly different when comparing enzyme production in glucose MM and CCMM (ANOVA, P $<$ 0.05) indicating higher enzymatic activity in CCMM and higher sensitivity of the fluorogenic substrates. We note that the N-acetylglucosaminidase and N-acetylgalactosaminidase substrates displayed a higher fluorescence compared to the β-1,3-glucanase substrate. We expect FD-Glc hydrolysis to be an indicator for β-1,3-glucanase since the enzyme has previously been reported to hydrolyze other glucopyranoside bound fluorogenic substrates.[244, 245, 246] However, previous reports show higher β-1,3-glucanase activity compared to chitinase activity, which we did not detect from the preliminary results above. [212, 232]

We identified two methods to improve the sensitive detection of filamentous fungi secreted products. First, we increased filamentous fungi droplet incubation time from previously reported 16 hours to 4 days, using solid-state fermentation media within nanoliter sized droplets. Next, we identified three sensitive fluorescein-based substrates that are commercially available of which we showed substrate sensitivity to cell-wall degrading enzymes.

3.2.3 Optimization and characterization of electrostatic sorter

Dielectrophoretic sorters often need to be experimentally tuned (potential, flow rate and frequency) based on specific droplet volume and content, to sort optimally.[225, 231, 31] However, after droplet incubation for extended time periods, droplets often display a variation in volume, which is especially true for long-term droplet incubation of filamentous fungi. Secondly, filamentous fungi hyphal tips are known to puncture droplets. Changing the shape of droplets extensively, through channel geometries or high-voltage DEP sorting (electrosplitting) can increase the risk of droplet breakage post-incubation.

We first tested the effect of changing flow rate and potential on droplet emulsions of identical droplet size and content ($\sim$ 1 nL, ddH$_2$O). Experimental results show sorting success (number of droplets that go into the disfavored channel (T) divided by the total (T+F)) modeled with a binomial regression model with an
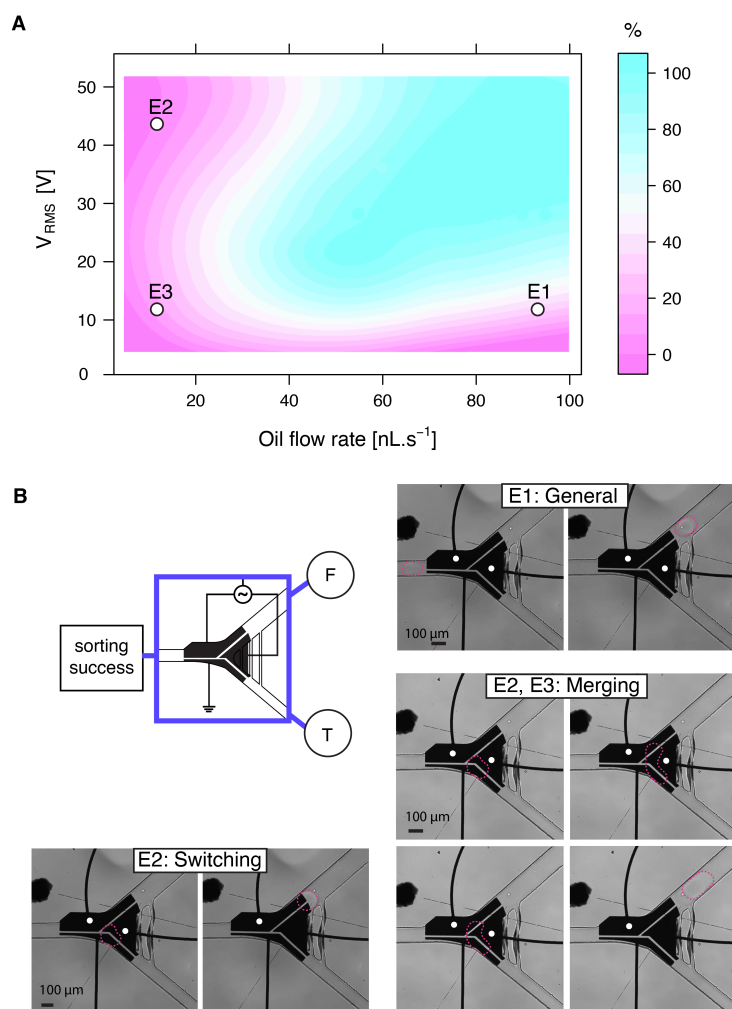
Figure 3.3: Evaluating the sorting efficiency under different flow rate and electric potential conditions. (A) A heat-map showing the efficiency of electrostatic droplet sorting (%) for different oil flow rates (nL/s) and applied potentials (V_{RMS}). The success rate of sorting was measured by counting the number of droplets that successfully enter the disfavored channel (true, T) and those that enter the main channel (false, F). The highest sorting success is displayed as a blue area with the lowest success being shown as the pink area. The optimal flow rate and potential to achieve 100% success is > 51.5 nL s^{-1}, 27.4 V_{RMS}. The lowest potential at which we observed perfect sorting (100%, N = 10) was at 12.5 V_{RMS}, 50 nL s^{-1}. This graph was created through a polynomial fit using a binomial regression with interaction term, AIC: 1029.1 with coefficients P$<$0.05), N = 10 per condition. Three failure sorting conditions were observed and labeled as E1, E2, and E3. (B) Time series images of three sorting failure conditions. Actuated electrodes are indicated with a white dot, and droplet is outlined. E1: droplets immediately enter the main channel (low potential, high flow rate). E2: droplets enter the disfavored channel, but droplet switches to main channel after the PE pulse (low flow rate high potential). E2 and E3: droplet could merge with the next arriving droplet (low flow rate).

interaction term (all terms P < 0.01) (Figure 3.3A). A potential was sent to the top constant electrode (CE) while grounding the other two electrodes (PE and GE). For each condition, sorting was performed manually by applying a potential pulse to the PE upon arrival of a droplet (300 ms; N = 10), to sort droplets at random. A sine wave of 10 kHz with varying AC potential was amplified to obtain a potential between 4.6 - 51.8 V_{RMS} (see linear calibration curve **Figure B.12**), and flow rates of the spacer oil were varied between 10 - 100 nL s^{-1}. As shown in **Figure 3.3 A**, reliable efficient sorting occurs at oil flow rates greater than 51.5 nL s^{-1} at an applied voltage of 27.4 V_{RMS} (P = 0.5, binomial regression inflection point). The lowest potential at which we observed perfect sorting (100%, N = 10) was at 12.5 V_{RMS}, with a flow rate of 50 nL s^{-1} (**Figure B.14**). As far as we are aware, the idea of electrostatic-based sorting has been reported previously [109, 24], but this is the first example of characterisation as a low-voltage sorting system with perfect fidelity. While the sorter performed efficiently in this region (shown in blue), we note that there are three regions (labeled as E1, E2, and E3) that sorting errors occur more frequently. E1 occurs when droplets enter the main channel. This frequently occurs when sorting at low voltages (< 27.4 V_{RMS}), higher flow rates (> 51.5 nL s^{-1}), where the hydrodynamic drag force is larger than the electrostatic force. The second scenario (E2, **Figure 3.3 B**) occurs at low flow rates (< 51.5 nL s-1). Here, sorting fails because the hydrodynamic drag force is not strong enough to overcome the channel resistance in the disfavoured channel and the droplet either moves towards the main channel or remains static at the entry of the disfavored channel on the gap between the grounded and the activated electrode due to a strong electrostatic field until the PE is turned off. In addition, if in this scenario a second droplet arrives at the sorter junction when the PE is still on, merging can occur at high potentials (>27.4 V_{RMS}) (E3, **Figure 3.3 B**). We hypothesize when the orthogonal hydrodynamic drag forces and the electrostatic forces (from the applied potentials) balance each other out, sorting will be successful. By using this co-planar electrode configuration with an electrode gap oriented in parallel with the flow streamlines, electrostatic force based sorting can be performed successfully at significantly lower applied voltages compared to dielectrophoresis techniques requiring up to 1.4 kV, without sending potentials through the droplet content.[225, 31] This can reduce deformation and the risk of droplet breakage, which is beneficial when working with fragile filamentous fungi containing droplet libraries.

Next, we tested sorting efficiency of sorting a polydisperse volume droplet emulsion under two different sorting regimes (60 nL s^{-1} or 80 nL s^{-1}). The droplet emulsion represents a reinjected droplet population of long-term droplet incubated filamentous fungi.

A

B

	Observed	
	Fluorescein Positive	Blue dye Negative
Disfavored Channel Positive	TP 27	FN 1
Main Channel Negative	FP 8	TN 207
	Sensitivity 77.14%	Specificity 99.52%
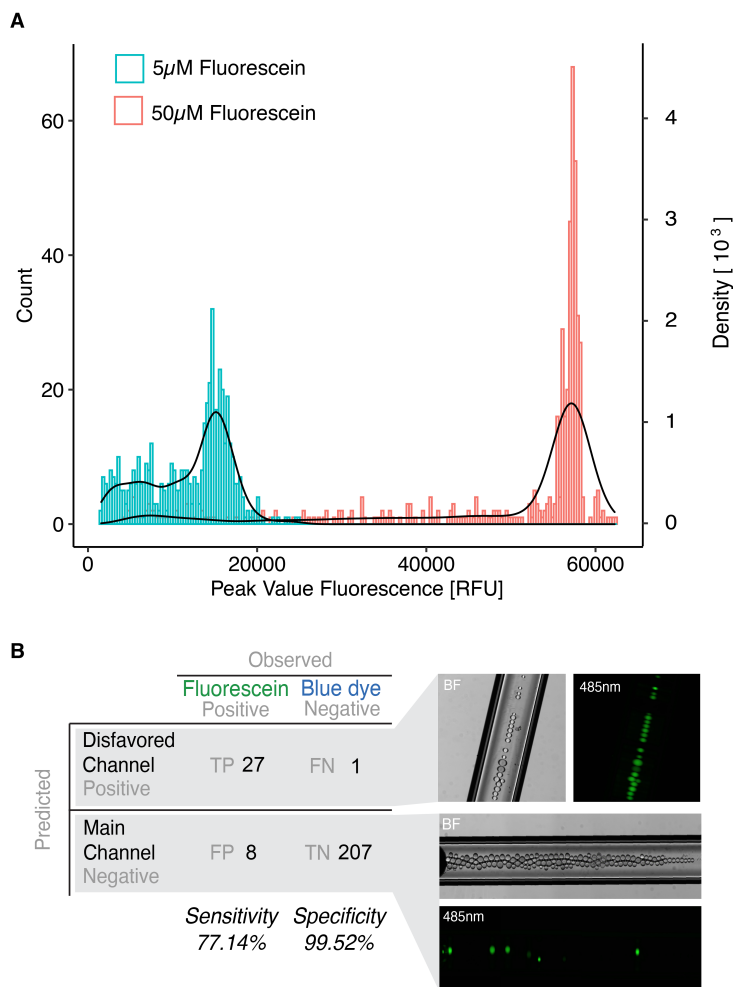
Figure 3.4: Calibration of the low-voltage sorter. (A) Gating histogram. Peak intensity of 5 μM (shown as blue) and 50 μM (shown as red) fluorescein containing droplets was measured when passing through the microfluidic sorter using a peak detection algorithm (N = 500). (B) Experimental overview. A mixed droplet library is reinjected into the sorter, of which the sorting gate is set to fit the 5μM Fluorescein histogram, and autonomous sorting with total oil flow of 0.03 μL/s, PE 10 kHz 15 V_{RMS} 0.3 s, and droplet travel time of 0.1 s. (C) Droplet populations from each outlet after autonomous sorting of a mixed population of fluorescein "positive (P)" (5 μM) droplets and "negative (N)" blue dye droplets. Sorted positive droplets are expected to flow into the 'disfavoured' channel with the negative droplets flowing into the 'main' channel. From observation of bright-field and 480 nm excited fluorescent microscopy images of droplets recovered from both sorting outlets, the sensitivity (77.14%) and specificity (99.52%) of the sorter were calculated.

As shown in **Figure B.15 A**, we observed droplets of different volumes passing through the binary sorter at two flow rates (60 nL s^{-1} or 80 nL s^{-1}), without actuating any electrodes. At 80 nL s^{-1}, the true probability r of a droplet entering the main channel is $> 90.6\%$ while at 60 nL s^{-1}, it's $> 94\%$ (99.9% confidence level). We can thus conclude that around 1% of true or false positive droplets could be due to the channel geometry. We also observed that at flow rates lower than 10 nL s^{-1} and increasing droplet size, droplet plugs increased the resistance in the main channel, resulting in droplets frequently entering the disfavored channel. Next, we used the previously described manual electrostatic sorting method in two experiments with different sorting regimes (36.34 V_{RMS}, 60 nL s^{-1} ; 44.20 V_{RMS}, 80 nL s^{-1}) to assess the ability of an electrostatic sorter to sort varying droplet sizes under the same sorting conditions (**Figure B.15 B**). Droplets with varying volumes smaller than $\sim$1 nL (at success $>$ 0.5; inflection point) could be sorted successfully under the same flow (60-80 nL s^{-1}) and potential (36.34 - 44.20 V_{RMS}). This indicates the ability to sort polydisperse volume droplet emulsions, without the need for re-tuning sorting parameters such as voltage, pulse length or oil flow rate for

different volumes.[247] This is beneficial to sort filamentous fungi containing droplets, which can often merge, or display polydispersity after long term incubation times due to differing growth rates, or evaporation.

After manually characterizing successful sorting regimes for sorting of polydisperse droplet emulsions, we analyzed the performance of fully autonomous sorting, under a single hardware configuration. All the sorting manipulation were controlled using our automation system (previously published [227]) with additionally developed software for droplet fluorescence detection and automated electrode pulsing, including a graphical user interface. We evaluated several performance measures such as the sensitivity, specificity, and throughput of sorting when auto-detecting and sorting positive droplets containing 5 μM fluorescein. For this, a droplet generator device containing two independent T-junction droplet generators was used to generate predefined droplet libraries for sorter calibration with fluorescein standard droplets (5 μM and 50 μM), and blue dyed ddH2O droplets (0 μM fluorescein) (device 2; **Figure B.9**). As a first step, to set the sorting gate, we measured the fluorescence of droplets of different concentrations of fluorescein by performing a peak finding algorithm (**Figure 3.4A** and Supplementary Note 2). We generated 5 μM and 50 μM droplets of fluorescein, reinjected the droplets into the sorter and determined the fluorescence intensity range for the 5 μM fluorescein droplets. Next, a mixed population of 5 μM fluorescein droplets with blue dyed droplets (representing 0 μM fluorescein) was generated and reinjected into the sorter. Using the previously determined 5μM fluorescein intensity range as a gate, a sorting voltage of 15.8 V_{RMS}, 10 kHz sine, and a flow rate of 30 nL/s, the device was left to sort autonomously (**Figure 3.4 B**). The results are shown in a confusion matrix (**Figure 4C**, **Supplementary Table 3**), display a sensitivity of 77.1% (true positives out of the total number of fluorescein droplets) and specificity of 99.2% (true negatives out of the total number of blue dyed droplets). The sensitivity is lower than other reported sorters, but this can be further increased by a more precise timing of PE actuation, given that our system relies on experimental (and no in-situ) measurement of droplet speed and derived droplet travel time to actuate the electrodes for sorting (**Figure B.16**). Although our sorting throughput of 7 Hz is lower than reported sorters,[31, 161] changing the system to a laser and PMT based detection system, the electrode configuration, the channel geometry or optimizing communication speed in electronics will increase the throughput of our sorting system to kHz range.[24, 231] Comparing our system to current filamentous fungi screening techniques, 7 Hz is faster than standard high-throughput well-plate based methods, and comparable to the previously reported microfluidic throughput for fungal sorting (Beneyton et al., 2016 (10 Hz)). To summarize, we developed an electrostatic

sorter that can efficiently sort polydisperse volume droplet libraries at 7 Hz throughput and with only an applied potential of 12.5 V_{RMS}, without exposing droplet content to electric fields and risking electrosplitting. This new sorter is an important contribution to aid the automated sorting of filamentous fungi droplet libraries.

3.2.4   Application: Screening glycoside hydrolases in *C.rosea* using droplet-based chitin fermentation

Mycoparasitism by degradation of pathogenic fungi cell walls (nercophytism) is a crucial mechanism of filamentous fungi used as biocontrol agents.[212] To show the use of our system, we generated a random mutant *C.rosea* conidia library and screened single clones for improved secreted CWDE. The generated UV mutant library showed a spore survival of on average 11.5% compared to an untreated sample.

To screen the mutants for cell-wall degrading enzymes activity, one fluorescein substrate at a final concentration of 100 μM was co-encapsulated with 2x CCMM with spores (1:1 microfluidic mixing). The resulting $\sim$ 1 nL droplets were subsequently incubated at 27 ^{o}C at varying times (2 – 4 days) depending on the substrate. Before active sorting, we detected the fluorescence for each droplet of the reinjected droplet population to assess the differing fluorescence between wild type and mutant libraries and differences in fluorescent profiles between substrates (**Figure 3.5 A**). The skewed populations (Pearson coefficient, mutant populations right skewed compared to wild-type) confirm a majority of empty droplets (Poisson distribution encapsulation), displaying the background fluorescence of the substrates in empty droplets. For FL-GlcNAc based sorting, the droplets were incubated for 2 days after which they showed strong fluorescence in spore containing droplets that was distinguishable from empty droplets. For FL-GalNAc based sorting, the droplets required incubation for 4 days to be able to observe fluorescence in the spore-containing droplets that was distinguishable from background fluorescence. For both substrates, the histogram showed a difference in variance between parent strain and mutant library (Levene Test, P < 0.05), which confirms droplets with higher fluorescence in the mutant library. FD-Glc containing droplets, however, showed a high degree of droplet breakage after 2 days and it was difficult to obtain intact droplets for sorting. Large clusters of hyphae were found indicating droplet merging events and faster growth rates. As a result of the shorter incubation time, the peak histogram of the parent strain population could not be distinguished from the mutant population (**Figure B.19**). While we confirmed that *C.rosea* generates β-1,3-glucanases

in CCMM, we observe from end-point and kinetic assays that the production was much lower as expected compared to previous reports.[232, 212] We hypothesize that C.rosea produces exo-glycosidases and exo-glucosidases in addition to endoglycosidases, which can lead to hydrolysis of FD-Glc and the release of glucose. The free glucose could expedite growth rates and droplet breakage. Due to the failed attempt to sort based on FD-Glc, we proceeded with autonomous sorting of the FL-GlcNAc (one sorting experiment) and FL-GalNAc populations (two sorting experiments). In a 30 min experiment, we screened on average around 12 500 droplets at 7Hz, which results in a screen of around 3800 unique single spores. The sorting gate was set to sort droplets above the 90% quantile of the mutant populations, with 500 nm $< \lambda_{em} <$ 520 nm. Using the sorting regime as previously optimized ($\sim$ 40 V_{RMS} potential, 60 nL s^{-1} oil flow), positive droplets with high-yield GH production were collected in a glass capillary and spread onto potato dextrose agar (PDA) for verification. Over fifty colonies were picked randomly and subjected to further enzymatic assays (**Figure 3.5 B**). Over fifty colonies were picked randomly and subjected to further enzymatic assays. Fourteen strains for the FL-GalNAc (MG strains) and four strains for the FL-GlcNAc based screen (MC strains) were studied using a 4-MU substrate end-point assay as previously described. From the results, we conclude that mutants that show increased activity on its screened compound, also show increased activity in other cell-wall degrading enzymes, as shown by additional 4-MU substrate end-point assays. When sorted based on FL-GlcNAc activity, *MC1*, *MC2* and *MC4* showed significantly improved enzymatic activity over wild-type (**Table B.4**). When sorted based on FL-GalNAc activity, *MG1*, *MG10*, *MG11*, and *MG12* showed increase activity in all three enzyme families (**Table B.5**). We identified three strains (*MG10*, *MG11*, and *MG12*) with $\sim$ four-fold improvement in chitinase activity over the wild-type strain and *MC2* with a 1.5 fold improvement. These results indicate that sorting based on end-point fluorescent measurement of a droplet based enzymatic assays of long-term droplet incubated filamentous fungi, is representative of the actual enzymatic activity confirmed in deep-well micro well plates. We then performed a biocontrol assay with mutant strains that showed increased enzymatic activity, to evaluate their ability to control plant pathogens *Fusarium graminearum* and *Botrytis cinerea*. *Fusarium* cultures in culture filtrate of *C.rosea* mutants *MG8* and *MC2* have a lower average dry weight compared to the wild-type inoculants, and these mutants show to have an effect and minimize biomass production. However, none of the mutants showed a significant strong biocontrol ability to either *Fusarium* or *Botrytis* (N=3, paired t-test, P $>$ 0.05) (**Figure B.20**).[212] From differentially expressed gene analysis, it is known that *C.rosea*'s regulatory response to

confrontation with pathogens is widely varying and there's upregulation of genes coding for proteins beyond cell-wall degrading enzymes, such as ABC transporters, membrane proteins, proteases, and secondary metabolites.[212, 211, 248] For cell-wall degrading enzymes, the response is also pathogen dependent, as Nygren et al. [248] showed a GH18 killer toxin-like chitinase *ChiC1* being induced upon confrontation with *F.graminearum*, but not with *B.cinerea*, while killer toxin-like chitinase *ChiC2* shows upregulation in the presence of *B. cinerea* and *R. solani* but not against *F. graminearum*.[212, 248] The results of our biocontrol assay indicate high chitinase activity mutants do not show increased activity of a pathogen specific chitinase. The successful microfluidic sorting based on a single enzymatic substrate lacks enzyme specificity, but could be used to speed up the process to find candidates for further research into complex phenotypic traits and transcriptomic analysis. Further investigation into expanding the repertoire of substrates and enzymes for the droplet based assays and looking into the expression of cell wall degrading enzymes in the selected *C.rosea* mutants via transcriptomics (or other gene expression studies) can offer a better insight into their bio-control ability.
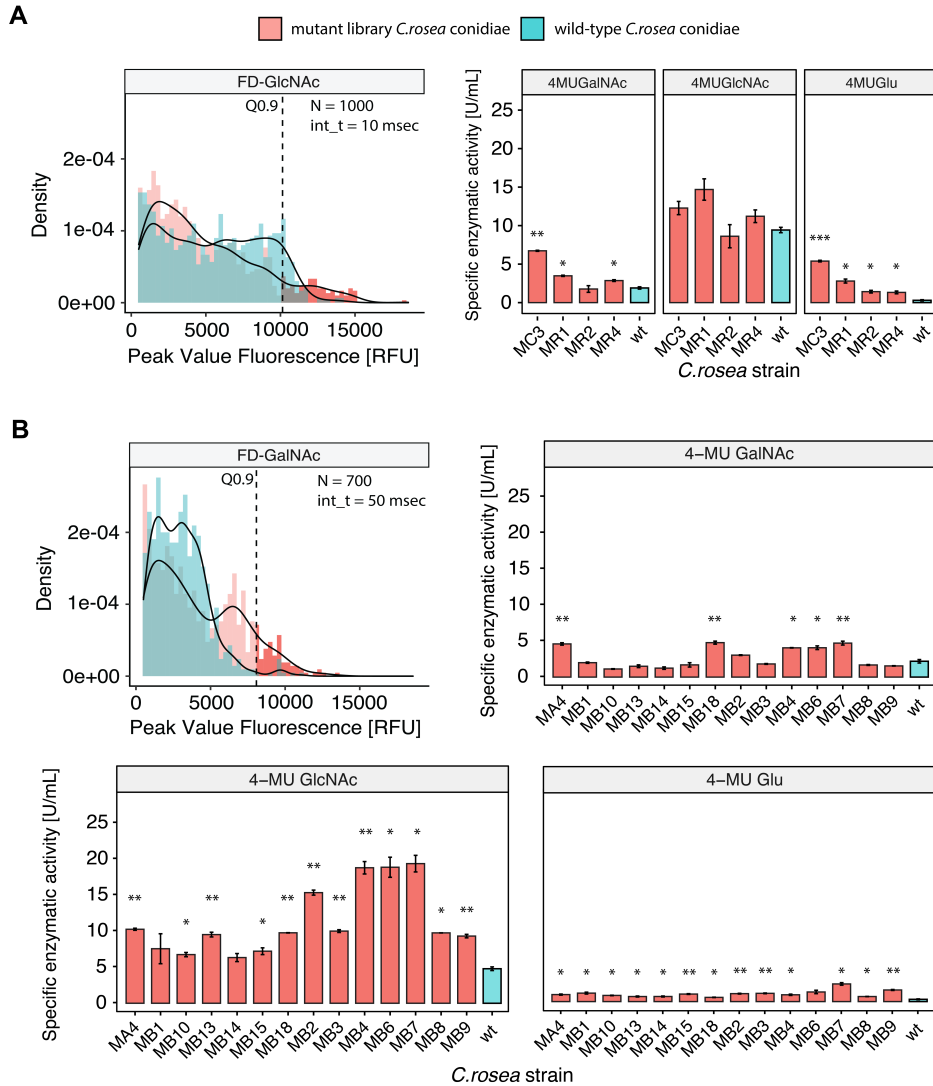
Figure 3.5: Sorting and recovery of *C. rosea* mutants based on cell-wall degrading enzyme (CWDE) activity. Peak intensity histogram and enzymatic assays using (A) FL-GlcNAc or (B) FL-GalNAc as the substrate for single spore libraries. For the histogram, fluorescence intensity of each droplet in a mutant population (shown as red) and a wild type (shown as blue) population incubated at 27 °C. Intensity of peaks between the wavelengths 510 nm and 520 nm were used for gating. To sort droplets, the intensity gate was set at the 0.9 quantile of the mutant population fluorescence (shown by the dotted line). Total number of peaks (N) and integration time are indicated on the plot. The top 10% droplets were recovered on plates and cultured to obtain distinct mutant colonies (MG for the FL-GalNAc sorted spores, MC for the FL-GlcNAc sorted spores). For enzymatic assays, three cell-wall degrading enzymes were assayed for on recovered strains: 4MU-GlcNAc (indicating chitinase activity), 4MU-GalNAc (indicating N-aceylgalactosaminidase activity) or 4MU-Glc (indicating β-1,3-glucanase activity). Values were obtained through an end-point enzymatic assay (pH 5.1, 30 min) with N= 3. Error bars are representing one standard deviation, paired t-test against WT, * P < 0.05, ** P < 0.01.

3.3 Conclusion

In this study, a novel filamentous fungi high-throughput screening approach was developed using a solid-state fermentation droplet incubation method and an electrostatic low-voltage droplet microfluidic sorter. The system was established using *C.rosea*, and successfully screened for high performing cell wall degrading enzymes. Compared with the traditional screening methods available for high-throughput screening of filamentous fungi, this method greatly increases the screening speed and reduces the labour and tedium associated to testing secreted proteins in fungi. To our knowledge, this is the first filamentous fungi microfluidic sorting work that shows advancement in long-term droplet culture based on solid-state fermentation, and a sorting method particularly designed to handle fungal droplet libraries. Compared to current filamentous fungi screening techniques available, the 7 Hz throughput is faster than macroscale high-throughput well-plate based methods, and comparable to the previously reported microfluidic methods for fungal screening. Given our longer incubation times ($>$ 3 days), we resolved enzymatic activity in *C.rosea*, which was previously hard to demonstrate with single spore libraries. We believe our system is the first step to further explore solid-state fermentation methods in nano or pico-liter sized droplets and to further investigate the effect of long term incubation on screening methods. Beyond electrostatic or DEP based sorting, the screening strategy we present here could be applied to other filamentous fungal strains and enzymes using other fluorescein based substrates, and can thus be used for many industrial biotechnology applications.

3.4 Experimental section

3.4.1 Reagents and materials

Fabrication materials for microfluidic devices include a transparent photomask (CAD/Art Services Inc., Bandon, OR), S1811 positive photoresist coated glass slides (Telic, Valencia, CA, USA), MF321 developer (Rohm and Haas, Marlborough, MA, USA), CR-4 chromium etchant (OM Group, Cleveland, OH, USA), AZ-300T photoresist stripper (AZ Electronic Materials, Somerville, NJ, USA),
$< 100 >$ Si wafers (Silicon Valley Microelectronics Inc., Santa Clara, CA, USA), Indium Tin Oxide coated

glass (Delta Technologies, Loveland, CO), SU-8 5, SU-8 2075, and SU-8 developer (Microchem, Westborough, MA, USA). Optical fibers, short pass filter were obtained from Thorlabs (Newton, NJ, USA). Polydimethylsiloxane (PDMS, 184 Sylgard) was purchased from Dow (Toronto, ON, CA) and chlorotrimethylsilane from Sigma-Aldrich (Oakville, ON, CA). Polylactic acid (PLA) material for 3D printing was purchased from Shop3D (Mississauga, ON, Canada). DI Water had a resistivity of $15 M\Omega cm^{-1}$.

Reagents for device operation include 3M Novec HFE7500 engineering fluid and the surfactant 3M Novec 1720 (M.G. Chemicals, Burlington, ON, CA), PEG fluoro-surfactant dissolved in HFE7500 (20 g of 5%wt) (Ran Biotechnologies, Beverly, MA, USA). All liquids were filtered prior to use with a Nylon filter cartridge ($0.22 \mu m$, Millex $^{®}$ GP, Millipore). All glass syringes were from Hamilton (Reno, NV, USA). All tubing and fittings were sourced from IDEX Health & Science LLC (Oak Harbor, WA).

Fluorescein and 4-Methillumbeliferyl based fluorescent substrates, chitin, Bradford assay reagent and all other cell culture and assay reagents were acquired from Sigma-Aldrich (Missisauga, Canada), unless specified otherwise

3.4.2 Microorganisms and culture conditions

Clonostachys rosea cultures were obtained from a commercial source. *Fusarium graminearum* DAOMC 215630 and *Botrytis cinerea* DAOMC 143576 were obtained from the Canadian Collection of Fungal Cultures (Ottawa, CA). All fungi were cultured on potato dextrose agar (PDA) or in potato dextrose broth (PDB), with 0.05 g L^{-1} chloramphenicol, at 27 ^{o}C with 12 h light/dark cycles. For *Clonostachys rosea* cultures, after around 3 weeks, dark green aerial conidia formed. The conidia were harvested by washing each culture with sterile 0.01% Tween-80 in ddH$_2$O, filtering the conidia through a 10 μm filter (Pluriselect, CA, US), centrifugation (8000 rpm, 2 min) and resuspension in the Tween-80 solution. The spore stock solution concentration was determined with a hemocytometer, and was kept at 4 ^{o}C until further use for up to 2 weeks. A mutant conidia library was generated by UV mutagenesis. Ten mL of a 5 x 10^7 spores/mL suspension were spread in a sterile petri dish and treated under UV light (254 nm, 100 mJ/cm^2) (UVP HL-2000 Hybrilinker cross-linker). Suspensions were kept in the dark and a small aliquot was taken, serially diluted in sterile water and spread on PDA plates to evaluate the number of viable spores. The remainder of the UV-treated suspension was plated on PDA, and germinated at room temperature for 10-14 days. Aerial spores were collected and the library was finally stored at -80 ^{o}C in 25% glycerol.

3.4.3   Enzyme production media

Minimal media (MM) was used as the base media for incubation in droplets and was adapted from Mania et al. (2010) with an EDTA based Hutners Trace element solution and 0.05% chloramphenicol.53 As a carbon source, the MM was supplemented with either glucose or colloidal chitin (1% w/v). Cell wall degrading enzyme production by *C. rosea* was induced by culture in liquid MM without glucose, and 1 % w/v colloidal chitin as carbon source. Colloidal chitin also served as a solid-state fermentation support. Colloidal chitin for enzymatic assays and droplet based assays was produced following Wu, Cheng and Li's (2019) method, dissolving chitin (enzymatic assay grade) in 1M HCl overnight at 40 ^{o}C.[207] The solution was centrifuged and neutralized by washing with distilled water until a pH of 2-4 was reached. The final wash was performed with 2X MM and the colloidal chitin was formulated to a 2% w/v solution in 2X MM. Colloidal chitin for the biocontrol assay was produced following Subramanian et al (2020) method [249], by dissolving chitin (practical grade) 1:10 in HCl (1M) while stirring, and incubating overnight at 40 ^{0}C. The colloidal chitin was precipitated by slowly adding five volumes of chilled ethanol, with constant stirring at 4 ^{0}C. The solution was centrifuged, and neutralized by washing with sterile distilled water and addition of sodium acetate. The supernatant was discarded, colloidal chitin pellets were dried and a 1%w/v colloidal chitin in MM was formulated for the biocontrol assay.

3.4.4   Well-plate enzymatic assays

For an end-point enzymatic assay, CCMM or PDB was inoculated with a 5 x 5mm mycelium stab of one week old cultures, and maintained in static culture at 27 ^{o}C for five days in a 2mL 96-well deep well plate. Cell free enzyme containing supernatant was collected by centrifugation (4000 rpm, 4 min) and filter sterilization of the supernatant (0.22 μm). The supernatant was kept at 4 ^{o}C until use. Three 4-methyllumbelliferyl enzymatic substrates – 4-methyllumbelliferyl-N-acetyl-β-D-glucosaminide (4-MU-GlcNAc), 4-methyllumbelliferyl-N-acetyl-β-D-galactosaminide (4-MU-GalNAc) (BioSynth Carbosynth, UK), 4-methyllumbelliferyl-β-D-glucopyranoside (4-MU-Glc) (BioSynth Carbosynth, UK) – were dissolved to a 500 mM stock concentration in DMSO. A 50mg mL^{-1} 4-MU standard stock solution was prepared in methanol. For the end-point assay performed on mutant or wild type *C. rosea*, a standard clear 96-well plate was loaded with each well containing a substrate at final concentration of 0.5 mM in a sodium acetate buffer (pH 5.1) (75 μL) and the sample supernatant or standard (1.9 nmol mL^{-1})(25 μL) , and incubated for 30

min at 37 ^{o}C . A stop solution of 100 μL sodium carbonate (0.4 M) was added, and the relative fluorescence was measured at 360 +- 20 ex / 450+-30 em (40 flashes per well, 200 rpm orbital shaking before each measurement) in a fluorescent well-plate reader (ClarioSTAR®, BMG Labtech). Background fluorescence was subtracted. To calculate enzymatic activity (U mL^{-1}), the following equation was used:

$$\text{Enzymatic activity} \left(\frac{\text{U}}{\text{ml}} \right) = \frac{1.9 V_T DF \left(FLU - FLU_{\text{blank}} \right)}{FLU_{\text{std}} \, t V_{\text{sample}}} \tag{3.1}$$

where FLU fluorescence of the well (RFU), FLU$_{\text{blank}}$ fluorescence of the substrate working solution (RFU), the final reaction volume (mL) , DF the enzyme dilution factor, FLU$_{\text{std}}$ the fluorescence of the Standard Solution minus the fluorescence of the Standard Blank, t the incubation time of 30 mins (min), V$_{\text{sample}}$ the volume of the sample in the well (mL). One unit of enzymatic activity will release 1 umole of 4-MU from the appropriate substrate per minute at pH 5.0 at 37 ^{0}C. A BCA total protein assay was performed on the same supernatant (Pierce$^{\text{TM}}$ BCA Protein Assay Kit, Thermo Scientific).The relative fluorescence was divided by the total protein content (determined using a bovine serum albumin standard curve).

For a kinetic enzymatic assay representative of droplet incubation, CCMM or MM (1% w/v glucose) was inoculated with 0.5 10^{7} spores mL^{-1} wild-type *C.rosea* per well. Three fluorogenic substrates – fluorescein N-acetyl-β-D-glucosaminidase (FL-GlcNAc) (Abcam, Waltham, MA, USA), fluorescein-N-acetyl-β-D-galactosaminidase (FL-GalNAc) and fluorescein-di-glucopyranoside (FD-Glc) - were dissolved in DMSO to obtain a stock concentration of 100 mM. The substrates were dissolved in ddH$_2$O and mixed with the samples to a final concentration of 100 μM. The assay was carried out overnight (16 hrs) in a 50 μL half area flat bottom dark well plate (Greiner Bio-One, AT) incubated at 27 ^{o}C in a fluorescent plate reader (ClarioSTAR®, BMG Labtech) and measured at 485+-15 ex / 530+-10 em (100 flashes per well, 200 rpm orbital shaking before each measurement).

3.4.5   Device fabrication and optical fiber setup

The microfluidic sorter was fabricated using standard photolithography and soft-lithography methods. Photomasks were designed using AutoCAD 2019. The co-planar sorter device, electrode and dielectric layer fabrication followed standard photolithography procedures reported previously.[227] Briefly, chromium-coated glass slides (50 x 75 mm), with S1811 positive were exposed (5 s at 38-50 mW cm^{-2}), developed in MF-321 developer, etched with CR-4 chromium etchant, and stripped with AZ-300T photoresist stripper.

For the dielectric layer, the resulting patterned electrode substrate was placed under plasma oxygen (Harrick Plasma PDC-001, Ithaca, NY) for 1 min 30 s, after which they were immediately spin coated with an SU-8 5 layer (10 s, 500 rpm, 30 s 2250 rpm), soft baked, and exposed to a sawtooth patterned mask. After post-bake, substrates were developed, rinsed with isopropyl alcohol, and underwent a hard baked cycle (180 ^{o}C, 10 min, gradual ramping). For the channel layer of the sorter device, a 4" Si wafer was treated under plasma oxygen for 1 min 30 s. SU-8 2075 was spin coated (500 rpm 10 s and 3250 rpm 30 s) to obtain an 70 μm layer, followed by a baking and exposure cycle according to the manufacturer datasheet. A second layer of SU-8 2075 was spin coated on top of the undeveloped first layer (500 rpm 10 s and 2250 rpm 30 s) to obtain a 90 μm thick layer. After pre-exposure bake, the second layer mask was feature aligned and exposed (UV-KUB 2, Kloé, France), followed with baking and development according to the manufacturer datasheet. The resulting master mold was exposed to chlorotrimethylsilane vapour deposition in a desiccator for 45 min. PDMS (1:10 w/w ratio curing agent to prepolymer), was poured over the mold and left to cure in an oven (65 ^{o}C, 3 hrs). PDMS layers were cut to size with an X-Acto knife. Inlets and outlets were made using 0.75 mm or 0.35 mm biopsy punchers (World Precision Instruments, FL, USA), fitting 1/32" OD tubing or 360 μm OD tubing respectively, after which the PDMS was carefully washed with IPA, ddH2O, air dried, and cleaned with tape to remove dust before device assembly. The PDMS channel layer was treated with oxygen plasma for 30 sec. Immediately after, the sorter was manually aligned with the dielectric coated electrodes under a dissecting fluorescence microscope (Olympus IX73, 10X). Device channels were then treated with Novec 1720 fluorosilane polymer surfactant [227]. Two flat cleave multi-mode optical fibers were prepared for droplet excitation (100 μm core, 0.22 N.A.) and detection (400 μm core, 0.49 N.A.) (Thorlabs, NJ, US). The cladding was stripped off, the fiber core was polished, cleaned and carefully inserted into the respective optical fiber channel. Fibers were then fixed with Kapton tape. To retrieve droplets from the sorter, two 3 cm pieces of PEEK tubing (360 μm OD) were cut and treated with similar Novec 1720 treatment. Outlet blockers were made by hot gluing one end of a 1" PEEK 1/32" OD tubing.

3.4.6   Microfluidic sorting setup and operation

Gastight 500 μL glass syringes were prepared with fittings and tubing as reported previously. 30 The spore containing syringe and the syringe for droplet reinjection were set up with a 1/32" OD , 0.381 mm ID PEEK tubing. All other syringes had a 1/32" OD , 0.127 mm ID tubing. Syringes were installed on a low-pressure neMESYS pump system (Cetoni, Korbussen, DE), and the spore containing syringe was

continuously stirred using a syringe stirrer (Nannostirus, V&P scientific, San Diego, CA, USA). The sorting device with installed optical fibers, was fixed in a 3D printed holder, and clamped in place with a pogo pin PCB providing contact with the electrode pads. The holder base plate fits in the scanning stage (XYZ Tango, Marzhauser, Wetzlar, DE) of an inverted epi-fluorescence microscope (Olympus IX78, Olympus, Montreal, Quebec, CA). For a description of the Arduino driven electrode control system, see SI. Next, the SMA end of the excitation fiber was coupled to a 500 nm short-pass filter in an in-line fiber optic filter mount (Thorlabs, NJ, US), connected to a high power (1mW) 470 nm fiber coupled LED light source. The SMA end of the emission fiber was coupled to a portable mini-spectrometer (FLAME-S UV-VIS, Ocean Insight, NY, USA). The flow inside the microfluidic channel was observed under a 4X or 10X objective under bright-field illumination. The spectrometer, pressure driven fluid flow and electrode actuation were controlled using an in-house Python based automation system and graphical user interface.

3.4.7   Spectrometer data processing

The raw spectrum was obtained by using the Seabreeze Python library and reading intensities [A.U.] in a threaded Python process. The SciPy signal processing library was used for spectrometer signal denoising and peak detection. Background subtraction was used to remove excitation signal noise and background light, and absolute values of resulting arbitrary fluorescence values were stored in a list as follows:

$$I = |I_{n-1} + (I_n - I_{\text{dark}})| \tag{3.2}$$

with I the raw intensity [R.F.U.] values from the spectrometer. For signal denoising, a third order Butterworth lowpass filter with 0.1 cut-off frequency (normalized) (f_c) was applied to the intensity spectrum (user set). The processed arbitrary fluorescence values, and gating area were plotted on a live plot. Peaks in the processed intensities list were detected based on height, peak base width, vertical distance to neighbouring peaks and peak prominence. Gated peaks were filtered to be within a certain wavelength and intensity range (user set gate), above the user set noise level. When the sorting process was started, the CE is turned on, all peaks are being detected, and the pulsing electrode (PE) is switched on when a gated peak was detected. All detected peaks were stored in a data file listing peak intensity and peak wavelength, which was converted to a csv file for generating gating plots.

3.4.8 Sorter characterization

Sorting efficiency was determined by a two-factor experiment with binary response. Both the applied AC signal amplitude (10 kHz, sine wave, 50 mV$_{PP}$ - 550 mV$_{PP}$, 7 levels) and the spacer oil speed (5 - 100 nL s^{-1}, 20 levels) were varied. Droplet generation was kept stable (water: 0.5 nL s^{-1}), oil: 1 nL sec^{-1}). Droplets were sorted by actuating the pulsing electrode (PE) while keeping negative channel electrode (CE) on. Out of 10 sorting attempts, the successes were counted, and the sorting efficiency was calculated in terms of percentage. To determine the effect of sorting polydisperse solutions, two conditions in the efficient sorting regime were chosen (350 mV$_{PP}$, 60 nL s^{-1} and 450 mV$_{PP}$, 80 nL s^{-1}) and the droplet volume was varied. Droplet area was measured using Fiji (ImageJ) and approximated by height of 70 μm. To optimize the efficiency of autonomous sorting, the droplet travel time between excitation point and sorting location was experimentally observed, by varying the oil flow rate and recording high speed image series (30 msec/frame) (Hamamatsu Flash LT+ 4.0, Hamamatsu, JP). For optimising the autonomous sorting, a mixed population of ddH$_2$O and 50 μM or 100 μM analytical standard fluorescein droplets in 2% Ran HFE 7500 oil was generated using a dual T-junction droplet generator, and transferred to the sorter using 360 μm OD PEEK capillary tubing. For each concentration fluorescein, a gating histogram was made by recording 500 positive peaks above a set noise level and within a wavelength range of 500-600 nm.

3.4.9 Sorting and recovery of glucoside hydrolase producing *C.rosea* strains

Before use, the colloidal chitin minimal media (CCMM) was filtered through a 40 μm filter. For droplet incubation, mutant or wild type spore stock solution was diluted in 2X CCMM to a final concentration of 0.35 x 10^6 spores/mL (λ = 0.35, Poisson distribution). Single spore encapsulation was performed, by mixing 0.35 x 10^6 spores mL^{-1} in 2X CCMM (30 nL s^{-1}) with 200 μM fluorescein substrate (30 nL s^{-1}) using a microfluidic mixer T-junction droplet generator (1% Ran HFE 7500 oil at 60 nL s^{-1}). Droplets were retrieved into a PCR tube containing 50 μL 2% Ran HFE 7500, and incubated in the dark at 27 ^{o}C for enzymatic production. After the appropriate incubation time, droplets were aspirated (0.2 μL s^{-1}) using a syringe pump, and injected into the microfluidic sorter (0.01- 0.02 μL s^{-1}). Autonomous sorting was performed at a sorting regime (oil flow rate and potential) with efficient sorting. Droplets from the positive outlet were recovered in a capillary or PCR tube, then plated on PDA (not more than 10 to 20 droplets per plate), and incubated at 27 ^{o}C. Mutant colonies were transferred to individual plates before neighbouring

hyphae touched (after around 3-4 days). Cultures were maintained for further assays. Glycoside hydrolase activity of recovered mutants was confirmed with a 4-MU and Bradford assay as described above.

3.4.10   Biocontrol assay

In a liquid culture filtrate assay, plant pathogen growth inhibition by *C.rosea* produced enzymes was measured. A 50 mL round bottom test tube with 30 mL 1X CCMM was inoculated with a 5x5 mm agar mycelium plug of a recovered *C.rosea* mutant or wild-type, and incubated at 27 ^{0}C for 7 days. The media was filtered (0.45 um), and 5 mL of PDB was added. The culture filtrate was inoculated with a 5x5 mm agar plug of active *Fusarium graminearum* DAOMC 215630 or *Botrytis cinerea* DAOMC 143576 culture (5 days old) and incubated at 27 ^{0}C in the dark on a rotary shaker (200rpm) for 5 days. To measure biomass production, the cultures were vacuum filtered through Wattman grade 2 paper, and the filter paper was dried overnight in an oven (65 ^{0}C). Mycelial dry weight was measured in triplicates and filter paper weight of a media control was subtracted.

3.4.11   Modeling and data analysis

Data analysis was performed with Fiji, Python 3.9 and R v3.6.2. Metadata of high-speed camera was exported using Fiji by ImageJ, and further analyzed with Python, to obtain the time it takes for a droplet to follow a specific path length. Droplet area was calculated using Fiji. Applied electrical signal was measured using an oscilloscope. Heat transfer, fluid and electric field simulations were performed with COMSOL Multiphysics v5.4 (**Appendix B.3**). All in-house code was written in Python 3.9, and is published under GNU GPL v3.0 on our repository (`https://bitbucket.org/shihmicrolab/fungalmicrofluidics/`).

Chapter 4

Droplet-digital sorting, mixing, incubation, and droplet generation for screening yeast

Abstract

Droplet microfluidics is a technique that has the ability to compartmentalize reactions in sub nano- (or pico-) liter volumes that can potentially enable millions of distinct biological assays to be performed on individual cells. In a typical droplet microfluidic system, droplets are manipulated by pressure-based flows. This has limited the fluidic operations that can be performed in these devices. Digital microfluidics is an alternative microfluidic paradigm with precise control and manipulation over individual droplets. Here, we implement an integrated droplet-digital microfluidic (which we call 'ID2M') system in which common fluidic operations (i.e. droplet generation, cell encapsulation, droplet merging and mixing, droplet trapping and incubation, and droplet sorting) can be performed. With the addition of electrodes, we have been able to create droplets on-demand, tune their volumes on-demand, and merge and mix several droplets to produce a dilution series. Moreover, this device can trap and incubate droplets over several days (> 48 h) that can consequently be sorted and analyzed in multiple n-ary channels (as opposed to typical binary channels). The ID2M platform has been validated as a robust on-demand screening system by sorting fluorescein

droplets of different concentration with an efficiency of ~ 96 %. The utility of the new system is further demonstrated by culturing and sorting tolerant yeast mutants and wild-type yeast cells in ionic liquid based on their growth profiles. This new platform for both droplet and digital microfluidics has the potential to be used for screening different conditions on-chip and for applications like directed evolution.

4.1   Introduction

Droplet microfluidics involves monodisperse aqueous droplets that are generated by a pressure-driven flow in a continuous oil phase where droplets are typically analysed and manipulated at very high rates ($>$ 1000 droplets per second). The use of droplet microfluidic technology has enabled a wide variety of applications, specifically in the area of high-throughput chemistry and biology.[4, 250, 251, 252] This two-phase microfluidic format can undergo a number of different fluidic operations – droplet generation, encapsulation, mixing, and sorting. Sorting is in particular an important operation that allows selection of subpopulation of cells, DNA, and biomolecules in the droplets.[253, 170, 30] A variety of sorting methods have been shown in literature using dielectrophoresis, magnetic, thermal, or acoustic methods.[254, 255, 256, 257] Each of these have their own advantages in terms of speed, reliability and ease of implementation. However, typical sorting methods are usually based only on binary sorting – i.e. sorting droplets that are based on two levels of output - which can limit the range of detecting rare events and to sort based on different constituents in the droplet (e.g., multiple concentrations of an additive).

There is an alternative type of microfluidics that enables on-demand droplet control called digital microfluidics. [13, 26] This platform allows manipulation of discrete droplets by electrostatic forces on an array of electrodes coated with an insulating dielectric. One of the main advantages of DMF is it facilitates precise control over many different reagents simultaneously and independently, by application of potentials (or by acoustic and contactless methods [258, 259, 260]). This has enabled DMF to be a well-suited platform to carry out many different types of applications, namely, cell-based assays [37, 261], synthetic biology [262, 110] and point-of-care diagnostics [263, 264]. Most of these types of applications are configured in a two-plate format, in which droplets are manipulated between a top and bottom substrate bearing a ground and driving electrodes respectively. There is another digital microfluidic configuration in which droplets are actuated on a single substrate with co-planar configuration of electrodes. Although in this configuration droplets lack the capacity to dispense, this format does allow better mixing which is useful in applications

carrying out chemical reactions.[265, 266] Likewise, it may be useful to couple single-plate DMF with microchannels as a chemical pre-processing unit without the need for pre-column reactions since DMF can rapidly mix different analytes in seconds and separated using the channels.[111, 112] The idea of integrating DMF with other microfluidic paradigms is an exciting innovation as it combines advantages of both systems while minimizing the disadvantages of the individual systems.

The work reported here combines the use of single-plate DMF and droplet-in-channel microfluidics. Our work joins a group of studies that have used digital microfluidics and combined it with other microfluidic paradigms.[111, 112, 107, 101, 267]. In most of these studies, DMF was integrated with microchannels and is used to control bulk fluid flow or for pre-separation of chemical reactions. There is one group (to our knowledge) that have implemented DMF with droplets-in-channel microfluidics. The Mugele group,[103, 101] have discussed the physical phenomenon behind the integration of electrowetting with microfluidics to control the size and frequency of drop formation and the binary sorting of droplets. We present a method that includes several advances relative to the methods described by Mugele et. al., including the integration of on-demand droplet generation with n-ary sorting (as opposed to binary [24, 109]) on the same device (which we call integrated digital-droplet microfluidic – ID2M). Furthermore, additional advancements of the device includes other important and essential operations for typical droplet-based microfluidic assays. (1) On-demand droplet mixing enabling control and creation of different concentration of droplets. Typical droplet-in-channel techniques have depended on fusion [268] or picoinjection [269] methods for mixing but these techniques only allow one reagent addition to an existing droplet and require exquisite control over flow rates, timing, and fluidic resistance. Our integrated device can create a range of different concentrations with multiple additions of reagent droplets by application of an electric potential without any consideration for other parameters (e.g., timing). (2) We also include areas for trapping and incubation of droplets in which droplets can be individually trapped and incubated for > 48 h. To date, this has not been shown on such a device and does not require delay lines [270, 271] or on- and off-chip reservoirs for incubation [272, 273]. Finally, we show the utility of our system by applying it to a biological study (instead of manipulation of water and oil [111, 112, 107]) that examines mutant and wild-type yeast cells under ionic liquid conditions which can be useful for applications related to biofuel production. We believe this is an important step in the field of digital and droplet microfluidics as this can possibly enable more control for droplet microfluidic devices while increase droplet throughput for digital microfluidic devices.
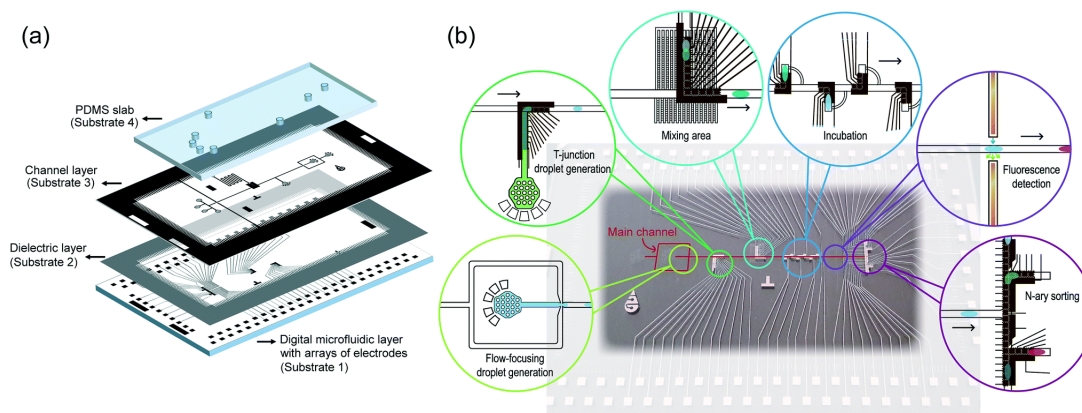
Figure 4.1: ID2M microfluidic device. (a) Exploded view of the ID2M microfluidic device. The bottom layer is the digital microfluidic (DMF) configuration which is covered with a dielectric SU-8 layer ~ 7 μm thickness. The channel layer with 300 μm wide and 110-120μm high was fabricated on top of this layer. A PDMS slab of thickness ~ 5 mm was bonded to seal the channel layer. (b) A photo of the device with schematics depicting the operations of the device, namely droplet dispensing (using T-junction and flow focusing), droplet mixing, droplet incubation, droplet detection, and droplet n-ary sorting. Highlighted in red shows the main channel on the device in which droplets are transported from one region to another. Mixing area contains sinking channels to reduce the oil flow rate. Reproduced from Ref. [108] with permission from the Royal Society of Chemistry.

4.2 Results and discussion

4.2.1 Device characterization and optimization

We have developed a new microfluidics architecture called ID2M, merging droplet microfluidics (useful for generating and sorting droplets) with digital microfluidics (useful for on-demand droplet manipulation and individual control of droplets). The ID2M device were formed by creating a single-plate DMF device (i.e. the ground and driving electrodes are co-planar) and fabricating a network of channels on top, with inlets and outlets for generating and sorting droplets respectively, and an area for droplet mixing. An exploded view (**Figure 4.1 A**) shows the digital microfluidic device as the bottom substrate with 104 patterned electrodes, the dielectric layer (substrate 1 and 2), the network of channels patterned in SU-8 photoresist, and a slab of PDMS with inlets and outlets (substrates 3 and 4). This multilayer integrated architecture facilitates pressure-based and on-demand droplet generation using flow focusing and T-junction configurations respectively, on-demand droplet mixing, on-demand droplet trapping and incubation, and on-demand droplet sorting. The combined multilayer architecture represents a significant advance over other types droplet-to-digital methods which relies on two separate design configurations which can cause difficulties in moving the droplet from one platform to the other as reported previously.[263, 264, 265, 110] Droplets in the main channel are moved by pressure flow and electrical potentials move droplets to the mixing, incubation,

and sorting regions (i.e. away from the main channel) (**Figure 4.1 B**). A central feature of this design is that droplets in the main channel can be moved to the mixing area to merge with other droplets. For example, a droplet containing dilution buffer is generated on-demand via actuation from the T-junction, then actuated to the mixing area, and merged and mixed with other droplets in the main channel. This process can be repeated to create of a diluent series of droplets. After generating the diluent droplet, these droplets can be actuated to the main channel and can be incubated in the trap and sorted in one of the channels (after incubation) using electrostatic actuation. Typical droplet microfluidic systems use electrocoalescence [274, 275] or picoinjection [269, 276] techniques to sequentially add reagents to droplets at different times. However, these techniques, as of yet, have not demonstrated the generation of a dilution series of droplets. In addition to generation of a diluent series of droplets, the droplets are capable to be sorted in four different channels. This allows for droplet samples to be sorted by multiple conditions based on a larger gradient, like multiple levels of fluorescence and absorbance, instead of typical binary sorters. This suggests that using a system (such as ID2M) can provide direct droplet control that enables generation of a droplet dilution series and droplet sorting in multiple fractions for droplet microfluidic systems.

Electrode shape and design is important to ensure high-fidelity droplet movement on the device (**Figure 4.1b**). In initial electrode designs, we followed an one electrode design on the bottom plate with alternating ground and driving potentials.[103, 277] However, droplets in the main channel were not able to overcome the pressure generated from the oil flow rate and could not be actuated into the mixing, incubation, or different sorting regions. A co-planar electrode configuration (i.e. with adjacent ground and actuated electrodes on the same plane), as shown by some groups [111, 278, 25] showed optimal droplet manipulation. The introduction of a ground electrode (or grounding line) on the same plane may not generate the highest applied force as compared to other electrode designs [111], but the selected design is easiest to fabricate and is capable to overcome the applied pressure on the droplet in our system (oil flow rate of 0.005– 0.05 μL/s).

The fabrication protocol for the ID2M devices needed to be optimized to ensure strong adhesion of the dielectric, channel, and PDMS layers during fabrication, and to allow droplets to be controlled by application of electric potentials in the in the mixing area. For the former challenge, we found that introducing 300 μm spaced repeated finger-like structures on the boundary of the dielectric layer increases adhesion to the substrate (**Figure C.4**). We observed that SU-8 5 tends to peel or crack easily in the absence of finger-like structures, or if the repeated finger like structures are spaced far apart (> 500 μm). We hypothesize these cracks are mostly made by internal stresses as high evaporation and heating/cooling rate in addition to

temperature differences in different layers of SU-8 5 causes residual stresses in the layer.[279] To increase the adhesion of the PDMS slab to the SU-8 layer, we used (3-aminopropyl)triethoxysilane (APTES) [280] vapor deposition after plasma treatment of the PDMS, the slab were exposed to the vapor of APTES in a desiccator for 30 min forming aminosilane molecule on the surface of the PDMS. This surface favorably reacts with the epoxy group from the SU-8 surface which strengthens the bond between the PDMS and SU-8 layer.

To slow down the flow rate and to enable droplets to be actuated from the main channel to the mixing area, we added sinking channels in the mixing area. We added multiple sink channels [281] to create flow eddies from the main flow channel which allow the oil phase to have multiple flow paths (**Figure 4.1 B** and **Figure C.5**). This reduction in oil flow rate enables droplets in the main channel to be actuated into the mixing channel. In our initial designs, we created a side channel (i.e. a channel branching out of the main channel) with the co-planar electrodes; however, droplets were not capable to be moved by actuation from the main channel to the mixing area. We explored increasing the voltage [281]; however the higher voltage tend to cause dielectric breakdown in the oil phase and cause droplet breakup which created small satellite droplets. The sink channels are particularly important when a droplet is already in the mixing area since the droplet acts as a plug (i.e. increasing the hydrodynamic resistance).[282] Since the hydrodynamic resistance in the mixing channel is higher than the main channel when a droplet is present, the generated droplets favour flow in the main channel. Alternatively, having multiple sink channels creates multiple flow paths (i.e. reducing the resistance in the mixing channel), leading to mixing of the droplets in this area.

An additional component for successful device operation was optimization of the configuration of the n-ary sorting channels. We initially tested with Y-shaped configuration, [253, 31] in which droplets are discriminated by two (or more [255, 283, 284]) physical characteristics. However, the Y-channels have a tendency to create a stagnation zone (i.e. an area where the droplet faces an uncontrolled choice for an outlet) even with the additional bias of the electric potentials. The additional bias also creates an asymmetric presence of drops (creating different resistances) when it is expanded to more than two channels.[24] Instead, we designed a symmetrical T-channel that consists of four different sorting areas with similar resistances. Pressure-driven droplets are detected using the optical interface and are biased directly to a channel by actuation. In the future, we may design rails [285] or linear electrodes [286] with the symmetric T-channels to reduce the footprint and to increase the number of sorting channels.

4.2.2 On-demand droplet generation, mixing, incubation, and sorting

The unique system that we have reported here enables integration of a variety of fluidic manipulations steps such as on-demand droplet generation, merging and mixing, and n-ary sorting. As shown in **Figure 4.2 A**, droplets can be generated through flow-focusing geometry or by on-demand generation using T-junction (Frame i, ii, and iii), stored (Frame iv and v), merged and mixed (Frame vi), incubated (Frame vii), and sorted (Frame viii and ix). The device can generate droplets on-demand by using a T-junction configuration which combines the pressure of the continuous oil phase and electrostatic actuation of the aqueous flow. As shown in **Figure 4.2 B**, the droplet volume generated by the T-junction can be tuned by only changing the oil flow rate (as opposed to tuning both aqueous and oil flows) [287, 288] and using actuation to move the aqueous flow. This setup enabled a wide range of volumes being generated (40-115 nL) by tuning the oil flow between 0.001 and 0.06 μL/s.

Figure 4.2: ID2M droplet operations. (a) Series of images from a movie (top-view) depicting the droplet operations on a device. Frames i-iii illustrate droplet generation from flow-focusing and on-demand (T-junction) techniques, and Frames iv – vi subsequent merging and mixing of droplets. Frames vii show droplet incubation (for incubating cells and other constituents) and Frames viii and ix show droplet sorting in four different channels. Fluids and droplets are highlighted for visual clarity. (b) Droplet size as a function of oil flow rate at a constant water flow rate (0.0005 μL/s) using flow-focusing and T-junction (on-demand) configurations. Each point represents 8 droplets sampled. The error bars represent one standard deviation.

As a comparison, we generated droplets hydrodynamically by changing the oil flow rate (while keeping the aqueous flow rate constant) which resulted in minimal changes in the volume when increasing the oil

flow rate > 0.01 μL/s. We hypothesize that traditional systems for tuning droplet sizes is limited by the orifice size and the relative strength of interfacial tension and hydrodynamic shear forces, [270] which can be alleviated using on-demand droplet generation. In addition to on-demand droplet generation, mixing and sorting are particularly useful capabilities, as most droplet microfluidic systems are incapable of generating dilutions of droplets and sorting them into multiple channels. In the design reported here, after droplet generation, droplets can be actuated to the mixing area and merged with another droplet (**Figure 4.2 A**, frame iv-vi) and transferred to the main channel area for sorting and analysis (**Figure 4.2 A**, frame vii-ix). To illustrate this, we used this method to generate calibration standards on this platform with sorting analysis.

Dilutions were formed by merging a droplet containing analyte (fluorescein) with a droplet of diluent (buffer). This merged droplet was mixed (by moving the merged droplet in a linear pattern – up-and-down – for several seconds [289]) producing a droplet with a 2x dilution of analyte. This droplet was analyzed by optical detection (**Figure 4.3 A**) and sorted for further processing. Subsequent droplets of analyte with different concentrations (4x and 8x) followed a similar protocol except the droplet containing fluorescein was mixed with two, three, or four droplets of diluent respectively (**Figure 4.3 B**). Note that this type of process, which includes on-demand droplet generation and mixing to create different droplets of different concentration of analytes was only made possible with the integration of digital microfluidics. Such operations were not possible with typical droplet microfluidic platforms unless we increase the number of inlets and injectors or reinject droplets into the device.[276] The devices used in this experiment were done in droplet-in-channels with minimal inlets, which allowed for a maximum 8x dilution of stock analyte. In the future, more dilutions could be implemented or mixing different types of analytes could be implemented by using these devices.
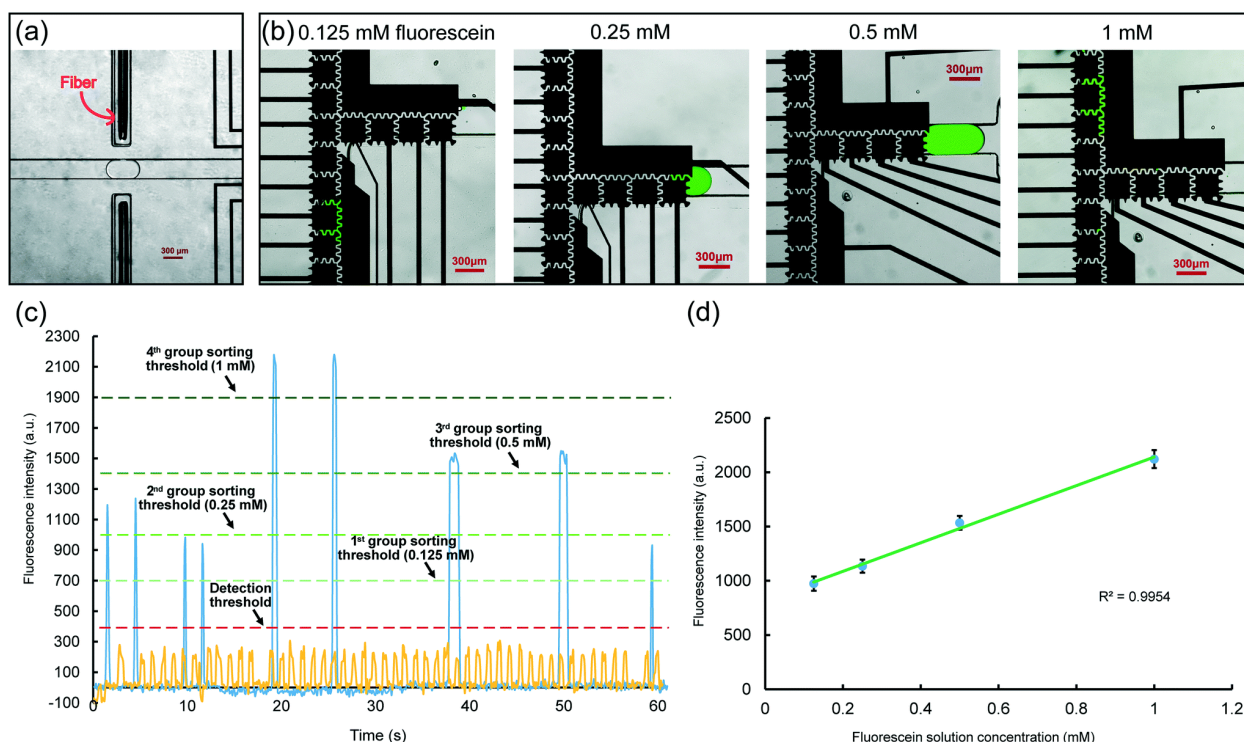
Figure 4.3: On-chip calibration. (a) Image of the detection region on the ID2M device. (b) Images of droplets containing fluorescein at four different concentrations (0.125, 0.25, 0.5, and 1 mM) being sorted into a respective channel. (c) Time series during a sort showing the fluorescence signal (blue) for four concentrations of fluorescein and for droplets with only diluent (i.e. no fluorescein, yellow). Each droplet containing fluorescein is sorted by their threshold fluorescence intensity values (green dashed lines). (d) A calibration curve showing the fluorescence as a function of fluorescein concentration. These average fluorescence values were used to create the threshold values for sorting. Error bars are ± 1 S.D. Reproduced from Ref. [108] with permission from the Royal Society of Chemistry.

Figure 4.3 C summarizes the results from the dilution series experiment with fluorescein. The emitted fluorescence from the droplet was detected by the spectrometer which outputted arbitrary units proportional to the emitted fluorescence of the droplet. As shown in **Figure 4.3**, the yellow curve depicts droplets that have minimal emitted fluorescence (i.e. droplets of diluent without fluorescein). The blue curve shows the fluorescence intensity for different concentrations of fluorescein. As expected, the highest fluorescein concentration (1 mM) showed the highest signal with a sorting threshold ~1900 arbitrary units and the lower fluorescein concentration (0.125 mM) showed the lowest signal with a threshold of ~ 700. A calibration curve (N = 10) was generated by plotting the ratio of analyte peak intensity as a function of analyte concentration (**Figure 4.3 D**). The precision in each measurement (RSD = 3.2%, 4.6 %, 7.5%, and 10.7% for the stock, 2x, 4x, and 8x dilution, respectively) and the correlation coefficient (R^2 = 0.99) demonstrates that the method is reproducible and linear. Furthermore, we measured the sorting efficiency by sorting positive-fluorescein (1 mM) vs. negative-fluorescein droplets and obtained ~96 % efficiency for positive

(i.e. fluorescent) droplets which is similar to other reported sorting efficiencies.[161]

4.2.3   ID2M application - effect of ionic liquid on yeast mutants

As an application of this work, we examined the effects of ionic liquid on wild-type and mutant yeast cells. Ionic liquid has been used as a promising pretreatment method for breaking down polysaccharides from typical feedstocks (e.g., lignin) for sustainable production of renewable biofuels. [290, 291] Typically, there has been a wide range of available ILs that are suitable for effectively breaking down the required biomass. [292, 293] However, a major disadvantage with typical ILs (especially imidazolium ILs) is their inherent microbial toxicity which can either arrest growth of microbial cells, like *E.coli* or *S. cerevisiae*, or inhibit biofuel-related enzymes which can reduce the overall yield of biofuel production. [294, 295] Hence, there is much interest in investigating the mechanisms of tolerance for microbes to different levels of IL.

Here, we compare the effects of IL on wild-type and mutant yeast cells and show the ability to interrogate each cell type with different IL concentrations and to sort cells based on their growth differences. To our knowledge, this is the first time that microbes have been cultured, mixed with ionic liquid and sorted based on multiple conditions (i.e. not binary). As a first step, we created a random mutant library (via ethylmethylsulfonate treatment) and verified their growth rates under IL conditions (**Figure 4.4 A**). We chose three types of yeast cells: wild-type and two best performing IL tolerant mutants and cultured them with and without 100 mM ionic liquid. As shown in **Figure 4.4 B**, the mutant cells grew at faster growth rates ($\sim$ 2.2 and $\sim$ 2.3 divisions per hour for mutant #1 and mutant #2, respectively) compared to the wild-type cells ($\sim$ 0 divisions per hour) in ionic liquid. In fact, the wild-type cells exhibited virtually no detectable growth in ionic liquid conditions. When cultured without ionic liquid, the wild type cells showed faster rates than both mutant cells ($\sim$ 3.4 and 3.7 divisions per hour for the mutants and $\sim$ 3.8 divisions per hour for the wild-type). The mechanisms of ionic liquid tolerance are still under debate, but we hypothesize that the location of the mutations in the yeast are in areas that are related to efflux pumps (i.e. to bring IL in-and-out of the cells) [296] and to transcriptional regulators that are related to stabilizing stress response [297]. Clearly, more work is required to determine the genotype location of the mutations (i.e. single-cell sequencing) [298], but this experiment confirmed that we are capable of obtaining three different strains that will be used to show the utility of our device.

After selecting mutant phenotypes, we implemented the yeast mutant library screening protocol on our ID2M device. **Figure C.6** shows the workflow for sorting yeast cells, starting with Poisson encapsulation of

single cells in droplets to ensure that each droplet only contains a single type of cell. The single cell droplet is pressure-driven in the main channel until it reaches the mixing area. In this area, the droplet is actuated away from the main channel and into the mixing channel where it will merge and mix with a droplet of 200 mM IL, generated from the on-demand T-channel configuration. Next the droplet containing a single cell in IL is actuated to the main channel and pressure-driven to the incubation channel. Upon arriving at the incubation region, the droplet is stored in one of the four incubation regions. After 24 h, the droplet was analyzed by absorbance and sorted by their growth (i.e. cell number). **Figure 4.4 C** shows droplets that contained wild-type and mutant-type yeast cells with 100 mM IL. Mutant-type cells showed significant difference in the cell density compared to wild-type cells which are matching the growth rate results. On this device, we have integrated four steps (single cell encapsulation, mixing with IL, incubation, and sorting) that are required to screen for yeast mutants in IL. The integration of electrodes has provided several advantages in terms of droplet control: (1) the on-demand droplet generator can be activated at any time to generate a droplet of IL without the manipulation of flow rates, (2) merging and mixing droplets are controlled operations by the user (or automated sequences) and eliminates the requirement to optimize the time on when to add reagents to the droplets,[276] (3) droplets can be individually incubated in the side channels and accessed in any particular order (i.e. non-serial droplet manipulation), and (4) droplets can be sorted based on a multi-dimensional space and not only on high-low producers. [170] Here, the sorting is based on absorbance and the droplets containing cells are sorted based on two OD levels (**Figure 4.4 D**). As shown, the droplets containing mutant cells show peaks at ~ 0.6 and ~ 1 OD after 24 h incubation. Using these values, droplets in IL can be sorted by three cell types: wild type, mutant 1, and mutant 2. The absorbance signals generated from the mutants (representing the cell density) increases in IL while the signal for wild-type cells is similar to the signal of the oil phase ($\sim$0.04-0.07; see **Figure C.7** for oil signal). In practice, the absorbance of the droplet is greater than that of the oil at higher cell densities (> 20 cells) and similar to oil at low cell densities (< 5 cells). Indeed, sensitivity of the signals depend on fiber alignment and background lighting which in our case we measure to be < 0.5 %. We propose that improvement on the optical setup [229] or device fabrication [299] can increase the sensitivity of our design and expanding the range of cell densities being observed. The method reported here enables a wide variety of droplet operations that is typically not possible with droplet or digital microfluidic systems – encapsulation, mixing (to generate different ionic liquid concentrations), culture and incubation, and n-ary sorting. Together the new methods described here may be particularly useful for high-throughput applications that require a creation of different drug concentrations or clonal

libraries and sorting them at multiple levels.
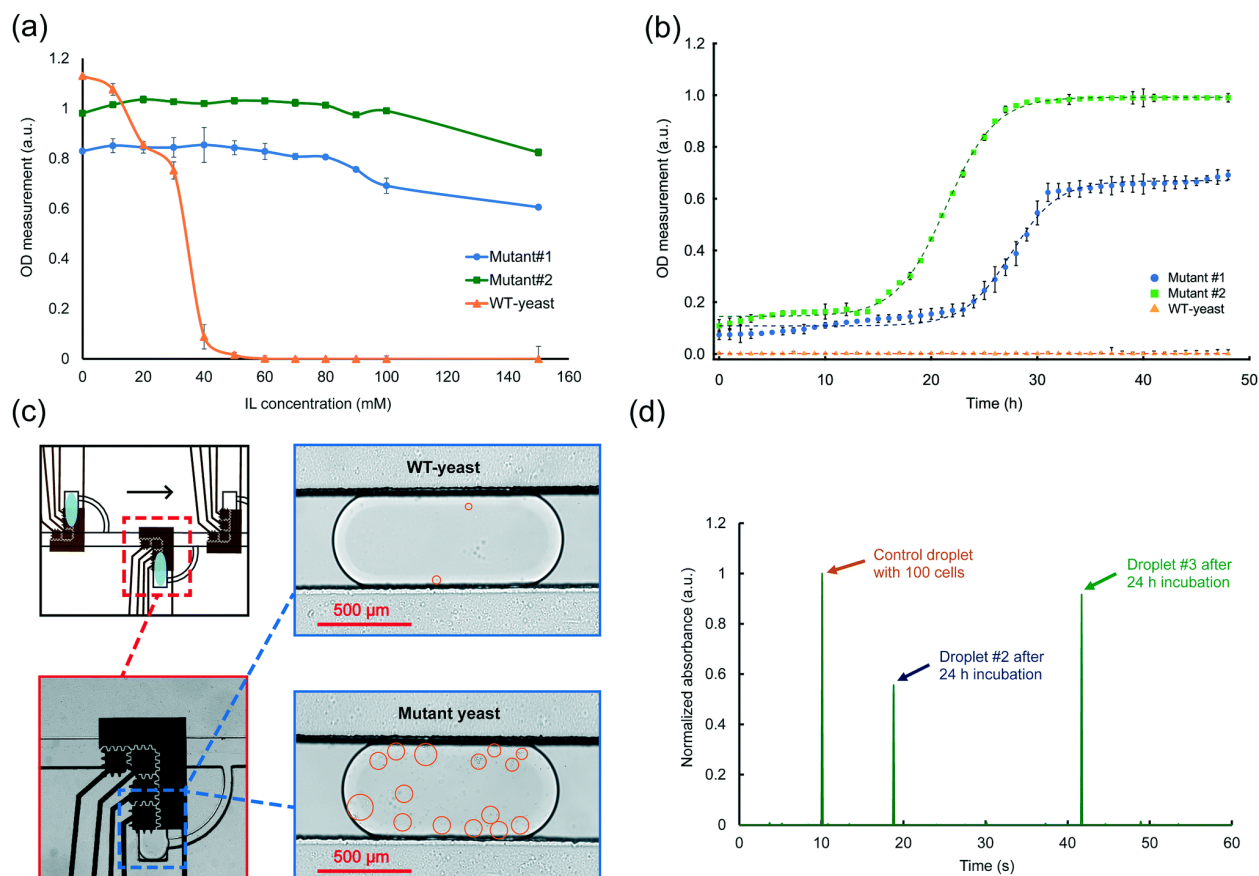
Figure 4.4: ID2M application – effect of ionic liquid on mutant yeast cells. (a) OD measurements as a function of ionic liquid concentrations for wild-type and two mutant yeast cells after 48 h incubation and at 30 °C. (b) Growth curves for the wild-type and mutant yeast cells in 100 mM ionic liquid. (c) Pictures of wild-type and mutant yeast cells cultured in incubation regions on the device for 48 h confirming the differences between two cell lines. (d) Raw data collected directly from the spectrometer showing the differences between the absorbance signals of droplets containing mutant and wild-type yeast. Reproduced from Ref. [108] with permission from the Royal Society of Chemistry.

4.3 Conclusion

We have developed an integrated droplet-digital microfluidic (ID2M) system that uses a combination of pressure- and electrical-based methods for the manipulation of droplets on chip. In this new method, four enhanced fluidic operations were created. First, droplets are generated by on-demand T-junction droplet generators (along with traditional flow-focusing techniques) which could generate a wide range of droplet volumes by tuning only the oil flow rate. Secondly, droplets were actuated to a mixing region that enabled merging with other droplets to form a dilution series of droplets. Third, after mixing, droplets could be trapped and incubated for several days simply by activating electrodes to guide the droplet into incubation

77

traps. Lastly, this design included four channels (i.e. n-ary) for sorting droplets that contained different concentrations or constituents using fluorescence or absorbance. We showed the utility of this microfluidic device by studying the effects of ionic liquid on wild-type and mutant yeast cells. Using the four controlled fluidic steps, we were able to sort the cells into different fractions based on absorbance that can be analyzed downstream. We hypothesize that this system will be useful for those who are developing high-throughput screening platforms for single-cell analysis or directed evolution applications.

4.4 Experimental section

4.4.1 Reagents and Materials

1-ethyl-3-methylimidazolium acetate $\geq$ 95 % (HPLC grade), ethyl methanesulfonate, sodium thiosulfate, sodium hydroxide (lab grade), fluorescein (free acid) dye content 95%, yeast nitrogen base without amino acids and with ammonium sulfate, bovine serum albumin (lyophilized powder) $\geq$ 96 %, and α-D-glucose anhydrous 96% were purchased from Sigma (Oakville, ON Canada), unless specified otherwise. L-leucine, L-histidine, L-methionine, and uracil were purchased from Bio Basic Canada Inc. Yeast BY4741 strain (genotype: MATa his3Δ1 leu2Δ0 met15Δ0 ura3Δ0) was generously donated from Dr. Vincent Martin. 3M Novec HFE7500 engineering fluid was purchased from M.G. Chemicals (Burlington, ON Canada). AquapelTM was purchased from Aquapel.ca (Lachute, QC Canada). 20 g of 5% wt of fluoro-surfactant dissolved in HFE7500 was purchased from Ran Biotechnologies (Beverly, MA). Sodium phosphate monobasic and sodium phosphate dibasic (Anhydrous, ASC grade) were purchased from BioShop (Burlington, ON).

Photolithography reagents and supplies included chromium coated with S1811 photoresist on glass slides from Telic (Valencia, CA), MF-321 positive photoresist developer from Rohm and Haas (Marlborough, MA), CR-4 chromium etchant from OM Group (Cleveland, OH), and AZ-300T photoresist stripper from AZ Electronic Materials (Somerville, NJ). Polylactic acid (PLA) material for 3D printing was purchased from 3Dshop (Mississauga, ON, Canada). Poly(dimethylsiloxane) (PDMS – Sylgard 194) was purchased from Krayden Inc. (Westminster, CO). SU8 photoresist and developer were purchased from Microchem (Westborough, MA). De-ionized (DI) water had a resistivity of 18 MΩ•cm at 25°C.

A 100 mM sodium phosphate buffer (SPB) was prepared by mixing 5.77 mL of 1 M Na$_2$HPO$_4$ and 4.23 mL of 1 M NaH$_2$PO$_4$ solutions (pH 7.0). 5 g of sodium thiosulfate salt was added to deionized water to produce a 5 % (w/v) sodium thiosulfate (STS) solution. Fluorescein solutions (0.5 mM) was prepared by

adding 1.66 mg of fluorescein powder (332.3 g/mol) to 10 mL 1 M NaOH solution that was made by adding 0.4 g NaOH to 10 mL DI water.

4.4.2   Device fabrication and operation

ID2M device masks were designed using AutoCAD 2016 and a transparent photomask was printed by CAD/Art Services Inc. (Bandon, OR). The ID2M microfluidic chip consisted of three layers: a digital microfluidic, dielectric, and channel layer (**Figure 4.1 A**). As described previously, [262, 300] electrodes were patterned on a glass substrate with chromium and coated with positive photoresist S1811, by UV exposure (5 s) on a Quintel Q-4000 mask aligner (Neutronix Quintel, Morgan Hill, CA). Exposed substrates were developed in Microposit MF-321 developer (2 min), rinsed with DI water, and post-baked on a hot plate (115 ^{o}C, 1 min). Substrates were etched in chromium (CR-4) etchant (2 min). Remaining photoresist was stripped in AZ300T (2 min). DMF devices were rinsed by acetone, isopropanol (IPA), and DI water. The device surface was treated with a plasma cleaner (Harrick Plasma PDC-001, Ithaca, NY) for 2 min and then immediately spin-coated (Laurell, North Wales, PA) with 7 μm SU8-5 photoresist (10 s, 500 rpm, 30 s 2000 rpm). SU-8 5 was soft-baked (1. 65 ^{o}C, 2 min, 2. 95 ^{o}C, 5 min) and exposed to UV light (5 s) under the dielectric mask. Post-exposure bake (1. 65 ^{o}C, 1 min, 2. 95 ^{o}C, 1 min) was followed by immersing in SU-8 developer (2 min). Substrates are rinsed with IPA and DI water, a hard bake was performed in three steps (1. 65 ^{o}C, 2 min, 2. 95 ^{o}C, 4 min, 3. 180 ^{o}C, 10 min). For the channel layer, devices were cleaned again with IPA and DI water prior to plasma cleaning (2 min). Next, SU-8 2075 photoresist was immediately spin-coated (1. 10 s 500 rpm, 2. 30 s 2000 rpm) on the chip as a 110-120 μm third layer, and soft-baked (65 ^{o}C, 3 min; 95 ^{o}C, 9 min). Following UV exposure (15 s), devices were post-baked (1. 65 ^{o}C, 2 min- 2. 95°C, 7 min), developed in SU-8 developer (7 min) and rinsed with IPA and DI water. The devices were hard-baked (1. 65 ^{o}C, 2 min, 2. 95 ^{o}C, 4 min, 3. 180 ^{o}C, 10 min). The integrated microfluidic chip was bonded to a slab (60 mm x 30 mm) of $\sim$ 0.5 mm thick PDMS (1:10 weight ratio, w/w curing agent to prepolymer, cured at 65 ^{o}C for 3 hours). Inlets and outlets were created using a 0.75 mm puncher (Biopsy Punch, Sklar, West Chester, PA). Before bonding, the PDMS slab was plasma-treated for $\sim$1 min and exposed to (3-aminopropyl)triethoxysilane 99% in a desiccator for 30 min. PDMS was immediately bonded to the device and baked at 160 ^{o}C for 20 min. Before operation, channels were treated with Aquapel^{TM} for $\sim$ 5 min and rinsed with HFE oil mixed with 0.75% fluorosurfactant. Syringes were prepared with the following fittings and tubing: 1/4-28 to 10-32 PEEK adapter, (10-32) peek union assembly, finger tight micro ferrule

10-32 coned for 1/32" OD, and PEEK tubing (1/32" diameter) from IDEX Health & Science, LLC (Oak Harbor, WA). Gastight glass 500 μL-syringes were purchased from Hamilton (Reno, NV) and installed on the neMESYS system (Cetoni, Korbussen, DE).

Device operation comprised of five stages: droplet generation by a flow-focusing or T-junction configuration followed by droplet mixing, incubation, detection, and sorting. Droplet generation by flow-focusing was implemented by initializing the flow rates using the neMESYS for the aqueous and oil flow rates to 0.0005 [μL/s] and 0.01 [μL/s] respectively. For the T-junction configuration, droplets were created on-demand by four steps: (1) the aqueous flow was initialized at 0.0005 [μL/s], (2) when the aqueous flow reaches the sixth electrode, an AC voltage (15 kHz, 200 Vrms) was used to drive the flow to the T-junction, (3) two electrodes were sequentially actuated (i.e. electrodes are turned on and off) to drag the fluid to the main channel (shown in red; **Figure 4.1b**) and (4) a $\sim$ 30 nL droplet is formed by both intersecting the oil phase with flow rate of 0.01 [μL/s] and turning on electrodes in the T-junction and main channel as shown in **Figure C.1**. After on-demand droplet generation, droplets were pressure-driven using the oil phase in the main channel and using actuation sequences to drive the droplet into the mixing region (15 kHz, 200 V$_{rms}$, under oil flowrate of 0.01 μL/s). Droplets were mixed by actuating underlying electrodes and the mixed droplet was actuated to the main channel. For incubation, droplets were directed to the traps actuating the designated electrodes. After incubation, droplets pass through a detection region which were further sorted by actuation of the electrodes. For droplet size calculations, images of the droplets were acquired and uploaded into ImageJ (National Institute of Health, USA). An imaging pipeline was created to calculate the droplet volume based on an ellipsoid volume formula given that the droplet height was set to 110 μm.

4.4.3   ID2M microfluidic optical fiber detection interface

The optical fiber detection interface consists of a Flame spectrometer (Ocean Optics, Largo, FL), two bare fiber (100 μm core) with numerical aperture of 0.22, and a multi-channel LED light sources that contains four high-power (1 mW) LED modules: 470, 530, 590, 627 nm. Two optical fibers were inserted into two fabricated 300 μm channels that were perpendicular to the direction of the fluid flow (see **Figure 4.1b**). One fiber was connected to the multi-channel LED source, while the other was connected to the Flame spectrometer. The fiber ends were polished carefully using the ocean optics termination kit and fitted with an SMA connector by the help of bare boots for guiding the bare fiber. The distance between the fiber and the channel is $\sim$ 200 μm. All data were collected using the Ocean View spectroscopy software (Ocean Optics,

Largo, FL) using the following settings: integration time 100 ms, boxcar smoothing width = 3, number of scans = 5, update rate = 1. Strip chart was enabled to collect data from a single wavelength (530 nm) and executed without stopping.

4.4.4   On-chip calibration curves – fluorescein measurement

A droplet containing fluorescein (1 mM each in 1M NaOH buffer, pH 9) was generated using the flow-focusing configuration with fluorescein (0.0005 μL/s) and HFE oil (0.01 μL/s). A droplet of buffer or water ($\sim$ 30 nL) was generated using the on-demand T-junction configuration. The droplets were merged and mixed by actuation of underlying electrodes. The number of buffer droplets added to one fluorescein droplet created four different concentrations: 1, 0.5, 0.25, and 0.125 mM. After mixing droplets were detected by using our optical fiber setup, and sorted by actuating a sorting sequence for one of the four different on-demand sorting channels. Peak intensities were recorded for each concentration with time traces of the recorded signals. The standard deviation was calculated from 20 replicates.

4.4.5   EMS mutagenesis and generating ionic liquid resistant yeast strains

Before generating the mutant library, wild-type *S. cerevisiae* BY4741 yeast cells were stored on agar plates containing synthetic defined medium (6.8 yeast nitrogen base without amino acids, 20 g agar, 20 g 2% glucose, 20 g methionine, 20 g histidine, 20 g uracil, 120 g leucine) at 4 ^{o}C. Wild-type yeast was grown in 50 mL of synthetic defined medium (30 ^{o}C, 200 rpm) for 48 hours. Aliquots of 2×10^8 yeast cells (O.D. $\sim$ 1) were transferred to four micro-centrifuge tubes corresponding to technical triplicate and one control sample. The cells were washed two times with phosphate buffered saline (PBS) and a single time with sodium phosphate buffer (SPB) (0.1 M- pH 7.0). After centrifugation, the pellets were re-suspended in 1.5 mL SPB. For mutagenesis, cells were exposed to ethyl methanesulfonate (EMS) according to Winston's protocol.[37] To generate a standard curve for viability after EMS mutagenesis, our 15 mL Falcon tubes (corresponding to three different EMS treatment time) were filled with 1 mL SPB and 0.7 mL cell solution of each micro-centrifuge tube. 50 μL of EMS was added to three of the 15 mL falcon tubes in a biological safety cabinet. The control sample (i.e. wild-type cells) were kept without EMS addition. All tubes were incubated at 30 ^{o}C on a shaker (200 rpm) for 30 min. Cells were exposed to EMS for 40, 50, 60, 75, and 90 min. Mutagenesis was stopped by adding 8 mL of 5 % (w/v) sterile sodium thiosulfate (STS) solution at

each time point. Aliquots of each falcon tubes diluted in SD media were plated on solid SD media. Plates were incubated at 30 ^{o}C for 48 h. Cell viability was measured by comparing colony formation of each EMS time point and the wild-type cells (**Figure C.2**).

To generate 1-ethyl-3-methylimidazolium acetate IL resistant cells, the mutagenesis is repeated for 60, 75, and 90 mins. Resulting aliquots were inoculated in 5 mL synthetic defined medium for 24 h at 30 ^{o}C on a shaker with 200 rpm. Next, the mutants were inoculated in 5 mL synthetic defined medium and 50, 75, or 100 mM 1-ethyl-3-methylimidazolium acetate IL and incubated for 24 h at 30 ^{o}C on a shaker with 200 rpm. 1 mL aliquots of each test tubes along with a wild-type sample were diluted 100 times with SD media and then were plated onto several solid SD plates containing 50, 75, or 100 mM IL. These plates were incubated for 4-6 days at 30 ^{o}C. Colonies were randomly selected from the plates and cultured in 5 mL SD media at 30 ^{o}C. After 24 h, we measured the OD of the culture and if the OD was greater than 0.3, samples were diluted and cultured in different ionic liquid conditions otherwise they were discarded. If selected, an aliquot (depending on IL concentration) from the 5 mL culture was added to the wells of a microwell plate to make up a final volume of 200 μL. In each well, the OD was measured every 20 min at 30 ^{o}C with shaking at 200 rpm for 48 hours using a Tecan Sunrise microplate reader (Tecan, Salzburg, Austria) with the following settings (measurement wavelength: 595 nm). Three replicates were measured for each condition.

4.4.6   N-ary sorting of yeast mutants library on ID2M device

For analyzing the effect of IL on wild-type and mutant yeast on chip, the two fastest growing IL tolerant mutants and wild-type yeast were cultured in SD without IL for 48 h. A 500 μL syringe was prepared with a cell suspension of 2×105 cells/mL in SD media containing 1% bovine serum albumin (BSA) and a syringe containing HFE oil with 2 % fluorinated surfactant. Both syringes were connected to the inlets of the device using PEEK tubing (1/32 inch diameter). Cell encapsulation was performed through flow focusing (using Poisson statistics) with flow rates of 0.0008 μL/s and 0.01 μL/s for cells and oil, respectively to generate a droplet with volume of $\sim$ 35 nL. For the T-junction droplet generator, a syringe was filled with 200 mM IL and $\sim$ 35 nL droplets were formed on demand. Droplets containing a single cell were actuated into the mixing region by sequentially applying $\sim$ 200 Vp-p (15 kHz) to the electrodes. The droplet was merged with an on-demand generated droplet of IL and mixed by moving the droplet back-and-forth along the linear path. Upon mixing the droplet with a 200 mM IL, the mixed droplet of cells and IL (with a final concentration of 100 mM IL) was actuated to the main channel and was trapped into incubation slot using actuation. This

process was repeated for three other incubation regions. After trapping all four droplets, the ID2M device was removed from the automation system and droplets were incubated for 48 h at 30 ^{o}C in a humidified chamber.

After incubation, droplets were actuated to the main channel and passed through the optical detection area where the two optical fibers were placed perpendicular to the main channel. According to the absorbance peaks differences, droplets were sorted into three groups using the three sorting channels. Any excess droplets in this procedure was actuated to the waste channel. During all droplet operation procedures (i.e. mixing, trapping, incubation, sorting) and when droplets were in the main channel, oil flow rates were maintained at 0.01 μL/s.

4.4.7   COMSOL simulation

We conducted a simulation of the mixing area with the sinking channels, using COMSOL Multiphysics V5.3 (COMSOL Inc., Cambridge, MA, USA). Parameters are shown in **Table C.1** and following assumptions were made for simplification: 1) Newtonian fluid, 2) no-slip boundary condition, and 3) incompressible flow. A single phase laminar flow using Navier Stokes model was selected as the physics of our stationary study with the assumption that our fluid is 3M^{TM} Novec^{TM} 7100 Engineered Fluid. Wall boundaries and inlet and outlet were defined as depicted in **Figure C.3**. The inlet velocity of the fluid flow was initialized to 0.033 ms^{-1}.

Chapter 5

Droplet-digital deterministic single-cell encapsulation for isoclonal cell line generation

Abstract

Generating a stable knockout cell line is a complex process that can take several months to complete. In this work, we introduce a microfluidic method that is capable of isolating single cells in droplets, selecting successful edited clones, and expansion of these isoclones. Using a hybrid microfluidic method, droplets in channels can be individually addressed using a co-planar electrode system. In our hybrid microfluidic device, we show that we can trap single cells and subsequently encapsulate them on demand into pL-sized droplets. Furthermore, individual cells inside the droplet can be released or kept in the traps, or merged with other droplets by the application of an electric potential to the electrodes that is actuated through an in-house user interface. We use this high precision control to successfully sort and recover single isoclones to establish monoclonal cell lines, which is demonstrated with a heterozygous NCI-H1299 lung squamous cell population resulting from loss-of-function eGFP and RAF1 gene knockout transfections.

5.1 Introduction

Gene editing in mammalian cells has become more accessible and less time consuming due to the availability of new editing tools that allow for rapid and precise edits. Using improved versions of CRISPR-Cas9 [301, 302], and better methods to control the cell's double-strand break (DSB) repair mechanisms [303], Cas9 has become a popular tool to engineer new cell lines. The utility of CRISPR is showing widespread benefits for generating new cellular therapies [304] and creating new genetic models for cancer.[305, 306] To fabricate these new edited cell lines, evaluating the properties of single clones (a single edited cell) is especially important, as biallelic editing differences can occur and non-homologous end-joining DSB repair mechanisms generate indels that differ between individual clones. [307, 308, 309] Isolating single clones provides a method for enriching correctly edited cells, of which one can correlate the phenotypic changes to a specific clonal genotype and facilitate downstream characterization.

The process of genome editing mammalian cells typically consists of in silico design of the guide, cloning the guide into an expression vector, transfection, selection, sorting, and expansion of homogeneous clonal lines.[310] Currently, the design of the guide and the act of transfecting cells can be done in less than a day.[310] And with new automation tools and methods continuously being developed, the process of synthesis [190] , assembly [311, 312], and transfection [313, 314, 315] are becoming faster, cheaper and more efficient. However, selection and enrichment of transfected clones, especially in knockout experiments, sensitive cell lines (e.g, hPSCs) or hard to transfect cell lines, remains a tedious and challenging task. Currently, common methods to isolate single clones are to use limited dilution or colony picking to separate single isoclones and to generate a homozygous progeny. [316, 317] The laborious and time-consuming process, the high dilution requirements, and inherent probabilistic nature for limited dilution are not ideal for increasing the chances to obtain a single clone. Fluorescence-activated cell sorting (FACS) , colony pickers and other automated tools can provide a method to generate clonal cell populations but are associated with high infrastructure and maintenance costs, downstream optimization usually requiring a large starting cell population, and can induce stress or apoptotic response in the cells due to their high voltage requirements and physical handling. [318, 319]

Droplet-based microfluidic systems are ideal systems for single-cell manipulation and analysis. These biocompatible systems mimic the physics of the cellular environment and in doing so, reduce the physical stresses often exerted on cells by traditional tools or robotic systems. They are also typically low in

infrastructure and operational costs and operate under much lower volumes ($\sim$pL range).[320, 4, 94, 74] Several researchers have already addressed multiple steps in the gene editing pipeline using microfluidics, including mammalian cell culture [37, 155], transfection of mammalian cells [321, 322, 323, 6, 324, 325, 326, 327, 156], as well as the sorting or selection of transfected mammalian cells. [328] Droplet-in-channel microfluidics can operate in ultra high-throughput ranges while generating single-cell containing droplets. [329, 3, 330, 30] A pitfall with these systems is that it is difficult to manipulate and to control the droplets in parallel. Digital microfluidic systems (DMF) can alleviate the challenges associated with droplet-in-channel systems since DMF are able to address each droplet individually. Having this control is especially useful in multi-step procedures such as transformation and enzymatic assays [331, 262], drug and inhibitor screening [332], and gene-editing [155]. Recently, we have combined both of these platforms together, in which we call a 'hybrid' microfluidic platform, placing co-planar electrodes (i.e. ground and activated electrodes on the same plate) under microfluidic channels to have individual control of the droplets in channels. [108] Given the increased control over droplets and droplet content that hybrid microfluidic technologies have shown [333, 334, 106, 110, 112, 109], there is an opportunity to use this technology as a method to control the isolation of mammalian isoclones.

Here, we developed a deterministic 'one-droplet-one-cell' hybrid microfluidic system that can trap single isoclones and subsequently encapsulate them in individual droplets. These single-cell containing droplets can be released from traps in two directions, kept in position, or have the opportunity to be merged with other droplets, allowing this device to be used for various manipulations of the individual clones. To show the versatility of our device, we have shown its ability to establish isoclonal mammalian loss-of-function cell lines from gene knockout experiments by sorting and recovering engineered clones of a NCI-H1299 lung squamous cell carcinoma.

5.2 Results and Discussion

5.2.1 The design of a hybrid microfluidics system for single-cell manipulations

Figure 5.1 depicts the representative device used for single-cell trapping, single-cell droplet generation and droplet operations. As shown in **Figure 5.1 A**, the microfluidic device consists of three layers: a patterned electrode layer, a 7 μm SU-8 5 dielectric layer and a PDMS-based channel layer of 35 μm height and a main channel width of 50μm. The 'hybrid' integrated droplet digital microfluidic device consists of

a bottom digital microfluidic layer (i.e. electrodes and dielectric) along with a top patterned channel layer in which cells are trapped (single-phase) or droplets are manipulated in an oil phase (two-phase). [108] The device is divided into two sections: 1) an on-demand T-junction droplet generator and 2) a single-cell droplet array. As shown in **Figure 5.1 B**, the on-demand droplet generation consists of co-planar electrodes that will actuate the aqueous flow (using electric potentials) to the orthogonal continuous oil flow that will break the continuous aqueous flow into discreet droplets. The single-cell droplet array (**Figure 5.1 C**) can trap single cells, after which they are encapsulated in droplets that are generated within the traps by the application of an electric field. It contains 12 traps, of which six are equipped with electrodes. Tubing connects the two parts of the device to transfer the droplets from the droplet generator to the single analysis part of the device. The device contains two inlets - I1 for oil and droplets and I2 for cells and priming - and two outlets - O1 for waste and O2 for sample recovery and flow reversal - (**Figure D.1**). In designing the system shown in **Figure 5.1**, there is a design element that requires consideration for reliable cell trapping and encapsulation. Two commonly used methods for single cell isolation – trapping and encapsulation – are used complementary. The traps are designed such that they could trap single cells with high efficiencies, yet also allow for a smooth phase change to a two-phase flow. We followed resistance based design guidelines as reported for microfluidic serpentine trap designs for droplets and cells. [284, 285, 283, 31, 282, 335] The design element concerns the location of the traps relative to the main channel such that both single-cell trapping and phase change can occur. By modeling flowrate profile and velocity streamlines, we optimized the channel geometry (**Figure D.2**), such that volumetric flow rate through the trap (Q_{trap}) is greater than volumetric flow rate through the bypass channel (Q_{bypass}) when there is no cell in the trap. We found that positioning the trap near the curvature of the main channel (i.e. the end of a serpentine channel) along with a narrow ($\sim$50 μm) trap entrance and a narrow ($\sim$50 μm) width of the main channel immediately after the trap opening, prevented cells bypassing the empty traps. The optimized placement offers a higher effective hydrodynamic resistance in the bypass channel (R_{bypass}) than through the trap (R_{trap}). Hence, the flowrate in the trap is higher compared to the bypass channel ($Q_{trap} > Q_{bypass}$) to maintain the same pressure drop (as shown from other studies [286]). Furthermore, the design offers two additional advantages: (1) if a cell is trapped, it is unlikely for another cell to flow into the same trap since this increases the R_{trap} (and reduces Q_{trap}) and (2) during a phase change for single-cell encapsulation (trap based droplet generation) (described below), the resistance in the trap is sufficiently higher than the bypass channel which will help preventing squeezing the cells out of their traps. A mathematical description and the simulation details are described in

Appendix D.1 and **D.2**.
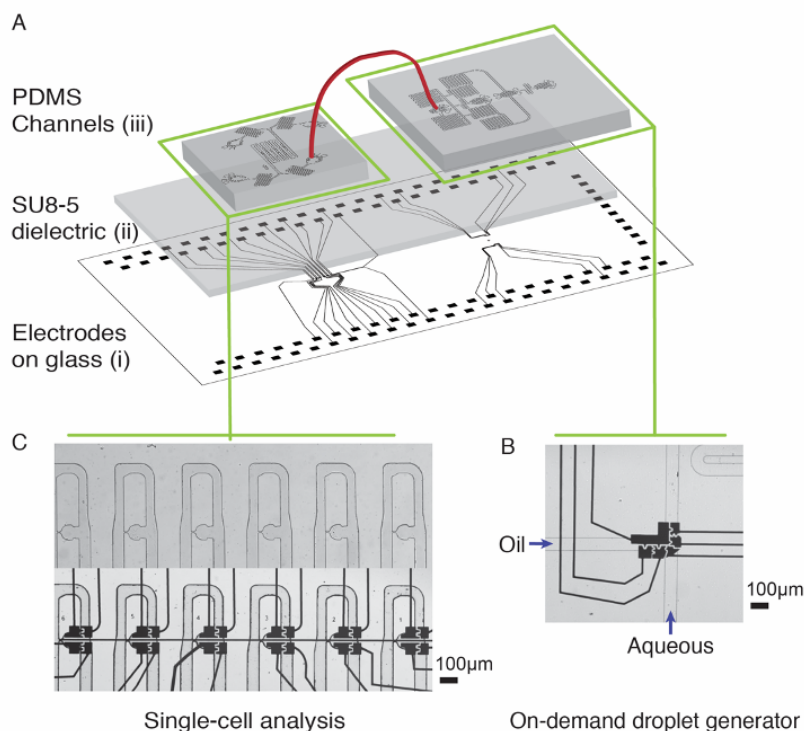
Figure 5.1: Integrated droplet digital device for on-demand single-cell encapsulation and analysis. The three layer device consists of a digital microfluidic layer with chromium electrodes patterned on glass, a 7 μm thick SU-8 5 dielectric layer and a PDMS channel layer of channels of height 35 μm and width of 50-75 μm. B) The droplet generation device contains two T-junction droplet generators, under which several electrodes are located for on-demand droplet generation. C) The single-cell analysis device contains two inlets, and two outlets. The trapping area contains cell traps with 8 μm constrictions, under which 4 electrodes are located. The droplet generation device. For details on channel, electrode and wiring sizes, see Appendix D.1. Reproduced from Samlali et al. [227], with permission from John Wiley and Sons.

Finally, we also note that one of the main goals of this work is to automate the process of actuation and droplet manipulation, but a key challenge is to integrate and to control the multiple pieces of hardware into one software framework. In this work, the microfluidic device is connected to two main hardware components: the in-house automation system (i.e. optical switches) and a syringe pump system (**Figure D.3**, **Appendix D.3**). The automation system serves the purpose to provide electrode actuation and the syringe pump system is to control the flow rates in the device. [262, 300] Since these two hardware systems are operating on different software protocols, we developed our own Python based framework with a simple user interface. The system user can control the flow of certain fluids (start stop, flow rate), and perform several pre-programmed droplet manipulations with the click a button ('encapsulate', 'forward release', 'reverse release', and 'keep' for a specific actuation time and trap number). The software is open-source available at `http://bitbucket.org/shihmicrolab`.

5.2.2 Hydrodynamic single-cell trapping and deterministic single-cell encapsulation through *in situ* droplet generation

Figure 5.2 illustrates the optimized device operation procedures for trapping single cells and encapsulating the cells inside droplets using a 'hybrid'-based microfluidics platform. As detailed in the Experimental Section, the device operation procedure consisted of priming, cell loading, phase change, and encapsulation followed by droplet release (**Appendix D.1**). This workflow, and the procedure for trapping and *in situ* encapsulation are represented as a schematic (**Figure 5.2**). First, devices were primed with 2% Pluronics F-127 for at least 5 min to decrease cell adhesion to PDMS. Second, an aqueous flow containing fresh media with mammalian cells (MCF-7 breast cancer cell line) was introduced into the trapping device at a concentration of 10^5 - 10^6 cells mL^{-1} (see **Figure 5.3 A** for an image of six in-

Figure 5.2: Workflow of device operation. Priming the device with 2% Pluronics F-127 in PBS for 5 min. MCF-7 cells in PBS are trapped. On-demand droplet generation can be selected to generate droplets, after which the aqueous flow is stopped. When all traps are loaded, oil (HFE 7500 2% Ran Fluorosurfactant) is loaded at 4 nL s^{-1} by connecting the droplet bridge. Oil flow shears off a small volume of remaining PBS, which forms a droplet around the cells. Droplets are brought in through the droplet bridge and droplet operations can be performed. Oil flow can be reversed to collect droplets. The inlet (I#) and outlets (O#) that are used for each operation are designated for each operation. Reproduced from Samlali et al. [227], with permission from John Wiley and Sons.

dividually trapped cells). We evaluated the efficiency of cell trapping as a function of flow rate. Using our design, the optimal range of flow rates to trap individual cells is between $1 - 4$ nL s^{-1} (**Figure 5.3 B**). At this range of flow rates, cells are unlikely to occupy traps with multiple cells and the MCF-7 cells do not squeeze through the traps (unlike at high flow rates). Single cells are most efficiently trapped ($\sim$88.3 %) at 5 nL s^{-1} - an efficiency similar to previous studies which required displacement structures or other external forces to trap cells.[288, 289, 161] We counted over 54 consecutive events (out of 54 observations) of MCF-7 cells

passing by a single MCF-7 cell occupied trap, without trapping a second one. The conditions defining the success at these flowrates are (1) the optimized channel flow velocity profile and slanted overhang along the main channel (close to the trapping region) to steer the flow towards the trap (2) designing a 8 μm constriction which is smaller than the cell size, and (3) the physical properties of MCF-7 cells (i.e. lower deformability).[92, 28]

Following the trapping of the cells is the generation of a droplet within a trap which results in the encapsulation of a single cell inside a droplet. Popular passive single-cell encapsulation is known to be a procedure that follows Poisson statistics, generating droplets with none, one or more cells.[72] Using the hybrid device, we can generate a droplet *in situ*, and thus deterministically encapsulate the trapped cell. This is done by moving from a single-phase flow to a two-phase flow using a phase change procedure by: (1) flowing an oil phase through the entire channel and, and (2) applying an electric potential to the electrodes below the trap when the oil flow approaches. **Figure 5.3 C** shows three images taken from video frames showing the on-demand, in situ droplet generation process. Four co-planar electrodes (size = $\sim$100 μm, area 0.06 mm^2) were used for the generation event – two electrodes below the main channel and two electrodes below the trap. In Frame I, all electrodes are grounded. An oil flow enters the main channel for the purpose of a phase change. In Frame II, the electrode below the trap is activated while the other electrodes are grounded. The aqueous phase and the single-cell remain inside the trap when the oil flow (in the main channel) "cuts" the aqueous phase at both ends of the trap. Generated cell containing droplets are on average 150.3 $\pm$ 5.6 pL in volume (N = 11). In Frame III, all potentials are grounded, and the oil phase flow continues to the next trap to perform the next encapsulation procedure. To aid the design of the trap and to determine the optimal actuation sequence, we have simulated the electric potential and electric field distributions (**Figure D.4** and **Figure D.5**). As shown, the electric field density ($\sim$ 5 x 106 V m^{-1}) is induced between the main channel and the trapping region. This field gradient induces an electrostatic force that will pull the liquid towards the trap (similar to droplet actuation on a DMF device [23]). Given this capability, the device has means to encapsulate cells in droplets on-demand without Poisson-based statistics. The details of the simulation are described in the Appendix **Appendix D.2**, **Table D.1**. To our knowledge, this is the first occurrence of trap based in situ droplet generation for deterministic single-cell encapsulation, providing an alternative to Poisson based encapsulation methods.
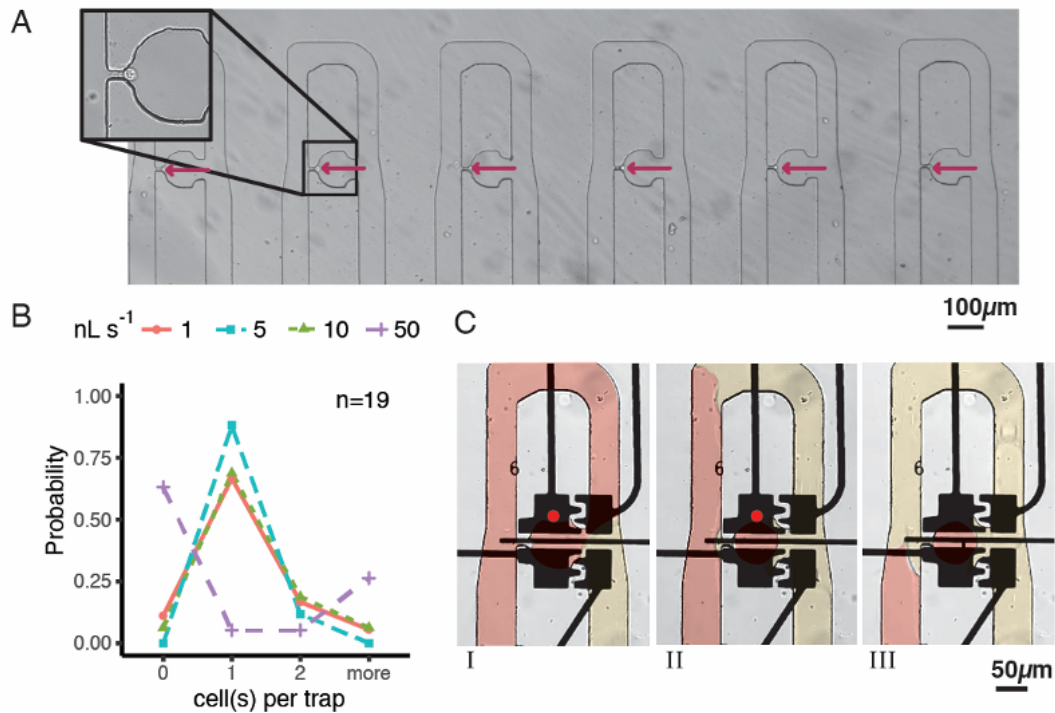
Figure 5.3: Cell trapping and encapsulation A) Single MCF-7 cells trapped, in PBS (bright-field, 4X). B) Efficiency of trapping cells at different flowrates. The cell concentration was kept constant at 5 x 10^5 cells/mL PBS and experiment was performed during 10 min. C) Encapsulation procedure. Frame I: A single MCF-7 cell trapped. An HFE 7500 + 2% Ran surfactant was loaded into the device at 4 nL s^{-1}. The trap electrode is actuated (15 kHz, 126 V_{RMS}). Frame II: A droplet is formed within the trap and the oil phase continues through the bypass channel. Frame III: Encapsulated MCF-7 cell. Reproduced from Samlali et al. [227], with permission from John Wiley and Sons.

The success of trapping and encapsulation is highly dependent on device fabrication and operation methods. For example, the reliability of electrode actuations and resulting droplet operations heavily depends on the alignment of the electrodes and channels. To minimize the strenuous task of alignment, we used the ground wire and the gap between electrodes to serve as an alignment mark. Since these are clear marks, alignment can be performed swiftly under a microscope without losing the oxygen plasma treatment on the PDMS.[336] Furthermore, we divided the device into two components (droplet generator and serpentine trapping channel) to fit the features within the view field of the microscope, and to minimize PDMS shrinkage.[337] The process of inserting and removing tubing from the inlets and outlets also requires slow manipulation. The air bubbles are most likely to occur while changing from priming solution to cell solution

and when initiating the oil flow. The bubbles can block flow inside traps, can push cells out of their traps or disturb the stability flow causing diverging flow rates. The air bubbles can also cause unwanted pressure differences inside the channel, which may lead to droplet breakup and movement. Our solution is to insert the tubing gently at high flow rates and use a small diameter tubing to connect the droplet generation and trapping devices (more info in Appendix D). Lastly, it is important to perform a thorough cleaning of the traps by removing the remaining oil emulsions in the 8 μm trap constrictions to ensure high cell trapping efficiency for the next set of trapping experiments.

5.2.3 Two-phase on-demand droplet operations: droplet generation, releasing and keeping of droplets in traps

After trapping and phase change, we turned our attention to other droplet operations such as droplet generation or keeping and releasing the droplets containing single cells. Generally, in droplet-based microfluidic devices, controlling droplet positions inside the channels is performed by using passive structures [92, 84, 28], valves [338, 339], or external forces (optical, acoustic, dielectrophoresis).[84, 95, 31] For example, Sauzade and Brouzes [92] uses serpentine channels containing droplet traps under forward flow to trap droplets and uses reverse flow to hydrodynamically release droplets. The platform presented here can perform multiple droplet operations, such as a trapping operation under forward flow, release operation under forward/reverse flow, and keep operation under reverse flow. Our device has no additional channel structures that have been fabricated to guide cell and there is no reliance on timing the droplet flow to control the droplets as required by previous works. [340, 276] The main contributor to controlling the droplets on our device is the application of electric potentials to the electrodes (similar to digital microfluidic systems [26] such that the above-mentioned operations can be performed with high fidelity.

To characterize releasing operations, we have tested the likelihood for droplet release at different flow rates (for the forward and reverse flow directions) using electric potential or via pressure-driven flow. **Figure 5.4 A** (Frames I-IV) shows the actuation sequence for releasing a droplet under forward flow. The droplet is released by actuating electrodes below the trap (Frame II) followed by activating an electrode below the main channel and the trap (Frame III). By using this specific sequence, the electric field density directs the droplet from the trap towards the main channel in the direction of the flow (**Figure D.5**). We also tested the likelihood for droplet release at different flow rates in forward direction (from inlets to outlets) (**Figure 5.4**

B). As shown, low forward flow rates (< 1 nL s^{-1}) give rise to high probability (> 95 %) of being able to release the droplet. Since droplets are trapped due to the hydrodynamic pressure, P_h, of the oil flow and the droplet is controlled by using electrostatic forces (F_{elec}), droplets can be released when the electrostatic force F_{elec} is greater than the P_h generated by the flow in the main channel. This relationship also holds true when there is no flow rate applied. In this case, the droplet is released from the trap but is static at the entrance of the trap since there is no flow. While without any electrostatic force (i.e. no electric field applied) at any given flow rate, the droplet is never released from the trap.
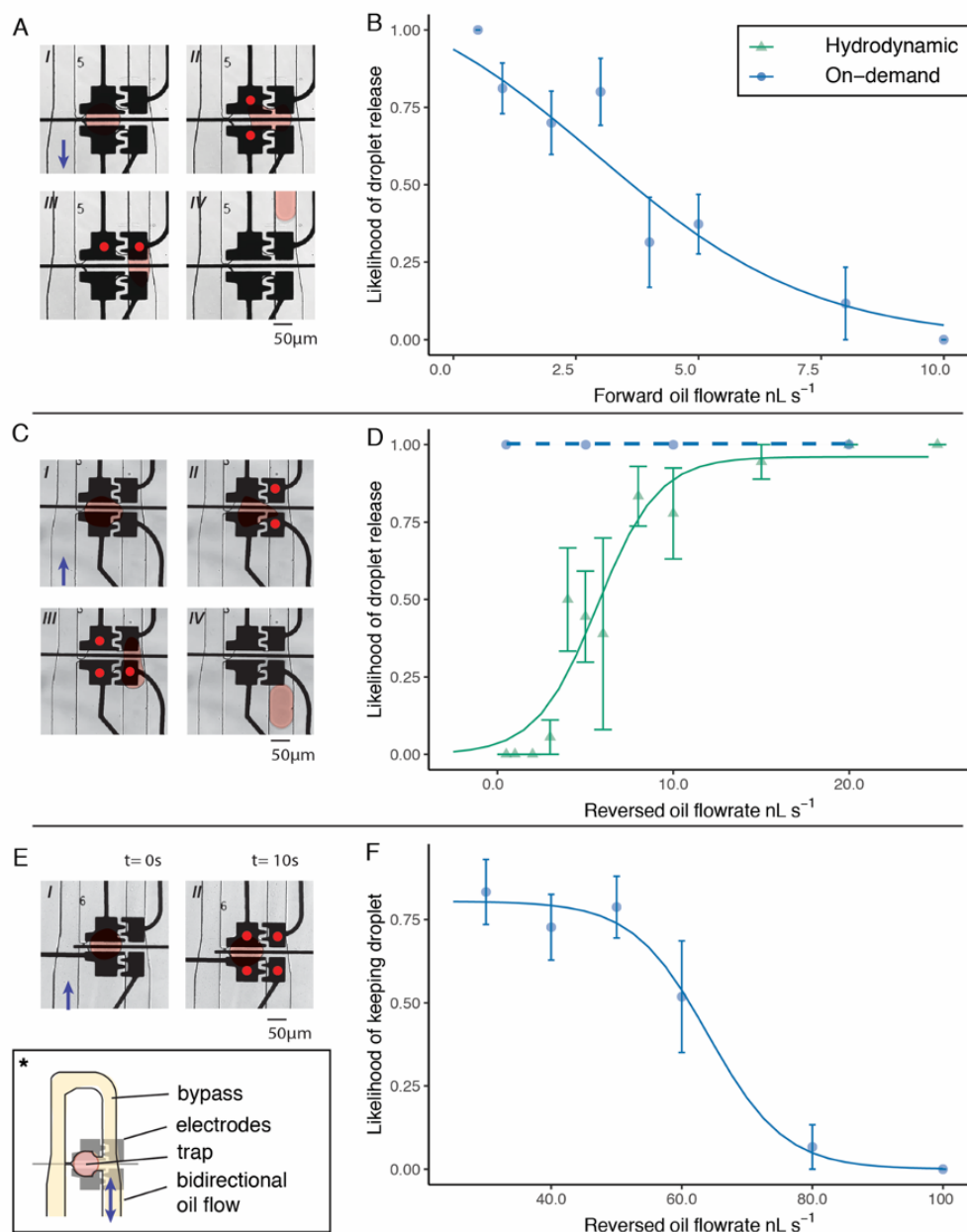
Figure 5.4: On-demand droplet operations. Actuation patterns are indicated with a red dot (bright field, 15X). Bypass channel, trap and flow are as indicated (*). The droplet is overlayed with a red mask. A) Actuation sequence of releasing droplet towards outlet on demand (15 kHz, 126 V_{RMS}). B) Efficiency of release of droplets under forward flowrate, under increasing flowrates. (n=8, 10 replicates per trap) C) Actuation sequence of releasing droplet towards inlets on demand (15 kHz, 126 V_{RMS}) D) Efficiency of release of droplets under reversed flowrate. Hydrodynamically, droplets are released more efficiently towards the inlets, under increasing flow rate. With on-demand release, droplet show efficient release with flow rates as low as 0.5 nL s^{-1}. E) Actuation sequence of keeping droplets within trap under reversed flow rate (15 kHz, 126 V_{RMS}, 10 s) F) Efficiency of keeping droplets on-demand under reversed flow rate. Droplets can be kept efficiently for flow rate lower than 45.4 nL s^{-1}. Reproduced from Samlali et al. [227], with permission from John Wiley and Sons.

Next, we tested the likelihood of releasing droplets with reverse oil flow, with and without on-demand actuation. As shown in **figure 5.4 C** (Frames I-IV), the actuation sequence under reverse flow (from outlets to inlets) is similar to the actuation sequence for the droplet release under forward flow. In contrast to with forward flow, the probability of releasing a droplet is most likely to occur at higher flow rates (>10.92 nL s^{-1}) (without actuation; hydrodynamic flow only). The lower flow rates are more likely to keep the droplet inside the trap (**Figure 5.4 D**) – a similar trend observed in other studies.[74] When actuation is implemented, the droplet can be released from the trap at any time and there is no dependence on the reverse flow rate using a specific actuation pattern. This is an exciting result since it enables the user to release and to select droplets on-demand and in parallel without the need for dielectrophoretic, acoustic or magnetic sorting techniques. Thus, this represents a significant advance over other droplet-based microfluidic systems that implement trapping and releasing droplets.

In some cases keeping droplets inside a trap is also a desired operation.[108, 341, 342] **Figure 5.4 E** shows the actuation sequence for keeping a droplet. Four electrodes are activated to ensure the highest electric field density is centered at the opening of the trap to prevent the droplet from escaping into the main channel (**Figure D.5**). The likelihood of the droplet being released when different flow rates are applied from the narrow to the wider region of the trap showed flow rates below 45.4 nL s^{-1} give rise to high probability on keeping the droplet ($> 95\%$ logistic regression model asymptote) (N = 10) (**Figure 5.4 D**). The main reason for this trend is that after a certain flow rate, $P_h > F_{elec}$. However, if the flowrate decreases, droplets reside for a longer period within the main channel, which can be disadvantageous for fast sorting procedures (**Figure D.6**). It is possible to increase the applied potential (> 126 V$_{RMS}$) to the electrodes (to increase the electrostatic force and work under higher flow rates), but this may induce dielectric breakdown [77–79], followed by electrolysis or Joule heating which can ultimately lead to cell stress and to changes in genomic regulation in cells. [80] Hence, for gene-editing experiments discussed below, we used flow rates below 45 nL s^{-1} to keep the droplets inside the trap while maintaining applied potentials below 126 V$_{RMS}$.

Similar to our previous work, we generate droplets on-demand to have the capability to add reagents to other droplets in the device. Ahmadi et al. [108] recently reported the first hybrid microfluidic device that is capable of generating droplets on-demand by combining the pressure of the continuous oil phase and the electrostatic actuation of the aqueous flow. The desire to have control over droplet generation is an important step forward for the field, as the enthusiasm for droplet control in droplet-based microfluidic devices is well-documented.[81] We improved upon this work by designing an automated replenishment of the aqueous

flow, which removes the limit on the number of droplets that can be generated. Using this droplet generator, we are able to generate droplets on-demand using a T-junction configuration with oil flow rates between 2 to 2.5 nL s^{-1} (**Figure D.7**). From our observation, lower flow rates than 2.0 nL s^{-1}, on-demand droplet generation became difficult due to the inability of the oil flow to shear off a droplet, while at higher flow rates than 2.5 nL s^{-1} the pressure of the oil flow is larger than the electrostatic force removing the force balance at the interface to generate droplets. After droplet generation, we showed the capacity of the device to merge droplets. As shown in **Figure D.8**, we can merge incoming droplets with trapped droplets on demand. An advantage of on-demand merging is that it does not rely on the tedious synchronization of two streams of droplets for droplet coalescence nor does it require any pressurized channel.[46,72,82–87] Generating droplets on-demand with a T-junction and generating single-cell containing droplets by phase change, show high monodispersity (250.9 ± 39 pL and 150.3 ± 55.6 pL respectively) (Appendix **Figure D.7**, **Table D.3**).

The compendium of results in **Figure 5.4** represent important additions of multiple on-demand droplet manipulations with individual and parallel droplet control for droplet-based microfluidic devices. These droplet operations in addition to the deterministic encapsulation provide a powerful device for sorting or assays on individual isoclones (as described below). Droplet-based microfluidic platforms typically use short pulses of electric potentials to either sort

Figure 5.5: Viability assay of MCF-7 cells. A) Trapped MCF-7 cells stained with FDA/PI after 10 min incubation on device (top), and after total actuation time of electrodes of 30 s (15 kHz, 126 V$_{RMS}$) and 10 min incubation on device (bottom). FDA stain reveals live cells and PI stain reveals dead cells. B) No significant difference in viability can be detected between the control (87.5±7.2%) and after actuation of electrodes (82.5±8.1%) (unpaired two-sample T-test, P=0.6687, N=3). Reproduced from Samlali et al. [227], with permission from John Wiley and Sons.

droplets [164] or manipulate droplets on an array of electrodes.[155] In these platforms, a droplet containing a biological cell experience a negligible electrical field and therefore their viability is maintained.[343, 272] We further investigated the effects of electrode actuation on cells in single-phase fluid, before cells were encapsulated. This is representative of electrode actuation for single-cell encapsulation. After priming the

device and trapping the single MCF-7 cells, we performed a viability assay by flowing a solution of fluorescein diacetate (λ_{ex}: 490 nm, λ_{em}: 526 nm) and propidium iodide (λ_{ex}: 488 nm, λ_{em}: 617 nm) through the channel labeling live and dead cells respectively. We compared the viability of voltage-potentiated and non-potentiated cells immediately after 30 s application of a low frequency AC electric potential. As **Figure 5.5 A** illustrates, the single cells are generally viable (shown in green) after being exposed to electric fields on the hybrid device compared to non-exposed cells. There was no significant difference between the cells directly exposed to the potentials and non-potentiated cells (**Figure 5.5 B**; P = 0.6687). We do observe a small loss of viability ($\sim$18 %) in the potentiated cells and observe a similar viability (87.5 $\pm$ 7.2%) in the non-potentiated cells. We believe the reduction in viability is attributed to the pre-processing sample handling procedures outside their native cell culture environment – e.g., cell sample preparation in the syringe. Regardless of the reasons for the loss, these initial results for viability suggests that actuating electrodes in our hybrid device does not significantly alter the cell viability ($>$ 80 %) and is suitable for our isoclonal procedures (described below).

5.2.4 Recovery and expansion of single-cell isoclones from a heterogeneous engineered cell population

To illustrate that our hybrid platform is suitable for single cell isoclonal sorting, we followed a gene-editing workflow to isolate the engineered cell from a heterogeneous cell population of an NCI-H1299 lung squamous cell carcinoma cell line.[344, 345] As shown in **Figure 5.6 A**, two plasmids containing Cas9 and a sgRNA, targeting either the eGFP or the RAF1 gene were used for transient lipid based transfection. We evaluated the transfection efficiency for each knockout experiment and observed a $\sim$25.3% and a $\sim$13.7% efficiency for eGFP and RAF1 respectively (**Figure 5.6 B**; Appendix Figure D.9). Knockout efficiencies were determined by a genomic cleavage detection assay and were calculated to be 4.95% and 8.3 % for eGFP and RAF1 respectively (**Figure 5.6 C**). Since we obtained a heterozygous population (**Figure D.10**), this called for a precise mechanism to sort and to isolate the low population of successful clones. Hence, for this part of the workflow, we used our hybrid device by trapping the cells in the device such that they can be imaged by fluorescence microscopy to determine which cells have been transfected (mCherry expression) (**Figure 5.6 D**; **Figure D.11**). Given the low number of successful clones, we predict that only 1 out of 6 traps are to contain a successful transfected cell ($\sim$16.7 %) (**Figure 5.6 E**). Indeed, there are times when

the traps did not fill with a transfected clone, however, with fine-tuned control and automation, our system can increase the flow rate in the forward direction which enabled the cells to squeeze through the traps such that a new cell can be trapped. This is one of the key capabilities of this device – trapping and releasing of isoclonal cells can be performed iteratively. In merely 45 minutes (instead of hours), isoclones can be trapped, encapsulated and sorted since (1) there is no requirement for iterative sample preparation or (2) isolation of a clonal cell line by limited dilution or other time-consuming techniques such as FACS is no longer needed.[11] After encapsulation of a successful isoclone, on-demand forward release of a single-isoclone in a droplet was performed to recover the isoclone (**Figure 5.6 F**).
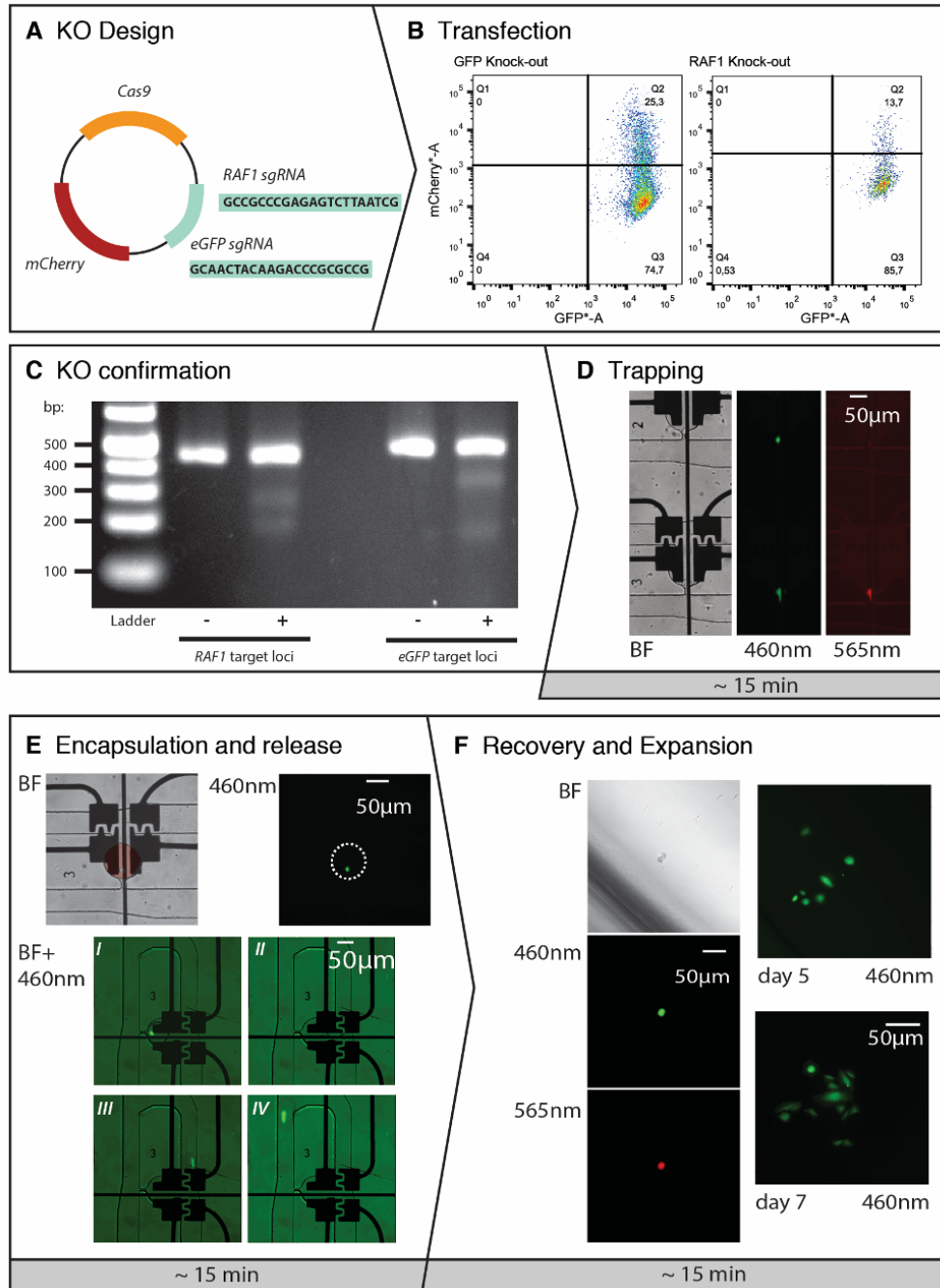
Figure 5.6: Gene-editing pipeline: screening and sorting of edited H1299 isoclone. A) Design of CRISPR-Cas9 based knockout cell line using a transient plasmid expressing Cas9 and guide RNA (sgRNA). B) Flow cytometry indicating transfection efficiencies. C) Knockout confirmation through a genomic cleavage detection assay. D) H1299 cells (eGFP+) resulting from lipid mediated transfection were trapped and screened for mCherry expression (red). Trapped cells show successfully transfected cells expressing mCherry (red) and GFP (green) (trap 3) and a cell only expressing native GFP (green) (trap 2). E) The transfected isoclone was encapsulated and subsequently released on-demand towards the outlets (trap 3, Frames I-IV from a video show the release of a single clone in a droplet). F) The droplet containing the isoclonal knocked out cell is collected from the outlet into a capillary and recovered into a 96-well plate. Two images showing expansion of the knocked-out GFP isoclonal cell on day 5 and day 7. Reproduced from Samlali et al. [227], with permission from John Wiley and Sons.

Expansion is a key step for the development of a new clonal cell line. After droplet sorting in microfluidic devices, the droplets can be recovered by directly flowing them into a different substrate for the recovery of cells using a chemical emulsion breaking method [253], centrifugal methods, [166, 346] or automated dispensing methods.[347, 348] As these methods are performed on emulsion of multiple droplets, we were unsuccessful at using these techniques to recover only the content of a single drop. The deterministic encapsulation and on-demand release of droplets in our platform allowed us to develop a method to recover the content of a single droplet from a water-in-oil microfluidic emulsion into a single well of a 96-well plate (see **Figure D.12**). Following an on-demand forward release of a single isoclone, we used a method similar to Langer and Joensson [349] by transferring the droplet into a capillary and onto a hydrophobic PTFE membrane (**Figure D.12**). The oleophilic membrane absorbs the HFE 7500 oil, removing the surrounding oil around the aqueous droplet. We washed the emulsions with FC-40 oil to remove excess HFE and surfactants and to release the isoclone into a media droplet which is subsequently transferred to a 96-well plate. As shown in **Figure 5.6 G** are images on day 5 and 7 showing the eGFP knockout isoclonal cells being expanded in a 96 well plate format. Transient plasmid based mCherry expression is lost after cell division.

The results described above demonstrate that hybrid-based microfluidics can be used to expedite the gene-editing workflow with very high performance and efficiency. With efficient trapping, encapsulation, releasing, recovery, and expansion procedures, hybrid microfluidic devices outperform the standard FACS and limited dilution assays for isolating single clones. These data presented here gives researchers interested in gene-editing the ability to establish monoclonal lines from heterozygous transfected populations, without the excessive manual handling steps required for selection, sorting, dilution, and clonal selection. In continuing work, we are using these devices (or derivative thereof) for low-transfection cell lines, which should highlight the advantages further by application to engineering cellular-based therapies.

5.3   Conclusion

The combination of hydrodynamic pressure and electrostatic force offered in the three-layer hybrid microfluidics device, was used to control flow in a cell and droplet trapping channel. First, we showed that reliable single-cell trapping can be followed with a deterministic encapsulation of the trapped single-cells. Using a phase change and electrode actuations, the one-phase cell containing aqueous flow can be turned into a droplet based two-phase flow. Next, we have shown efficient droplet controllability and fully characterized

100

the efficiency of droplet generation, bi-directional release and keeping. All of these operations, including deterministic encapsulation, can be performed with a 'click of a button' automation approach.

We applied this system to sort and recover gene-edited single cells from a NCI-H1299 non-small cell lung carcinoma cell population. Single cells from the heterozygous knockout population were encapsulated and sorted based on expression of a reporter protein. Next, we developed a methodology for recovery of an isoclone from a single droplet into a standard 96-well plate, and demonstrated this for a knockout cell line generation pipeline. Compared to automated systems used for sorting out isoclones in the cell engineering pipeline, such as FACS, limited dilution and clone picking, our system can work with low sample volumes ($< 200 \ \mu L$) and extremely low subpopulation levels (i.e. hard-to-transfect cell lines). The procedure is rapid (~ 45 min), and gentle on the cells, as our viability and expansion results show. We believe this could be of particular interest for use with other types of cells such as primary or stem cells.

Moving forward, improving alignment, and increasing the number of traps, will greatly improve the functionality of the device. To further increase the throughput of the system, we recommend the integration of image recognition algorithms in our Python based control system. We can also recommend automation of the cell recovery process, by combining our single-cell recovery technique with other automated microfluidic device and recovery substrate interfaces.[349, 347] Taken together, we can envision this multi-functional platform to be used for delivering reagents to isoclones on device, deterministic merging of two populations of single-cell containing droplets, non-binary single-cell sorting, expansion of isoclonal cultures based on their production of extracellular compounds and many other applications. Hybrid microfluidics creates a new pathway for many new mammalian cell assays that have been previously difficult to translate on microfluidic platforms.

5.4 Experimental section

5.4.1 Reagents and materials

Fabrication materials for hybrid microfluidic devices include a transparent photomask (CAD/Art Services Inc., Bandon, OR), S1811 positive photoresist coated glass slides (Telic, Valencia, CA, USA), MF321 developer (Rohm and Haas, Marlborough, MA, USA), CR-4 chromium etchant (OM Group, Cleveland, OH, USA), AZ-300T photoresist stripper (AZ Electronic Materials, Somerville, NJ, USA), <100> Si

wafers (Silicon Valley Microelectronics Inc., Santa Clara, CA, USA), and SU-8 5, SU-8 2035, SU-8 developer (Microchem, Westborough, MA, USA). Polydimethylsiloxane (PDMS) was purchased from Krayden Inc. (Westminster, CO) and chlorotrimethylsilane from Sigma-Aldrich (Oakville, ON, CA). Polylactic acid (PLA) material for 3D printing was purchased from Shop3D (Mississauga, ON, Canada). DI Water had a resistivity of 15 MΩ cm^{-1}.

Reagents for device preparation include 3M Novec HFE7500 engineering fluid and the surfactant 3M Novec 1720 (M.G. Chemicals, Burlington, ON, CA), PEG fluoro-surfactant dissolved in HFE7500 (20 g of 5% wt) (Ran Biotechnologies, Beverly, MA, USA), Fluorinert FC-40 (Sigma-Aldrich), Pluronics F-127 (EMD Millipore Corp, Billerica, MA, USA), and Triton X-100 (Sigma-Aldrich). All glass syringes were from Hamilton, Reno, NV, USA. All tubing and fittings were acquired from IDEX Health & Science, LLC, Oak Harbor, WA. Glass capillaries were purchased from World Precision Instruments (FL, USA). 0.22μm hydrophobic PTFE membrane was purchased from Thomas Scientific (NJ, USA).

All cell culture and preparation reagents were purchased from Thermo Fisher (Mississauga, ON, Canada). The cell culture reagents include DMEM, RPMI-1640, fetal bovine serum (FBS), penicillin/streptomycin and phosphate buffer saline (PBS) (Ca^{2+}/ Mg^{2+} free). The cell viability reagents include Fluorescein diacetate (FDA) (5 μg mL^{-1}) and Propiodium Iodine (PI) stock solutions (2 μg mL^{-1}). For transfection, a Neon Transfection kit (Mississauga, ON, Canada) and Lipofectamine^{TM} 3000 Transfection Reagent, Genomic Cleavage Detection kit were also purchased. EndoFree Plasmid Maxi Kit for plasmid purification was acquired from Qiagen (Toronto, ON, CA).

5.4.2 Device fabrication and assembly

The photomasks for the hybrid microfluidic devices were designed using AutoCAD 2017, with an electrode design and dielectric layer on a glass slide (50 x 75 mm), and a channel design fitting a 4"-Si wafer. Electrode and dielectric layer fabrication followed standard photolithography procedures reported previously.[45] Briefly, chromium-coated substrates with S1811 positive were exposed (11 s at 38-50 mW cm^{-2}), developed in MF-321 developer, etched with CR-4 chromium etchant, and stripped with AZ-300T photoresist stripper. For the dielectric layer, the devices are placed under plasma oxygen (Harrick Plasma PDC-001, Ithaca, NY) for 1 min 30 s, after which they are immediately spin coated with a SU-8 5 layer (10 s, 500 rpm, 30 s 2000 rpm), soft baked, and exposed to a sawtooth patterned mask. After post-bake, substrates were developed in SU-8 5 developer. A final hard bake cycle was performed by ramping up to 180°C in

15 min, baking at 180°C for 10 min and gradual cooling to room temperature. For the channel layer, soft-lithography procedure was followed. Si-wafers were placed under plasma oxygen for 1 min 30s, after which they are immediately spin coated with SU-8 2035 (500 rpm 10 s and 4000 rpm 30 s). The substrate was soft baked (55°C 1 min, 75°C 1 min, 95°C 5 min) and exposed under a Quintel Q-4000 mask aligner (Neutronix Quintel, Morgan Hill, CA) (10 sec at 38-50 mW cm$^{-2)}$. Substrates were post baked (55°C 1 min, 75°C 1 min, 95°C 5 min), and developed in SU-8 5 developer for 3 min 30 s upside down, without shaking. We followed a final hard bake cycle ramping up slowly to 165°C for 10 min and cooling slowly to room temperature. The master mold was treated with chlorotrimethylsilane vapour deposition in a desiccator for 45 min. PDMS (1:10 w/w ratio curing agent to prepolymer), was poured over the mold and left to cure in an oven at 65°C for 3 hours. Inlets and outlets were made using 0.75 mm or 0.35 mm biopsy punchers (World Precision Instruments, FL, USA), fitting 1/32" OD tubing or 360 μm OD tubing respectively, after which the PDMS was carefully washed with IPA, DI water, and cleaned with tape to remove debris before device assembly. The PDMS slabs were treated with oxygen plasma for 30 s and directly aligned with the dielectric coated electrodes under a dissecting fluorescence microscope (Olympus IX73, 10X). Device channels were immediately treated with Novec 1720 fluorosilane polymer surfactant for 20 min, under a weight of 750 g. Devices were then air dried (20 min) and baked (150°C, 30 min). To connect the droplet generator and the serpentine trap part of the device, a 2 cm piece of PEEK tubing (360 μm OD) was cut and treated with similar Novec 1720 treatment. Outlet blockers were made by hot gluing one end of a 1" PEEK 1/32" OD tubing.

5.4.3 Device operation

Gastight 500 μL glass syringes were prepared with the fittings and tubing as reported previously, adding one 2.5 mL syringe with a 1.87 mm magnetic stirring disk (V&P Scientific, San Diego, CA, USA). Syringes were installed on a low-pressure neMESYS pump system (Cetoni, Korbussen, DE), installed with a clamp holding a syringe stirrer (Nannostirus, V&P scientific, San Diego, CA, USA). The microfluidics device was placed inside a 3D printed pogo pin holder of which the base plate fits on the stage of an inverted microscope. The flow inside the microfluidic channel was observed under a 4X or 10X objective under bright-field illumination. Fluid flow and electrode actuation were controlled using an in-house automation system and graphical user interface. In experiments that consisted of trapping, encapsulation, keeping and releasing, we followed a 5-step procedure (**Appendix D.3**, **Figure 5.4**). First, priming was performed at

a flow rate of 0.8 to 8 nL s^{-1} with PBS (Ca^{2+}/ Mg^{2+} free) containing 2% Pluronics F-127 for 5 min, from inlet 1, to remove air bubbles and prevent cells sticking to the channel walls. The priming solution was then moved to outlet 1. The droplet generator was flushed with HFE-7500 with 2% fluorosurfactant, from inlet 4. Second, cells were loaded from inlet 1 at a flow rate of 1 nL s^{-1}, in PBS (Ca^{2+}/ Mg^{2+} free) or in complete media. Once cells are entering the inlet, the priming solution is turned off. We used MCF-7 cells as a model cell line and all reagents prior to operation were filtered sterilized. For trapping the cells, the filtered MCF-7 cells were resuspended in PBS (Ca^{2+} Mg^{2+} free) and pipetted into a UV sterilized 2.5 mL glass gastight syringe with stirring disk in a laminar hood. Third, droplets were generated using HFE 7500 with 2% w/v fluorosurfactant from inlet 4 with varying flow rates and PBS or media at 0.6 nL s^{-1} from inlet 3. On-demand droplet generation was performed by actuating electrodes with 15kHz 126 V$_{RMS}$. Fourth, single-cell encapsulation can be performed. Droplet generation was paused after it stabilized, the cell flow was stopped, and the tubing was connected from outlet 3 to inlet 2 , to the single-cell analysis chip. Phase change for encapsulation was performed using HFE 7500 with 2% w/v fluorosurfactant at a flow rate of 4 nL s^{-1}. Fifth, under forward flow several operations (droplet releasing, keeping or merging) can be performed using electrode actuation patterns. To reverse the flow, the tubing in inlet 1 and outlet 1 need to be carefully removed, and a second oil syringe can be connected to outlet 2.

5.4.4   Cell culture

MCF-7 cells were grown and maintained in DMEM containing 10%fetal bovine serum (FBS) with no antibiotics in an incubator at 37°C with 5% CO$_2$. Human lung squamous cell carcinoma dual-labeled (eGFP, Luciferase) stable NCI-H1299 cells (SCL-C01-HLG; Genecopoeia, Inc, Rockville, MD) were grown in RPMI-1640 containing 10% FBS without antibiotics at 37°C with 5% CO$_2$. For assays on device, cells were washed with PBS, trypsinized and resuspended in complete growth media. The cells were then centrifuged at 200 rcf for 4 min and the cell pellet was resuspended in either PBS or complete media without FBS to obtain an initial cell concentration of approximately 2 x 10^6 cells mL^{-1}. Cells were filtered through a 40 μm cell strainer (VWR, Mississauga, ON, CA) to remove cell clumps. An aliquot of the cell suspension ($\sim$250 μL) was pipetted into a syringe for operation. Conditioned media for cell expansion was made by collecting complete growth media from 1-day old 80% confluent NCI-H1299 cells (RPMI-1640 10% FBS, 1% penicillin/streptomycin) and adding 50% fresh complete growth media filter sterilizing and storing it at -80°C until used.

5.4.5 Viability assays

For viability assays, a 1X FDA/PI solution was prepared with 10 μL PI stock and 2.5 μL FDA stock, kept on ice, and used within 2 h. FDA/PI solution was placed in a 500 μL syringe covered with aluminium foil. After trapping of MCF-7 cells, the two top electrodes under each trap (top left under the trap, top right under the main channel) were actuated for 10 s (15 kHz 126 V_{RMS}), after which the ground electrode was actuated for 10 s (15 kHz 126 V_{RMS}) followed by activating the two bottom electrodes for 10 s (15 kHz 126 V_{RMS}). 1X FDA/PI was then flushed through the device at 1 nL s^{-1} and the device was incubated in the dark for 10 min. After incubation, MCF-7 cells were imaged (FDA: λ_{ex} = 495 nm, λ_{em} = 520 nm, 300 ms exposure; PI: λ_{ex} = 535 nm, λ_{em} = 617 nm, 3 s exposure) under a fluorescent microscope (Olympus IX73 Inverted Microscope; Québec City, Canada) and images were analyzed using ImageJ. This process was repeated for control cells (i.e. non-voltage potentiated cells).

5.4.6 H1299 Transfection

pCRISPR_eGFP_314, pCRISPR_RAF1_94 and pCRISPR/Cas9_All_in_one_LacZ plasmids (Appendix **Table D.4**) were transformed into DH5α stocks, grown overnight in LB with ampicillin, and purified (endo-toxin free). For forward lipid transfection of NCI-H1299 cells with an All-in-one pCRISPR/sgRNA plasmid, on day 0, cells were subcultured in a 24-well plate to reach confluency the day after (day 1). On Day 1, cells were transfected using 5 μg DNA per well. After 48 hours (Day 3), cells were harvested or subcultured into a 6-well plate. Confluent cells were trypsinized, centrifuged (200 rcf, 4 min), strained through a 40 μm filter, and resuspended in either PBS or flow cytometry buffer.

5.4.7 On-chip sorting, clonal recovery and expansion

For microfluidic sorting and cell recovery, PBS resuspended cells were loaded into a sterile 2.5 mL syringe with stir disk and 1/32" OD PEEK tubing. The device was primed with PBS with 2% F-127, and transfected NCI-H1299 cells were trapped at 4 nL s^{-1}. Capillary tubes were filled with HFE-7500 2% fluorosurfactant and placed on the outlet of the single-cell trapping device. pCRISPR_eGFP_sg314 and pCRISPR_RAF1_sg94 transfected cells were sorted by forward releasing mCherry+/eGFP+ cell containing droplets on-demand. A single droplet containing an isoclone was loaded individually into each capillary. The oil flow was reversed to hydrodynamically release the remaining droplets to waste. For expansion,

20 μL conditioned media was placed on a hydrophobic PTFE membrane situated on a custom 3D printed holder at 37 ^{o}C. The single capillary containing the recovered droplet was immediately flushed on top of the conditioned media droplet by 10 μL of FC-40 oil. After 1 min incubation, the droplet was recovered in a 96-well plate containing 50 μL conditioned media per well at 37 ^{o}C. After 24 h, single adherent clones could be observed based, representing eGFP or RAF1 knockouts. After five days, the expanded cells were maintained by changing the culture media complete growth media. Clones were incubated in a 96-well plate at 5 % CO2, 37 ^{o}C to allow expansion to 50 % confluency.

5.4.8   Flow cytometry and genomic cleavage analysis

To obtain transfection efficiency, transfected and control cells were resuspended in sorting buffer (1X PBS (Ca^{2+}/ Mg^{2+} free), 1mM EDTA, 25 mM HEPES pH 7.0, 1% FBS, sterilized using a 0.2 μm filter), placed on ice, and loaded in a BD FACS Melody (BD Biosciences, San Jose, CA) after 24 h post-transfection. Gating was performed for forward versus side scatter (FSC vs SSC) on control population after which the positive control fluorescence and transfected population were measured (GFP: 488 nm laser, BP 585/40 nm and mCherry: 488 nm, LP 670 nm). To obtain an estimate of knockout efficiency, a genomic cleavage detection assay (GCD) was performed (GeneArt Genomic Cleavage detection kit, Thermo Scientific) following the manufacturer protocol. Briefly, cell genomic DNA was extracted 48 h post-transfection and ∼500bp fragments containing gRNA target sites were amplified using PCR and primers, designed using NCBI primer-BLAST (Appendix **Table D.5**) and BLASTed against *Homo sapiens*. The fragments were re-annealed, and a cleavage reaction was performed using the manufacturer provided endonuclease. A 2% lithium acetate borate gel (10 mM lithium acetate, 10 mM boric acid) was used to resolve the cleavage bands in 20 min at 220 V. Parent and cleavage band intensities were compared to calculate the cleavage efficiency. Expected cleavage bands were shown in Appendix **Table D.6**.

5.4.9   Data analysis

Data analysis was performed with R v3.6.2. Data from **Figure 5.3** was fitted with a 3-parameter logistic regression model with continuous predictors (Hosmer-Lemeshow goodness of fit test P < 0.05 for all three models) (Appendix **Table D.2**). Image analysis to calculate droplet volume, and gel analysis were performed using Fiji by ImageJ. Flow cytometry density plots were generated using FlowJo v10. Fluid and electric

field simulations were performed with COMSOL 5.4 Multiphysics (**Appendix D.2**). All in-house code was

written in Python v2.7.15.

Chapter 6

Conclusion, Future Work and Reflections

6.1 Future directions

To support future advances in single-cell analysis, new developments in software, hardware and biological tools are needed. Given the massive availability of single cell data, computational methods and theoretical knowledge on cell complexity are increasingly available, yet the limited number of hardware tools restrict the applied work that can be done. Meeting this need is difficult. Researchers that develop microfluidic technologies, do so at labs that are dedicated to the design and fabrication of microfluidic devices. As a result, in many cases today, implementing new microfluidic technologies in a clinical setting, industry, or academia is difficult. The expertise required is extensive, and the equipment is too specialized. Currently, if one would want to implement a microfluidic system to automate a particular single-cell assay, custom designs and collaboration with academia, or an entrepreneurial spirit are needed.

We believe in a future in which hospitals have their own custom microfluidics labs, spearheading new solutions in precision medicine. In this future, microfluidics can empower us to perform diagnostics in the palm of our hand, with deployable and accessible droplet screening technologies. In clinical settings it could help us gain insights into patient specific tumor heterogeneity which can lead to patient derived gene therapies. Droplet-digital tools can be a part of this story, when they are designed with flexible and robust implementation in mind. To work towards this future we can recommend further work on:

- Developing droplet-digital technology to be compatible with mass manufacturing techniques such as injection molding, hot embossing, PCB fabrication.

- Developing a digital library of standardized droplet-digital components such as on-demand droplet generators or sorters, for standardizing the design of these devices

- Using and improving programming languages designed to translate biological protocols into computer-readable code

- Developing additional droplet-digital devices with clinically relevant end-to-end workflows

This relates to the work presented in this thesis by:

- Increasing the throughout of the device presented in Chapter 5

- Expanding the applications of the device presented in Chapter 5 to include cell-cell communications studies by deterministic two-cell encapsulation

- Expanding the single cell detection methods of the device presented in Chapter 5 by using transparent electrodes, image-based learning techniques, impedance-based cell sensing techniques

- Developing new droplet digital manufacturing protocols such as a silicon based architectures for the device presented in Chapter 5, bonding techniques for PCB's and thermoplastics, etc

- Exploring smaller footprint electronics, and further open-sourcing our software to increase the accessibility of the automation system presented in Chapter 3

6.2 Conclusion

In this work we have demonstrated several on-demand droplet operations in channels, including high-throughput binary droplet sorting, droplet isolation, droplet generation, droplet mixing, n-ary sorting, droplet trapping and releasing, and finally, deterministic single-cell encapsulation. We have shown that droplet-digital technology has increased the control over droplets compared to existing droplet-in-channel technology, without losing high throughput capabilities. This has allowed us to screen single spore derived fragile filamentous droplet libraries, screen yeast libraries based on culture conditions, and precisely sort a small population of edited mammalian cells.

We believe the droplet digital platforms presented here have expanded the application space of droplet-digital platforms and have proven to be useful to automate end-to-end workflows relevant for synthetic

biologists. In particular, we expect that these droplet-digital devices are extremely valuable in work where quality matters over quantity. For example, the use of droplet-digital devices in single-cell studies with sensitive or small cell populations, such as patient derived immune cells, can be important for precision medicine. Delivering reagents to isoclones on device, deterministic merging of two populations of single-cell containing droplets, non-binary single-cell sorting, expansion of isoclonal cultures based on their production of extracellular compounds, spatio-temporal Omics analysis, and many other applications

Short-term, we hope that researchers have a line of sight of how these technologies can be used within their facilities, and applied to their particular problems. We expect that droplet-digital devices will be more frequently demonstrated. To support the advancement of the microfluidics field and the adoption of droplet-digital tools, we made all of our software open-source. We think continued development of droplet-digital technologies will refine fabrication and operation of these devices. Engineering cells using microfluidic devices like ours will show increased success rates, and we expect in particular to see its use for engineering primary cells of low cell counts, and other applications with mammalian cells.

Appendix A

List of publications

Peer-reviewed journal articles

- Davis, A. N., Samlali, K., Kapadia, J. B., Perreault, J., Shih, S. C. C., & Kharma, N. (2021). Digital Microfluidics Chips for the Execution and Real-Time Monitoring of Multiple Ribozymatic Cleavage Reactions. ACS Omega, 6(35), 22514–22524. `https://doi.org/10.1021/acsomega.1c00239`

- Little, S. R., Perry, J. M., Samlali, K., & Shih, S. C. C. (2020). Chapter 8:Droplet Microfluidics: Applications in Synthetic Biology. In Droplet Microfluidics (pp. 193–222). `https://doi.org/10.1039/9781839162855-00193`

- Samlali, K., Ahmadi, F., Quach, A. B. V., Soffer, G., & Shih, S. C. C. (2020). One Cell, One Drop, One Click: Hybrid Microfluidics for Mammalian Single Cell Isolation. Small, 16(34), 2002400. `https://doi.org/10.1002/smll.202002400`. **Journal cover page**

- Ahmadi, F., Samlali, K., Vo, P. Q. N., & Shih, S. C. C. (2019). An integrated droplet-digital microfluidic system for on-demand droplet creation, mixing, incubation, and sorting. Lab on a Chip, 19(3), 524-535. `https://doi.org/10.1039/C8LC01170B`

Conference talks and proceedings

- Leal Alves, C., Samlali, K., Selim, A., Ahmadi, F., & Shih, S. (2021, July 5). The use of droplet-digital (D2) microfluidics to study protein-protein interaction in a cell-free system. Proceedings of the Emerging Investigators in Microfluidics Conference. Emerging Investigators in Microfluidics Conference, Online, Spain.

  `https://www.nanoge.org/proceedings/EIMC/60c388e770174629ad886773`

- Samlali, K., Leal Alves, C., Jezernik, M., Beauchemin, M., Oeser, M., & Shih, S. C. C. (2021, July 5). A low voltage co-planar microfluidic sorter for screening fungal bio-control agents. Proceedings of the Emerging Investigators in Microfluidics Conference. Emerging Investigators in Microfluidics Conference, Online, Spain. `https://www.nanoge.org/proceedings/EIMC/60c23a0a70174629ad8865d2`

- Samlali, K., Ahmadi, F., Quach, A.B.V., Soffer, G., Shih, S. C. C. Society for Laboratory Automation and Screening International Conference SLAS 2020, San Diego, US. January 2020. **Podium talk**

- Samlali, K., Ahmadi, F., Quach, A.B.V., Soffer, G., Shih, S. C. C. One cell, one drop, one click: hybrid microfluidic mammalian single-cell engineering. The 23rd International Conference on Miniaturized Systems for Chemistry and Life Sciences MicroTAS2019, Basel, CH. October 2019. **Podium talk**

- Samlali K., Alaa Selim, Cell-free protein synthesis on chip: a fresh approach to biosensors. 4th Annual Synthetic Biology Symposium SynBio 4.0, Waterloo, CA. May 2019. **Best talk award**

Appendix B

Supplementary Info Chapter 3

B.1 Substrate Structures
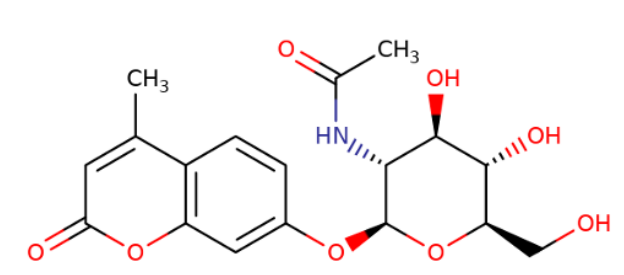
Figure B.1: 4-methylumbelliferyl-N-Acetyl-beta-D-glucosaminide or 4-MU 2-acetamido-2-deoxy-b-D-glucopyranoside (4MU-GlcNAc). Image retrieved from Biosynth Carbosynth, https://www.carbosynth.com
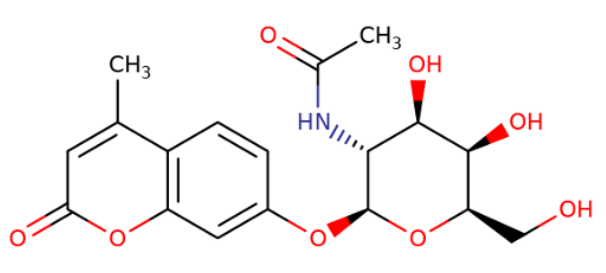
Figure B.2: 4-methylumbelliferyl-N-Acetyl-beta-D-galactosaminide or 4-MU 2-acetamido-2-deoxy-b-D-galactopyranoside (4MU-GalNAc). Image retrieved from Biosynth Carbosynth, https://www.carbosynth.com
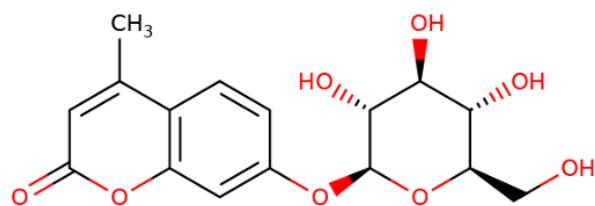
Figure B.3: 4-methylumbelliferyl beta-D-glucopyranoside (4MU-Glc). Image retrieved from Biosynth Carbosynth, https://www.carbosynth.com
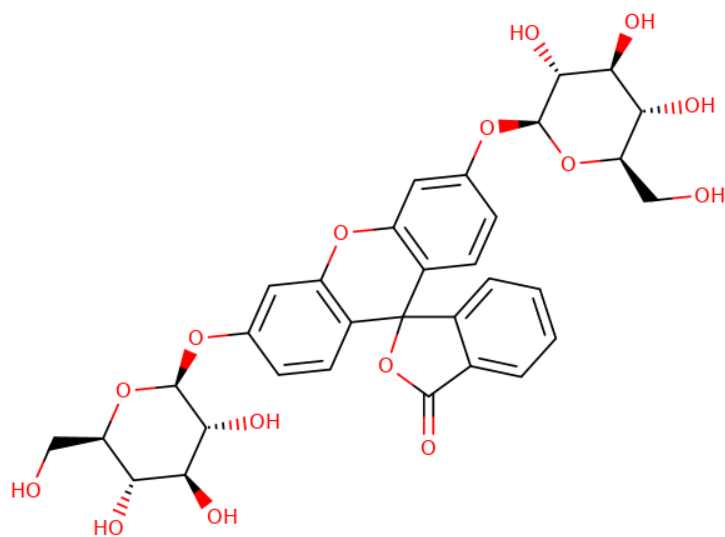
Figure B.4: Fluorescein-di-(beta-D-glucopyranoside) (FDGlc). Image retrieved from Biosynth Carbosynth, https://www.carbosynth.com
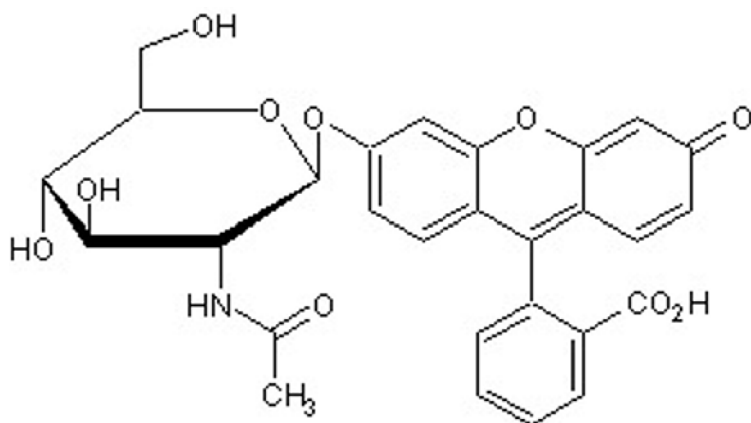
Figure B.5: Fluorescein mono-beta-D-N-acetylglucosaminidase (FL-GlcNAc). Image retrieved from Abcam, www.abcam.com
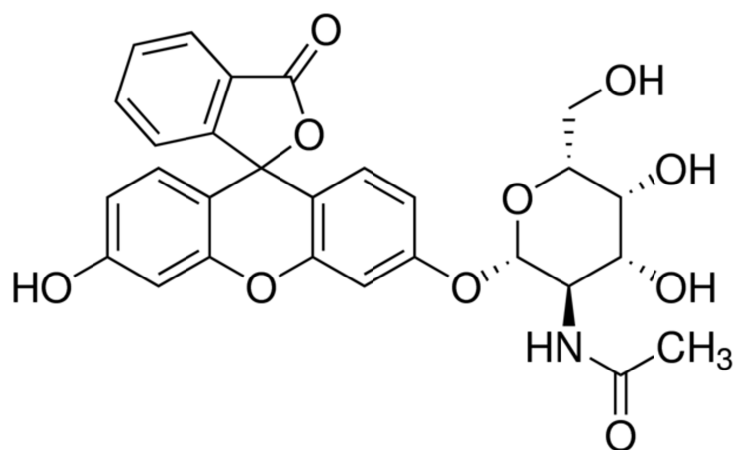
Figure B.6: Fluorescein mono-(N-Acetyl beta-D-galactosaminidase) (FMGalNAc). Image retrieved from Sigma-Aldrich, www.sigmaaldrich.com
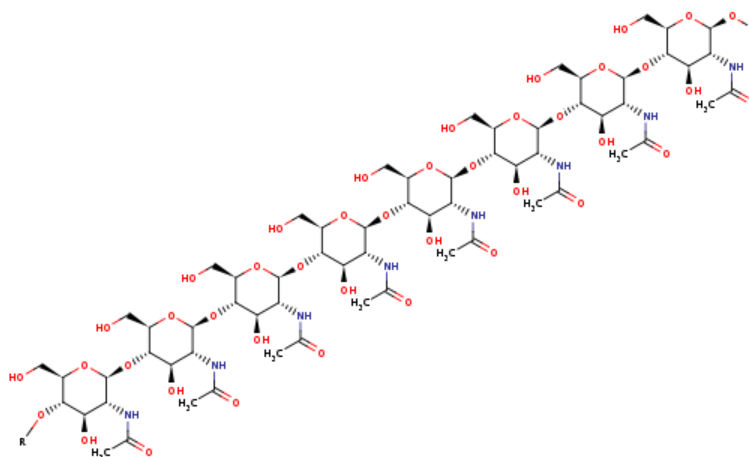
Figure B.7: Chitin is a fungal cell wall constituent. Homopolysaccharide consisting of repeated units of N-acetyl-glucosamine covalently linked by β-1,4 linkages. Structure retrieved from the BRENDA database,www.brenda-enzymes.org
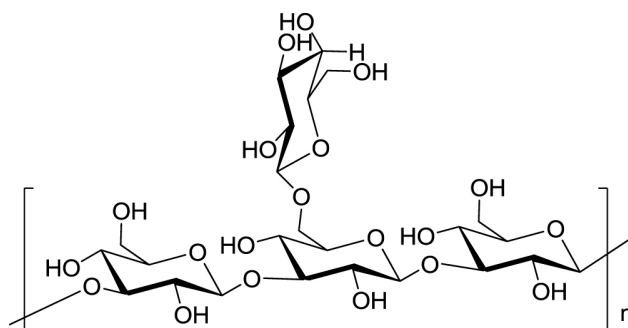
Figure B.8: Laminarin is a fungal cell wall constituent. Polysaccharide cosisting of repeated glucose units, covalently linked by β-1,3 linkages with β-1,6 side branches. Image retrieved from Mai Huong Le et al 2016 Adv. Nat. Sci: Nanosci. Nanotechnol. 7 045019, under CC 4.0

B.2 Device and automation system

Microfluidic devices shown in **Figure 1**, the PDMS-fabricated channel height was 70 μm. The electrode gap is 15 μm, and a dielectric (SU 8-5) of 7 μm (smaller than half the size of the gap) was deposited on top. All other dimensions and architecture can be found in **Figure B.9**.

To apply potentials for sorting droplets, an AC potential was generated using a function generator

(33201A Agilent, Allied Electronics, Ottawa, ON) and an amplifier (PZD-700A, Trek Inc., Lockport, NY) and sent to a custom board with Arduino UNO controlled optocoupler switches. For a detailed hardware overview, we refer to our previous work.[227] Pump (Nemesys CETONI) and electrode operation were driven using python-based software as described in our previous work.[227] In addition, background subtraction, gating and sorting were all be performed through our Python based open-source software with GUI (**Figure B.17**).

See `https://bitbucket.org/shihmicrolab/fungalmicrofluidics.git`, GNU GPLv3. Seabreeze was used as a Python library for communication with the spectrometer, allowing for compatibility of this software with several other affordable spectrometers `https://python-seabreeze.readthedocs.io`. The graphical user interface consisted out of two main windows: one window contained the control interface, and another window contained a plot viewer with a raw spectrum and a processed spectrum (denoised and indicating the sorting gate) (**Figure B.18**).

B.3   Spectrum detection and signal processing

To eliminate the background signal, we initially placed a band-pass filter in-line between the spectrometer and the outgoing 400 μm emission optical fiber. For peak detection, a program was created for detecting any intensity above a user-defined threshold intensity. Although the band-pass filter reduced the intensity of the peaks (loss-of-signal but leading to a higher LOD, useful information outside the band-pass filter range was lost. The resulting spectrum provided useful information on the sample type. For example, air droplets reflected excitation light and showed peaks with a large base (> 200 nm) and high intensity often overlapping with the sample band-pass range. Air droplets were accidentally misidentified as droplets within the sorting gate. We finally opted to not use an emission band-pass filter and use a background subtraction method and peak detection algorithm instead. A background frame of experimental light conditions (excitation light, background light, noise, with oil sample) was recorded and subtracted from future frames (**Figure B.11**). The peak detection algorithm detects peaks (local maxima) in a subset (gate) of the spectrum. By setting the peak height range, peak base width, a wavelength and maximum peak height gate, and distance to neighboring peaks, reliable detection of emission spectra could be performed. As such, this peak detection method offers several advantages over specific wavelength based raw intensity detection performed with PMT's.

B.4 Tables and figures

Table B.1: COMSOL electric field model parameters

Property	Value	Unit
PDMS relative permittivity	2.75	
PDMS electrical conductivity	4e-13	S/m
HFE 7500 oil relative permittivity	5.8	
HFE 7500 electrical conductivity	3e-8	S/m
Dielectric thickness SU-8 5	7.0	μm
SU8-5 relative Permittivity	4	
SU8 electrical conductivity	2.8e-14	S/m

Table B.2: Comparison of system needs between typical FADS sorting setup and our system.

	Equipment	
Purpose	Typical FADS Sorting setup	Samlali et al. sorting setup
Excitation	Laser, microscope, objectives for focusing	High power LED, optical fiber, in-line short pass filter
Detection	PMT	Optical fiber, mini-spectrometer
High-voltage electronics	Amplifier, function generator, high-voltage and frequency switchboard	None – only require low-voltage electronics (< 36 V)
Sorting efficiency	$>90\%$	$\sim 86\%$
Estimated costs	$>\$10$k	\$5k (most expensive is the spectrometer)

Table B.3: Confusion matrix evaluation measures

Measure	Value	
Error rate	ERR	0.03703704
Accuracy	ACC	0.96296296
Sensitivity	SN	0.77142857
True positive rate	TPR	
Recall	REC	
Specificity	SP	0.99519231
True negative rate	TNR	
Precision	PREC	0.96428571
Positive predictive value	PPV	
False positive rate	FPR	0.00480769
Matthews Correlation coefficient	MCC	127.202795
F-score	F	5
Beta		0.5

Table B.4: Paired t-test of enzymatic activity of FL-GlcNAc sorted and recovered strains compared to wild-type *C.rosea*

	Strain	Mean	P	P Adj	Significance
	WT	**2.104461**			
	MC1	6.890289	1.34E-04	0.00201	**
	MC5	2.288303	2.75E-01	0.351064	ns
4-MU GalNAc	MC6	2.458805	1.27E-01	0.177209	ns
	MC2	3.680456	2.00E-03	0.010909	*
	MC4	3.060147	8.00E-03	0.02087	*
	WT	**9.627257**			
	MC1	12.4445	6.40E-02	0.112941	ns
	MC5	10.10992	3.01E-01	0.3612	ns
4-MU GlcNAc	MC6	10.26913	4.31E-01	0.453684	ns
	MC2	14.88973	5.50E-02	0.1	ns
	MC4	11.4168	1.48E-01	0.201818	ns
	WT	**0.497538**			
	MC9	1.236722	9.60E-02	0.144	ns
	MC1	5.554288	4.33E-06	0.00026	***
	MC5	0.799743	4.20E-02	0.07875	ns
	MC6	0.913543	2.67E-01	0.348261	ns
4-MU Glc	MC7	0.835237	1.99E-01	0.265333	ns
	MC8	1.075781	3.20E-02	0.061935	ns
	MC2	3.001162	6.00E-03	0.02087	*
	MC3	1.623214	1.10E-02	0.025385	*
	MC4	1.525666	1.60E-02	0.034286	*

Table B.5: Paired t-test of enzymatic activity of of FL-GalNAc sorted and recovered strains compared to wild-type *C.rosea*

	Strain	Mean	P	P Adj	Significance
	WT	**2.391399**			
	MG1	4.796552	2.00E-03	0.009	**
	MG7	4.975938	1.00E-03	0.006545	**
	MG8	3.241116	6.70E-02	0.094588	ns
4-MU GalNAc	MG10	4.258935	1.50E-02	0.03375	*
	MG21	2.350239	8.96E-01	0.896	ns
	MG11	**4.269993**	6.00E-03	0.018783	*
	MG12	4.911983	2.00E-03	0.009	**
	WT	**4.987652**			
	MG1	10.46049	2.45E-04	0.003528	**
	MG16	5.318272	3.24E-01	0.343059	ns
	MG2	7.75972	3.13E-01	0.336358	ns
	MG3	**6.947886**	8.00E-03	0.022154	*
	MG18	6.439087	3.90E-02	0.0624	ns
	MG3	9.721721	4.48E-04	0.00468	**
	MG4	6.537106	9.20E-02	0.120436	ns
	MG5	7.417304	1.90E-02	0.036973	*
4-MU GlcNAc	MG19	4.812144	6.37E-01	0.645972	ns
	MG7	9.966263	2.00E-03	0.009	**
	MG8	15.53919	3.34E-05	0.002405	**
	MG9	10.2046	1.37E-04	0.003528	**
	MG10	18.98473	2.00E-03	0.009	**
	MG21	13.56671	3.20E-02	0.053581	ns
	MG11	19.05737	8.00E-03	0.022154	*
	MG12	19.55865	5.00E-03	0.016364	*
	MG13	9.95441	3.00E-03	0.011368	*
	MG14	9.514313	2.15E-04	0.003528	**
	WT	**0.513789**			
	MG15	0.557189	5.41E-01	0.556457	ns
	MG1	1.170213	3.00E-03	0.011368	*

MG2	1.376019	1.10E-02	0.029333	*
MG3	1.052171	3.00E-03	0.011368	*
MG18	0.699876	8.00E-02	0.108679	ns
MG3	0.902477	1.40E-02	0.032516	*
MG4	0.908055	1.30E-02	0.032276	*
MG5	1.246052	7.90E-04	0.00632	**
MG19	0.648324	2.70E-01	0.299077	ns
MG7	0.785153	2.50E-02	0.042857	*
MG8	1.300507	6.00E-04	0.0054	**
MG9	1.343989	4.55E-04	0.00468	**
MG10	1.143305	7.00E-03	0.021	*
MG21	1.729655	1.00E-03	0.006545	**
MG11	1.53515	4.20E-02	0.065739	ns
MG12	2.649297	4.00E-03	0.0144	*
MG13	0.900675	1.40E-02	0.032516	*
MG14	1.808683	1.55E-04	0.003528	**
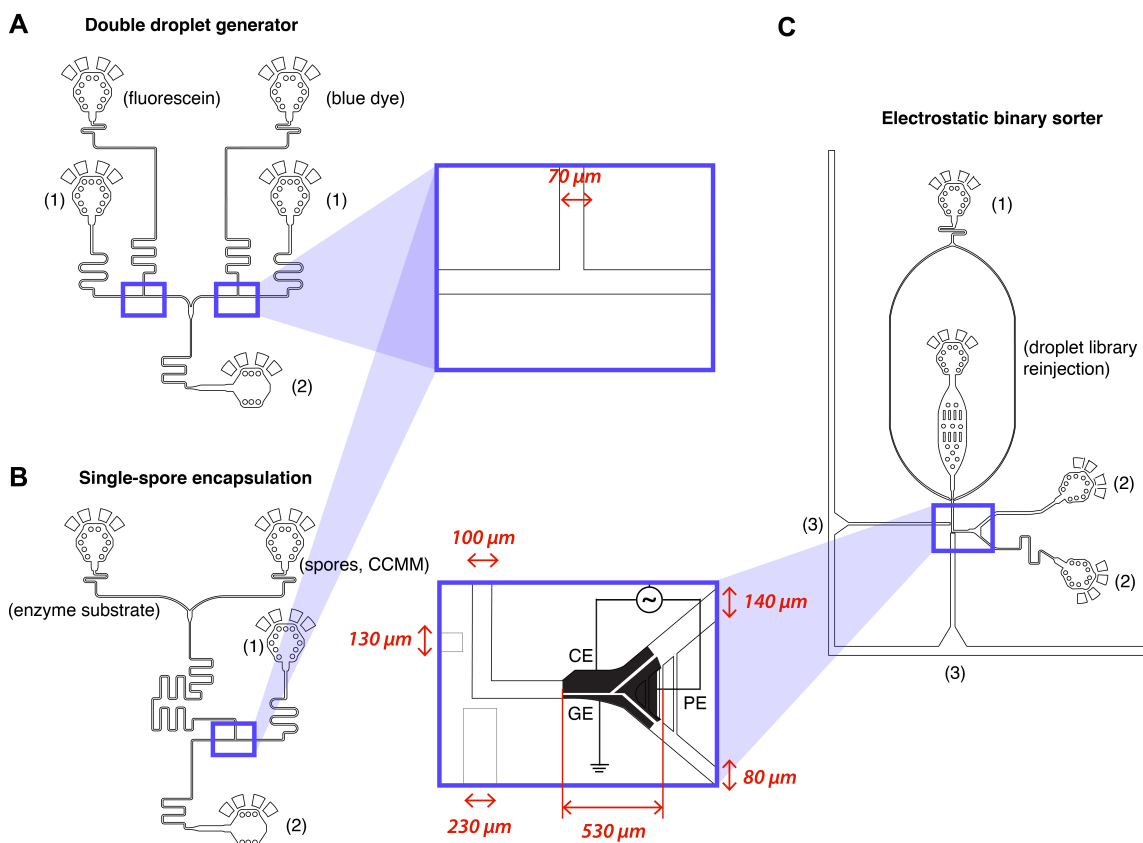
Figure B.9: Microfluidic devices for (A) optimizing sorting parameters and (B and C) fungal enzyme screening. Two T-junction droplet generators (left) were designed with 70 x 70 (w x h) μm channel dimensions. (A) A first droplet generator was used for creating a mixed droplet library for sorter characterization. Fluorescein and blue dye droplets were generated with two separately controlled T-junction droplet generators that produced droplets of the same size (oil/aqueous flow ratio identical) at different flow rates. (B) A second droplet generator was used to generate a filamentous fungi droplet library. An enzymatic substrate and a spore solution were injected at the same flow rates ($\sim$100 nL/s), and mixed through a serpentine mixer before droplet generation. Droplets were collected from the outlet (labeled as (2)) into a PCR tube. For both devices, fluorinated oil (HFE 7500 2% fluoro-based surfactant) was injected into the inlet (labeled as (1)). (C) The microfluidic binary sorter was designed with co-planar electrodes under a dielectric (fabrication similar to our previously reported work 1,2). The emission fiber channel (3) has a 100 μm height for the excitation fiber and a 170 μm height for the emission fiber. All other dimensions are as indicated on the zoomed in sorting region. The droplet library was reinjected into the device inlet and droplets were spaced with spacer oil (1). After sorting, droplets were collected from the outlets (2).
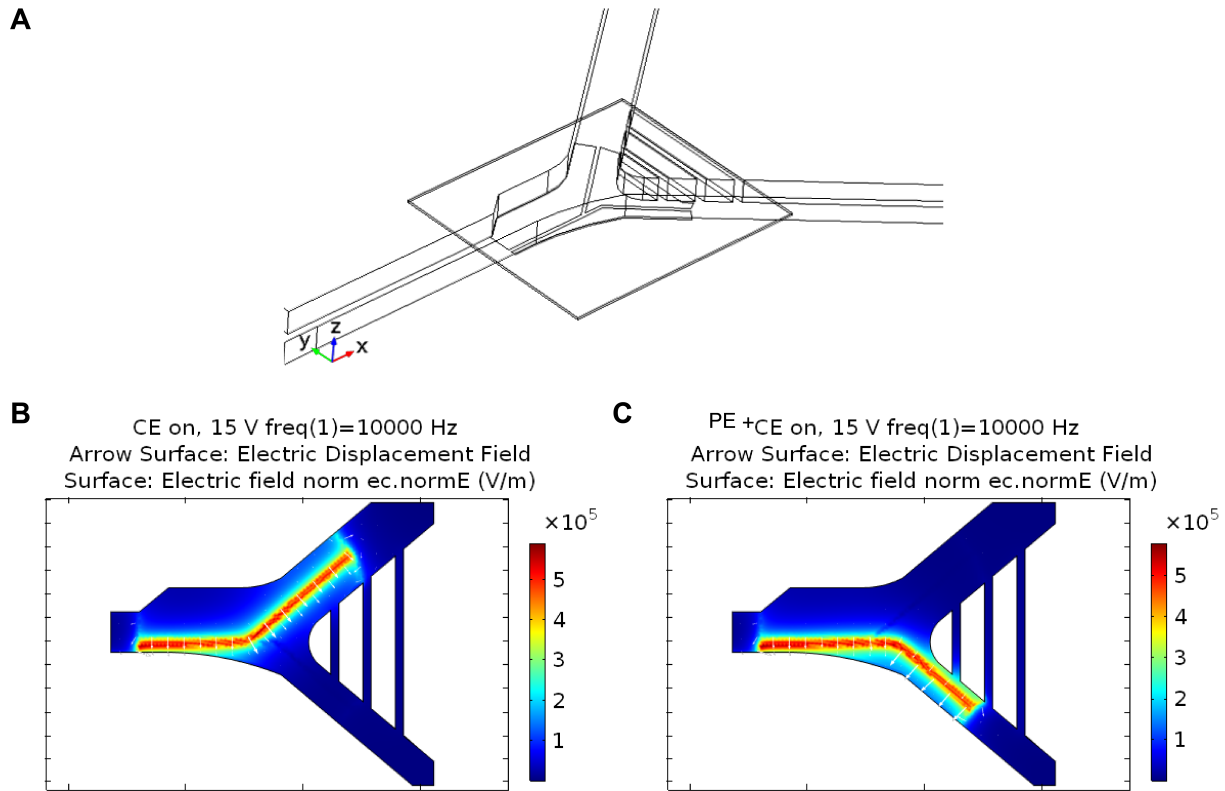
Figure B.10: Simulation of the electric displacement field above the electrodes. (A) Model components include a channel layer with PDMS boundary and HFE 7500 domain, a 7μm thick dielectric layer and three electrode terminals. (B) Top view of electrostatic displacement field vectors and electric field strength (V/m) at z = 7 μm (SU8 5 dielectric – HFE7500 oil interface) when the constant electrode (CE) is on with 15 $V_R MS$, 10kHz applied. The electrostatic force vectors are perpendicular to the gap and the flow velocity. (C) Top view of electrostatic field strength at z = 7 μm when both the CE and the pulsing electrode (PE) are on with 124 V applied.
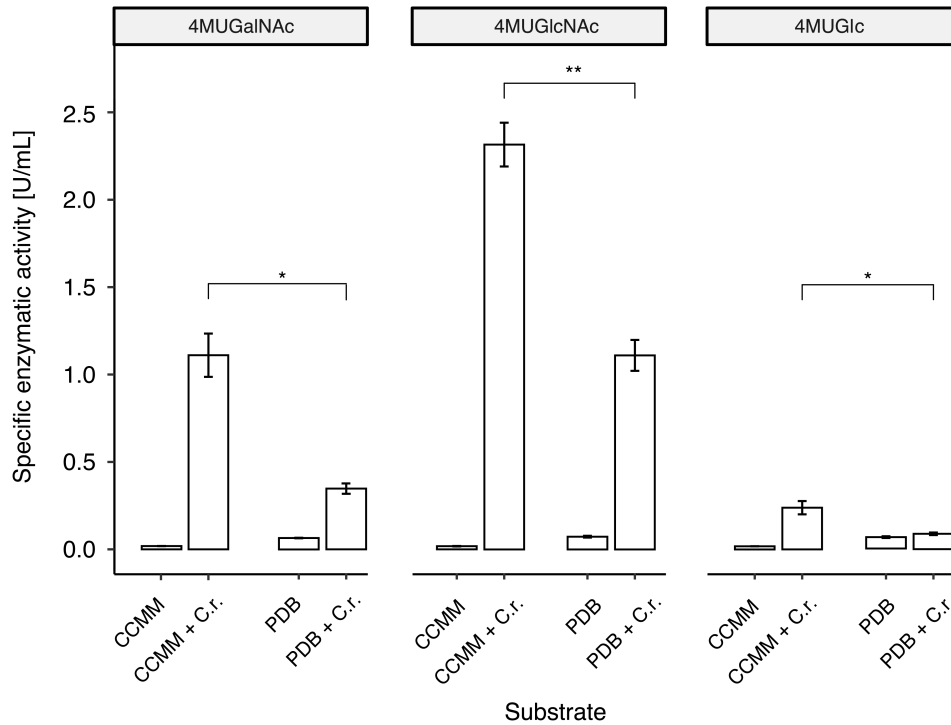
Figure B.11: *C.rosea* **well-plate end-point enzymatic assay**. The enzymatic activity of cell wall degrading enzymes in C. rosea cultures (27 ^{o}C, 5 days) was compared in different media formulations (colloidal chitin minimal media, CCMM, solid, and potato dextrose broth, PDB, liquid). Enzymatic activity is displayed as an end-point a specific enzymatic activity (U/mL) of substrate 4-MU-GlcNAc for chitinase activity, 4-MU-GalNAc for galactosaminidase activity, and 4-MU-Glu for β-1,3-glucanase activity. A unpaired Welch t-test was performed between the enzymatic activity in *C.rosea* grown in solid and liquid media (* for $P < 0.05$, ** for $P < 0.01$) (30 min, 37 ^{o}C, pH 5.1). Error bars represent one standard deviation, N = 3.
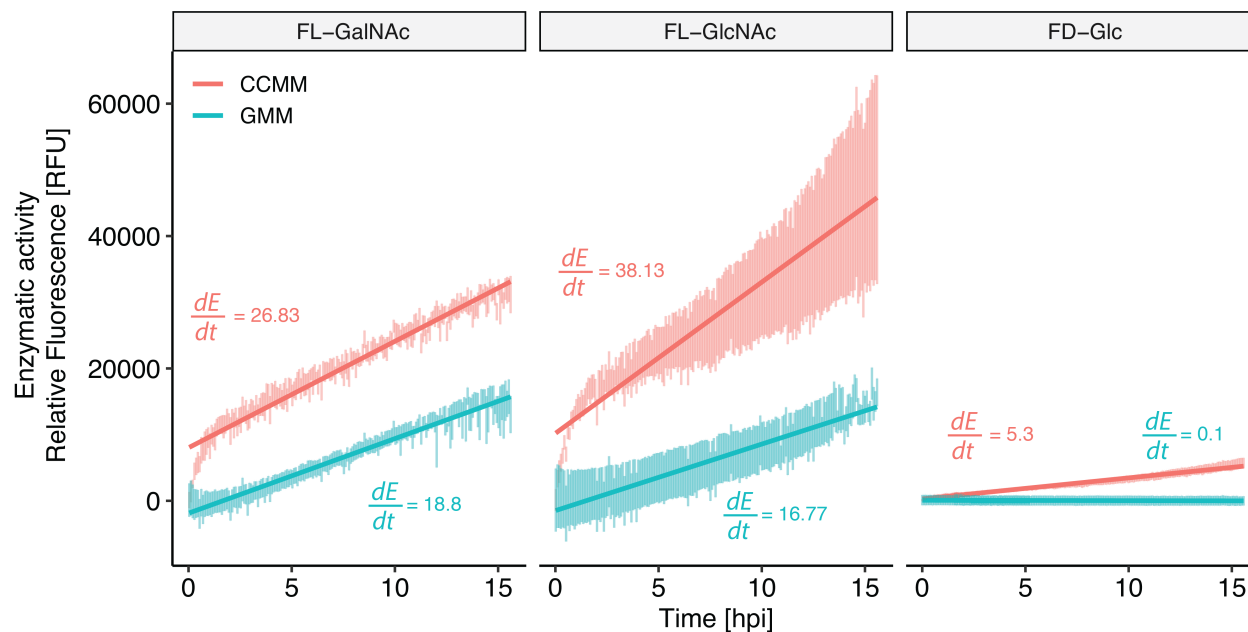
Figure B.12: *C.rosea* **conidia well-plate kinetic assay with fluorescein based substrates**. The enzymatic activity of cell wall degrading enzymes in *C. rosea* cultures was compared between different media (colloidal chitin minimal media, CCMM (red) and glucose minimal media, GMM (blue)) over 15 h post-incubation. Germination started at 0 h from parent strain spores at concentrations as in droplets (0.5×10^7 spores mL^{-1}) and were incubated (27 ^{o}C, 16 h) with either FD-GlcNAc, FD-GalNAc or FD-Glu as the substrate. At each measured time point, one standard deviation is shown, N = 3. Relative fluorescence is normalized with a control (media and substrate without spores) and slopes dE/dt represent change in enzymatic activity over time. Colloidal chitin media offers a faster increase in fluorescence over time, which will allow for shorter incubation times in droplets.
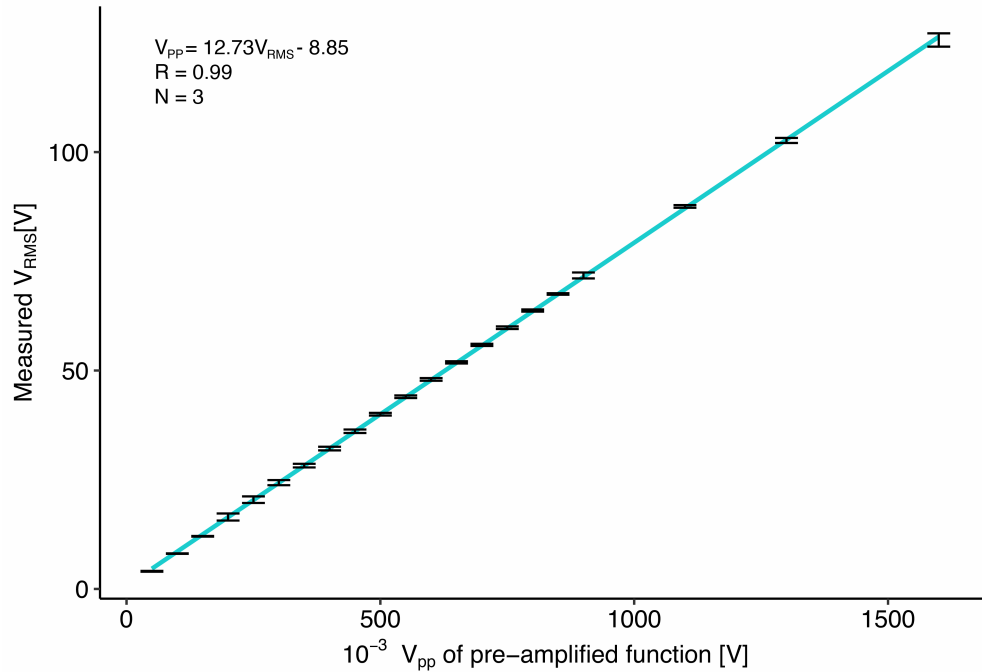
Figure B.13: Amplifier calibration curve. Measured root-mean squared voltage at the electrode, after amplification of a sine wave (10 kHz, VPP) using a PZD-700A, Trek Inc. amplifier. The gain at 10 kHz was determined to be 78.85. The resulting linear relationship was used to calculate the true applied potential (V_{RMS}) in experiments and simulations.
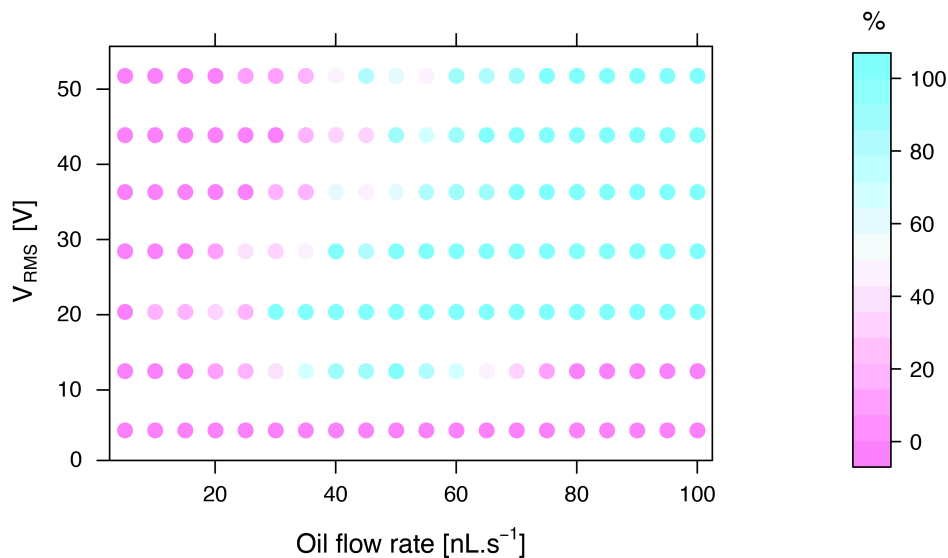
Figure B.14: Efficiency of sorting under different flow and applied potential. Dot plot showing the success rate of sorting ([# successfully sorted droplets (T) / # of total droplets sorted (T+F)]* 100 %) in a 7 x 20 factorial design experiment with binary outcome (N = 10). For each dot (or condition), the applied potential to the sorting electrodes were kept at constant frequency (10 kHz AC sine wave), while the spacer oil flowrate was varied. Droplets were generated at 0.5 nL/s (water) and 1 nL/s (oil and surfactant). Blue dots indicate sorting conditions with 100 % sorting success
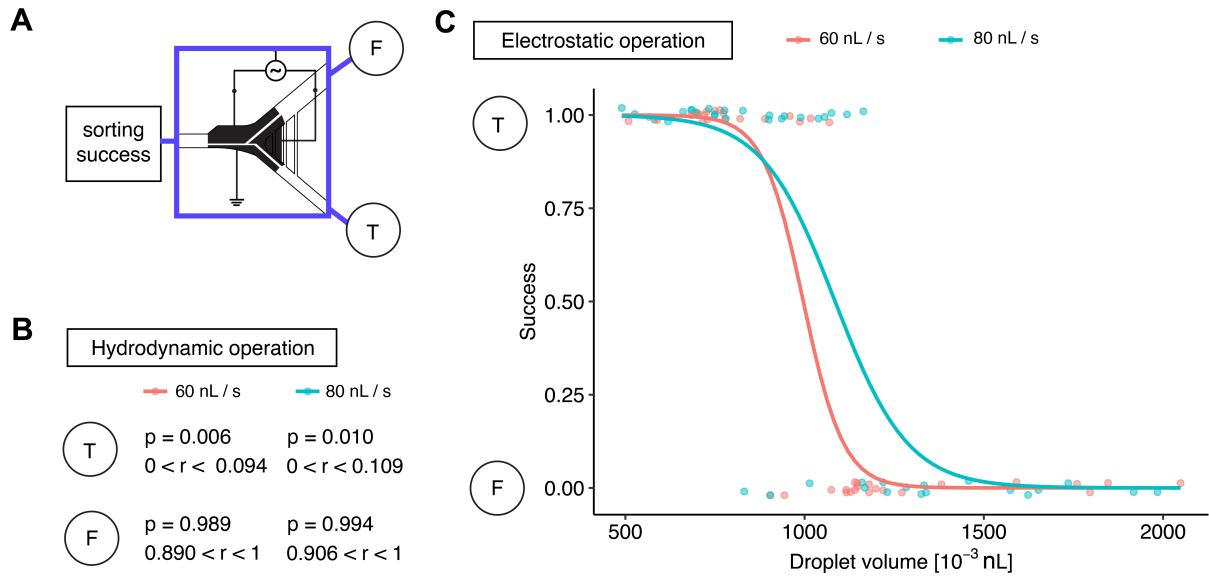
Figure B.15: Polydisperse volume droplet library sorting success rate. (A) Droplets were sorted using a co-planar sorter. A "positive" droplet going into the main channel was considered a sorting failure (F), while a droplet going into the disfavored channel was considered a sorting success (T) (see sorting design schematic). (B) Sorting logic outcome under hydrodynamic operation (free flow without the use of electrodes). Sorting success of polydisperse volume droplet libraries was measured under two flow conditions (60 nL/s spacer oil ; 80 nL/s spacer oil). At 60 nL/s, the probability p of sorting failure (droplet entering the disfavored channel, F) is 0.6% or the true probability r (99.9% confidence) is < 0.9%. At 80 nL/s, the sorting failure is < 1%. (C) Sorting logic outcome under electrostatic sorting. Sorting success of polydisperse volume droplet libraries was measured under two electrostatic sorting regimes (350 mVPP actuation, 60 nL s^{-1} spacer oil; 450 mVPP actuation, 80 nL s^{-1} spacer oil). Logic outcome fitted with logarithmic binomial regression. On average droplets smaller than $\sim$ 1 nL can be sorted with near-perfect efficiency.
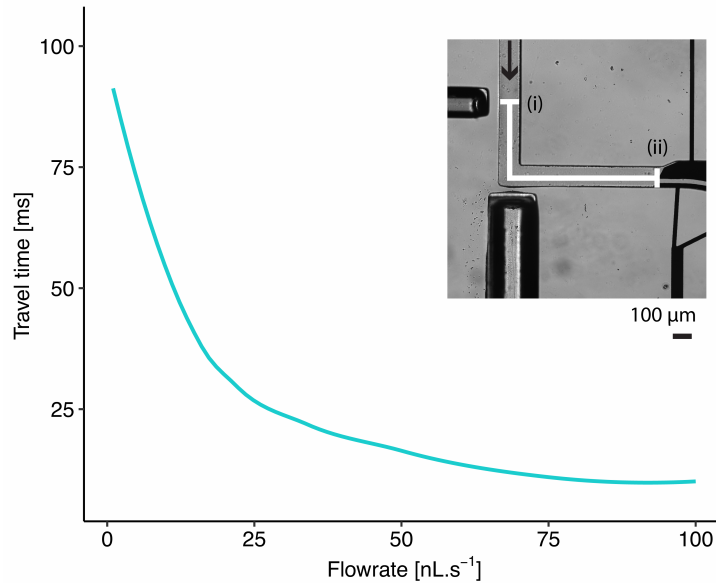
Figure B.16: Droplet sorting timing calibration. Droplet travel time from detection point (i) to sorting point (ii) ($\sim$ 1.1 mm) under different oil flow rates. Droplet generation was kept at 3 nL s^{-1} aqueous (ddH2O) and 4 nL s^{-1} oil phase (HFE 7500 0.5% fluorosurfactant), while the spacer oil phase varied in flow rate. Time was measured by summing up exposure times of frames in high-speed image series (each frame on $\sim$ 33 ms).
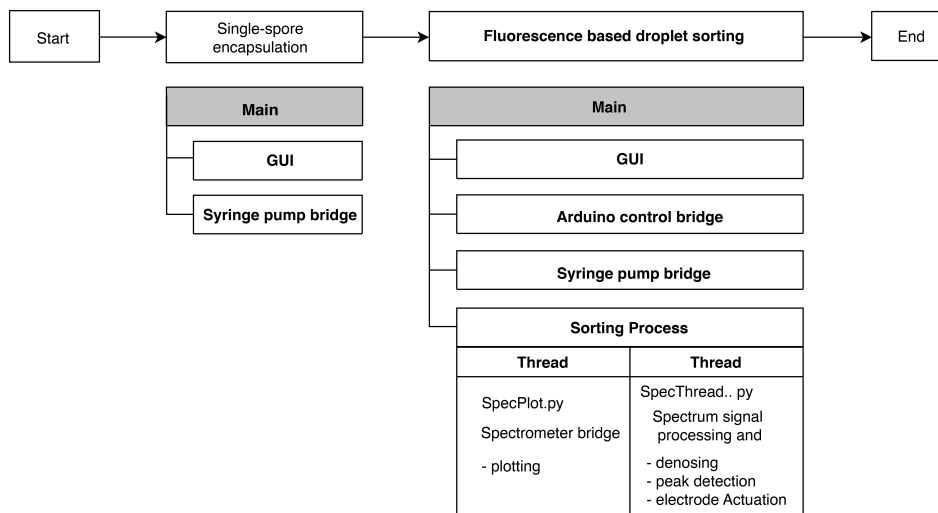
Figure B.17: Software logical workflow diagram. The Python 3.9 based software is used for two independent experimental steps: single-spore encapsulation and fluorescence based droplet sorting. For each experiment, a main python process is started to drive hardware and provide a user interface. For single-cell encapsulation, the main process runs a GUI process and a syringe pump bridge process, controlling the pressure driven syringe pumps. For fluorescence based droplet sorting, the main process runs a GUI process, an Arduino control bridge which operates switches supplying high-voltage to the electrodes, a syringe pump process, and a sorting process. The sorting process contains two sub-processes: a bridge with the spectrometer instrument continuously reading raw intensities and wavelengths, and a signal processing process for signal denoising, background subtraction, peak detection and electrode actuation. Software can be found under GNU GPL v3.0 on `https://bitbucket.org/shihmicrolab/fungalmicrofluidics/`.
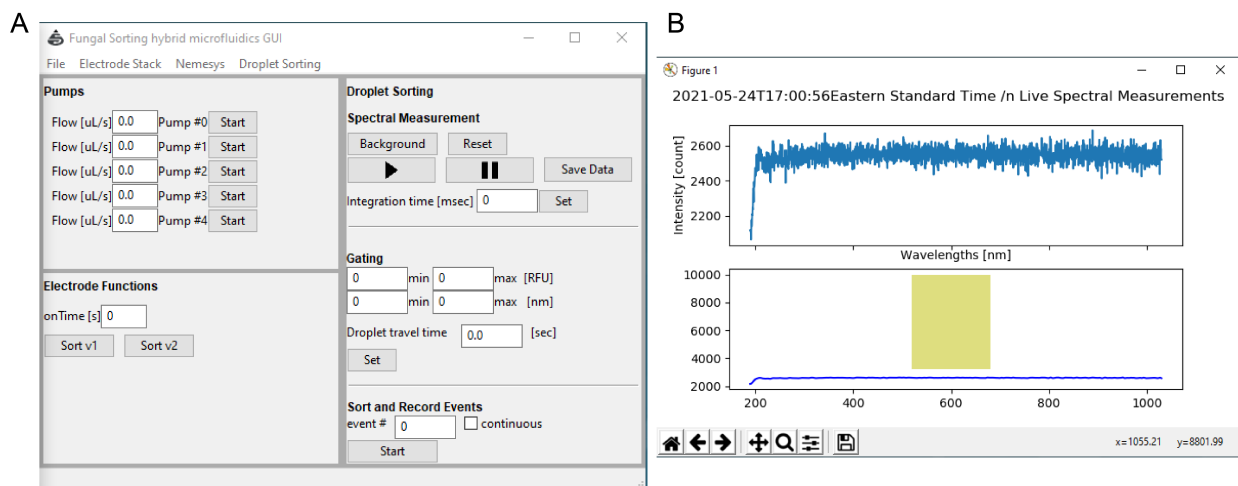
Figure B.18: Graphical user interface. (A) Control panel graphical user interface for fungal screening. After running a main script, the GUI can be used to control pumps, the electrode switching board, and the spectrometer. The menu ribbon can be used to control the hardware interface and to start and stop communication with the hardware. Pumps can be controlled in the pump panel by configuring the flow rates of the respective pump and using the start button to start and stop fluid dispensing. Electrodes can be controlled in the electrode panel. Electrode 'onTime' can be entered and buttons are present to which users can program custom actuation sequences (e.g. Sort v1 and Sort v2). The Droplet Sorting panel is used to perform automated droplet sorting. A spectrum viewer can be controlled using the play buttons, data snapshots can be saved, spectrometer integration time can be set, and background fluorescence can be subtracted using the top panel. These operations can be applied to live measurements. In the middle panel, the sorting gate (wavelength and intensity) and droplet travel time can be set. Finally, the user can start the autonomous sorting by performing a continuous measurement or a number of events. The procedure can be paused, and events can be saved in a data file. (B) Spectrum viewer graphical user interface. Live raw spectrum (blue) of the emission fiber transferred signal, showing the wavelength and measured intensities (RFU), measured by the spectrometer (top). The spectrum after signal processing (bottom) is also displayed through live plotting. The plotted signal (blue) has the recorded background noise subtracted and is denoised using a third order Butterworth lowpass filter. The user set sorting gate is displayed in green.
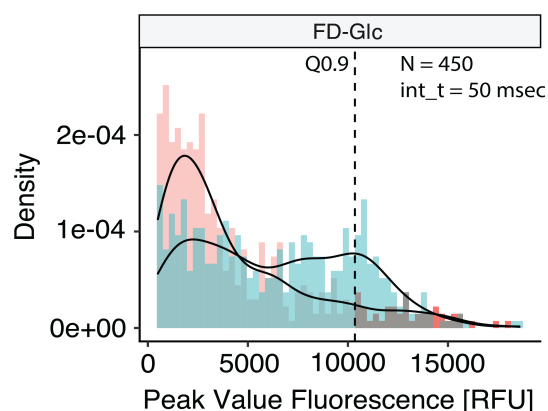
Figure B.19: Fluorescence intensity of each droplet in a mutant population (shown as red) and a wild type (shown as blue) population incubated at 27 ^{o}C. Intensity of peaks between the wavelengths 510 nm and 520 nm were used for gating. To sort droplets, the intensity gate was set at the 0.9 quantile of the mutant population fluorescence (shown by the dotted line). Total number of peaks (N) and integration time are indicated on the plot.
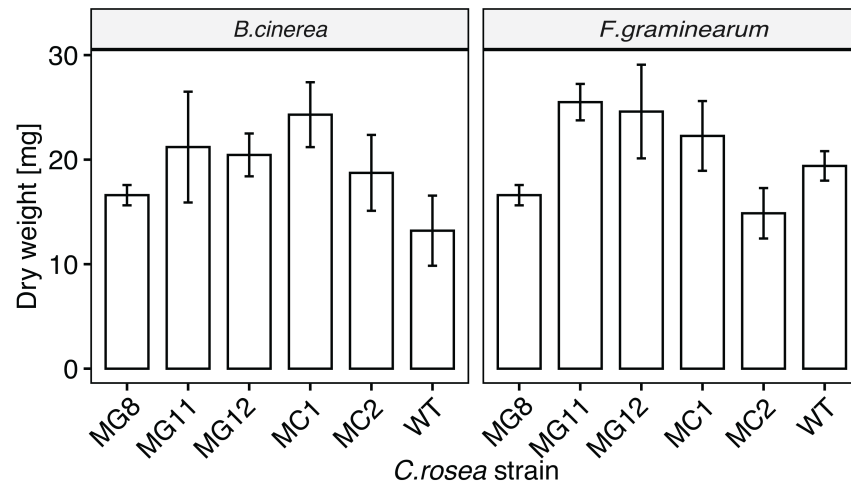
Figure B.20: Several microfluidic device selected high enzymatic activity *C.rosea* mutants were screened for their ability to reduce growth of two plant pathogens. Dry mycelial biomass of two plant pathogens was measured after inoculation in culture filtrate media, in which previously *C.rosea* grew. Biomass of pathogens grown in mutant culture filtrate was not significantly different from those grown in wild-type culture filtrate. (N = 3, P > 0.05)

Appendix C

Supplementary Info Chapter 4

C.1   ID2M automation system

Droplet manipulation was controlled by a GUI (Figure C.8) generated in a MATLAB (Mathworks, Natlick, MA) which controlled an Arduino Uno that interfaced to a control board consisting of a network of high-voltage relays (AQW216 Panasonic, Digikey, Winnipeg, MB). The control board delivered AC signals from a high-voltage amplifier (PZD-700A, Trek Inc., Lockport, NY) paired with a function generator (33201A Agilent, Allied Electronics, Ottawa, ON) to initiate actuation sequences on the device (Figure S9). Additionally, the GUI controlled the neMESYS syringe pump and Flame spectrometer (Ocean Optics, Largo, FL). The ID2M microfluidic chip is mounted on a pogo pin-control board (104 pins) with a 3D printed base platform as previously reported[1, 2] and was placed on the stage of an inverted IX-73 Olympus microscope (Olympus Canada, Mississauga, ON).

C.2   Tables and figures

Table C.1: COMSOL simulation parameters used for modeling the sinking channels in the mixing area.

Parameter	Value	Units
Oil density (ρ)	1614	$Kg.m^{-3}$
dynamic viscosity μ	0.00124	Pa.s
Inlet velocity (u_0)	0.0003	$m.s^{-1}$
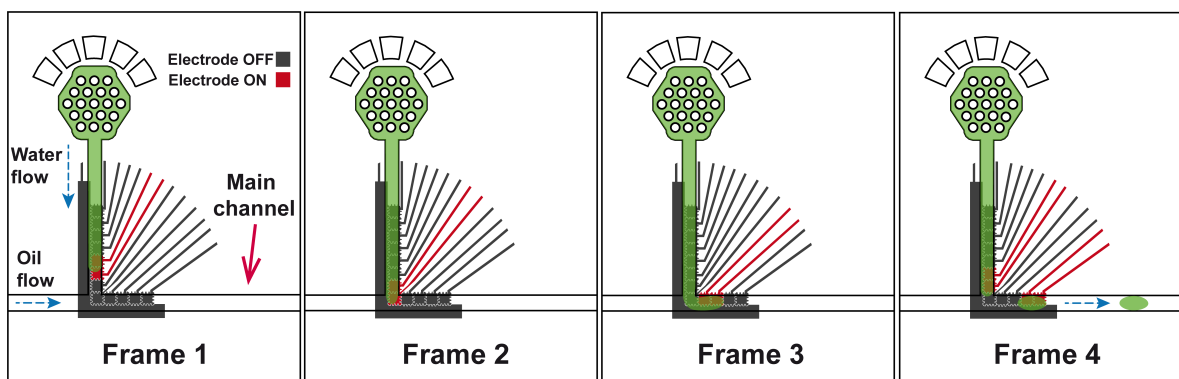
Figure C.1: A series of images showing on-demand droplet generation with T-junction configuration. Frame 1 shows a water flow 0.0005 [μL/s] with initialization of the electrodes. Frame 2-3 shows actuation sequences to drag the fluid to the main channel and Frame 4 shows the required sequence to break-off a droplet. A constant oil flow rate of 0.01 [μL/s] was maintained during this procedure. Reproduced from Ref. [108] with permission from the Royal Society of Chemistry.

$$y = 267.93e^{-0.058x}$$

$$R^2 = 0.9482$$
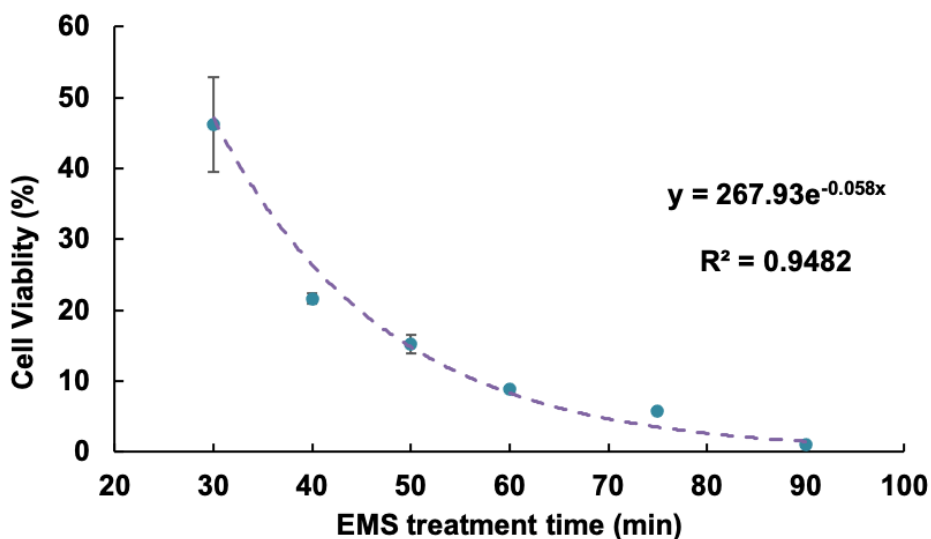
Figure C.2: Cell viability of yeast BY4741 strain as a function of different EMS treatment time. Cell viability was calculated by counting colonies growing on SD media plates after 48 h incubation at 30 ^{o}C. Reproduced from Ref. [108] with permission from the Royal Society of Chemistry.
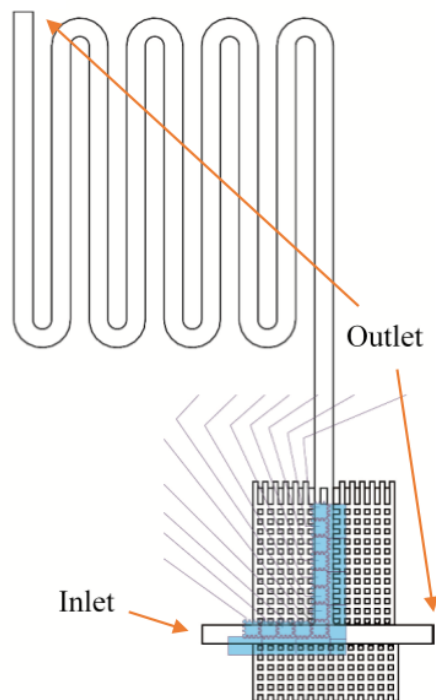
Figure C.3: The CAD model design for simulating the sink channel in COMSOL Multiphysics V5.2. For simplification, we only modeled the mixing and sinking channels with the following inlet and outlets of the system. Reproduced from Ref. [108] with permission from the Royal Society of Chemistry.
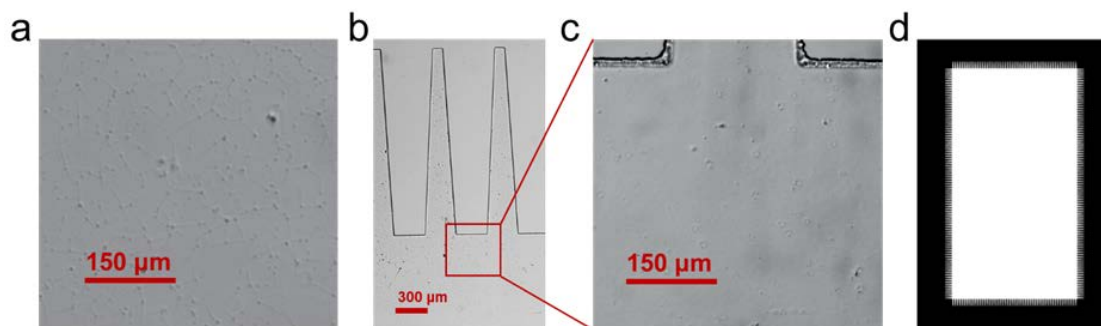
Figure C.4: Finger-like structures on the boundary of the SU-8 5 negative photoresist layer. (a) Cracks distributed in the resist layer fabricated with a straight edge mask, (b) and (c) show 10X and 20X images of the same layer fabricated with mask design with fingers, and d) the final mask design with finger-like boundaries. Reproduced from Ref. [108] with permission from the Royal Society of Chemistry.
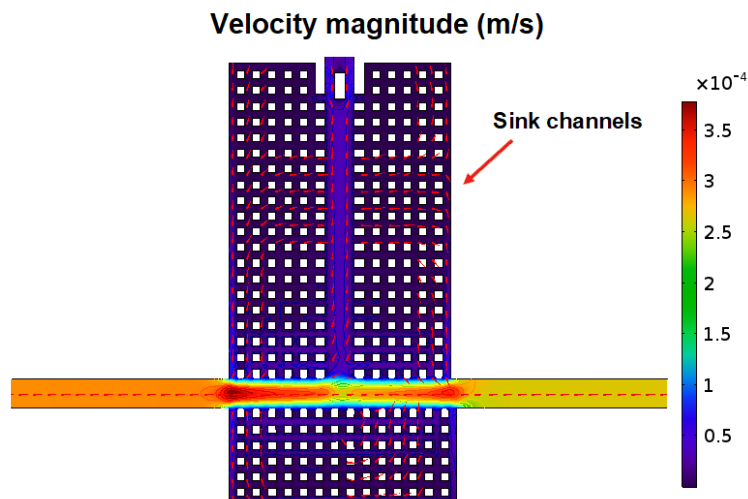
Figure C.5: COMSOL simulation of the oil flow velocity in the mixing area, indicating a visible decrease in its velocity. Red arrows indicate the flow direction of the velocity field. Reproduced from Ref. [108] with permission from the Royal Society of Chemistry.
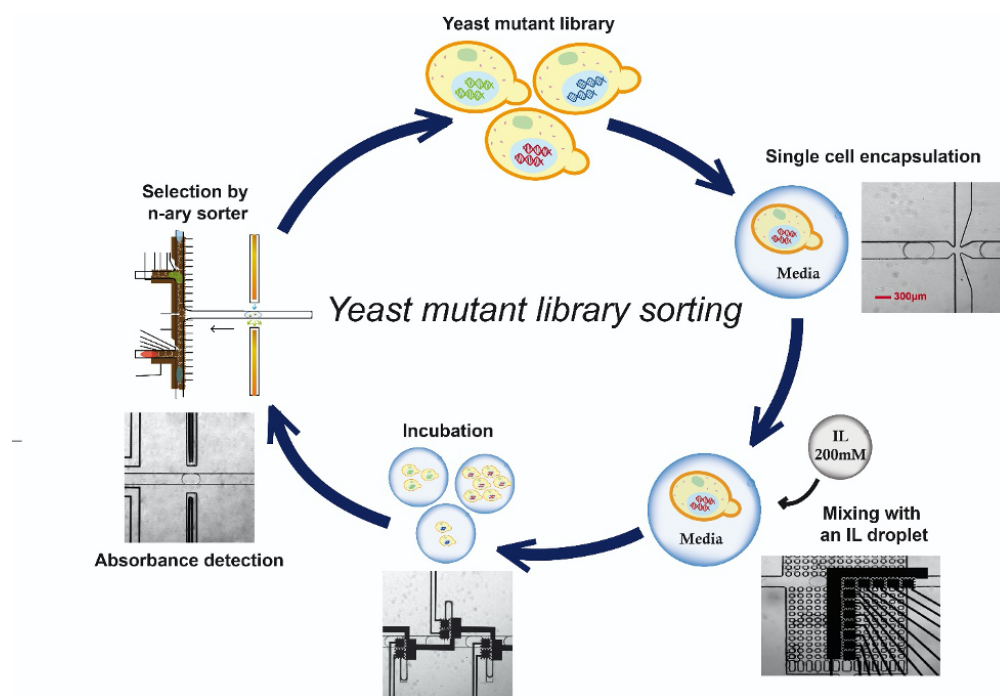
Figure C.6: Schematic of the ID2M work flow for screening of a yeast mutant library for ionic liquid resistance based on growth (i.e. absorbance). All steps (except generating the mutant library) was conducted on the ID2M system. Reproduced from Ref. [108] with permission from the Royal Society of Chemistry.
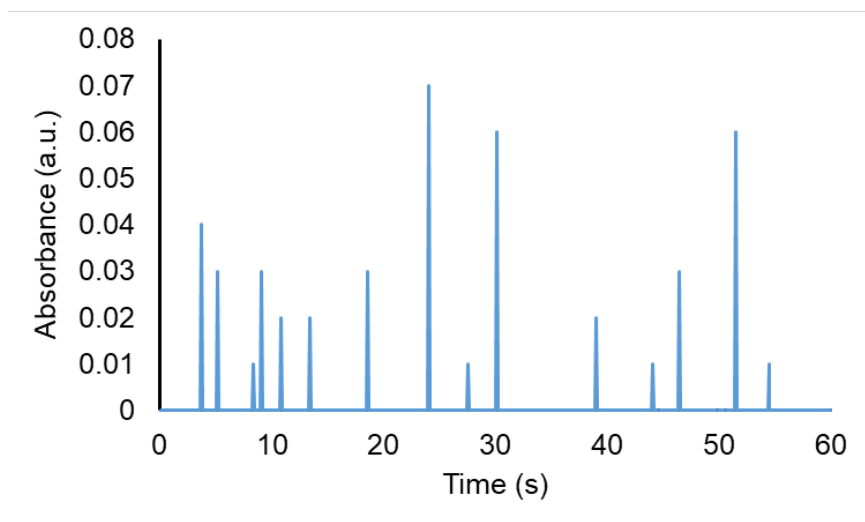
Figure C.7: The time course (absorbance vs. time) plot for only oil phase (i.e. no droplets). Reproduced from Ref. [108] with permission from the Royal Society of Chemistry.
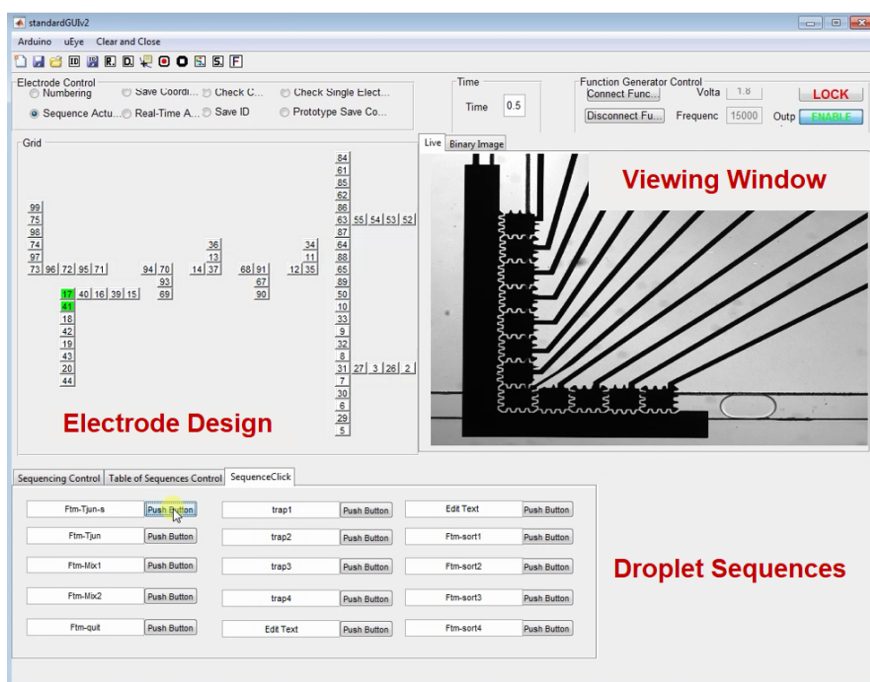
Figure C.8: MATLAB GUI. This is the interfaced used to automate our droplet operations which contains a region showing the electrode design (1), the real-time view of the device (2), the voltage and frequency control for the droplet actuations (3), the creation of user-defined droplet sequences that are preprogrammed (4). Reproduced from Ref. [108] with permission from the Royal Society of Chemistry.
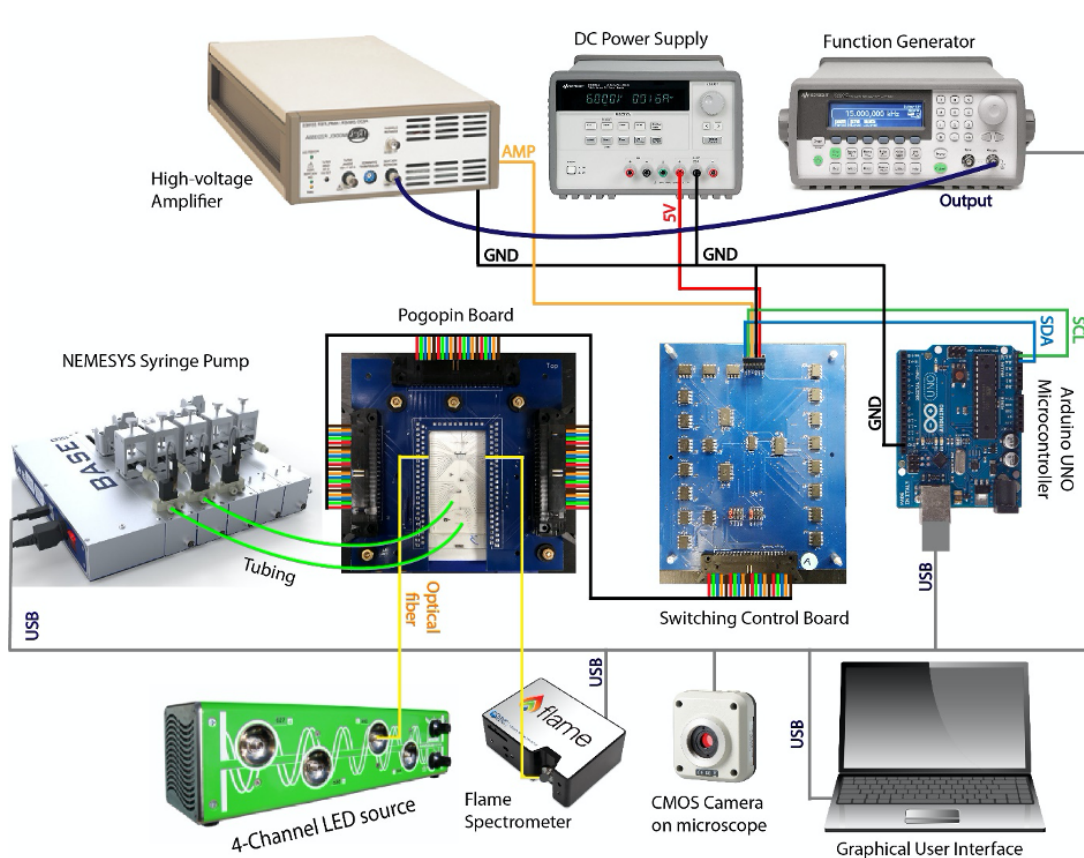
Figure C.9: The ID2M automation setup. An image showing the connectivity of all the different components used in this system. Reproduced from Ref. [108] with permission from the Royal Society of Chemistry.

Appendix D

Supplementary Info Chapter 5

D.1   Device channel and electrode design

Optimizing single-cell trapping and encapsulation was done by designing the channel microfluidics device following hydrodynamic resistance (R_h) and using streamline based design rules [84, 92].

$$\Delta P = R_h Q \tag{D.1}$$

with R_h the hydrodynamic resistance, Q the volumetric flow rate and ΔP the pressure drop in the channel. The hydrodynamic resistance can be described as follows:

$$R_h = \frac{12\mu L}{wh^3\left(1 - 0.63\frac{h}{w}\right)} \tag{D.2}$$

We define three hydraulic resistances: The trap constriction R_2, the trap R_3, and the bypass channel R_1 (Supplementary Figure 2).

Determining the width of the opening of the trap, the depth of the trap, the height of the channel, and the length of the bypass, we can calculate the three resistances. Before the cells are loaded, we aim for $R_2 + R_3 > R_1$ to encourage cell trapping. When a cell is trapped, we want $R_2 + R_3 \leq R_1$ to encourage $Q_1 > Q_{2+3}$ (or $Q_{bypass} > Q_{trap}$) while taking into account R_3 increases when a cell is trapped. Taking this into account, we looked at the velocity streamline profile and positioned the trap near the curvature of the main channel (i.e. the end of a serpentine channel) along with narrowing the width of channel near trap to improve cell trapping.

For the electrode design, four electrodes were sufficient to perform desired operations. A common ground electrode wire going through the center of the trap was chosen to act as a ground in case all four electrodes receive a potential. Interdigitation was used and electrodes have a minimum gap of 14 μm. The wiring has a thickness of 20

μm. The wiring density through channels is minimized, as actuations through wiring can manipulate the flow. This limited us to only equip 6 out of 12 traps with 4 electrodes each.

D.2   Computational fluid dynamics and electric field simulations

The model portraying the channel geometry with flow velocity profile, velocity streamlines and pressure was stationary simulated using COMSOL Multiphysics 2D creeping flow physics. Inertia and turbulence were neglected, and no slip was set for channel walls. The fluid within the channels was PBS, the boundaries were PDMS.

Conditions used for modeling:

$P = 0$ Pa for outlet pressure

$\boldsymbol{u} = \begin{cases} x = 0 \\ y = 0 \end{cases}$ m s^{-1} for initial velocity profile

$V_0 = 0.0008 \mu$Ls^{-1} for volumetric laminar inflow

The model portraying the electric field generated by different actuation patterns, was simulated in COMSOL Multiphysics with a static electricity module (Figure D.6). Electrodes were modeled as 2D surfaces without thickness, under a 7 μm SU-8 surface, covered with an HFE oil of 30 μm thickness (Figure D.1). The top PDMS features on the device were omitted from the simulation.

Conditions used for modeling the electric field above the dielectric:

T = 293.15 K is the temperature

As potential V_0 :

1.8V_{pp} = 142V_{RMS} for droplet generation

1.6V_{pp} = 126V_{RMS} for droplet release, keep and encapsulate

And with ground potential and initial potential $V_{RMS} = 0V$.

The model was static, stationary and materials were continuous. For each model, the not actuated electrodes were selected as ground. Under static conditions, the electric potential, V, is defined by the relationship

$$\mathbf{E} = -\nabla V$$

and the electric displacement or flux density $\boldsymbol{D}$ is defined by the relationship

$$\mathbf{D} = \varepsilon_0 \mathbf{E} + \mathbf{P}$$

with the dielectric constant ε_0, electric field E, and P the polarization density. Following Gauss' Law:

$$\nabla \cdot \mathbf{D} = \rho$$

with ρ the total electric charge density, we can fill in.

$$\nabla \cdot (-\varepsilon_0 \nabla V + P) = \rho$$

In our simulations, the magnitude of the electric vector field (V m^{-1}) is calculated with:

$$E = \sqrt{E_x{}^2 + E_y^2 + E_z^2}$$

D.3 Automation setup and device operation

Software that we used for this work can be found here: `http://bitbucket.org/shihmicrolab`. The microfluidics device is placed inside a 3D printed pogo pin PCB board holder of which the base plate fits on the stage of an inverted microscope (Olympus IX7). The flow is observed under a 4X or 10X objective under bright-field illumination. A NeMESYS Low Pressure pump (Cetoni) with five syringe units, and an Arduino Uno were connected to a PC, and operated through Python 2.7. The Arduino Uno is connected to a stack of 120 optocouplers, powered by a 5 V DC power supply. A 15 kHz sinusoidal signal (function generator), is amplified. The Python protocol is run and the GUI is started after which flows are started with disconnected tubing to remove air bubbles in the system. Tubing is carefully connected to the device (Figure 5.3).

When tubing is inserted into the device, high flow rates ($\sim$500 nL s^{-1}) are to be used in order to avoid air bubbles within the inlets. Priming is done from inlet 1 with PBS containing 2% Pluronics F-127, filled in a 500 μL gastight syringe. After the device is primed (for at least 5 min), the priming solution is moved from the inlet to outlet and turned to a lower flowrate ($\sim$ 1 nL s^{-1}). Cells are loaded from inlet 1, either re-suspended in PBS or their original media, and placed in a 2.5 mL syringe with a 7 mm magnetic stirring disk. The syringe is stirred continuously throughout the procedure. Once cells entered the device, and leaving through inlet 2, the flow of the priming solution can be stopped and cells will enter the trapping array. Phase change for single-cell encapsulation is performed using HFE 7500 with 2% fluorosurfactant arriving from the droplet generator with inlet 4 connected to a 500 μL syringe. Inlet 3 is connected to a 500 μL syringe with an aqueous solution (droplet content). Outlet 3 is connected to Inlet 2 with PEEK tubing, after all air has been pushed out the droplet bridge. Electrodes are actuated using the GUI. Once the cells are encapsulated, additional droplets can be generated on-demand using the GUI, by using HFE 7500 with 2% fluorosurfactant at Inlet 4 with varying flow rates, and aqueous flow from Inlet 3 at 0.6 nL s^{-1}. In- or outlets can be blocked using PEEK tubing with glued ends, if needed.

D.4   Device assembly and channel treatment

Novec 1720 contains a fluorosilane polymer surfactant dissolved in an ether solution. It is a volatile solvent and ideal to avoid remaining surfactant clogs in the traps. This solvent swells PDMS, and care should be taken to follow this procedure accordingly. Clean PDMS channel slabs are treated with oxygen plasma for 30 s and directly aligned on top of a clean dielectric coated electrode patterned glass, under a microscope (4X). The device is sealed with transparent adhesive tape and pressure is applied. Immediately, treat the device channels for 20 min with Novec 1720 and dry for 20 min at room temperature. Bake device at 150 ^{o}C for 30 min, while applying 750 g weight on the device. For the droplet bridge, a 2 cm piece of PEEK tubing is treated with Novec 1720 for 20 min by flowing it through.

To reuse of devices, flush the device with Fluorinert FC-40 to remove the oil containing surfactant in the traps, and then bake at 100 ^{o}C for 2 h. If actuation took place, wash the device with FC-40, treat the device with Novec 1720 as before. Chips not used for 14 days should be treated again with Novec 1720. If needed, chips can be washed with a 1% Triton X-100 solution to flush out debris, and then continue with an FC-40 wash.

D.5   Tables and figures

Table D.1: Parameters for multi-physics modeling

Property	Value
SU8-5 Relative Permittivity	4.5
PDMS Relative permittivity	2.75
PDMS density	970 [kg m^{-3}]
PBS density	1000 [kg m^{-3}]
PBS dynamic viscosity	0.0008882 [Pa s]
HFE 7500 oil relative permittivity	5.8
HFE 7500 oil boundary size	500x500 $\left[\mu\text{m}^2\right]$
Dielectric thickness SU-8 5	7.0[μm]
SU-8 5 boundary size	500×500 $\left[\mu\text{m}^2\right]$
Electrode sizes	110×110 and 110×40 $\left[\mu\text{m}^2\right]$
Ground electrode size	10[μm]
Electrode gap width	14[μm]

$$y = \frac{A}{1 + e^{\frac{B-x}{C}}} \tag{D.3}$$

Table D.2: Three parameter logistic regression model. Parameters and the Hosmer-Lemeshow goodness of fit statistic of each fitted model.

Data	Asymptote (A)	Inflection point (B)	Scale (C)	P (Goodness of fit)
Forward flow on-demand droplet release	1.1646	3.23	−1.92	0.9888
Reverse flow Hydrodynamic droplet release	0.96059	5.68	1.73	0.9616
Reverse flow on demand droplet keeping	0.80613	64.01	−5.87	0.9967

Table D.3: Additional device statistics

Dispersed	Continuous	Contact angle (°)	sd	N
PBS	HFE $7500 + 2\%$ Ran	139.55	4.90	10
DI Water		128.97	4.53	10

Droplet volume	Volume in pL	Sd		N
After single-cell encapsulation	150.25	55.58		11
On-demand droplet-generation	250.90	39		44
Before entering droplet bridge	76.19	9.41		10
After exiting droplet bridge	72.97	4.59		10

Table D.4: Cells and plasmids

Cells Lines	Transgene integration	Source
NCI-H1299	Luciferase, eGFP, KanR	Genecopeia SL001
MCF-7	N/A	Donated by Piekny Lab

Plasmids	Relevant characteristics	Source
pCRISPR eGFP 497	AmpR, Neo/KanR	Addgene #111824
pCRISPR_RAF1_94	AmpR, Neo/KanR	Addgene #111824
All_in_one_CRISPR/Cas9_LacZ	AmpR	Addgene #74293

Table D.5: Primers for genomic cleavage detection

Targeted gene	Name	Orientation	Primer Sequence (5' to 3')
elGFP	P1	Forward	TGACCACCCTGACCTACGG
eGFP	P2	Reverse	ATGTGATCGCGCTTCTCGTT
RAF1	P3	Forward	CGATTACCGAGTGCCTCTCC
RAF1	P4	Reverse	CCGCATCGTAGCAAACGC

Table D.6: Expected cleavage band size for GCD

Target gene	Primer pair	Amplicon	Amplicon size	Expected cleavag band size
eGFP	P1, P2	TGACCACCCTGACCTACGGCGTGCAGTGCT TCAGCCGCTACCCCGACCACATGAAGC CCGAAGGCTACGTCCAGGAGCGCACCA TCTTCTTCAAGGA**CGACGGCAACTACA AGACCCGCGCCG**AGGTGAAGTTCGAG GGCGACACCCTGGTGAACCGCATCGAG CTGAAGGGCATCGACTTCAAGGAGGACG GCAACATCCTGGGGCACAAGCTGGAGTA CAACTACAACAGCCACAACGTCTATATC ATGGCGACAAGCAGAAGAACGGCATCAA GGTGAACTTCAAGATCCGCCACAACATC GAGGACGGCAGCGTGCAGCTCGCCGACC ACTACCAGCAGAACACCCCCATCGGC GACGGCCCCGTGCTGCTGCCGACAACCACT ACCTGAGCACCCAGTCCGCCCTGAGCAAAGACCCCA ACGAGAAGCGCGATCACAT	472	132, 340
RAF1	P3, P4	CGATTACCGAGTGCCTCTCCTGAAAGCAAGTC AGCGTCGCCTAACCTCTTCAGCTTCGAAATGGCGGCCA CCAGATCGCTAGGCCACGCCCCGGGGGCGGGGCCTGAGTTCAGGCC AGAGCGATGGATGCCCGAGCCAAGTTAGAAGTCGACTGCCAGTAGGGCT CGCGCAGAATCGGAGAGCCGGTGGCGTCGCAGGTCGGGAGGACGAG CACCGAGTCGAGGGCTCGCTCGTCTGG**GCCGCCCGAGA GTCTTAATCG**CGGGCGCTTGGGCCGCCATCTTAGATGGCGGGAGTA AGAGGAAAACGATTGTGAGGCGGGAACGGCTTTCTGCTGCCTTTT TTGGGCCCCGAAAAGGGTCAGCTGGCCGGGCTTTGGGGCGCGTGCC CTGAGGCGCGGAGCGCGTTTGCTACGATGCGG	418	241, 177
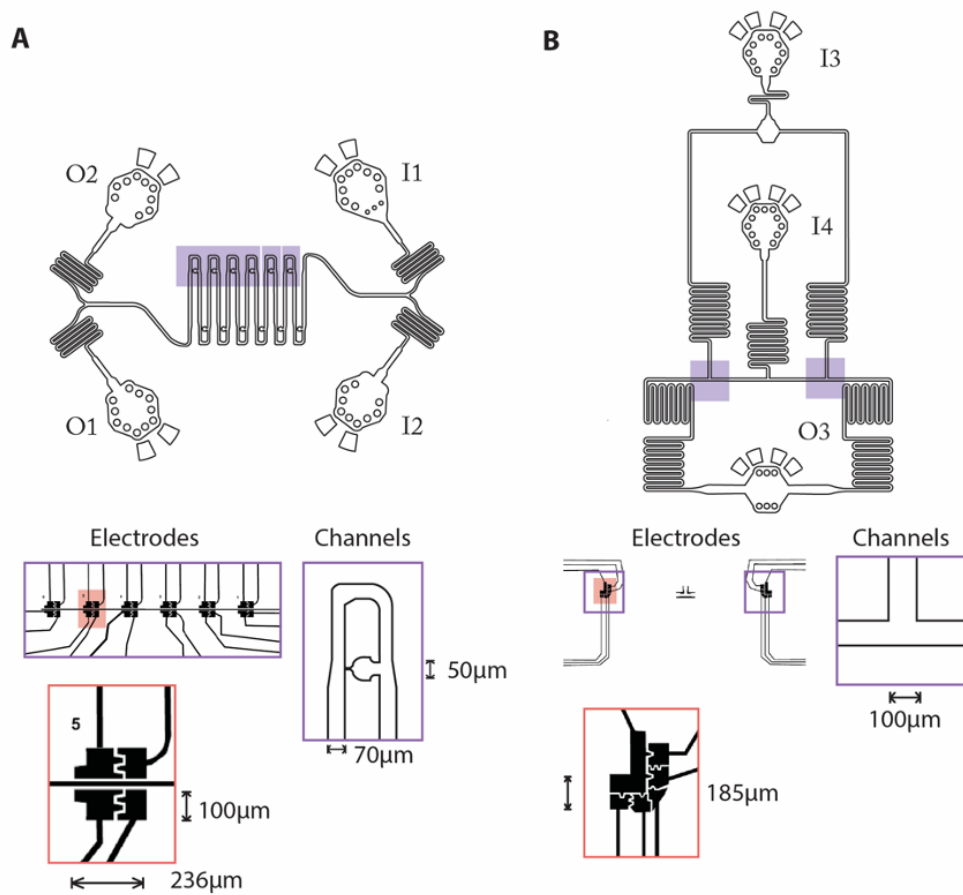
Figure D.1: Device electrode and channel geometry. The device consists out of two separate PDMS layers, a serpentine trapping channel and a droplet generator. A) The serpentine trapping channel contains two inlets (I1, I2) and two outlets (O1, O2). The channel width is 70μm with bypass width of 50 μm, and height of 35 μm. Highlighted top area of 6 traps is lined with electrodes (enlarged). B) The droplet generator has two inlets (I3, I4) and one outlet (O3). The channel width is 100 μm, and height is 35 μm. Highlighted area is lined with electrodes (enlarged). Reproduced from Samlali et al. [227], with permission from John Wiley and Sons.
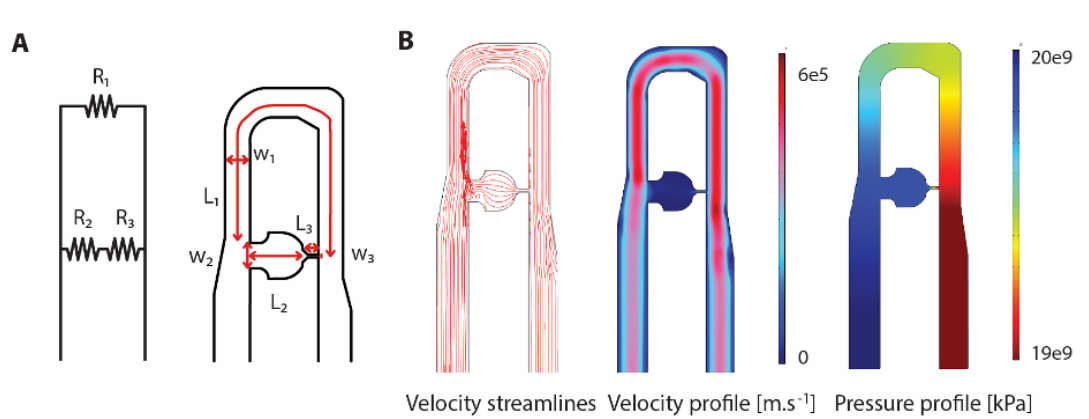
Figure D.2: Resistance based channel design. A) Overlay of a resistor diagram on the trapping device Hydrodynamic resistance in the cell trap (R_3) will increase upon trapping a cell. The flow prefers the path of least resistance and the bypass path (R_1) is usually preferred. The length and width of the bypass (L_1 = 1000 μm, W_1= 50 μm) and trap (L_2 = W_2 = 50 μm; L_3 = 30 μm W_3 = 8 μm) were modified such that it satisfied the conditions for trapping cells (see Supplemental Note 1). Dimensions are as indicated. B) Numerical simulations with COMSOL Multiphysics show flow velocity pattern across trapping array. Reproduced from Samlali et al. [227], with permission from John Wiley and Sons.
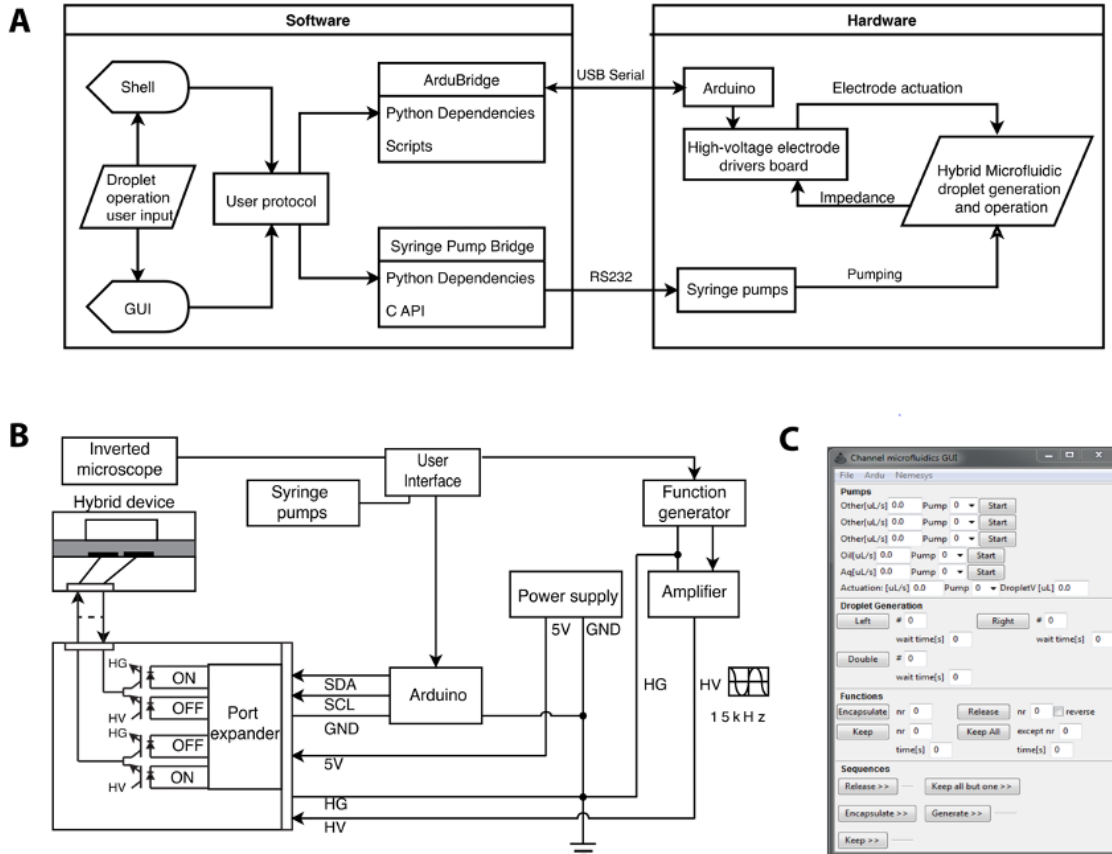
Figure D.3: Software and hardware diagram. A) Diagram showing communication lines between software and hardware, with integration of pump and electrode operation through Python 2.7. Through a graphical user interface (GUI), the user can perform on-demand droplet operations such as droplet generation, encapsulation, keeping or releasing a droplet. For example, the user can create x droplets with set time interval or can perform on-demand encapsulation in trap number 5, release or keeping of a specific droplet, with the click of a button. The GUI accesses a Bridge that writes to an Arduino or a syringe pump system. The software is accessible on `http://bitbucket.org/shihmicrolab`. B) Hardware setup. Arduino controls an I2C communication protocol to address specific optocouplers. Automation system hardware setup is similar to previously reported [3] C) Screenshot of the graphical user interface. Reproduced from Samlali et al. [227], with permission from John Wiley and Sons.
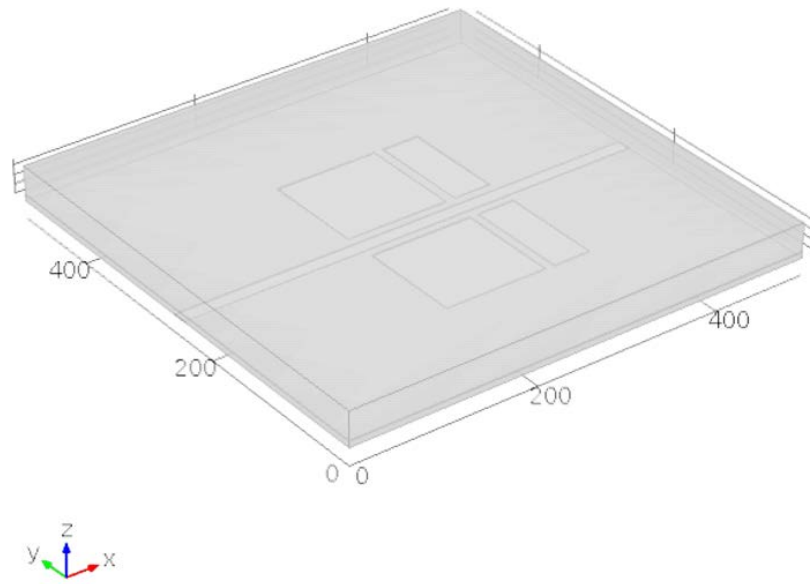
Figure D.4: Geometry used for electrostatic field calculations. Geometry used for electric potential (V) and electric field (V m^{-1}) modeling on 7 μm SU-8 5 dielectric layer above co-planar electrode surfaces using COMSOL Multiphysics electrostatics numerical modelling. Dimensions are in microns. Top layer is a 35 μm HFE 7500 oil layer, under which a 7μm thick SU-8 5 layer is positioned with defined areas of potential or grounding. Reproduced from Samlali et al. [227], with permission from John Wiley and Sons.
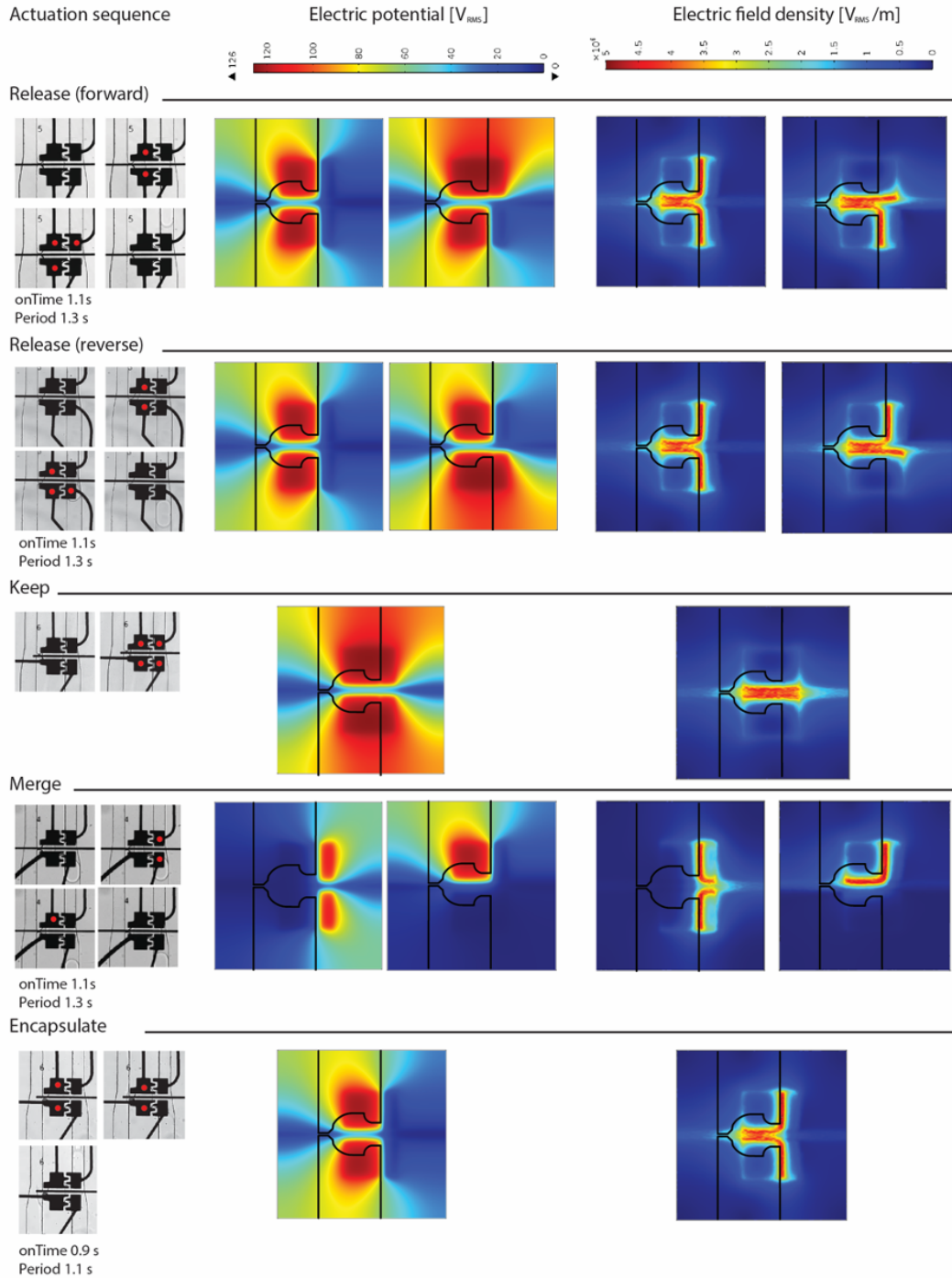
Figure D.5: Electrode sequences of on-demand droplet operations. Electric potential (V) and electric field (V m^{-1}) on 7μm SU-8 5 dielectric layer above co-planar electrode surfaces were modelled using COMSOL Multiphysics electrostatics numerical modelling. Actuated electrodes are marked by a red dot (bright field image, 15X). All droplet operations (encapsulation, release, merging, and keeping) were simulated using a potential of 126 V$_{RMS}$ at a frequency of 15 kHz with varying pulse width (0.9 – 1.1s) and period (1.1-1.3s). Reproduced from Samlali et al. [227], with permission from John Wiley and Sons.
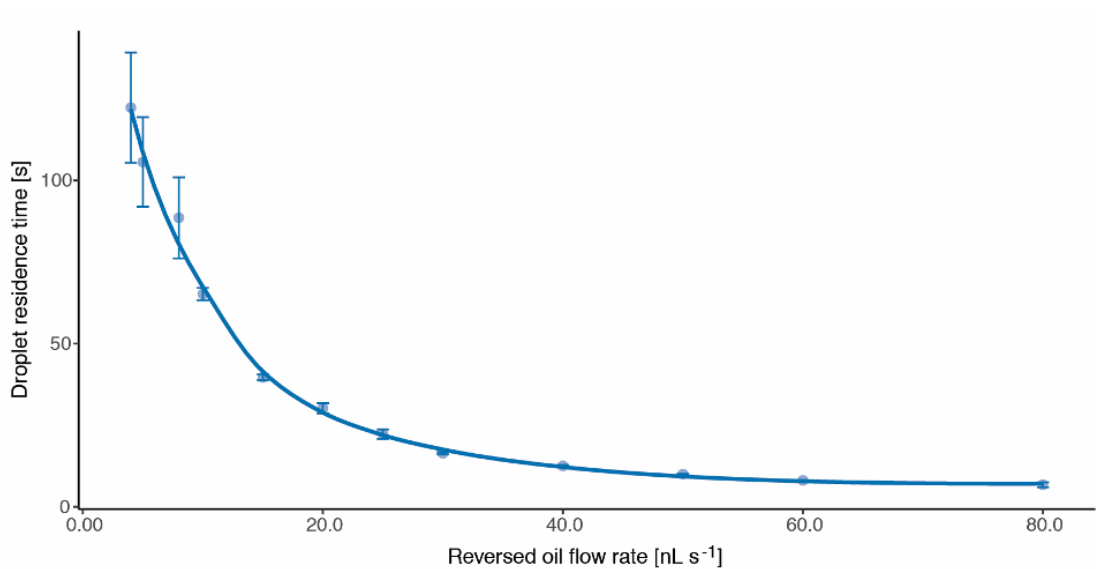
Figure D.6: Droplet residence time. The time for the last droplet (from trap 6) to leave the trapping array under different flow rates. At low flow rates ($4 - 8$ nL s^{-1}), residence time is highly variable. At high flow rates (> 20 nL s^{-1}), all droplets are usually released within $\sim$30 s. Droplet residence time is an important parameter for sorting droplets under flow reversal and for keeping desired droplets such that an automation sequence can be executed for these operations. One standard error, N=3 displayed. Reproduced from Samlali et al. [227], with permission from John Wiley and Sons.
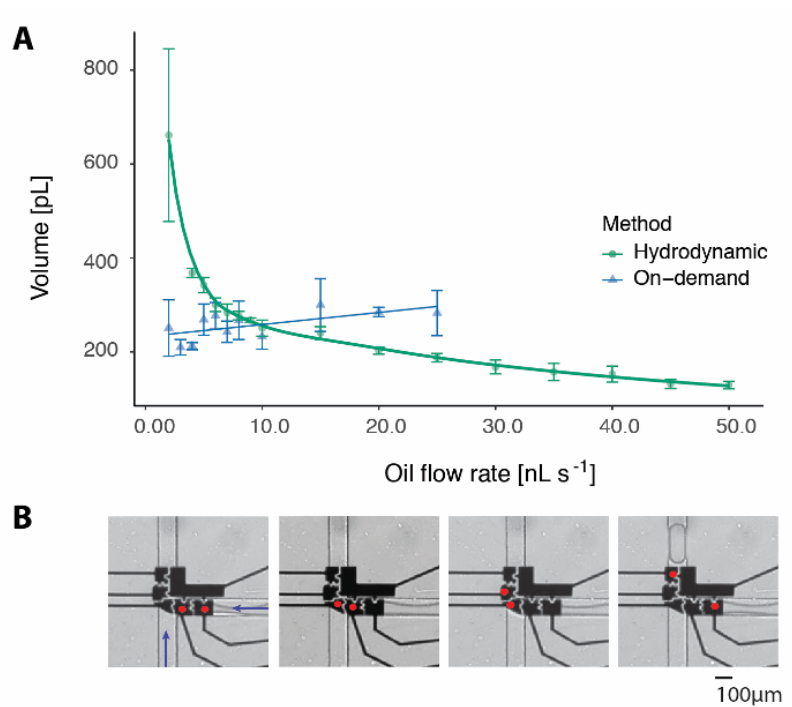
Figure D.7: Characterization of on-demand droplet generation. A) Electrodes are serially actuated to generate droplets on-demand at a potential of 126 V_{RMS} and a frequency of 15 kHz (bright field image, 10X). B) Average droplet volume (in pL) of on-demand generated and hydrodynamically generated droplets. Droplets are generated with a double T-junction of 100 μm width. On-demand droplet-generation shows a linear relationship with respect to oil flow rates. An average droplet volume of 207.5 pL was achieved for on-demand droplet generation. Droplet volume was calculated by multiplying droplet area and a channel height of 35 μm using Fiji (Image J). All error bars are one standard deviation (N = 4). Reproduced from Samlali et al. [227], with permission from John Wiley and Sons.
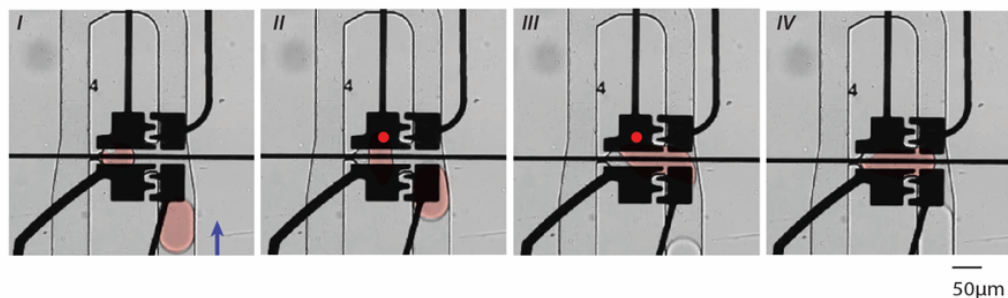
Figure D.8: Droplet merging. A series of four frames from a movie showing on-demand merging of two droplets at 4 nl s^{-1} oil flow rate. The trapped droplet contains a single MCF-7 cells A red false color is shown to highlight the droplet. Reproduced from Samlali et al. [227], with permission from John Wiley and Sons.
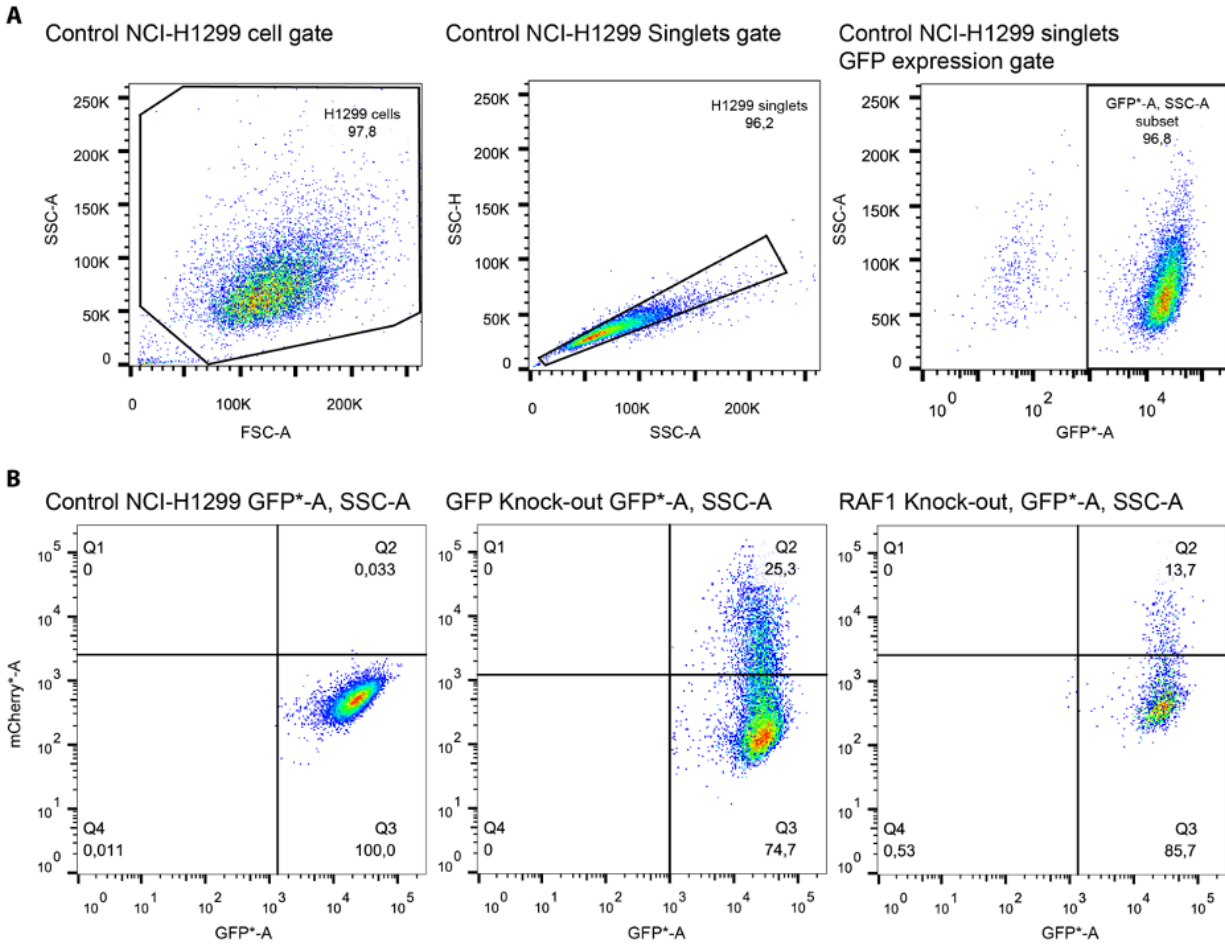
Figure D.9: Transfection efficiency determined with flow cytometry A) Gating strategy demonstrated with untransfected NCI-H1299 cells B) Left: mCherry vs. eGFP of control NCI-H1299 lung squamous cell carcinoma singlets Middle: mCherry vs. eGFP of NCI-H1299 lung squamous cell carcinoma singlets transfected with a plasmid expressing an sgRNA directed to knock out the stably integrated eGFP cassette. The determined transfection efficiency is 25.3%. Right: mCherry vs. eGFP of NCI-H1299 lung squamous cell carcinoma singlets transfected with a plasmid expressing an sgRNA directed to knock out the RAF1 oncogene. The determined transfection efficiency is 13.7%. Reproduced from Samlali et al. [227], with permission from John Wiley and Sons.
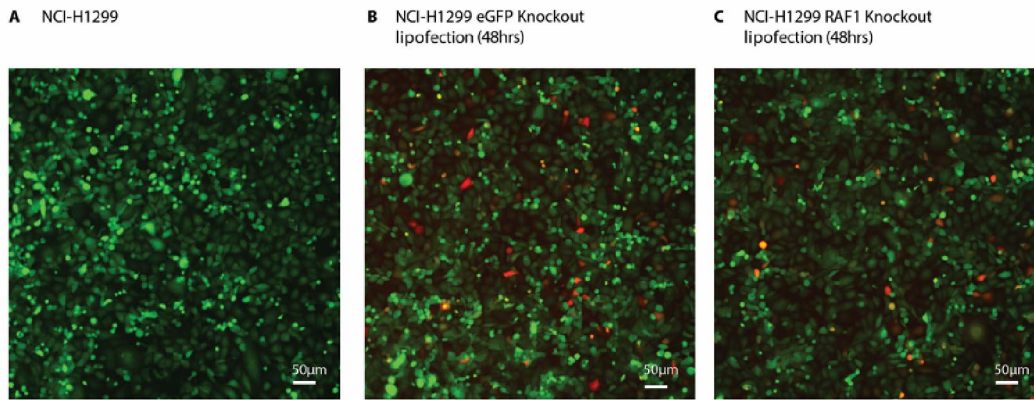
Figure D.10: Fluorescent microscopy images of NCI-H1299 lung squamous carcinoma cells. A) NCI-H1299 cells containing eGFP integrated at the AAVS1 site. B) NCI-H1299 cells 48 h after lipid-mediated transfection with eGFP targeting sgRNA encoding plasmid. C) NCI-H1299 cells 48 h after lipid-mediated transfection with RAF1 targeting sgRNA encoding plasmid. mCherry expression (λ_{Ex}: 585 nm / λ_{Em} 608 nm), native eGFP expression (λ_{Ex}: 488 nm / λ_{Em}: 509 nm). Reproduced from Samlali et al. [227], with permission from John Wiley and Sons.
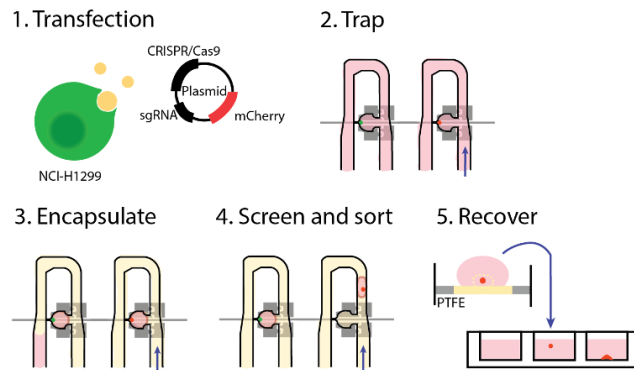
Figure D.11: Overview of hybrid microfluidics assisted isoclonal recovery pipeline. After transfection (1), the device is loaded with a heterozygous transfected cell suspension and single isoclones are trapped (2). An HFE-7500 2% Ran surfactant oil flow is flown through the device and electrodes are actuated in order to encapsulate single-cells in droplets (3). Single isoclone containing droplets can be selected and released on demand. After capillary recovery and centrifugation, isoclones are recovered in 96-well plates and maintained for expansion (4). Reproduced from Samlali et al. [227], with permission from John Wiley and Sons.
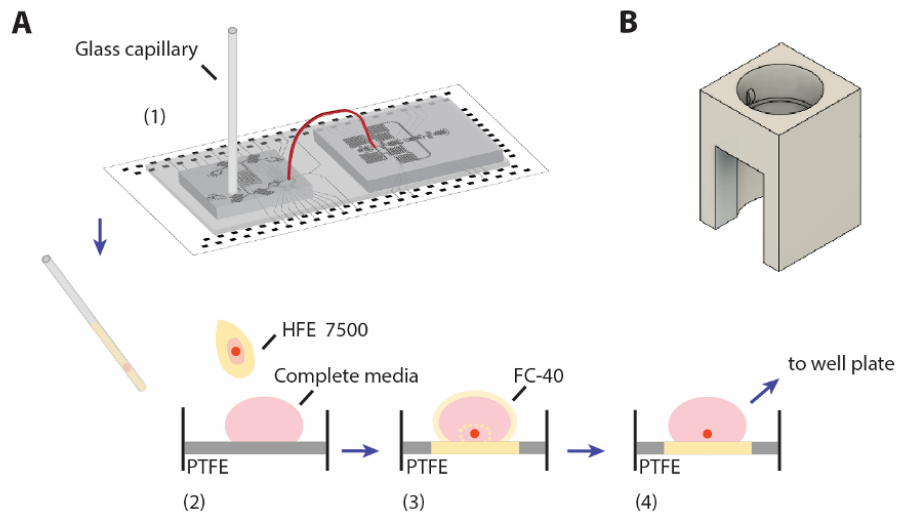
Figure D.12: Overview of single-clone recovery method. A) A four-step droplet isclonal recovery procedure. (1) After on-demand release of an isoclone containing droplet from the device, an HFE7500 filled glass capillary is held on top of the outlet. (2) The capillary content is flushed out using FC-40, on top of a complete media droplet situated on top of a PTFE membrane. (3) The FC-40 further destabilizes the surfactant held emulsion, and the oils are absorbed by the membrane. (4) The remaining media and single-cell containing droplet can be transferred to a culturing platform. B) 3D printed PTFE membrane holder allows for airflow and fast oil evaporation in a biosafety cabinet. Reproduced from Samlali et al. [227], with permission from John Wiley and Sons.

Bibliography

[1] Sanjay M. Prakadan, Alex K. Shalek, and David A. Weitz. Scaling by shrinking: Empowering single-cell 'omics' with microfluidic devices. *Nature Reviews Genetics*, 18(6):345–361, June 2017. ISSN 1471-0064. doi: 10.1038/nrg.2017.15.

[2] Xing Xu, Junxia Wang, Lingling Wu, Jingjing Guo, Yanling Song, Tian Tian, Wei Wang, Zhi Zhu, and Chaoyong Yang. Microfluidic Single-Cell Omics Analysis. *Small*, 16(9):1903905, 2020. ISSN 1613-6829. doi: 10.1002/smll.201903905.

[3] Evan Z. Macosko, Anindita Basu, Rahul Satija, James Nemesh, Karthik Shekhar, Melissa Goldman, Itay Tirosh, Allison R. Bialas, Nolan Kamitaki, Emily M. Martersteck, John J. Trombetta, David A. Weitz, Joshua R. Sanes, Alex K. Shalek, Aviv Regev, and Steven A. McCarroll. Highly Parallel Genome-wide Expression Profiling of Individual Cells Using Nanoliter Droplets. *Cell*, 161(5):1202–1214, May 2015. ISSN 0092-8674. doi: 10.1016/j.cell.2015.05.002.

[4] Jeremy J. Agresti, Eugene Antipov, Adam R. Abate, Keunho Ahn, Amy C. Rowat, Jean-Christophe Baret, Manuel Marquez, Alexander M. Klibanov, Andrew D. Griffiths, and David A. Weitz. Ultrahigh-throughput screening in drop-based microfluidics for directed evolution. *Proceedings of the National Academy of Sciences*, 107(9):4004–4009, February 2010. ISSN 0027-8424, 1091-6490. doi: 10.1073/pnas.0910781107.

[5] Anna Alemany, Maria Florescu, Chloé S. Baron, Josi Peterson-Maduro, and Alexander van Oudenaarden. Whole-organism clone tracing using single-cell sequencing. *Nature*, 556(7699):108–112, April 2018. ISSN 1476-4687. doi: 10.1038/nature25969.

[6] Tia DiTommaso, Julie M. Cole, Luke Cassereau, Joshua A. Buggé, Jacquelyn L. Sikora Hanson, Devin T. Bridgen, Brittany D. Stokes, Scott M. Loughhead, Bruce A. Beutel, Jonathan B. Gilbert,

Kathrin Nussbaum, Antonio Sorrentino, Janine Toggweiler, Tobias Schmidt, Gabor Gyuelveszi, Howard Bernstein, and Armon Sharei. Cell engineering with microfluidic squeezing preserves functionality of primary immune cells in vivo. *Proceedings of the National Academy of Sciences*, 115(46): E10907–E10914, November 2018. ISSN 0027-8424, 1091-6490. doi: 10.1073/pnas.1809671115.

[7] Rapolas Zilionis, Juozas Nainys, Adrian Veres, Virginia Savova, David Zemmour, Allon M. Klein, and Linas Mazutis. Single-cell barcoding and sequencing using droplet microfluidics. *Nature Protocols*, 12(1):44–73, January 2017. ISSN 1750-2799. doi: 10.1038/nprot.2016.154.

[8] Jellert T. Gaublomme, Nir Yosef, Youjin Lee, Rona S. Gertner, Li V. Yang, Chuan Wu, Pier Paolo Pandolfi, Tak Mak, Rahul Satija, Alex K. Shalek, Vijay K. Kuchroo, Hongkun Park, and Aviv Regev. Single-Cell Genomics Unveils Critical Regulators of Th17 Cell Pathogenicity. *Cell*, 163(6):1400–1412, December 2015. ISSN 0092-8674. doi: 10.1016/j.cell.2015.11.009.

[9] Charles Gawad, Winston Koh, and Stephen R. Quake. Dissecting the clonal origins of childhood acute lymphoblastic leukemia by single-cell genomics. *Proceedings of the National Academy of Sciences*, 111(50):17947–17952, December 2014. ISSN 0027-8424, 1091-6490. doi: 10.1073/pnas.1420822111.

[10] Nate J. Cira, Adrien Benusiglio, and Manu Prakash. Dancing droplets: Autonomous surface tension-driven droplet motion. *Physics of Fluids*, 26(9):091113, September 2014. ISSN 1070-6631. doi: 10.1063/1.4894407.

[11] J. P. Brody, P. Yager, R. E. Goldstein, and R. H. Austin. Biotechnology at low Reynolds numbers. *Biophysical Journal*, 71(6):3430–3441, December 1996. ISSN 0006-3495. doi: 10.1016/S0006-3495(96)79538-3.

[12] E. M. Purcell. Life at low Reynolds number. *American Journal of Physics*, 45(1):3–11, January 1977. ISSN 0002-9505. doi: 10.1119/1.10903.

[13] Kihwan Choi, Alphonsus H. C. Ng, Ryan Fobel, and Aaron R. Wheeler. Digital Microfluidics. *Annual Review of Analytical Chemistry*, 5(1):413–440, 2012. doi: 10.1146/annurev-anchem-062011-143028.

[14] VolTRAX. http://nanoporetech.com/products/voltrax.

[15] Digital Microfluidics Technology. https://www.illumina.com/science/technology/digital-microfluidics.html.

[16] Technology — GenMark Diagnostics. https://genmarkdx.com/education/technology/.

[17] Meet Alto™ — High-Throughput Benchtop SPR Instrument —.

[18] Miroculus — Science Simplified™. https://miroculus.com/.

[19] Nuclera. https://www.nuclera.com/.

[20] Wyatt C. Nelson and Chang-Jin 'CJ' Kim. Droplet Actuation by Electrowetting-on-Dielectric (EWOD): A Review. *Journal of Adhesion Science and Technology*, ahead-of-print(ahead-of-print): 1–25, January 2012. ISSN 0169-4243. doi: 10.1163/156856111X599562.

[21] Debalina Chatterjee, Heather Shepherd, and Robin L. Garrell. Electromechanical model for actuating liquids in a two-plate droplet microfluidic device. *Lab on a Chip*, 9(9):1219–1229, 2009. doi: 10.1039/B901375J.

[22] T. B. Jones. An electromechanical interpretation of electrowetting. *Journal of Micromechanics and Microengineering*, 15(6):1184, 2005. ISSN 0960-1317. doi: 10.1088/0960-1317/15/6/008.

[23] Mohamed Abdelgawad, Philip Park, and Aaron R. Wheeler. Optimization of device geometry in single-plate digital microfluidics. *Journal of Applied Physics*, 105(9):094506, May 2009. ISSN 0021-8979. doi: 10.1063/1.3117216.

[24] Arjen M. Pit, Riëlle de Ruiter, Anand Kumar, Daniel Wijnperlé, Michèl H. G. Duits, and Frieder Mugele. High-throughput sorting of drops in microfluidic chips using electric capacitance. *Biomicrofluidics*, 9(4):044116, July 2015. doi: 10.1063/1.4928452.

[25] U. C. Yi and C. J. Kim. Characterization of electrowetting actuation on addressable single-side coplanar electrodes. *Journal of Micromechanics and Microengineering*, 16(10):2053–2059, October 2006. ISSN 0960-1317. doi: 10.1088/0960-1317/16/10/018.

[26] Mais J. Jebrail, Michael S. Bartsch, and Kamlesh D. Patel. Digital microfluidics: A versatile tool for applications in chemistry, biology and medicine. *Lab on a Chip*, 12(14):2452–2463, June 2012. ISSN 1473-0189. doi: 10.1039/C2LC40318H.

[27] Sara Lindström and Helene Andersson-Svahn. Miniaturization of biological assays — Overview on microwell devices for single-cell analyses. *Biochimica et Biophysica Acta (BBA) - General Subjects*, 1810(3):308–316, March 2011. ISSN 0304-4165. doi: 10.1016/j.bbagen.2010.04.009.

[28] Eric Brouzes, Martina Medkova, Neal Savenelli, Dave Marran, Mariusz Twardowski, J. Brian Hutchison, Jonathan M. Rothberg, Darren R. Link, Norbert Perrimon, and Michael L. Samuels. Droplet microfluidic technology for single-cell high-throughput screening. *Proceedings of the National Academy of Sciences*, 106(34):14195–14200, August 2009. ISSN 0027-8424, 1091-6490. doi: 10.1073/pnas.0903542106.

[29] Josephin M. Holstein, Christian Gylstorff, and Florian Hollfelder. Cell-free Directed Evolution of a Protease in Microdroplets at Ultrahigh Throughput. *ACS Synthetic Biology*, 10(2):252–257, February 2021. doi: 10.1021/acssynbio.0c00538.

[30] Fabrice Gielen, Raphaelle Hours, Stephane Emond, Martin Fischlechner, Ursula Schell, and Florian Hollfelder. Ultrahigh-throughput–directed enzyme evolution by absorbance-activated droplet sorting (AADS). *Proceedings of the National Academy of Sciences*, 113(47):E7383–E7389, November 2016. ISSN 0027-8424, 1091-6490. doi: 10.1073/pnas.1606927113.

[31] Jean-Christophe Baret, Oliver J. Miller, Valerie Taly, Michaël Ryckelynck, Abdeslam El-Harrak, Lucas Frenz, Christian Rick, Michael L. Samuels, J. Brian Hutchison, Jeremy J. Agresti, Darren R. Link, David A. Weitz, and Andrew D. Griffiths. Fluorescence-activated droplet sorting (FADS): Efficient microfluidic cell sorting based on enzymatic activity. *Lab on a Chip*, 9(13):1850–1858, July 2009. ISSN 1473-0189. doi: 10.1039/B902504A.

[32] Balint Kintses, Christopher Hein, Mark F. Mohamed, Martin Fischlechner, Fabienne Courtois, Céline Lainé, and Florian Hollfelder. Picoliter Cell Lysate Assays in Microfluidic Droplet Compartments for Directed Enzyme Evolution. *Chemistry & Biology*, 19(8):1001–1009, August 2012. ISSN 1074-5521. doi: 10.1016/j.chembiol.2012.06.009.

[33] Stephen A. Campbell. *Fabrication Engineering at the Micro- and Nanoscale*. The Oxford Series in Electrical and Computer Engineering. Oxford University Press, New York, fourth edition edition, 2013. ISBN 978-0-19-986122-4.

[34] M. Leester-Schädel, T. Lorenz, F. Jürgens, and C. Richter. Fabrication of Microfluidic Devices. In Andreas Dietzel, editor, *Microsystems for Pharmatechnology*, pages 23–57. Springer International Publishing, Cham, 2016. ISBN 978-3-319-26918-4 978-3-319-26920-7. doi: 10.1007/978-3-319-26920-7_2.

[35] Younan Xia and and George M. Whitesides. Soft Lithography. *Annual Review of Materials Science*, 28(1):153–184, 1998. doi: 10.1146/annurev.matsci.28.1.153.

[36] Liangcai Xiong, Peng Chen, and Quansheng Zhou. Adhesion promotion between PDMS and glass by oxygen plasma pre-treatment. *Journal of Adhesion Science and Technology*, 28(11):1046–1054, June 2014. ISSN 0169-4243. doi: 10.1080/01694243.2014.883774.

[37] I. Barbulovic-Nad, H. Yang, P. S. Park, and A. R. Wheeler. Digital microfluidics for cell-based assays. *Lab Chip*, 8(4):519–26, April 2008. ISSN 1473-0197 (Print) 1473-0189 (Linking). doi: 10.1039/b717759c.

[38] N. J. Shirtcliffe, R. Toon, and P. Roach. Surface treatments for microfluidic biocompatibility. *Methods in Molecular Biology (Clifton, N.J.)*, 949:241–268, 2013. ISSN 1940-6029. doi: 10.1007/978-1-62703-134-9_17.

[39] C. Holtze, A. C. Rowat, J. J. Agresti, J. B. Hutchison, F. E. Angilè, C. H. J. Schmitz, S. Köster, H. Duan, K. J. Humphry, R. A. Scanga, J. S. Johnson, D. Pisignano, and D. A. Weitz. Biocompatible surfactants for water-in-fluorocarbon emulsions. *Lab on a Chip*, 8(10):1632–1639, September 2008. ISSN 1473-0189. doi: 10.1039/B806706F.

[40] Kenneth C. Lowe. Perfluorochemical respiratory gas carriers: Benefits to cell culture systems. *Journal of Fluorine Chemistry*, 118(1-2):19–26, December 2002. ISSN 00221139. doi: 10.1016/S0022-1139(02)00200-2.

[41] Yao Lu, Qiong Xue, Markus R. Eisele, Endah S. Sulistijo, Kara Brower, Lin Han, El-ad David Amir, Dana Pe'er, Kathryn Miller-Jensen, and Rong Fan. Highly multiplexed profiling of single-cell effector functions reveals deep functional heterogeneity in response to pathogenic ligands. *Proceedings of the National Academy of Sciences*, 112(7):E607–E615, February 2015. ISSN 0027-8424, 1091-6490. doi: 10.1073/pnas.1416756112.

[42] Ahmad Ali Manzoor, Lauren Romita, and Dae Kun Hwang. A review on microwell and microfluidic geometric array fabrication techniques and its potential applications in cellular studies. *The Canadian Journal of Chemical Engineering*, 99(1):61–96, 2021. ISSN 1939-019X. doi: 10.1002/cjce.23875.

[43] Todd M. Gierahn, Marc H. Wadsworth, Travis K. Hughes, Bryan D. Bryson, Andrew Butler, Rahul Satija, Sarah Fortune, J. Christopher Love, and Alex K. Shalek. Seq-Well: Portable, low-cost RNA sequencing of single cells at high throughput. *Nature Methods*, 14(4):395–398, April 2017. ISSN 1548-7105. doi: 10.1038/nmeth.4179.

[44] Jinzhou Yuan and Peter A. Sims. An Automated Microwell Platform for Large-Scale Single Cell RNA-Seq. *Scientific Reports*, 6(1):33883, September 2016. ISSN 2045-2322. doi: 10.1038/srep33883.

[45] Navin Varadarajan, Douglas S. Kwon, Kenneth M. Law, Adebola O. Ogunniyi, Melis N. Anahtar, James M. Richter, Bruce D. Walker, and J. Christopher Love. Rapid, efficient functional characterization and recovery of HIV-specific human CD8+ T cells using microengraving. *Proceedings of the National Academy of Sciences*, 109(10):3885–3890, March 2012. ISSN 0027-8424, 1091-6490. doi: 10.1073/pnas.1111205109.

[46] Khashayar Moshksayan, Navid Kashaninejad, Majid Ebrahimi Warkiani, John G. Lock, Hajar Moghadas, Bahar Firoozabadi, Mohammad Said Saidi, and Nam-Trung Nguyen. Spheroids-on-a-chip: Recent advances and design considerations in microfluidic platforms for spheroid formation and culture. *Sensors and Actuators B: Chemical*, 263:151–176, June 2018. ISSN 0925-4005. doi: 10.1016/j.snb.2018.01.223.

[47] Päivi Järvinen, Ashkan Bonabi, Ville Jokinen, and Tiina Sikanen. Simultaneous Culturing of Cell Monolayers and Spheroids on a Single Microfluidic Device for Bridging the Gap between 2D and 3D Cell Assays in Drug Research. *Advanced Functional Materials*, 30(19):2000479, 2020. ISSN 1616-3028. doi: 10.1002/adfm.202000479.

[48] Sang Woo Lee, Soyoung Hong, Boyoung Jung, Soo Yeon Jeong, Jae Hee Byeon, Gi Seok Jeong, Jaesoon Choi, and Changmo Hwang. In vitro lung cancer multicellular tumor spheroid formation using a microfluidic device. *Biotechnology and Bioengineering*, 116(11):3041–3052, 2019. ISSN 1097-0290. doi: 10.1002/bit.27114.

[49] H. Antypas, M. Veses-Garcia, E. Weibull, H. Andersson-Svahn, and A. Richter-Dahlfors. A universal platform for selection and high-resolution phenotypic screening of bacterial mutants using the nanowell slide. *Lab on a Chip*, 18(12):1767–1777, 2018. doi: 10.1039/C8LC00190A.

[50] Nien-Tsu Huang, Yuh-Jen Hwong, and Richard Lee Lai. A microfluidic microwell device for immunomagnetic single-cell trapping. *Microfluidics and Nanofluidics*, 22(2):16, January 2018. ISSN 1613-4990. doi: 10.1007/s10404-018-2040-x.

[51] Bob Chen, Sungwon Lim, Arvind Kannan, Spencer C. Alford, Fanny Sunden, Daniel Herschlag, Ivan K. Dimov, Thomas M. Baer, and Jennifer R. Cochran. High-throughput analysis and protein engineering using microcapillary arrays. *Nature Chemical Biology*, 12(2):76–81, February 2016. ISSN 1552-4469. doi: 10.1038/nchembio.1978.

[52] Kiki C. Andree, Fikri Abali, Lisa Oomens, Fiona R. Passanha, Joska J. Broekmaat, Jaco Kraan, Pauline A. J. Mendelaar, Stefan Sleijfer, and Leon W. M. M. Terstappen. Self-Seeding Microwells to Isolate and Assess the Viability of Single Circulating Tumor Cells. *International Journal of Molecular Sciences*, 20(3):477, January 2019. doi: 10.3390/ijms20030477.

[53] Ansgar Huebner, Dan Bratton, Graeme Whyte, Min Yang, Andrew J. deMello, Chris Abell, and Florian Hollfelder. Static microdroplet arrays: A microfluidic device for droplet trapping, incubation and release for enzymatic and cell-based assays. *Lab on a Chip*, 9(5):692–698, March 2009. ISSN 1473-0189. doi: 10.1039/B813709A.

[54] Kwanghun Chung, Catherine A. Rivet, Melissa L. Kemp, and Hang Lu. Imaging Single-Cell Signaling Dynamics with a Deterministic High-Density Single-Cell Trap Array. *Analytical Chemistry*, 83 (18):7044–7052, September 2011. ISSN 0003-2700. doi: 10.1021/ac2011153.

[55] Stefan Kobel, Ana Valero, Jonas Latt, Philippe Renaud, and Matthias Lutolf. Optimization of microfluidic single cell trapping for long-term on-chip culture. *Lab on a Chip*, 10(7):857–863, 2010. doi: 10.1039/B918055A.

[56] Dino Di Carlo, Liz Y. Wu, and Luke P. Lee. Dynamic single cell culture array. *Lab on a Chip*, 6(11): 1445–1449, October 2006. ISSN 1473-0189. doi: 10.1039/B605937F.

[57] Robert M. Johann. Cell trapping in microfluidic chips. *Analytical and Bioanalytical Chemistry*, 385 (3):408–412, June 2006. ISSN 1618-2642, 1618-2650. doi: 10.1007/s00216-006-0369-6.

[58] Vigneswaran Narayanamurthy, Sairam Nagarajan, Al'aina Yuhainis Firus Khan, Fahmi Samsuri, and T. M. Sridhar. Microfluidic hydrodynamic trapping for single cell analysis: Mechanisms, methods and applications. *Analytical Methods*, 9(25):3751–3772, 2017. doi: 10.1039/C7AY00656J.

[59] Mahnoush Tayebi, Yinning Zhou, Pallavi Tripathi, Rajesh Chandramohanadas, and Ye Ai. Exosome Purification and Analysis Using a Facile Microfluidic Hydrodynamic Trapping Device. *Analytical Chemistry*, 92(15):10733–10742, August 2020. ISSN 0003-2700. doi: 10.1021/acs.analchem.0c02006.

[60] Reya Ganguly, Byungjin Lee, Solib Kang, Yong Sic Kim, Seong-Geun Jeong, Jae Seong Kim, So Young Park, Yamauchi Yohei, and Chang-Soo Lee. Microfluidic Single-cell Trapping and Cultivation for the Analysis of Host-viral Interactions. *Biotechnology and Bioprocess Engineering*, 26(2): 179–187, April 2021. ISSN 1976-3816. doi: 10.1007/s12257-020-0143-1.

[61] Quang D. Tran, Tian Fook Kong, Dinglong Hu, Marcos, and Raymond H. W. Lam. Deterministic sequential isolation of floating cancer cells under continuous flow. *Lab on a Chip*, 16(15):2813–2819, July 2016. ISSN 1473-0189. doi: 10.1039/C6LC00615A.

[62] Huichao Chai, Yongxiang Feng, Fei Liang, and Wenhui Wang. A microfluidic device enabling deterministic single cell trapping and release. *Lab on a Chip*, 21(13):2486–2494, 2021. doi: 10.1039/D1LC00302J.

[63] Avanish Mishra, Jae-Sung Kwon, Raviraj Thakur, and Steve Wereley. Optoelectrical microfluidics as a promising tool in biology. *Trends in Biotechnology*, 32(8):414–421, August 2014. ISSN 0167-7799. doi: 10.1016/j.tibtech.2014.06.002.

[64] Yuling Qin, Li Wu, Thomas Schneider, Gloria S. Yen, Jiasi Wang, Shihan Xu, Min Li, Amy L. Paguirigan, Jordan L. Smith, Jerald P. Radich, Robbyn K. Anand, and Daniel T. Chiu. A Self-Digitization Dielectrophoretic (SD-DEP) Chip for High-Efficiency Single-Cell Capture, On-Demand Compartmentalization, and Downstream Nucleic Acid Analysis. *Angewandte Chemie*, 130(35): 11548–11553, 2018. ISSN 1521-3757. doi: 10.1002/ange.201807314.

[65] Hyungsoo Kim, In-Kyu Lee, Kendra Taylor, Karl Richters, Dong-Hyun Baek, Jae Ha Ryu, Sang June Cho, Yei Hwan Jung, Dong-Wook Park, Joseph Novello, Jihye Bong, Aaron J. Suminski, Aaron M. Dingle, Robert H. Blick, Justin C. Williams, Erik W. Dent, and Zhenqiang Ma. Single-neuronal cell culture and monitoring platform using a fully transparent microfluidic DEP device. *Scientific Reports*, 8(1):13194, September 2018. ISSN 2045-2322. doi: 10.1038/s41598-018-31576-2.

[66] David J. Collins, Belinda Morahan, Jose Garcia-Bustos, Christian Doerig, Magdalena Plebanski, and Adrian Neild. Two-dimensional single-cell patterning with one cell per well driven by surface acoustic waves. *Nature Communications*, 6(1):8686, November 2015. ISSN 2041-1723. doi: 10. 1038/ncomms9686.

[67] Ping Wang, Lydia Robert, James Pelletier, Wei Lien Dang, Francois Taddei, Andrew Wright, and Suckjoon Jun. Robust Growth of Escherichia coli. *Current Biology*, 20(12):1099–1103, June 2010. ISSN 0960-9822. doi: 10.1016/j.cub.2010.04.045.

[68] Matthias Kaiser, Florian Jug, Thomas Julou, Siddharth Deshpande, Thomas Pfohl, Olin K. Silander, Gene Myers, and Erik van Nimwegen. Monitoring single-cell gene regulation under dynamically controllable conditions with integrated microfluidics and software. *Nature Communications*, 9(1): 212, January 2018. ISSN 2041-1723. doi: 10.1038/s41467-017-02505-0.

[69] Laurent Potvin-Trottier, Nathan D. Lord, Glenn Vinnicombe, and Johan Paulsson. Synchronous long-term oscillations in a synthetic gene circuit. *Nature*, 538(7626):514–517, October 2016. ISSN 1476-4687. doi: 10.1038/nature19841.

[70] Korine A. Ohiri, Sean T. Kelly, Jeffrey D. Motschman, Kevin H. Lin, Kris C. Wood, and Benjamin B. Yellen. An acoustofluidic trap and transfer approach for organizing a high density single cell array. *Lab on a Chip*, 18(14):2124–2133, 2018. doi: 10.1039/C8LC00196K.

[71] Jinjie Shi, Daniel Ahmed, Xiaole Mao, Sz-Chin Steven Lin, Aitan Lawit, and Tony Jun Huang. Acoustic tweezers: Patterning cells and microparticles using standing surface acoustic waves (SSAW). *Lab on a Chip*, 9(20):2890–2895, 2009. doi: 10.1039/B910595F.

[72] David J. Collins, Adrian Neild, Andrew deMello, Ai-Qun Liu, and Ye Ai. The Poisson distribution

and beyond: Methods for microfluidic droplet production and single cell encapsulation. *Lab on a Chip*, 15(17):3439–3459, August 2015. ISSN 1473-0189. doi: 10.1039/C5LC00614G.

[73] Tamar Hashimshony, Naftalie Senderovich, Gal Avital, Agnes Klochendler, Yaron de Leeuw, Leon Anavy, Dave Gennert, Shuqiang Li, Kenneth J. Livak, Orit Rozenblatt-Rosen, Yuval Dor, Aviv Regev, and Itai Yanai. CEL-Seq2: Sensitive highly-multiplexed single-cell RNA-Seq. *Genome Biology*, 17 (1):77, April 2016. ISSN 1474-760X. doi: 10.1186/s13059-016-0938-8.

[74] Maryam Navi, Niki Abbasi, Morteza Jeyhani, Vaskar Gnyawali, and Scott S. H. Tsai. Microfluidic diamagnetic water-in-water droplets: A biocompatible cell encapsulation and manipulation platform. *Lab on a Chip*, 18(22):3361–3370, November 2018. ISSN 1473-0189. doi: 10.1039/C8LC00867A.

[75] Peng Xu, Cyrus Modavi, Benjamin Demaree, Frederick Twigg, Benjamin Liang, Chen Sun, Wenjun Zhang, and Adam R. Abate. Microfluidic automated plasmid library enrichment for biosynthetic gene cluster discovery. *Nucleic Acids Research*, 48(8):e48, May 2020. ISSN 1362-4962. doi: 10.1093/nar/gkaa131.

[76] Jianbin Wang, H. Christina Fan, Barry Behr, and Stephen R. Quake. Genome-wide Single-Cell Analysis of Recombination Activity and De Novo Mutation Rates in Human Sperm. *Cell*, 150(2): 402–412, July 2012. ISSN 0092-8674. doi: 10.1016/j.cell.2012.06.030.

[77] Feng Guo, Sixing Li, Mehmet Umut Caglar, Zhangming Mao, Wu Liu, Andrew Woodman, Jamie J. Arnold, Claus O. Wilke, Tony Jun Huang, and Craig E. Cameron. Single-Cell Virology: On-Chip Investigation of Viral Infection Dynamics. *Cell Reports*, 21(6):1692–1704, November 2017. ISSN 2211-1247. doi: 10.1016/j.celrep.2017.10.051.

[78] Burak Okumus, Charles J. Baker, Juan Carlos Arias-Castro, Ghee Chuan Lai, Emanuele Leoncini, Somenath Bakshi, Scott Luro, Dirk Landgraf, and Johan Paulsson. Single-cell microscopy of suspension cultures using a microfluidics-assisted cell screening platform. *Nature Protocols*, 13(1):170–194, January 2018. ISSN 1750-2799. doi: 10.1038/nprot.2017.127.

[79] Weikai Zhang, Qin Li, Fei Jia, Zhiyuan Hu, and Zewen Wei. A Microfluidic Chip for Screening and Sequencing of Monoclonal Antibody at a Single-Cell Level. *Analytical Chemistry*, 93(29):10099–10105, July 2021. ISSN 0003-2700. doi: 10.1021/acs.analchem.1c00918.

[80] Joshua S. Marcus, W. French Anderson, and Stephen R. Quake. Microfluidic Single-Cell mRNA Isolation and Analysis. *Analytical Chemistry*, 78(9):3084–3089, May 2006. ISSN 0003-2700. doi: 10.1021/ac0519460.

[81] Ryan A. Kellogg, Rafael Gómez-Sjöberg, Anne A. Leyrat, and Savaş Tay. High-throughput microfluidic single-cell analysis pipeline for studies of signaling dynamics. *Nature Protocols*, 9(7): 1713–1726, July 2014. ISSN 1750-2799. doi: 10.1038/nprot.2014.120.

[82] Hsiu-Kang Huang, Ho-Wen Cheng, Cheng-Chieh Liao, Shang-Jyun Lin, Yi-Zih Chen, Juen-Kai Wang, Yuh-Lin Wang, and Nien-Tsu Huang. Bacteria encapsulation and rapid antibiotic susceptibility test using a microfluidic microwell device integrating surface-enhanced Raman scattering. *Lab on a Chip*, 20(14):2520–2528, 2020. doi: 10.1039/D0LC00425A.

[83] Peng Zhang, Jennifer Crow, Divya Lella, Xin Zhou, Glenson Samuel, Andrew K. Godwin, and Yong Zeng. Ultrasensitive quantification of tumor mRNAs in extracellular vesicles with an integrated microfluidic digital analysis chip. *Lab on a Chip*, 18(24):3790–3801, 2018. doi: 10.1039/C8LC01071D.

[84] Wei-Heong Tan and Shoji Takeuchi. A trap-and-release integrated microfluidic system for dynamic microarray applications. *Proceedings of the National Academy of Sciences*, 104(4):1146–1151, January 2007. ISSN 0027-8424, 1091-6490. doi: 10.1073/pnas.0606625104.

[85] Margaux Duchamp, Thamani Dahoun, Clarisse Vaillier, Marion Arnaud, Sara Bobisse, George Coukos, Alexandre Harari, and Philippe Renaud. Microfluidic device performing on flow study of serial cell–cell interactions of two cell populations. *RSC Advances*, 9(70):41066–41073, 2019. doi: 10.1039/C9RA09504G.

[86] Lijun Li, Huirong Wang, Lu Huang, Sean Alan Michael, Wei Huang, and Hongkai Wu. A Controllable, Centrifugal-Based Hydrodynamic Microfluidic Chip for Cell-Pairing and Studying Long-Term Communications between Single Cells. *Analytical Chemistry*, 91(24):15908–15914, December 2019. ISSN 0003-2700. doi: 10.1021/acs.analchem.9b04370.

[87] Xiaotian Du, Xiao Ma, Hang Li, Yaqing Ning, Xuanhong Cheng, and James C.M. Hwang. Validation of Clausius-Mossotti Function in Single-Cell Dielectrophoresis. In *2018 IEEE International*

Microwave Biomedical Conference (IMBioC), pages 94–96, June 2018. doi: 10.1109/IMBIOC.2018. 8428917.

[88] Berkeley Lights. https://www.berkeleylights.com/.

[89] Lightcast Discovery - Next generation cell biology. https://www.lightcastdiscovery.co.uk.

[90] Heng-Dong Xi, Hao Zheng, Wei Guo, Alfonso M. Gañán-Calvo, Ye Ai, Chia-Wen Tsao, Jun Zhou, Weihua Li, Yanyi Huang, Nam-Trung Nguyen, and Say Hwa Tan. Active droplet sorting in microfluidics: A review. *Lab on a Chip*, 17(5):751–771, February 2017. ISSN 1473-0189. doi: 10.1039/C6LC01435F.

[91] Mathias Girault, Hyonchol Kim, Hisayuki Arakawa, Kenji Matsuura, Masao Odaka, Akihiro Hattori, Hideyuki Terazono, and Kenji Yasuda. An on-chip imaging droplet-sorting system: A real-time shape recognition method to screen target cells in droplets with single cell resolution. *Scientific Reports*, 7, January 2017. ISSN 2045-2322. doi: 10.1038/srep40072.

[92] M. Sauzade and E. Brouzes. Deterministic trapping, encapsulation and retrieval of single-cells. *Lab on a Chip*, 17(13):2186–2192, June 2017. ISSN 1473-0189. doi: 10.1039/C7LC00283A.

[93] Adam R. Abate, Chia-Hung Chen, Jeremy Agresti, and David A. Weitz. Beating Poisson encapsulation statistics using close-packed ordering. *Lab on a Chip*, 9(18):2628–2631, 2009. doi: 10.1039/B909386A.

[94] Mingyan He, J. Scott Edgar, Gavin D. M. Jeffries, Robert M. Lorenz, J. Patrick Shelby, and Daniel T. Chiu. Selective Encapsulation of Single Cells and Subcellular Organelles into Picoliter- and Femtoliter-Volume Droplets. *Analytical Chemistry*, 77(6):1539–1544, March 2005. ISSN 0003-2700. doi: 10.1021/ac0480850.

[95] David J. Collins, Tuncay Alan, Kristian Helmerson, and Adrian Neild. Surface acoustic waves for on-demand production of picoliter droplets and particle encapsulation. *Lab on a Chip*, 13(16):3225–3231, July 2013. ISSN 1473-0189. doi: 10.1039/C3LC50372K.

[96] Say Hwa Tan, Benoît Semin, and Jean-Christophe Baret. Microfluidic flow-focusing in ac electric fields. *Lab on a Chip*, 14(6):1099–1106, February 2014. ISSN 1473-0189. doi: 10.1039/C3LC51143J.

[97] Stefan Haeberle, Roland Zengerle, and Jens Ducrée. Centrifugal generation and manipulation of droplet emulsions. *Microfluidics and Nanofluidics*, 3(1):65–75, December 2006. ISSN 1613-4982, 1613-4990. doi: 10.1007/s10404-006-0106-7.

[98] Maria Antfolk, Soo Hyeon Kim, Saori Koizumi, Teruo Fujii, and Thomas Laurell. Label-free single-cell separation and imaging of cancer cells using an integrated microfluidic system. *Scientific Reports*, 7(1):46507, April 2017. ISSN 2045-2322. doi: 10.1038/srep46507.

[99] Yufu Zhou, Ning Shao, Ricardo Bessa de Castro, Pengchao Zhang, Yuan Ma, Xin Liu, Feizhou Huang, Rong-Fu Wang, and Lidong Qin. Evaluation of Single-Cell Cytokine Secretion and Cell-Cell Interactions with a Hierarchical Loading Microwell Chip. *Cell Reports*, 31(4):107574, April 2020. ISSN 2211-1247. doi: 10.1016/j.celrep.2020.107574.

[100] Zhiliang Bai, Yanxiang Deng, Dongjoo Kim, Zhuo Chen, Yang Xiao, and Rong Fan. An Integrated Dielectrophoresis-Trapping and Nanowell Transfer Approach to Enable Double-Sub-Poisson Single-Cell RNA Sequencing. *ACS Nano*, 14(6):7412–7424, June 2020. ISSN 1936-0851. doi: 10.1021/acsnano.0c02953.

[101] H. Gu, F. Malloggi, S. A. Vanapalli, and F. Mugele. Electrowetting-enhanced microfluidic device for drop generation. *Applied Physics Letters*, 93(18), November 2008. ISSN 0003-6951. doi: Artn18350710.1063/1.3013567.

[102] I-Ming Chen, Hsin-Hsien Tsai, Che-Wei Chang, Gaofeng Zheng, and Yu-Chuan Su. Electric-field triggered, on-demand formation of sub-femtoliter droplets. *Sensors and Actuators B: Chemical*, 260:541–553, May 2018. ISSN 0925-4005. doi: 10.1016/j.snb.2017.12.152.

[103] F. Malloggi, H. Gu, A. G. Banpurkar, S. A. Vanapalli, and F. Mugele. Electrowetting –A versatile tool for controlling microdrop generation. *The European Physical Journal E*, 26(1):91–96, May 2008. ISSN 1292-895X. doi: 10.1140/epje/i2007-10252-x.

[104] Mostafa Shojaeian, François-Xavier Lehr, H. Ulrich Göringer, and Steffen Hardt. On-Demand Production of Femtoliter Drops in Microchannels and Their Use as Biological Reaction Compartments. *Analytical Chemistry*, 91(5):3484–3491, March 2019. ISSN 0003-2700. doi: 10.1021/acs.analchem.8b05063.

[105] Darren R. Link, Erwan Grasland-Mongrain, Agnes Duri, Flavie Sarrazin, Zhengdong Cheng, Galder Cristobal, Manuel Marquez, and David A. Weitz. Electric Control of Droplets in Microfluidic Devices. *Angewandte Chemie International Edition*, 45(16):2556–2560, 2006. ISSN 1521-3773. doi: 10.1002/anie.200503540.

[106] Xize Niu, Fabrice Gielen, Andrew J. deMello, and Joshua B. Edel. Electro-Coalescence of Digitally Controlled Droplets. *Analytical Chemistry*, 81(17):7321–7325, September 2009. ISSN 0003-2700. doi: 10.1021/ac901188n.

[107] Steve C.C. Shih, Philip C. Gach, Jess Sustarich, Blake A. Simmons, Paul D. Adams, Seema Singh, and Anup K. Singh. A droplet-to-digital (D2D) microfluidic device for single cell assays. *Lab on a Chip*, 15(1):225–236, 2015. doi: 10.1039/C4LC00794H.

[108] Fatemeh Ahmadi, Kenza Samlali, Philippe Q. N. Vo, and Steve C. C. Shih. An integrated droplet-digital microfluidic system for on-demand droplet creation, mixing, incubation, and sorting. *Lab on a Chip*, 19(3):524–535, January 2019. ISSN 1473-0189. doi: 10.1039/C8LC01170B.

[109] Riëlle de Ruiter, Arjen M. Pit, Vitor Martins de Oliveira, Michèl H. G. Duits, Dirk van den Ende, and Frieder Mugele. Electrostatic potential wells for on-demand drop manipulation in microchannels. *Lab on a Chip*, 14(5):883–891, February 2014. ISSN 1473-0189. doi: 10.1039/C3LC51121A.

[110] Steve C. C. Shih, Garima Goyal, Peter W. Kim, Nicolas Koutsoubelis, Jay D. Keasling, Paul D. Adams, Nathan J. Hillson, and Anup K. Singh. A Versatile Microfluidic Device for Automating Synthetic Biology. *ACS Synthetic Biology*, 4(10):1151–1164, October 2015. doi: 10.1021/acssynbio.5b00062.

[111] M. Abdelgawad, M. W. Watson, and A. R. Wheeler. Hybrid microfluidics: A digital-to-channel interface for in-line sample processing and chemical separations. *Lab Chip*, 9(8):1046–51, April 2009. ISSN 1473-0197 (Print) 1473-0189 (Linking). doi: 10.1039/b820682a.

[112] Michael W. L. Watson, Mais J. Jebrail, and Aaron R. Wheeler. Multilayer Hybrid Microfluidics: A Digital-to-Channel Interface for Sample Processing and Separations. *Analytical Chemistry*, 82(15):6680–6686, August 2010. ISSN 0003-2700. doi: 10.1021/ac101379g.

[113] Samuel R. Little, James M. Perry, Kenza Samlali, and Steve C. C. Shih. CHAPTER 8:droplet Microfluidics: Applications in Synthetic Biology. In *Droplet Microfluidics*, pages 193–222. Royal Society Chemistry, November 2020. doi: 10.1039/9781839162855-00193.

[114] Rosalind Franklin and R. G. Gosling. Molecular configuration in sodium thymonucleate. *Nature*, 171 (2):720–724, 1953.

[115] Francis Crick and James Watson. Molecular structure of nucleic acids. *Nature*, 171(2):720–724, 1953.

[116] S. N. Cohen, A. C. Chang, and L. Hsu. Nonchromosomal antibiotic resistance in bacteria: Genetic transformation of Escherichia coli by R-factor DNA. *Proceedings of the National Academy of Sciences of the United States of America*, 69(8):2110–2114, 1972. ISSN 00278424. doi: 10.1073/pnas.69.8.2110.

[117] U. Güldener, M. Münsterkötter, G. Kastenmüller, N. Strack, J. van Helden, C. Lemer, J. Richelles, S. J. Wodak, J. García-Martínez, J. E. Pérez-Ortín, H. Michael, A. Kaps, E. Talla, B. Dujon, B. André, J. L. Souciet, J. De Montigny, E. Bon, C. Gaillardin, and H. W. Mewes. CYGD: The comprehensive yeast genome database. *Nucleic Acids Research*, 33(DATABASE ISS.):364–368, 2005. ISSN 03051048. doi: 10.1093/nar/gki053.

[118] Stacia R. Engel, Fred S. Dietrich, Dianna G. Fisk, Gail Binkley, Rama Balakrishnan, Maria C. Costanzo, Selina S. Dwight, Benjamin C. Hitz, Kalpana Karra, Robert S. Nash, Shuai Weng, Edith D. Wong, Paul Lloyd, Marek S. Skrzypek, Stuart R. Miyasato, Matt Simison, and J. Michael Cherry. The reference genome sequence of saccharomyces cerevisiae: Then and now. *G3: Genes, Genomes, Genetics*, 4(3):389–398, 2014. ISSN 21601836. doi: 10.1534/g3.113.008995.

[119] Daniel C. Koboldt, Karyn Meltz Steinberg, David E. Larson, Richard K. Wilson, and Elaine R. Mardis. The next-generation sequencing revolution and its impact on genomics. *Cell*, 155(1):27, 2013. ISSN 10974172. doi: 10.1016/j.cell.2013.09.006.

[120] Michael L. Metzker. Sequencing technologies the next generation. *Nature Reviews Genetics*, 11(1): 31–46, 2010. ISSN 14710056. doi: 10.1038/nrg2626.

[121] Elaine R. Mardis. A decade's perspective on DNA sequencing technology. *Nature*, 470(7333):198–203, 2011. ISSN 00280836. doi: 10.1038/nature09796.

[122] Martin Jinek, Krzysztof Chylinski, Ines Fonfara, Michael Hauer, Jennifer A Doudna, and Emmanuelle Charpentier. A programmable Dual-RNA–Guided DNA endonuclease in adaptive bacterial immunity. *Science (New York, N.Y.)*, 337(6096):816–822, 2012. doi: 10.1126/science.1225829.

[123] C. J. Paddon, P. J. Westfall, D. J. Pitera, K. Benjamin, K. Fisher, D. McPhee, M. D. Leavell, A. Tai, A. Main, D. Eng, D. R. Polichuk, K. H. Teoh, D. W. Reed, T. Treynor, J. Lenihan, H. Jiang, M. Fleck, S. Bajad, G. Dang, D. Dengrove, D. Diola, G. Dorin, K. W. Ellens, S. Fickes, J. Galazzo, S. P. Gaucher, T. Geistlinger, R. Henry, M. Hepp, T. Horning, T. Iqbal, L. Kizer, B. Lieu, D. Melis, N. Moss, R. Regentin, S. Secrest, H. Tsuruta, R. Vazquez, L. F. Westblade, L. Xu, M. Yu, Y. Zhang, L. Zhao, J. Lievense, P. S. Covello, J. D. Keasling, K. K. Reiling, N. S. Renninger, and J. D. Newman. High-level semi-synthetic production of the potent antimalarial artemisinin. *Nature*, 496(7446): 528–532, 2013. ISSN 00280836. doi: 10.1038/nature12051.

[124] Stephanie Galanie, Kate Thodey, Isis J. Trenchard, Maria Filsinger Interrante, and Christina D. Smolke. Complete biosynthesis of opioids in yeast. *Science (New York, N.Y.)*, 349(6252):1095–1100, 2015. ISSN 10959203. doi: 10.1126/science.aac9373.

[125] Xiaozhou Luo, Michael A. Reiter, Leo d'Espaux, Jeff Wong, Charles M. Denby, Anna Lechner, Yunfeng Zhang, Adrian T. Grzybowski, Simon Harth, Weiyin Lin, Hyunsu Lee, Changhua Yu, John Shin, Kai Deng, Veronica T. Benites, George Wang, Edward E.K. Baidoo, Yan Chen, Ishaan Dev, Christopher J. Petzold, and Jay D. Keasling. Complete biosynthesis of cannabinoids and their unnatural analogues in yeast. *Nature*, 567(7746):123–126, 2019. ISSN 14764687. doi: 10.1038/s41586-019-0978-9.

[126] Charles E. Nakamura and Gregory M. Whited. Metabolic engineering for the microbial production of 1,3-propanediol. *Current Opinion in Biotechnology*, 14(5):454–459, 2003. ISSN 09581669. doi: 10.1016/j.copbio.2003.08.005.

[127] Michael Sauer, Hans Marx, and Diethard Mattanovich. Microbial production of 1,3-Propanediol. *Recent Patents on Biotechnology*, 2(3):191–197(7), 2008. doi: 10.2174/187220808786240999.

[128] Leqian Liu, Chiraj Dalal, Ben Heineike, and Adam Abate. High throughput gene expression profiling of yeast colonies with microgel-culture Drop-seq. *Lab on a Chip*, 19(10):1838–1849, 2018. doi: 10.1101/416966.

[129] Fayin Zhu, Xiaofang Zhong, Mengzhu Hu, Lei Lu, Zixin Deng, and Tiangang Liu. In vitro reconstitution of mevalonate pathway and targeted engineering of farnesene overproduction in Escherichia coli. *Biotechnology and Bioengineering*, 111(7):1396–1405, 2014. ISSN 10970290. doi: 10.1002/bit.25198.

[130] Gregory J. Tsongalis. Branched DNA technology in molecular diagnostics. *American Journal of Clinical Pathology*, 126(3):448–453, 2006. ISSN 00029173. doi: 10.1309/90BU6KDXANFLN4RJ.

[131] Keith Pardee, Alexander A. Green, Tom Ferrante, D. Ewen Cameron, Ajay Daleykeyser, Peng Yin, and James J. Collins. Paper-based synthetic gene networks. *Cell*, 159(4):940–954, 2014. ISSN 10974172. doi: 10.1016/j.cell.2014.10.004.

[132] Miguel-Angel Perales, Partow Kebriaei, Leslie S Kean, and Michel Sadelain. Building a safer and faster CAR: Seatbelts, airbags and crispr. Building a safer and faster CAR: Seatbelts, airbags and crispr. *Biology of Blood and Marrow Transplantation*, 24(1):27–31, 2017. ISSN 1083-8791. doi: 10.1016/j.bbmt.2017.10.017.

[133] Carl H. June and Michel Sadelain. Chimeric antigen receptor therapy. *New England Journal of Medicine*, 379(1):64–73, 2018. ISSN 15334406. doi: 10.1056/NEJMra1706169.

[134] Persis J. Amrolia and Martin Pule. Chimeric antigen receptor T cells for ALL. *The Lancet*, 385 (9967):488–490, 2015. ISSN 1474547X. doi: 10.1016/S0140-6736(14)61729-3.

[135] Alec A.K. Nielsen, Bryan S. Der, Jonghyeon Shin, Prashant Vaidyanathan, Vanya Paralanov, Elizabeth A. Strychalski, David Ross, Douglas Densmore, and Christopher A. Voigt. Genetic circuit design automation. *Science (New York, N.Y.)*, 352(6281), 2016. ISSN 10959203. doi: 10.1126/science.aac7341.

[136] Nathan J. Hillson, Rafael D. Rosengarten, and Jay D. Keasling. J5 DNA assembly design automation software. *ACS Synthetic Biology*, 1(1):14–21, 2012. ISSN 21615063. doi: 10.1021/sb2000116.

[137] Afaf H. El-Sagheer and Tom Brown. Click chemistry with DNA. *Chemical Society Reviews*, 39(4): 1388, March 2010. ISSN 0306-0012. doi: 10.1039/b901971p.

[138] Carola Engler, Romy Kandzia, and Sylvestre Marillonnet. A one pot, one step, precision cloning method with high throughput capability. *PLoS ONE*, 3(11):e3647, 2008. doi: 10.1371/journal.pone. 0003647.

[139] Carola Engler, Ramona Gruetzner, Romy Kandzia, and Sylvestre Marillonnet. Golden Gate Shuffling: A One-Pot DNA Shuffling Method Based on Type IIs Restriction Enzymes. *PLoS ONE*, 4(5), May 2009. ISSN 1932-6203. doi: 10.1371/journal.pone.0005553.

[140] Daniel G Gibson, Lei Young, Ray-Yuan Chuang, J Craig Venter, Clyde A Hutchison, and Hamilton O Smith. Enzymatic assembly of DNA molecules up to several hundred kilobases. *Nature methods*, 6 (5):343–5, 2009. ISSN 1548-7105. doi: 10.1038/nmeth.1318.

[141] Daniel G. Gibson. Synthesis of DNA fragments in yeast by one-step assembly of overlapping oligonucleotides. *Nucleic Acids Research*, 37(20):6984–6990, 2009. ISSN 03051048. doi: 10.1093/nar/gkp687.

[142] Mazhar Adli. The CRISPR tool kit for genome editing and beyond. *Nature Communications*, 9(1): 1–13, May 2018. ISSN 2041-1723. doi: 10.1038/s41467-018-04252-2.

[143] Pierre Crozet, Francisco J. Navarro, Felix Willmund, Payam Mehrshahi, Kamil Bakowski, Kyle J. Lauersen, Maria Esther Pérez-Pérez, Pascaline Auroy, Aleix Gorchs Rovira, Susana Sauret-Gueto, Justus Niemeyer, Benjamin Spaniol, Jasmine Theis, Raphael Trösch, Lisa Desiree Westrich, Konstantinos Vavitsas, Thomas Baier, Wolfgang Hübner, Felix De Carpentier, Mathieu Cassarini, Antoine Danon, Julien Henri, Christophe H. Marchand, Marcello De Mia, Kevin Sarkissian, David C. Baulcombe, Gilles Peltier, José Luis Crespo, Olaf Kruse, Poul Erik Jensen, Michael Schroda, Alison G. Smith, and Stéphane D. Lemaire. Birth of a photosynthetic chassis: A MoClo toolkit enabling synthetic biology in the microalga chlamydomonas reinhardtii. *ACS Synthetic Biology*, 7(9):2074–2086, 2018. ISSN 21615063. doi: 10.1021/acssynbio.8b00251.

[144] Michael E. Lee, William C. DeLoache, Bernardo Cervantes, and John E. Dueber. A highly characterized yeast toolkit for modular, multipart assembly. *ACS Synthetic Biology*, 4(9):975–986, 2015. ISSN 21615063. doi: 10.1021/sb500366v.

[145] Ernst Weber, Carola Engler, Ramona Gruetzner, Stefan Werner, and Sylvestre Marillonnet. A modular cloning system for standardized assembly of multigene constructs. *PLoS ONE*, 6(2), 2011. doi: 10.1371/journal.pone.0016765.

[146] Hung En Lai, Simon Moore, Karen Polizzi, and Paul Freemont. EcoFlex: A multifunctional moclo kit for E. coli synthetic biology. *Methods in Molecular Biology*, 1772:429–444, 2018. ISSN 10643745. doi: 10.1007/978-1-4939-7795-6_25.

[147] Ginkgo bioworks. https://www.ginkgobioworks.com/.

[148] Nathan Hillson, Mark Caddick, Yizhi Cai, Jose A. Carrasco, Matthew Wook Chang, Natalie C. Curach, David J. Bell, Rosalind Le Feuvre, Douglas C. Friedman, Xiongfei Fu, Nicholas D. Gold, Markus J. Herrgård, Maciej B. Holowko, James R. Johnson, Richard A. Johnson, Jay D. Keasling, Richard I. Kitney, Akihiko Kondo, Chenli Liu, Vincent J.J. Martin, Filippo Menolascina, Chiaki Ogino, Nicola J. Patron, Marilene Pavan, Chueh Loo Poh, Isak S. Pretorius, Susan J. Rosser, Nigel S. Scrutton, Marko Storch, Hille Tekotte, Evelyn Travnik, Claudia E. Vickers, Wen Shan Yew, Yingjin Yuan, Huimin Zhao, and Paul S. Freemont. Building a global alliance of biofoundries. *Nature Communications*, 10(1):1038–1041, 2019. ISSN 20411723. doi: 10.1038/s41467-019-10079-2.

[149] EGF cuba. https://cuba.genomefoundry.org/, 2017.

[150] Agile biofoundry. http://www.agilebiofoundry.org/.

[151] Paulina Kanigowska, Yue Shen, Yijing Zheng, Susan Rosser, and Yizhi Cai. Smart DNA fabrication using sound waves: Applying acoustic dispensing technologies to synthetic biology. *Journal of Laboratory Automation*, 21(1):49–56, 2016. ISSN 22110690. doi: 10.1177/2211068215593754.

[152] Jennifer A. Doudna and Emmanuelle Charpentier. The new frontier of genome engineering with CRISPR-Cas9. *Science (New York, N.Y.)*, 346(6213):1258096–6, 2014. doi: 10.1126/science.1258096.

[153] Prashant Mali, Kevin M. Esvelt, and George M. Church. Cas9 as a versatile tool for engineering biology. *Nature Methods*, 10(10):957–963, 2013. ISSN 15487091. doi: 10.1038/nmeth.2649.

[154] Le; Cong, Ann; Ran, David; Cox, Shuailaang; Lin, Robert; Barretto, Naomi; Habib, Patrick; Hsu, Xuebing; Wu, Wenyan; Jiang, Luciano; Marraffini, and Feng; Zhang. Multiplex genome engineering using CRISPR/Cas systems. *Science (New York, N.Y.)*, (February):819–824, 2013.

[155] Hugo Sinha, Angela B. V. Quach, Philippe Q. N. Vo, and Steve C. C. Shih. An automated microfluidic gene-editing platform for deciphering cancer genes. *Lab on a Chip*, 18(15):2300–2312, July 2018. ISSN 1473-0189. doi: 10.1039/C8LC00470F.

[156] Xuan Li, Mohammad Aghaamoo, Shiyue Liu, Do Hyun Lee, and Abraham P. Lee. Lipoplex-mediated single-cell transfection via droplet microfluidics. *Small (Weinheim an der Bergstrasse, Germany)*, 14 (40):1–10, 2018. ISSN 16136829. doi: 10.1002/smll.201802055.

[157] Xin Han, Zongbin Liu, Li Zhao, Feng Wang, Yang Yu, Jianhua Yang, Rui Chen, and Lidong Qin. Microfluidic cell deformability assay for rapid and efficient kinase screening with the CRISPR-Cas9 system. *Angewandte Chemie - International Edition*, 55(30):8561–8565, 2016. ISSN 15213773. doi: 10.1002/anie.201601984.

[158] Xin Han, Zongbin Liu, Myeong chan Jo, Kai Zhang, Ying Li, Zihua Zeng, Nan Li, Youli Zu, and Lidong Qin. CRISPR-Cas9 delivery to hard-to-transfect cells via membrane deformation. *Science Advances*, 1(7):e1500454, 2015. doi: 10.1126/sciadv.1500454.

[159] Philip C. Gach, Steve C.C. Shih, Jess Sustarich, Jay D. Keasling, Nathan J. Hillson, Paul D. Adams, and Anup K. Singh. A droplet microfluidic platform for automating genetic engineering. *ACS Synthetic Biology*, 5(5):426–433, 2016. ISSN 21615063. doi: 10.1021/acssynbio.6b00011.

[160] Yun Ding, Jaebum Choo, and Andrew J. deMello. From single-molecule detection to next-generation sequencing: Microfluidic droplets for high-throughput nucleic acid analysis. *Microfluidics and Nanofluidics*, 21(3):1–20, 2017. ISSN 16134990. doi: 10.1007/s10404-017-1889-4.

[161] Adam Sciambi and Adam R. Abate. Accurate microfluidic sorting of droplets at 30 kHz. *Lab on a Chip*, 15(1):47–51, December 2014. ISSN 1473-0189. doi: 10.1039/C4LC01194E.

[162] James M. Wagner, Leqian Liu, Shuo Fu Yuan, Maya V. Venkataraman, Adam R. Abate, and Hal S. Alper. A comparative analysis of single cell and droplet-based FACS for improving production phenotypes: Riboflavin overproduction in Yarrowia lipolytica. *Metabolic Engineering*, 47(February): 346–356, 2018. ISSN 10967184. doi: 10.1016/j.ymben.2018.04.015.

[163] Ouriel Caen, Simon Schütz, M. S. Suryateja Jammalamadaka, Jérémy Vrignon, Philippe Nizard, Tobias M. Schneider, Jean-Christophe Baret, and Valérie Taly. High-throughput multiplexed fluorescence-activated droplet sorting. *Microsystems & Nanoengineering*, 4(1):33, December 2018. ISSN 2055-7434. doi: 10.1038/s41378-018-0033-2.

[164] Nachiket Shembekar, Hongxing Hu, David Eustace, and Christoph A. Merten. Single-Cell Droplet Microfluidic Screening for Antibodies Specifically Binding to Target Cells. *Cell Reports*, 22(8): 2206–2215, February 2018. ISSN 2211-1247. doi: 10.1016/j.celrep.2018.01.071.

[165] Joanna C. Sadler, Andrew Currin, and Douglas B. Kell. Ultra-high throughput functional enrichment of large monoamine oxidase (MAO-N) libraries by fluorescence activated cell sorting. *The Analyst*, 143(19):4747–4755, 2018. ISSN 0003-2654. doi: 10.1039/C8AN00851E.

[166] Kazuki Nakamura, Ryo Iizuka, Shinro Nishi, Takao Yoshida, Yuji Hatada, Yoshihiro Takaki, Ayaka Iguchi, Dong Hyun Yoon, Tetsushi Sekiguchi, Shuichi Shoji, and Takashi Funatsu. Culture-independent method for identification of microbial enzyme-encoding genes by activity-based single-cell sequencing using a water-in-oil microdroplet platform. *Scientific Reports*, 6:22259, February 2016. ISSN 2045-2322. doi: 10.1038/srep22259.

[167] Ziyi Yu, Christian R. Boehm, Julian M. Hibberd, Chris Abell, Jim Haseloff, Steven J. Burgess, and Ivan Reyna-Llorens. Droplet-based microfluidic analysis and screening of single plant cells. *PLoS ONE*, 13(5):1–15, 2018. ISSN 19326203. doi: 10.1371/journal.pone.0196810.

[168] Mingtao Huang, Yunpeng Bai, Staffan L. Sjostrom, Björn M. Hallström, Zihe Liu, Dina Petranovic, Mathias Uhlén, Haakan N. Joensson, Helene Andersson-Svahn, and Jens Nielsen. Microfluidic screening and whole-genome sequencing identifies mutations associated with improved protein secretion by yeast. *Proceedings of the National Academy of Sciences*, 112(34):E4689–E4696, August 2015. ISSN 0027-8424, 1091-6490. doi: 10.1073/pnas.1506460112.

[169] Philip A. Romero, Tuan M. Tran, and Adam R. Abate. Dissecting enzyme function with microfluidic-based deep mutational scanning. *Proceedings of the National Academy of Sciences*, 112(23):7159–7164, 2015. ISSN 0027-8424. doi: 10.1073/pnas.1422285112.

[170] Joseph Abatemarco, Maen F. Sarhan, James M. Wagner, Jyun Liang Lin, Leqian Liu, Wafa Hassouneh, Shuo Fu Yuan, Hal S. Alper, and Adam R. Abate. RNA-aptamers-in-droplets (RAPID) high-throughput screening for secretory phenotypes. *Nature Communications*, 8(1):1–9, 2017. doi: 10.1038/s41467-017-00425-7.

[171] Lewis A Fraser, Andrew B Kinghorn, Marco S L Tang, Yee-wai Cheung, Bryce Lim, Shaolin Liang, Roderick M Dirkzwager, and Julian A Tanner. Oligonucleotide functionalised microbeads : Indispensable tools for high-throughput aptamer selection. *Molecules (Basel, Switzerland)*, 1:21298–21312, 2015. doi: 10.3390/molecules201219766.

[172] Lewis A. Fraser, Yee Wai Cheung, Andrew B. Kinghorn, Wei Guo, Simon Chi Chin Shiu, Chandra Jinata, Mengping Liu, Soubhagya Bhuyan, Lang Nan, Ho Cheung Shum, and Julian A. Tanner. Microfluidic technology for nucleic acid aptamer evolution and application. *Advanced Biosystems*, 1900012:1–16, 2019. ISSN 23667478. doi: 10.1002/adbi.201900012.

[173] Paul Datlinger, André F Rendeiro, Christian Schmidl, Thomas Krausgruber, Peter Traxler, Johanna Klughammer, Linda C Schuster, Amelie Kuchler, Donat Alpar, and Christoph Bock. Pooled CRISPR screening with single-cell transcriptome readout. *Nature methods*, 14(3):297–301, 2017. ISSN 1548-7105. doi: 10.1038/nmeth.4177.

[174] Angela R Wu, Norma F Neff, Tomer Kalisky, Piero Dalerba, Barbara Treutlein, Michael E Rothenberg, Francis M Mburu, Gary L Mantalas, Sopheak Sim, Michael F Clarke, and Stephen R Quake. Quantitative assessment of single-cell RNA-sequencing methods. *Nature methods*, 11(1):41–6, January 2014. ISSN 1548-7105. doi: 10.1038/nmeth.2694.

[175] Aaron M. Streets, Xiannian Zhang, Chen Cao, Yuhong Pang, Xinglong Wu, Liang Xiong, Lu Yang, Yusi Fu, Liang Zhao, Fuchou Tang, and Yanyi Huang. Microfluidic single-cell whole-transcriptome sequencing. *Proceedings of the National Academy of Sciences*, 111(19):7048–7053, May 2014. ISSN 0027-8424, 1091-6490. doi: 10.1073/pnas.1402030111.

[176] Efthymia Papalexi and Rahul Satija. Single-cell RNA sequencing to explore immune cell heterogeneity. *Nature Reviews Immunology*, 18(1):35–45, January 2018. ISSN 1474-1741. doi: 10.1038/nri.2017.76.

[177] Feiqiao Brian Yu, Paul C Blainey, Frederik Schulz, Tanja Woyke, Mark A Horowitz, and Stephen R Quake. Microfluidic-based mini-metagenomics enables discovery of novel microbial lineages from complex environmental samples. *eLife*, 6:e26580, 2017. doi: 10.7554/eLife.26580.

[178] Diego Adhemar Jaitin, Ephraim Kenigsberg, Hadas Keren-Shaul, Naama Elefant, Franziska Paul, Irina Zaretsky, Alexander Mildner, Nadav Cohen, Steffen Jung, Amos Tanay, and Ido Amit. Massively parallel single-cell RNA-Seq for marker-free decomposition of tissues into cell types. *Science (New York, N.Y.)*, 343(6172):776–779, February 2014. ISSN 0036-8075, 1095-9203. doi: 10.1126/science.1247651.

[179] Hadas Keren-Shaul, Ephraim Kenigsberg, Diego Adhemar Jaitin, Eyal David, Franziska Paul, Amos Tanay, and Ido Amit. MARS-seq2.0: An experimental and analytical pipeline for indexed sorting combined with single-cell RNA sequencing. *Nature Protocols*, 14(6):1841–1862, June 2019. ISSN 1750-2799. doi: 10.1038/s41596-019-0164-4.

[180] Daniel Ramsköld, Shujun Luo, Yu-Chieh Wang, Robin Li, Qiaolin Deng, Omid R. Faridani, Gregory A. Daniels, Irina Khrebtukova, Jeanne F. Loring, Louise C. Laurent, Gary P. Schroth, and Rickard Sandberg. Full-length mRNA-Seq from single-cell levels of RNA and individual circulating tumor cells. *Nature Biotechnology*, 30(8):777–782, August 2012. ISSN 1546-1696. doi: 10.1038/nbt.2282.

[181] Johannes W. Bagnoli, Christoph Ziegenhain, Aleksandar Janjic, Lucas E. Wange, Beate Vieth, Swati Parekh, Johanna Geuder, Ines Hellmann, and Wolfgang Enard. Sensitive and powerful single-cell RNA sequencing using mcSCRB-seq. *Nature Communications*, 9(1):2937, July 2018. ISSN 2041-1723. doi: 10.1038/s41467-018-05347-6.

[182] Simone Picelli, Åsa K. Björklund, Omid R. Faridani, Sven Sagasser, Gösta Winberg, and Rickard Sandberg. Smart-seq2 for sensitive full-length transcriptome profiling in single cells. *Nature Methods*, 10(11):1096–1098, November 2013. ISSN 1548-7105. doi: 10.1038/nmeth.2639.

[183] Yohei Sasagawa, Hiroki Danno, Hitomi Takada, Masashi Ebisawa, Kaori Tanaka, Tetsutaro Hayashi, Akira Kurisaki, and Itoshi Nikaido. Quartz-Seq2: A high-throughput single-cell RNA-sequencing method that effectively uses limited sequence reads. *Genome Biology*, 19(1):29, March 2018. ISSN 1474-760X. doi: 10.1186/s13059-018-1407-3.

[184] Robert Salomon, Dominik Kaczorowski, Fatima Valdes-Mora, Robert E. Nordon, Adrian Neild, Nona Farbehi, Nenad Bartonicek, and David Gallego-Ortega. Droplet-based single cell RNAseq tools: A practical guide. *Lab on a Chip*, 19(10):1706–1727, 2019. doi: 10.1039/C8LC01239C.

[185] Esben Bjoern Madsen, Thomas Kvist, Ida Hoijer, Adam Ameur, and Marie Just Mikkelsen. Xdrop: Targeted sequencing of long DNA molecules from low input samples using droplet sorting. *bioRxiv : the preprint server for biology*, page 409086, 2018. doi: 10.1101/409086.

[186] Alphonsus H. C. Ng, Songming Peng, Alexander M. Xu, Won Jun Noh, Katherine Guo, Michael T. Bethune, William Chour, Jongchan Choi, Sung Yang, David Baltimore, and James R. Heath. MATE-Seq: Microfluidic antigen-TCR engagement sequencing. *Lab on a Chip*, 19(18):3011–3021, August 2019. doi: 10.1039/C9LC00538B.

[187] Elham Azizi, Ambrose J. Carr, George Plitas, Andrew E. Cornish, Catherine Konopacki, Sandhya Prabhakaran, Juozas Nainys, Kenmin Wu, Vaidotas Kiseliovas, Manu Setty, Kristy Choi, Rachel M. Fromme, Phuong Dao, Peter T. McKenney, Ruby C. Wasti, Krishna Kadaveru, Linas Mazutis, Alexander Y. Rudensky, and Dana Pe'er. Single-Cell Map of Diverse Immune Phenotypes in the Breast Tumor Microenvironment. *Cell*, 174(5):1293–1308.e36, August 2018. ISSN 1097-4172. doi: 10.1016/j.cell.2018.05.060.

[188] Freeman Lan, John R. Haliburton, Aaron Yuan, and Adam R. Abate. Droplet barcoding for massively parallel single-molecule deep sequencing. *Nature Communications*, 7(1):1–10, June 2016. ISSN 2041-1723. doi: 10.1038/ncomms11784.

[189] Wai Keung Chu, Peter Edge, Ho Suk Lee, Vikas Bansal, Vineet Bafna, Xiaohua Huang, and Kun Zhang. Ultraaccurate genome sequencing and haplotyping of single human cells. *Proceedings of the National Academy of Sciences of the United States of America*, 114(47):12512–12517, November 2017. ISSN 1091-6490. doi: 10.1073/pnas.1707609114.

[190] Randall A. Hughes and Andrew D. Ellington. Synthetic DNA Synthesis and Assembly: Putting the Synthetic in Synthetic Biology. *Cold Spring Harbor Perspectives in Biology*, 9(1):a023812, January 2017. ISSN , 1943-0264. doi: 10.1101/cshperspect.a023812.

[191] Daniel J. Steyer and Robert T. Kennedy. High-Throughput Nanoelectrospray Ionization-Mass Spectrometry Analysis of Microfluidic Droplet Samples. *Analytical Chemistry*, 91(10):6645–6651, May 2019. ISSN 0003-2700. doi: 10.1021/acs.analchem.9b00571.

[192] Joshua Heinemann, Kai Deng, Steve C.C. Shih, Jian Gao, Paul D. Adams, Anup K. Singh, and Trent R. Northen. On-chip integration of droplet microfluidics and nanostructure-initiator mass spectrometry for enzyme screening. *Lab on a Chip*, 17(2):323–331, 2017. ISSN 14730189. doi: 10.1039/c6lc01182a.

[193] Camille Lombard-Banek, Sally A. Moody, M. Chiara Manzini, and Peter Nemes. Microsampling capillary electrophoresis mass spectrometry enables single-cell proteomics in complex tissues: Developing cell clones in live ¡i¿Xenopus laevis¡/i¿ and zebrafish embryos. *Analytical Chemistry*, 91 (7):4797–4805, April 2019. ISSN 0003-2700. doi: 10.1021/acs.analchem.9b00345.

[194] Samuel C. Kim, Gayatri Premasekharan, Iain C. Clark, Hawi B. Gemeda, Pamela L. Paris, and Adam R. Abate. Measurement of copy number variation in single cancer cells using rapid-emulsification digital droplet MDA. *Microsystems and Nanoengineering*, 3:17018, 2017. doi: 10.1038/micronano.2017.18.

[195] Ying Zhu and Qun Fang. Analytical detection techniques for droplet microfluidics—A review. *Analytica Chimica Acta*, 787:24–35, July 2013. ISSN 0003-2670. doi: 10.1016/j.aca.2013.04.064.

[196] Jyun Liang Lin, James M. Wagner, and Hal S. Alper. Enabling tools for high-throughput detection of metabolites: Metabolic engineering and directed evolution applications. *Biotechnology Advances*, 35 (8):950–970, 2017. ISSN 07349750. doi: 10.1016/j.biotechadv.2017.07.005.

[197] Derek Vallejo, Ali Nikoomanzar, and John C. Chaput. Directed evolution of custom polymerases using droplet microfluidics. *Methods in Enzymology*, 644:227–253, 2020. ISSN 1557-7988. doi: 10.1016/bs.mie.2020.04.056.

[198] Yu Dong Ma, Kang Luo, Wen Hsin Chang, and Gwo Bin Lee. A microfluidic chip capable of generating and trapping emulsion droplets for digital loop-mediated isothermal amplification analysis. *Lab on a Chip*, 18(2):296–303, 2018. ISSN 14730189. doi: 10.1039/c7lc01004d.

[199] Brandon G Wong, Christopher P Mancuso, Szilvia Kiriakov, Caleb J Bashor, and Ahmad S Khalil. Precise, automated control of conditions for high-throughput growth of yeast and bacteria with eVOLVER. *Nature biotechnology*, 36(7):614–623, 2018. doi: 10.1038/nbt.4151.

[200] Guokun Wang, Sara M. Björk, Mingtao Huang, Quanli Liu, Kate Campbell, Jens Nielsen, Haakan N. Joensson, and Dina Petranovic. RNAi expression tuning, microfluidic screening, and genome recombineering for improved protein production in Saccharomyces cerevisiae. *Proceedings of the National Academy of Sciences*, 116(19):9324–9332, 2019. doi: 10.1073/pnas.1820561116.

[201] Hanaa M. Hegab, Ahmed ElMekawy, and Tim Stakenborg. Review of microfluidic microbioreactor technology for high-throughput submerged microbiological cultivation. *Biomicrofluidics*, 7(2):1–14, 2013. ISSN 19321058. doi: 10.1063/1.4799966.

[202] Lisa Mahler, Miguel Tovar, Thomas Weber, Susanne Brandes, Martin Michael Rudolph, Josef Ehgartner, Torsten Mayr, Marc Thilo Figge, Martin Roth, and Emerson Zang. Enhanced and homogeneous oxygen availability during incubation of microfluidic droplets. *RSC Advances*, 5(123):101871–101878, 2015. ISSN 20462069. doi: 10.1039/c5ra20118g.

[203] Tuan M Tran, Samuel C Kim, and Adam R Abate. Robotic automation of droplet microfluidics. *bioRxiv : the preprint server for biology*, page 278556, 2018. doi: 10.1101/278556.

[204] Han A B Wösten. Filamentous fungi for the production of enzymes, chemicals and materials. *Current Opinion in Biotechnology*, 59:65–70, October 2019. ISSN 0958-1669. doi: 10.1016/j.copbio.2019.02.010.

[205] Marina Venturini Copetti. Fungi as industrial producers of food ingredients. *Current Opinion in Food Science*, 25:52–56, February 2019. ISSN 2214-7993. doi: 10.1016/j.cofs.2019.02.006.

[206] Lauryn G. Chan, Joshua L. Cohen, and Juliana Maria Leite Nobrega de Moura Bell. Conversion

of Agricultural Streams and Food-Processing By-Products to Value-Added Compounds Using Filamentous Fungi. *Annual Review of Food Science and Technology*, 9(1):503–523, March 2018. ISSN 1941-1413, 1941-1421. doi: 10.1146/annurev-food-030117-012626.

[207] Yue-Jin Wu, Chih-Yu Cheng, and Yaw-Kuen Li. Cloning and Expression of Chitinase A from Serratia Marcescens for Large-Scale Preparation of N,N-Diacetyl Chitobiose. *Journal of the Chinese Chemical Society*, 56(4):688–695, 2009. ISSN 2192-6549. doi: 10.1002/jccs.200900103.

[208] Hans-Josef Schroers, Gary J. Samuels, Keith A. Seifert, and Walter Gams. Classification of the Mycoparasite Gliocladium roseum in Clonostachys as C. rosea, Its Relationship to Bionectria ochroleuca, and Notes on Other Gliocladium-like Fungi. *Mycologia*, 91(2):365–385, 1999. ISSN 0027-5514. doi: 10.2307/3761383.

[209] D. F. Jensen, I. M. B. Knudsen, M. Lü beck, M. Mamarabadi, J. Hockenhull, and B. Jensen. Development of a biocontrol agent for plant disease control with special emphasis on the near commercial fungal antagonist Clonostachys rosea strain 'IK726'. *Australasian Plant Pathology*, 36(2):95–101, March 2007. ISSN 1448-6032. doi: 10.1071/AP07009.

[210] Z.-B. Sun, S.-D. Li, Q. Ren, J.-L. Xu, X. Lu, and M.-H. Sun. Biology and applications of Clonostachys rosea. *Journal of Applied Microbiology*, 129(3):486–495, September 2020. ISSN 1365-2672. doi: 10.1111/jam.14625.

[211] Magnus Karlsson, Mikael Brandström Durling, Jaeyoung Choi, Chatchai Kosawang, Gerald Lackner, Georgios D. Tzelepis, Kristiina Nygren, Mukesh K. Dubey, Nathalie Kamou, Anthony Levasseur, Antonio Zapparata, Jinhui Wang, Daniel Buchvaldt Amby, Birgit Jensen, Sabrina Sarrocco, Emmanuel Panteris, Anastasia L. Lagopodi, Stefanie Pöggeler, Giovanni Vannacci, David B. Collinge, Dirk Hoffmeister, Bernard Henrissat, Yong-Hwan Lee, and Dan Funck Jensen. Insights on the evolution of mycoparasitism from the genome of Clonostachys rosea. *Genome Biology and Evolution*, 7(2): 465–480, January 2015. ISSN 1759-6653. doi: 10.1093/gbe/evu292.

[212] Georgios Tzelepis, Mukesh Dubey, Dan Funck Jensen, and MagnusYR 2015 Karlsson. Identifying glycoside hydrolase family 18 genes in the mycoparasitic fungal species Clonostachys rosea. *Microbiology*, 161(7):1407–1419, 2015. ISSN 1465-2080,. doi: 10.1099/mic.0.000096.

[213] Helena Nevalainen, Robyn Peterson, and Natalie Curach. Overview of Gene Expression Using Filamentous Fungi. *Current Protocols in Protein Science*, 92(1):e55, 2018. ISSN 1934-3663. doi: 10.1002/cpps.55.

[214] Janina Kluge, Dominik Terfehr, and Ulrich Kück. Inducible promoters and functional genomic approaches for the genetic engineering of filamentous fungi. *Applied Microbiology and Biotechnology*, 102(15):6357–6372, August 2018. ISSN 1432-0614. doi: 10.1007/s00253-018-9115-1.

[215] Robert-Jan Bleichrodt and Nick D. Read. Flow cytometry and FACS applied to filamentous fungi. *Fungal Biology Reviews*, 33(1):1–15, January 2019. ISSN 1749-4613. doi: 10.1016/j.fbr.2018.06. 001.

[216] H. Mathis, A. Margeot, and M. Bouix. Optimization of flow cytometry parameters for high-throughput screening of spores of the filamentous fungus Trichoderma reesei. *Journal of Biotechnology*, 321:78–86, September 2020. ISSN 0168-1656. doi: 10.1016/j.jbiotec.2020.05.015.

[217] Hyun Soo Kim, Shih-Chi Hsu, Song-I Han, Hem R. Thapa, Adrian R. Guzman, Daniel R. Browne, Mehmet Tatli, Timothy P. Devarenne, David B. Stern, and Arum Han. High-throughput droplet microfluidics screening platform for selecting fast-growing and high lipid-producing microalgae from a mutant library. *Plant Direct*, 1(3):e00011, 2017. ISSN 2475-4455. doi: 10.1002/pld3.11.

[218] Derek Vallejo, Ali Nikoomanzar, Brian M. Paegel, and John C. Chaput. Fluorescence-Activated Droplet Sorting for Single-Cell Directed Evolution. *ACS Synthetic Biology*, 8(6):1430–1440, June 2019. doi: 10.1021/acssynbio.9b00103.

[219] Ming Li, Mark van Zee, Carson T. Riche, Bobby Tofig, Sean D. Gallaher, Sabeeha S. Merchant, Robert Damoiseaux, Keisuke Goda, and Dino Di Carlo. A Gelatin Microdroplet Platform for High-Throughput Sorting of Hyperproducing Single-Cell-Derived Microalgal Clones. *Small*, 14(44): 1803315, 2018. ISSN 1613-6829. doi: 10.1002/smll.201803315.

[220] Staffan L. Sjostrom, Yunpeng Bai, Mingtao Huang, Zihe Liu, Jens Nielsen, Haakan N. Joensson, and Helene Andersson Svahn. High-throughput screening for industrial enzyme production hosts by droplet microfluidics. *Lab on a Chip*, 14(4):806–813, 2014. doi: 10.1039/C3LC51202A.

[221] Emerson Zang, Susanne Brandes, Miguel Tovar, Karin Martin, Franziska Mech, Peter Horbert, Thomas Henkel, Marc Thilo Figge, and Martin Roth. Real-time image processing for label-free enrichment of Actinobacteria cultivated in picolitre droplets. *Lab on a Chip*, 13(18):3707–3713, 2013. doi: 10.1039/C3LC50572C.

[222] Lisa Mahler, Konstantin Wink, R. Julia Beulig, Kirstin Scherlach, Miguel Tovar, Emerson Zang, Karin Martin, Christian Hertweck, Detlev Belder, and Martin Roth. Detection of antibiotics synthetized in microfluidic picolitre-droplets by various actinobacteria. *Scientific Reports*, 8(1):13087, August 2018. ISSN 2045-2322. doi: 10.1038/s41598-018-31263-2.

[223] Ran Tu, Yue Zhang, Erbing Hua, Likuan Bai, Huamei Huang, Kaiyue Yun, and Meng Wang. Droplet-based microfluidic platform for high-throughput screening of Streptomyces. *Communications Biology*, 4(1):1–9, May 2021. ISSN 2399-3642. doi: 10.1038/s42003-021-02186-y.

[224] Ronglin He, Ruihua Ding, John A Heyman, Dongyuan Zhang, and Ran Tu. Ultra-high-throughput picoliter-droplet microfluidics screening of the industrial cellulase-producing filamentous fungus Trichoderma reesei. *Journal of Industrial Microbiology and Biotechnology*, 46(11):1603–1610, November 2019. ISSN 1367-5435. doi: 10.1007/s10295-019-02221-2.

[225] Thomas Beneyton, I. Putu Mahendra Wijaya, Prexilia Postros, Majdi Najah, Pascal Leblond, Angélique Couvent, Estelle Mayot, Andrew D. Griffiths, and Antoine Drevelle. High-throughput screening of filamentous fungi using nanoliter-range droplet-based microfluidics. *Scientific Reports*, 6:27223, June 2016. ISSN 2045-2322. doi: 10.1038/srep27223.

[226] Larry J. Millet, Jayde Aufrecht, Jessy Labbé, Jessie Uehling, Rytas Vilgalys, Myka L. Estes, Cora Miquel Guennoc, Aurélie Deveau, Stefan Olsson, Gregory Bonito, Mitchel J. Doktycz, and Scott T. Retterer. Increasing access to microfluidics for studying fungi and other branched biological structures. *Fungal Biology and Biotechnology*, 6(1):1, June 2019. ISSN 2054-3085. doi: 10.1186/s40694-019-0071-z.

[227] Kenza Samlali, Fatemeh Ahmadi, Angela B. V. Quach, Guy Soffer, and Steve C. C. Shih. One Cell, One Drop, One Click: Hybrid Microfluidics for Mammalian Single Cell Isolation. *Small*, 16(34): 2002400, 2020. ISSN 1613-6829. doi: 10.1002/smll.202002400.

[228] Zerihun A. Demissie, Thomas Witte, Kelly A. Robinson, Amanda Sproule, Simon J. Foote, Anne Johnston, Linda J. Harris, David P. Overy, and Michele C. Loewen. Transcriptomic and Exometabolomic Profiling Reveals Antagonistic and Defensive Modes of Clonostachys rosea Action Against Fusarium graminearum. *Molecular plant-microbe interactions: MPMI*, 33(6):842–858, June 2020. ISSN 0894-0282. doi: 10.1094/MPMI-11-19-0310-R.

[229] Russell H. Cole, Niek de Lange, Zev J. Gartner, and Adam R. Abate. Compact and modular multicolour fluorescence detector for droplet microfluidics. *Lab on a Chip*, 15(13):2754–2758, 2015. ISSN 1473-0197, 1473-0189. doi: 10.1039/C5LC00333D.

[230] Kanako Saito, Yuri Ota, Dieter M. Tourlousse, Satoko Matsukura, Hirotsugu Fujitani, Masamune Morita, Satoshi Tsuneda, and Naohiro Noda. Microdroplet-based system for culturing of environmental microorganisms using FNAP-sort. *Scientific Reports*, 11(1):9506, May 2021. ISSN 2045-2322. doi: 10.1038/s41598-021-88974-2.

[231] A. Isozaki, Y. Nakagawa, M. H. Loo, Y. Shibata, N. Tanaka, D. L. Setyaningrum, J.-W. Park, Y. Shirasaki, H. Mikami, D. Huang, H. Tsoi, C. T. Riche, T. Ota, H. Miwa, Y. Kanda, T. Ito, K. Yamada, O. Iwata, K. Suzuki, S. Ohnuki, Y. Ohya, Y. Kato, T. Hasunuma, S. Matsusaka, M. Yamagishi, M. Yazawa, S. Uemura, K. Nagasawa, H. Watarai, D. Di Carlo, and K. Goda. Sequentially addressable dielectrophoretic array for high-throughput sorting of large-volume biological compartments. *Science Advances*, 6(22):eaba6712, May 2020. ISSN 2375-2548. doi: 10.1126/sciadv.aba6712.

[232] Syama ChattertonS Chatterton and Zamir K. PunjaZ K. Punja. Chitinase and β-1,3-glucanase enzyme production by the mycoparasite Clonostachys rosea f. catenulata against fungal plant pathogens. *Canadian Journal of Microbiology*, April 2009. doi: 10.1139/W08-156.

[233] Bruno C. Aita, Stéfani S. Spannemberg, Silvana Schmaltz, Giovani L. Zabot, Marcus V. Tres, Raquel C. Kuhn, and Marcio A. Mazutti. Production of cell-wall degrading enzymes by solid-state fermentation using agroindustrial residues as substrates. *Journal of Environmental Chemical Engineering*, 7(3):103193, June 2019. ISSN 2213-3437. doi: 10.1016/j.jece.2019.103193.

[234] Stefanie Utech, Radivoje Prodanovic, Angelo S. Mao, Raluca Ostafe, David J. Mooney, and David A. Weitz. Microfluidic Generation of Monodisperse, Structurally Homogeneous Alginate Microgels for

Cell Encapsulation and 3D Cell Culture. *Advanced Healthcare Materials*, 4(11):1628–1633, 2015. ISSN 2192-2659. doi: 10.1002/adhm.201500021.

[235] Marta Napiorkowska, Luzius Pestalozzi, Sven Panke, Martin Held, and Steven Schmitt. High-Throughput Optimization of Recombinant Protein Production in Microfluidic Gel Beads. *Small*, 17(2):2005523, 2021. ISSN 1613-6829. doi: 10.1002/smll.202005523.

[236] Ye-Jin Eun, Andrew S. Utada, Matthew F. Copeland, Shoji Takeuchi, and Douglas B. Weibel. Encapsulating Bacteria in Agarose Microparticles Using Microfluidics for High-Throughput Cell Analysis and Isolation. *ACS Chemical Biology*, 6(3):260–266, March 2011. ISSN 1554-8929. doi: 10.1021/cb100336p.

[237] Yung-Sheng Lin, Chih-Hui Yang, Kang Lu, Keng-Shiang Huang, and Ying-Zhen Zheng. Synthesis of agar microparticles using temperature-controlled microfluidic devices for Cordyceps militaris cultivation. *ELECTROPHORESIS*, 32(22):3157–3163, 2011. ISSN 1522-2683. doi: 10.1002/elps.201100343.

[238] Gabriel Amselem, Cyprien Guermonprez, Benoît Drogue, Sébastien Michelin, and Charles N. Baroud. Universal microfluidic platform for bioassays in anchored droplets. *Lab on a Chip*, 16(21):4200–4211, 2016. doi: 10.1039/C6LC00968A.

[239] Martina Kiel and Karl-Heinrich Engesser. The biodegradation vs. biotransformation of fluorosubstituted aromatics. *Applied Microbiology and Biotechnology*, 99(18):7433–7464, September 2015. ISSN 0175-7598, 1432-0614. doi: 10.1007/s00253-015-6817-5.

[240] Nancy Merino, Meng Wang, Rocio Ambrocio, Kimberly Mak, Ellen O'Connor, An Gao, Elisabeth L. Hawley, Rula A. Deeb, Linda Y. Tseng, and Shaily Mahendra. Fungal biotransformation of 6:2 fluorotelomer alcohol. *Remediation Journal*, 28(2):59–70, March 2018. ISSN 1051-5658, 1520-6831. doi: 10.1002/rem.21550.

[241] Francesc X. Prenafeta-Boldú, Dion M. A. M. Luykx, Jacques Vervoort, and Jan A. M. de Bont. Fungal Metabolism of Toluene: Monitoring of Fluorinated Analogs by [19] F Nuclear Magnetic Resonance Spectroscopy. *Applied and Environmental Microbiology*, 67(3):1030–1034, March 2001. ISSN 0099-2240, 1098-5336. doi: 10.1128/AEM.67.3.1030-1034.2001.

[242] Syama Chatterton and Zamir K. Punja. Interactions Between Clonostachys rosea f. catenulata, Fusarium oxysporum and Cucumber Roots Leading to Biological Control of Fusarium Root and Stem Rot. In Ulrich Gisi, I. Chet, and Maria Lodovica Gullino, editors, *Recent Developments in Management of Plant Diseases*, Plant Pathology in the 21st Century, pages 93–106. Springer Netherlands, Dordrecht, 2009. ISBN 978-1-4020-8804-9. doi: 10.1007/978-1-4020-8804-9_8.

[243] Gloria Innocenti, Roberta Roberti, Matteo Montanari, and Eva Zakrisson. Efficacy of microorganisms antagonistic to Rhizoctonia cerealis and their cell wall degrading enzymatic activities. *Mycological Research*, 107(4):421–427, April 2003. ISSN 0953-7562. doi: 10.1017/S0953756203007640.

[244] Michel Fevre. Intracellular and cell wall associated $(1 \rightarrow 3)$ β glucanases of Saprolegnia. *Mycopathologia*, 67(2):89–94, January 1979. ISSN 1573-0832. doi: 10.1007/BF00440678.

[245] Anna A. Kulminskaya, Karl K. Thomsen, Konstantin A. Shabalin, Irina A. Sidorenko, Elena V. Eneyskaya, Andrew N. Savel'Ev, and Kirill N. Neustroev. Isolation, enzymatic properties, and mode of action of an exo-1,3-β-glucanase from T. viride. *European Journal of Biochemistry*, 268(23): 6123–6131, 2001. ISSN 1432-1033. doi: 10.1046/j.0014-2956.2001.02558.x.

[246] Marjorie A. Tingle and Harlyn O. Halvorson. A comparison of β-glucanase and β-glucosidase in Saccharomyces lactis. *Biochimica et Biophysica Acta (BBA) - Enzymology*, 250(1):165–171, October 1971. ISSN 0005-2744. doi: 10.1016/0005-2744(71)90130-6.

[247] Iain C. Clark, Rohan Thakur, and Adam R. Abate. Concentric electrodes improve microfluidic droplet sorting. *Lab on a Chip*, 18(5):710–713, 2018. doi: 10.1039/C7LC01242J.

[248] Kristiina Nygren, Mukesh Dubey, Antonio Zapparata, Mudassir Iqbal, Georgios D. Tzelepis, Mikael Brandström Durling, Dan Funck Jensen, and Magnus Karlsson. The mycoparasitic fungus Clonostachys rosea responds with both common and specific gene expression during interspecific interactions with fungal prey. *Evolutionary Applications*, 11(6):931–949, July 2018. ISSN 1752-4571. doi: 10.1111/eva.12609.

[249] Kumaran Subramanian, Balamurugan Sadaiappan, Wilson Aruni, Alagappan Kumarappan, Rajasekar

Thirunavukarasu, Guru Prasad Srinivasan, Selvaraj Bharathi, Prasannabalaji Nainangu, Pugazhvendan Sampath Renuga, Anandajothi Elamaran, Deivasigamani Balaraman, and Mahendran Subramanian. Bioconversion of chitin and concomitant production of chitinase and N-acetylglucosamine by novel Achromobacter xylosoxidans isolated from shrimp waste disposal area. *Scientific Reports*, 10 (1):11898, December 2020. ISSN 2045-2322. doi: 10.1038/s41598-020-68772-y.

[250] M. T. Guo, A. Rotem, J. A. Heyman, and D. A. Weitz. Droplet microfluidics for high-throughput biological assays. *Lab Chip*, 12(12):2146–55, June 2012. ISSN 1473-0189 (Electronic) 1473-0189 (Linking). doi: 10.1039/c2lc21147e.

[251] T. Schneider, J. Kreutz, and D. T. Chiu. The potential impact of droplet microfluidics in biology. *Anal Chem*, 85(7):3476–82, April 2013. ISSN 1520-6882 (Electronic) 0003-2700 (Linking). doi: 10.1021/ac400257c.

[252] H. N. Joensson and H. A. Svahn. Droplet Microfluidics-A Tool for Single-Cell Analysis. *Angewandte Chemie-International Edition*, 51(49):12176–12192, 2012. ISSN 1433-7851. doi: 10.1002/anie. 201200460.

[253] Linas Mazutis, John Gilbert, W. Lloyd Ung, David A. Weitz, Andrew D. Griffiths, and John A. Heyman. Single-cell analysis and sorting using droplet-based microfluidics. *Nature Protocols*, 8(5): 870–891, May 2013. ISSN 1750-2799. doi: 10.1038/nprot.2013.046.

[254] K. Ahn, C. Kerbage, T. P. Hunt, R. M. Westervelt, D. R. Link, and D. A. Weitz. Dielectrophoretic manipulation of drops for high-speed microfluidic sorting devices. *Applied Physics Letters*, 88(2), January 2006. ISSN 0003-6951. doi: Artn02410410.1063/1.2164911.

[255] K. Zhang, Q. L. Liang, S. Ma, X. A. Mu, P. Hu, Y. M. Wang, and G. A. Luo. On-chip manipulation of continuous picoliter-volume superparamagnetic droplets using a magnetic force. *Lab Chip*, 9(20): 2992–2999, 2009. ISSN 1473-0197. doi: 10.1039/b906229g.

[256] V. Miralles, A. Huerre, H. Williams, B. Fournie, and M. C. Jullien. A versatile technology for droplet-based microfluidics: Thermomechanical actuation. *Lab Chip*, 15(9):2133–2139, 2015. ISSN 1473-0197. doi: 10.1039/c5lc00110b.

[257] T. Franke, A. R. Abate, D. A. Weitz, and A. Wixforth. Surface acoustic wave (SAW) directed droplet flow in microfluidics for PDMS devices. *Lab Chip*, 9(18):2625–2627, 2009. ISSN 1473-0197. doi: 10.1039/b906819h.

[258] Orlin D. Velev, Brian G. Prevo, and Ketan H. Bhatt. On-chip manipulation of free droplets. *Nature*, 426(6966):515–516, December 2003. ISSN 1476-4687. doi: 10.1038/426515a.

[259] Chuyi Chen, Steven Peiran Zhang, Zhangming Mao, Nitesh Nama, Yuyang Gu, Po-Hsun Huang, Yun Jing, Xiasheng Guo, Francesco Costanzo, and Tony Jun Huang. Three-dimensional numerical simulation and experimental investigation of boundary-driven streaming in surface acoustic wave microfluidics. *Lab on a Chip*, 18(23):3645–3654, November 2018. ISSN 1473-0189. doi: 10.1039/C8LC00589C.

[260] Steven Peiran Zhang, James Lata, Chuyi Chen, John Mai, Feng Guo, Zhenhua Tian, Liqiang Ren, Zhangming Mao, Po-Hsun Huang, Peng Li, Shujie Yang, and Tony Jun Huang. Digital acoustofluidics enables contactless and programmable liquid handling. *Nature Communications*, 9(1):2928, July 2018. ISSN 2041-1723. doi: 10.1038/s41467-018-05297-z.

[261] N. Vergauwe, D. Witters, F. Ceyssens, S. Vermeir, B. Verbruggen, R. Puers, and J. Lammertyn. A versatile electrowetting-based digital microfluidic platform for quantitative homogeneous and heterogeneous bio-assays. *Journal of Micromechanics and Microengineering*, 21(5), May 2011. ISSN 0960-1317. doi: Artn05402610.1088/0960-1317/21/5/054026.

[262] Mathieu C. Husser, Philippe Q. N. Vo, Hugo Sinha, Fatemeh Ahmadi, and Steve C. C. Shih. An Automated Induction Microfluidics System for Synthetic Biology. *ACS Synthetic Biology*, 7(3):933–944, March 2018. doi: 10.1021/acssynbio.8b00025.

[263] D. G. Rackus, M. D. Dryden, J. Lamanna, A. Zaragoza, B. Lam, S. O. Kelley, and A. R. Wheeler. A digital microfluidic device with integrated nanostructured microelectrodes for electrochemical immunoassays. *Lab Chip*, 15(18):3776–84, 2015. ISSN 1473-0189 (Electronic) 1473-0189 (Linking). doi: 10.1039/c5lc00660k.

[264] A. H. C. Ng, R. Fobel, C. Fobel, J. Lamanna, D. G. Rackus, A. Summers, C. Dixon, M. D. M. Dryden, C. Lam, M. Ho, N. S. Mufti, V. Lee, M. A. M. Asri, E. A. Sykes, M. D. Chamberlain, R. Joseph,

M. Ope, H. M. Scobie, A. Knipes, P. A. Rota, N. Marano, P. M. Chege, M. Njuguna, R. Nzunza, N. Kisangau, J. Kiogora, M. Karuingi, J. W. Burton, P. Borus, E. Lam, and A. R. Wheeler. A digital microfluidic system for serological immunoassays in remote settings. *Science Translational Medicine*, 10(438), April 2018. ISSN 1946-6234. doi: ARTNeaar607610.1126/scitranslmed.aar6076.

[265] M. Abdelgawad, S. L. Freire, H. Yang, and A. R. Wheeler. All-terrain droplet actuation. *Lab Chip*, 8 (5):672–7, May 2008. ISSN 1473-0197 (Print) 1473-0189 (Linking). doi: 10.1039/b801516c.

[266] C. G. Cooney, C.-Y. Chen, M. R. Emerling, A. Nadim, and J. D. Sterling. Electrowetting droplet microfluidics on a single planar surface. *Microfluidics and Nanofluidics*, 2(5):435–446, March 2006. ISSN 1613-4990. doi: 10.1007/s10404-006-0085-8.

[267] D. Huh, A. H. Tkaczyk, J. H. Bahng, Y. Chang, H. H. Wei, J. B. Grotberg, C. J. Kim, K. Kurabayashi, and S. Takayama. Reversible switching of high-speed air-liquid two-phase flows using electrowetting-assisted flow-pattern change. *Journal of the American Chemical Society*, 125(48):14678–14679, December 2003. ISSN 0002-7863. doi: 10.1021/ja037350g.

[268] M. G. Simon, R. Lin, J. S. Fisher, and A. P. Lee. A Laplace pressure based microfluidic trap for passive droplet trapping and controlled release. *Biomicrofluidics*, 6(1):14110–1411013, March 2012. ISSN 1932-1058 (Electronic) 1932-1058 (Linking). doi: 10.1063/1.3687400.

[269] B. O'Donovan, D. J. Eastburn, and A. R. Abate. Electrode-free picoinjection of microfluidic drops. *Lab Chip*, 12(20):4029–32, October 2012. ISSN 1473-0189 (Electronic) 1473-0189 (Linking). doi: 10.1039/c2lc40693d.

[270] H. Song and R. F. Ismagilov. Millisecond kinetics on a microfluidic chip using nanoliters of reagents. *Journal of the American Chemical Society*, 125(47):14613–9, November 2003. ISSN 0002-7863 (Print) 0002-7863 (Linking). doi: 10.1021/ja0354566.

[271] L. Frenz, K. Blank, E. Brouzes, and A. D. Griffiths. Reliable microfluidic on-chip incubation of droplets in delay-lines. *Lab Chip*, 9(10):1344–8, May 2009. ISSN 1473-0197 (Print) 1473-0189 (Linking). doi: 10.1039/b816049j.

[272] Jenifer Clausell-Tormos, Diana Lieber, Jean-Christophe Baret, Abdeslam El-Harrak, Oliver J. Miller, Lucas Frenz, Joshua Blouwolff, Katherine J. Humphry, Sarah Köster, Honey Duan, Christian Holtze,

David A. Weitz, Andrew D. Griffiths, and Christoph A. Merten. Droplet-Based Microfluidic Platforms for the Encapsulation and Screening of Mammalian Cells and Multicellular Organisms. *Chemistry & Biology*, 15(5):427–437, May 2008. ISSN 1074-5521. doi: 10.1016/j.chembiol.2008.04.004.

[273] S. Koster, F. E. Angile, H. Duan, J. J. Agresti, A. Wintner, C. Schmitz, A. C. Rowat, C. A. Merten, D. Pisignano, A. D. Griffiths, and D. A. Weitz. Drop-based microfluidic devices for encapsulation of single cells. *Lab Chip*, 8(7):1110–5, July 2008. ISSN 1473-0197 (Print) 1473-0189 (Linking). doi: 10.1039/b802941e.

[274] M. Chabert, K. D. Dorfman, and J. L. Viovy. Droplet fusion by alternating current (AC) field electrocoalescence in microchannels. *Electrophoresis*, 26(19):3706–15, October 2005. ISSN 0173-0835 (Print) 0173-0835 (Linking). doi: 10.1002/elps.200500109.

[275] Keunho Ahn, Jeremy Agresti, Henry Chong, Manuel Marquez, and D. A. Weitz. Electrocoalescence of drops synchronized by size-dependent flow in microfluidic channels. *Applied Physics Letters*, 88 (26):264105, June 2006. ISSN 0003-6951. doi: 10.1063/1.2218058.

[276] Adam R. Abate, Tony Hung, Pascaline Mary, Jeremy J. Agresti, and David A. Weitz. High-throughput injection with microfluidics using picoinjectors. *Proceedings of the National Academy of Sciences*, 107(45):19163–19166, November 2010. ISSN 0027-8424, 1091-6490. doi: 10.1073/pnas.1006888107.

[277] A. Banerjee, E. Kreit, Y. G. Liu, J. Heikenfeld, and I. Papautsky. Reconfigurable virtual electrowetting channels. *Lab Chip*, 12(4):758–764, 2012. ISSN 1473-0197. doi: 10.1039/c2lc20842c.

[278] P. Y. Paik, V. K. Pamula, and K. Chakrabarty. Adaptive cooling of integrated circuits using digital microfluidics. *Ieee Transactions on Very Large Scale Integration (Vlsi) Systems*, 16(4):432–443, April 2008. ISSN 1063-8210. doi: 10.1109/Tvlsi.2007.915434.

[279] Ren Yang, Steven A. Soper, and Wanjun Wang. A new UV lithography photoresist based on composite of EPON resins 165 and 154 for fabrication of high-aspect-ratio microstructures. *Sensors and Actuators A: Physical*, 135(2):625–636, 2007/04/15/. ISSN 0924-4247. doi: 10.1016/j.sna.2006.09.009.

[280] Yufei Ren, Shun-Ho Huang, Sébastien Mosser, O. Marc Heuschkel, Arnaud Bertsch, C. Patrick Fraering, J. Jia-Jin Chen, and Philippe Renaud. A Simple and Reliable PDMS and SU-8 Irreversible

Bonding Method and Its Application on a Microfluidic-MEA Device for Neuroscience Research. *Micromachines*, 6(12), 2015. ISSN 2072-666X. doi: 10.3390/mi6121465.

[281] N. Yanagisawa and T. Higashiyama. Quantitative assessment of chemotropism in pollen tubes using microslit channel filters. *Biomicrofluidics*, 12(2), March 2018. ISSN 1932-1058. doi: Artn02411310. 1063/1.5023718.

[282] Swastika S. Bithi and Siva A. Vanapalli. Behavior of a train of droplets in a fluidic network with hydrodynamic traps. *Biomicrofluidics*, 4(4):044110, 12/06 08/24/received 10/28/accepted 2010. ISSN 1932-1058. doi: 10.1063/1.3523053.

[283] S. X. Li, X. Y. Ding, F. Guo, Y. C. Chen, M. I. Lapsley, S. C. S. Lin, L. Wang, J. P. McCoy, C. E. Cameron, and T. J. Huang. An On-Chip, Multichannel Droplet Sorter Using Standing Surface Acoustic Waves. *Anal Chem*, 85(11):5468–5474, June 2013. ISSN 0003-2700. doi: 10.1021/ac400548d.

[284] D. H. Yoon, J. Ito, T. Sekiguchi, and S. Shoji. Active and Precise Control of Microdroplet Division Using Horizontal Pneumatic Valves in Bifurcating Microchannel. *Micromachines*, 4(2):197–205, June 2013. ISSN 2072-666x. doi: 10.3390/mi4020197.

[285] E. Fradet, C. McDougall, P. Abbyad, R. Dangla, D. McGloin, and C. N. Baroud. Combining rails and anchors with laser forcing for selective manipulation within 2D droplet arrays. *Lab Chip*, 11(24): 4228–4234, 2011. ISSN 1473-0197. doi: 10.1039/c1lc20541b.

[286] Y. G. Liu, A. Banerjee, and I. Papautsky. Precise droplet volume measurement and electrode-based volume metering in digital microfluidics. *Microfluidics and Nanofluidics*, 17(2):295–303, August 2014. ISSN 1613-4982. doi: 10.1007/s10404-013-1318-2.

[287] Shelley L. Anna, Nathalie Bontoux, and Howard A. Stone. Formation of dispersions using "flow focusing" in microchannels. *Applied Physics Letters*, 82(3):364–366, January 2003. ISSN 0003-6951. doi: 10.1063/1.1537519.

[288] T. Ward, M. Faivre, M. Abkarian, and H. A. Stone. Microfluidic flow focusing: Drop size and scaling in pressure versus flow-rate-driven pumping. *Electrophoresis*, 26(19):3716–24, October 2005. ISSN 0173-0835 (Print) 0173-0835 (Linking). doi: 10.1002/elps.200500173.

[289] P. Paik, V. K. Pamula, and R. B. Fair. Rapid droplet mixers for digital microfluidic systems. *Lab Chip*, 3(4):253–259, 2003. ISSN 1473-0189. doi: 10.1039/b307628h.

[290] Chun-Zhao Liu, Feng Wang, Amanda R. Stiles, and Chen Guo. Ionic liquids for biofuel production: Opportunities and challenges. *Applied Energy*, 92:406–414, 2012/04/01/. ISSN 0306-2619. doi: 10.1016/j.apenergy.2011.11.031.

[291] H. W. Blanch, B. A. Simmons, and D. Klein-Marcuschamer. Biomass deconstruction to sugars. *Biotechnol J*, 6(9):1086–102, September 2011. ISSN 1860-7314 (Electronic) 1860-6768 (Linking). doi: 10.1002/biot.201000180.

[292] J. Sun, D. Liu, R. P. Young, A. G. Cruz, N. G. Isern, T. Schuerg, J. R. Cort, B. A. Simmons, and S. Singh. Solubilization and Upgrading of High Polyethylene Terephthalate Loadings in a Low-Costing Bifunctional Ionic Liquid. *ChemSusChem*, 11(4):781–792, February 2018. ISSN 1864-564X (Electronic) 1864-5631 (Linking). doi: 10.1002/cssc.201701798.

[293] Mario Ouellet, Supratim Datta, Dean C. Dibble, Pramila R. Tamrakar, Peter I. Benke, Chenlin Li, Seema Singh, Kenneth L. Sale, Paul D. Adams, Jay D. Keasling, Blake A. Simmons, Bradley M. Holmes, and Aindrila Mukhopadhyay. Impact of ionic liquid pretreated plant biomass on Saccharomyces cerevisiae growth and biofuel production. *Green Chemistry*, 13(10):2743–2749, 2011. ISSN 1463-9262. doi: 10.1039/C1GC15327G.

[294] J. I. Park, E. J. Steen, H. Burd, S. S. Evans, A. M. Redding-Johnson, T. Batth, P. I. Benke, P. D'Haeseleer, N. Sun, K. L. Sale, J. D. Keasling, T. S. Lee, C. J. Petzold, A. Mukhopadhyay, S. W. Singer, B. A. Simmons, and J. M. Gladden. A thermophilic ionic liquid-tolerant cellulase cocktail for the production of cellulosic biofuels. *PLoS One*, 7(5):e37010, 2012. ISSN 1932-6203 (Electronic) 1932-6203 (Linking). doi: 10.1371/journal.pone.0037010.

[295] Y. V. Nancharaiah and A. J. Francis. Alkyl-methylimidazolium ionic liquids affect the growth and fermentative metabolism of Clostridium sp. *Bioresour Technol*, 102(11):6573–8, June 2011. ISSN 1873-2976 (Electronic) 0960-8524 (Linking). doi: 10.1016/j.biortech.2011.03.042.

[296] T. L. Ruegg, E. M. Kim, B. A. Simmons, J. D. Keasling, S. W. Singer, T. S. Lee, and M. P. Thelen. An auto-inducible mechanism for ionic liquid resistance in microbial biofuel production. *Nature*

Communications, 5:3490, March 2014. ISSN 2041-1723 (Electronic) 2041-1723 (Linking). doi: 10.1038/ncomms4490.

[297] Marijke Frederix, Florence Mingardon, Matthew Hu, Ning Sun, Todd Pray, Seema Singh, Blake A. Simmons, Jay D. Keasling, and Aindrila Mukhopadhyay. Development of an E. coli strain for one-pot biofuel production from ionic liquid pretreated cellulose and switchgrass. *Green Chemistry*, 18(15): 4189–4197, 2016. ISSN 1463-9262. doi: 10.1039/C6GC00642F.

[298] H. S. Moon, K. Je, J. W. Min, D. Park, K. Y. Han, S. H. Shin, W. Y. Park, C. E. Yoo, and S. H. Kim. Inertial-ordering-assisted droplet microfluidics for high-throughput single-cell RNA-sequencing. *Lab Chip*, 18(5):775–784, February 2018. ISSN 1473-0189 (Electronic) 1473-0189 (Linking). doi: 10. 1039/c7lc01284e.

[299] R. Blue and D. Uttamchandani. Recent advances in optical fiber devices for microfluidics integration. *J Biophotonics*, 9(1-2):13–25, January 2016. ISSN 1864-0648 (Electronic) 1864-063X (Linking).

[300] Philippe Q. N. Vo, Mathieu C. Husser, Fatemeh Ahmadi, Hugo Sinha, and Steve C. C. Shih. Image-based feedback and analysis system for digital microfluidics. *Lab on a Chip*, 17(20):3437–3446, September 2017. ISSN 1473-0189. doi: 10.1039/C7LC00826K.

[301] Su Bin Moon, Do Yon Kim, Jeong-Heon Ko, Jin-Soo Kim, and Yong-Sam Kim. Improving CRISPR Genome Editing by Engineering Guide RNAs. *Trends in Biotechnology*, 37(8):870–881, August 2019. ISSN 0167-7799. doi: 10.1016/j.tibtech.2019.01.009.

[302] Christopher A. Vakulskas, Daniel P. Dever, Garrett R. Rettig, Rolf Turk, Ashley M. Jacobi, Michael A. Collingwood, Nicole M. Bode, Matthew S. McNeill, Shuqi Yan, Joab Camarena, Ciaran M. Lee, So Hyun Park, Volker Wiebking, Rasmus O. Bak, Natalia Gomez-Ospina, Mara Pavel-Dinu, Wenchao Sun, Gang Bao, Matthew H. Porteus, and Mark A. Behlke. A high-fidelity Cas9 mutant delivered as a ribonucleoprotein complex enables efficient gene editing in human hematopoietic stem and progenitor cells. *Nature Medicine*, 24(8):1216–1224, August 2018. ISSN 1546-170X. doi: 10.1038/s41591-018-0137-0.

[303] Takeshi Maruyama, Stephanie K. Dougan, Matthias C. Truttmann, Angelina M. Bilate, Jessica R.

Ingram, and Hidde L. Ploegh. Increasing the efficiency of precise genome editing with CRISPR-Cas9 by inhibition of nonhomologous end joining. *Nature Biotechnology*, 33(5):538–542, May 2015. ISSN 1546-1696. doi: 10.1038/nbt.3190.

[304] Xiaoyun Dai, Jonathan J. Park, Yaying Du, Hyunu R. Kim, Guangchuan Wang, Youssef Errami, and Sidi Chen. One-step generation of modular CAR-T cells with AAV–Cpf1. *Nature Methods*, 16(3): 247–254, March 2019. ISSN 1548-7105. doi: 10.1038/s41592-019-0329-7.

[305] Francisco J. Sánchez-Rivera and Tyler Jacks. Applications of the CRISPR–Cas9 system in cancer biology. *Nature Reviews Cancer*, 15(7):387–393, July 2015. ISSN 1474-1768. doi: 10.1038/nrc3950.

[306] Tianzuo Zhan, Niklas Rindtorff, Johannes Betge, Matthias P. Ebert, and Michael Boutros. CRISPR/Cas9 for cancer research and therapy. *Seminars in Cancer Biology*, 55:106–119, April 2019. ISSN 1044-579X. doi: 10.1016/j.semcancer.2018.04.001.

[307] Alexis C. Komor, Ahmed H. Badran, and David R. Liu. CRISPR-Based Technologies for the Manipulation of Eukaryotic Genomes. *Cell*, 168(1):20–36, January 2017. ISSN 0092-8674. doi: 10.1016/j.cell.2016.10.044.

[308] Van Trung Chu, Timm Weber, Benedikt Wefers, Wolfgang Wurst, Sandrine Sander, Klaus Rajewsky, and Ralf Kühn. Increasing the efficiency of homology-directed repair for CRISPR-Cas9-induced precise gene editing in mammalian cells. *Nature Biotechnology*, 33(5):543–548, May 2015. ISSN 1546-1696. doi: 10.1038/nbt.3198.

[309] Anob M. Chakrabarti, Tristan Henser-Brownhill, Josep Monserrat, Anna R. Poetsch, Nicholas M. Luscombe, and Paola Scaffidi. Target-Specific Precision of CRISPR-Mediated Genome Editing. *Molecular Cell*, 73(4):699–713.e6, February 2019. ISSN 1097-2765. doi: 10.1016/j.molcel.2018.11. 031.

[310] F. Ann Ran, Patrick D. Hsu, Jason Wright, Vineeta Agarwala, David A. Scott, and Feng Zhang. Genome engineering using the CRISPR-Cas9 system. *Nature Protocols*, 8(11):2281–2308, November 2013. ISSN 1750-2799. doi: 10.1038/nprot.2013.143.

[311] Andreas I. Andreou and Naomi Nakayama. Mobius Assembly: A versatile Golden-Gate framework

towards universal DNA assembly. *PLOS ONE*, 13(1):e0189892, January 2018. ISSN 1932-6203. doi: 10.1371/journal.pone.0189892.

[312] Simon J. Moore, Hung-En Lai, Richard J. R. Kelwick, Soo Mei Chee, David J. Bell, Karen Marie Polizzi, and Paul S. Freemont. EcoFlex: A Multifunctional MoClo Kit for E. coli Synthetic Biology. *ACS Synthetic Biology*, 5(10):1059–1069, October 2016. doi: 10.1021/acssynbio.6b00031.

[313] Martin P. Stewart, Armon Sharei, Xiaoyun Ding, Gaurav Sahay, Robert Langer, and Klavs F. Jensen. In vitro and ex vivo strategies for intracellular delivery. *Nature*, 538(7624):183–192, October 2016. ISSN 1476-4687. doi: 10.1038/nature19764.

[314] Hao Yin, Kevin J. Kauffman, and Daniel G. Anderson. Delivery technologies for genome editing. *Nature Reviews Drug Discovery*, 16(6):387–399, June 2017. ISSN 1474-1784. doi: 10.1038/nrd.2016.280.

[315] Xiquan Liang, Jason Potter, Shantanu Kumar, Yanfei Zou, Rene Quintanilla, Mahalakshmi Sridharan, Jason Carte, Wen Chen, Natasha Roark, Sridhar Ranganathan, Namritha Ravinder, and Jonathan D. Chesnut. Rapid and highly efficient mammalian cell engineering via Cas9 protein transfection. *Journal of Biotechnology*, 208:44–53, August 2015. ISSN 0168-1656. doi: 10.1016/j.jbiotec.2015.04.024.

[316] Joseph J. Priola, Nathan Calzadilla, Martina Baumann, Nicole Borth, Christopher G. Tate, and Michael J. Betenbaugh. High-throughput screening and selection of mammalian cells for enhanced protein production. *Biotechnology Journal*, 11(7):853–865, 2016. ISSN 1860-7314. doi: 10.1002/biot.201500579.

[317] Darrin Kuystermans and Mohamed Al-Rubeai. Mammalian Cell Line Selection Strategies for High-Producers. In Mohamed Al-Rubeai, editor, *Animal Cell Culture*, Cell Engineering, pages 327–372. Springer International Publishing, Cham, 2015. ISBN 978-3-319-10320-4. doi: 10.1007/978-3-319-10320-4_11.

[318] Kristina Lindgren, Andréa Salmén, Mats Lundgren, Lovisa Bylund, Åsa Ebler, Eric Fäldt, Lina Sörvik, Christel Fenge, and Ulrica Skoging-Nyberg. Automation of cell line development. *Cytotechnology*, 59(1):1–10, January 2009. ISSN 0920-9069. doi: 10.1007/s10616-009-9187-y.

[319] Krista Evans, Thomas Albanetti, Raghavan Venkat, Ronald Schoner, James Savery, Guillermo Miro-Quesada, Bhargavi Rajan, and Christopher Groves. Assurance of monoclonality in one round of cloning through cell sorting for single cell deposition coupled with high resolution cell imaging. *Biotechnology Progress*, 31(5):1172–1178, 2015. ISSN 1520-6033. doi: 10.1002/btpr.2145.

[320] David Bardin, Michael R. Kendall, Paul A. Dayton, and Abraham P. Lee. Parallel generation of uniform fine droplets at hundreds of kilohertz in a flow-focusing module. *Biomicrofluidics*, 7(3): 034112, May 2013. doi: 10.1063/1.4811276.

[321] Jing Li, Bu Wang, Brian M. Juba, Michael Vazquez, Steve W. Kortum, Betsy S. Pierce, Michael Pacheco, Lee Roberts, Joseph W. Strohbach, Lyn H. Jones, Erik Hett, Atli Thorarensen, Jean-Baptiste Telliez, Armon Sharei, Mark Bunnage, and Jonathan Brian Gilbert. Microfluidic-Enabled Intracellular Delivery of Membrane Impermeable Inhibitors to Study Target Engagement in Human Primary Cells. *ACS Chemical Biology*, 12(12):2970–2974, December 2017. ISSN 1554-8929. doi: 10.1021/acschembio.7b00683.

[322] Armon Sharei, Nahyun Cho, Shirley Mao, Emily Jackson, Roberta Poceviciute, Andrea Adamo, Janet Zoldan, Robert Langer, and Klavs F Jensen. Cell Squeezing as a Robust, Microfluidic Intracellular Delivery Platform. *Journal of Visualized Experiments : JoVE*, (81), November 2013. ISSN 1940-087X. doi: 10.3791/50980.

[323] Armon Sharei, Radiana Trifonova, Siddharth Jhunjhunwala, George C. Hartoularos, Alexandra T. Eyerman, Abigail Lytton-Jean, Mathieu Angin, Siddhartha Sharma, Roberta Poceviciute, Shirley Mao, Megan Heimann, Sophia Liu, Tanya Talkar, Omar F. Khan, Marylyn Addo, Ulrich H. von Andrian, Daniel G. Anderson, Robert Langer, Judy Lieberman, and Klavs F. Jensen. Ex Vivo Cytosolic Delivery of Functional Macromolecules to Immune Cells. *PLOS ONE*, 10(4):e0118803, April 2015. ISSN 1932-6203. doi: 10.1371/journal.pone.0118803.

[324] Gregory Lee Szeto, Debra Van Egeren, Hermoon Worku, Armon Sharei, Brian Alejandro, Clara Park, Kirubel Frew, Mavis Brefo, Shirley Mao, Megan Heimann, Robert Langer, Klavs Jensen, and Darrell J. Irvine. Microfluidic squeezing for intracellular antigen loading in polyclonal B-cells as cellular vaccines. *Scientific Reports*, 5:10276, May 2015. ISSN 2045-2322. doi: 10.1038/srep10276.

[325] Xiaoyun Ding, Martin P. Stewart, Armon Sharei, James C. Weaver, Robert S. Langer, and Klavs F. Jensen. High-throughput nuclear delivery and rapid expression of DNA via mechanical and electrical cell-membrane disruption. *Nature Biomedical Engineering*, 1(3):0039, March 2017. ISSN 2157-846X. doi: 10.1038/s41551-017-0039.

[326] Pranav Agrawal, Nilesh P. Ingle, William S. Boyle, Emily Ward, Jakub Tolar, Kevin D. Dorfman, and Theresa M. Reineke. Fast, Efficient, and Gentle Transfection of Human Adherent Cells in Suspension. *ACS Applied Materials & Interfaces*, 8(14):8870–8874, April 2016. ISSN 1944-8244. doi: 10.1021/acsami.6b01702.

[327] Fangyuan Chen, Yihong Zhan, Tao Geng, Hongzhen Lian, Peisheng Xu, and Chang Lu. Chemical Transfection of Cells in Picoliter Aqueous Droplets in Fluorocarbon Oil. *Analytical Chemistry*, 83 (22):8816–8820, November 2011. ISSN 0003-2700. doi: 10.1021/ac2022794.

[328] Annamaria Mocciaro, Theodore L. Roth, Hayley M. Bennett, Magali Soumillon, Abhik Shah, Joseph Hiatt, Kevin Chapman, Alexander Marson, and Gregory Lavieu. Light-activated cell identification and sorting (LACIS) for selection of edited clones on a nanofluidic device. *Communications Biology*, 1(1):1–8, May 2018. ISSN 2399-3642. doi: 10.1038/s42003-018-0034-6.

[329] Freeman Lan, Benjamin Demaree, Noorsher Ahmed, and Adam R. Abate. Single-cell genome sequencing at ultra-high-throughput with microfluidic droplet barcoding. *Nature Biotechnology*, 35(7): 640–646, July 2017. ISSN 1546-1696. doi: 10.1038/nbt.3880.

[330] Payam Shahi, Samuel C. Kim, John R. Haliburton, Zev J. Gartner, and Adam R. Abate. Abseq: Ultrahigh-throughput single cell protein profiling with droplet microfluidic barcoding. *Scientific Reports*, 7:44447, March 2017. ISSN 2045-2322. doi: 10.1038/srep44447.

[331] Ehsan Moazami, James M. Perry, Guy Soffer, Mathieu C. Husser, and Steve C. C. Shih. Integration of World-to-Chip Interfaces with Digital Microfluidics for Bacterial Transformation and Enzymatic Assays. *Analytical Chemistry*, 91(8):5159–5168, April 2019. ISSN 0003-2700. doi: 10.1021/acs.analchem.8b05754.

[332] Laura M. Y. Leclerc, Guy Soffer, David H. Kwan, and Steve C. C. Shih. A fucosyltransferase inhibition assay using image-analysis and digital microfluidics. *Biomicrofluidics*, 13(3):034106, May 2019. ISSN 1932-1058. doi: 10.1063/1.5088517.

[333] Hesam Babahosseini, Tom Misteli, and Don L. DeVoe. Microfluidic on-demand droplet generation, storage, retrieval, and merging for single-cell pairing. *Lab on a Chip*, 19(3):493–502, January 2019. ISSN 1473-0189. doi: 10.1039/C8LC01178H.

[334] Sanghyun Lee, Hojin Kim, Dong-Joon Won, Jaehyung Lee, and Joonwon Kim. On-demand, parallel droplet merging method with non-contact droplet pairing in droplet-based microfluidics. *Microfluidics and Nanofluidics*, 20(1):1, January 2016. ISSN 1613-4990. doi: 10.1007/s10404-015-1676-z.

[335] W. W. Cui, M. L. Zhang, X. X. Duan, W. Pang, D. H. Zhang, and H. Zhang. Dynamics of Electrowetting Droplet Motion in Digital Microfluidics Systems: From Dynamic Saturation to Device Physics. *Micromachines*, 6(6):778–789, June 2015. ISSN 2072-666x. doi: 10.3390/mi6060778.

[336] R. W. R. L. Gajasinghe, S. U. Senveli, S. Rawal, A. Williams, A. Zheng, R. H. Datar, R. J. Cote, and O. Tigli. Experimental study of PDMS bonding to various substrates for monolithic microfluidic applications. *Journal of Micromechanics and Microengineering*, 24(7):075010, June 2014. ISSN 0960-1317. doi: 10.1088/0960-1317/24/7/075010.

[337] Seok Woo Lee and Seung S. Lee. Shrinkage ratio of PDMS and its alignment method for the wafer level process. *Microsystem Technologies*, 14(2):205–208, February 2008. ISSN 1432-1858. doi: 10.1007/s00542-007-0417-y.

[338] Sungho Jang, Byungjin Lee, Heon-Ho Jeong, Si Hyung Jin, Sungyeon Jang, Seong Gyeong Kim, Gyoo Yeol Jung, and Chang-Soo Lee. On-chip analysis, indexing and screening for chemical producing bacteria in a microfluidic static droplet array. *Lab on a Chip*, 16(10):1909–1916, 2016. doi: 10.1039/C6LC00118A.

[339] Kaston Leung, Hans Zahn, Timothy Leaver, Kishori M. Konwar, Niels W. Hanson, Antoine P. Pagé,

Chien-Chi Lo, Patrick S. Chain, Steven J. Hallam, and Carl L. Hansen. A programmable droplet-based microfluidic device applied to multiparameter analysis of single microbes and microbial communities. *Proceedings of the National Academy of Sciences*, 109(20):7665–7670, May 2012. ISSN 0027-8424, 1091-6490. doi: 10.1073/pnas.1106752109.

[340] Adrian M. Nightingale, Thomas W. Phillips, James H. Bannock, and John C. de Mello. Controlled multistep synthesis in a three-phase droplet reactor. *Nature Communications*, 5(1):1–8, May 2014. ISSN 2041-1723. doi: 10.1038/ncomms4777.

[341] Mohammad Ali Khorshidi, Prem Kumar Periyannan Rajeswari, Carolina Wählby, Haakan N. Joensson, and Helene Andersson Svahn. Automated analysis of dynamic behavior of single cells in picoliter droplets. *Lab on a Chip*, 14(5):931–937, February 2014. ISSN 1473-0189. doi: 10.1039/C3LC51136G.

[342] Alim Dewan, Jihye Kim, Rebecca H. McLean, Siva A. Vanapalli, and Muhammad Nazmul Karim. Growth kinetics of microalgae in microfluidic static droplet arrays. *Biotechnology and Bioengineering*, 109(12):2987–2996, 2012. ISSN 1097-0290. doi: 10.1002/bit.24568.

[343] Sam H. Au, Ryan Fobel, Salil P. Desai, Joel Voldman, and Aaron R. Wheeler. Cellular bias on the microscale: Probing the effects of digital microfluidic actuation on mammalian cell health, fitness and phenotype. *Integrative Biology*, 5(8):1014–1025, August 2013. doi: 10.1039/c3ib40104a.

[344] Aleksandra Spiegel, Mandy Bachmann, Gabriel Jurado Jiménez, and Mihail Sarov. CRISPR/Cas9-based knockout pipeline for reverse genetics in mammalian cell culture. *Methods*, 164–165:49–58, July 2019. ISSN 1046-2023. doi: 10.1016/j.ymeth.2019.04.016.

[345] Ambrin Fatima, Jens Schuster, Talia Akram, Maria Sobol, Jan Hoeber, and Niklas Dahl. Generation of a human Neurochondrin deficient iPSC line KICRi002-A-3 using CRISPR/Cas9. *Stem Cell Research*, 44:101758, April 2020. ISSN 1873-5061. doi: 10.1016/j.scr.2020.101758.

[346] Qiang Zhang, Tingting Wang, Qian Zhou, Peng Zhang, Yanhai Gong, Honglei Gou, Jian Xu, and Bo Ma. Development of a facile droplet-based single-cell isolation platform for cultivation and genomic analysis in microorganisms. *Scientific Reports*, 7:41192, January 2017. ISSN 2045-2322. doi: 10.1038/srep41192.

[347] Russell H. Cole, Shi-Yang Tang, Christian A. Siltanen, Payam Shahi, Jesse Q. Zhang, Sean Poust, Zev J. Gartner, and Adam R. Abate. Printed droplet microfluidics for on demand dispensing of picoliter droplets and cells. *Proceedings of the National Academy of Sciences*, 114(33):8728–8733, August 2017. ISSN 0027-8424, 1091-6490. doi: 10.1073/pnas.1704020114.

[348] J. Schoendube, D. Wright, R. Zengerle, and P. Koltay. Single-cell printing based on impedance detection. *Biomicrofluidics*, 9(1):014117, January 2015. ISSN 1932-1058. doi: 10.1063/1.4907896.

[349] Krzysztof Langer and Haakan N. Joensson. Rapid Production and Recovery of Cell Spheroids by Automated Droplet Microfluidics. *SLAS TECHNOLOGY: Translating Life Sciences Innovation*, page 2472630319877376, September 2019. ISSN 2472-6303. doi: 10.1177/2472630319877376.